TRANSPORTATION RESEARCH RECORD 1095

Design and Performance of Flexible Pavements

TRB
TRANSPORTATION RESEARCH BOARD
NATIONAL RESEARCH COUNCIL
WASHINGTON, D.C. 1986

Transportation Research Record 1095
Price $16.20
Editor: Elizabeth W. Kaplan
Compositor: Lucinda Reeder
Layout: Betty L. Hawkins

modes
1 highway transportation
3 rail transportation

subject area
24 pavement design and performance

Transportation Research Board publications are available by ordering directly from TRB. They may also be obtained on a regular basis through organizational or individual affiliation with TRB; affiliates or library subscribers are eligible for substantial discounts. For further information, write to the Transportation Research Board, National Research Council, 2101 Constitution Avenue, N.W., Washington, D.C. 20418.

Printed in the United States of America

Library of Congress Cataloging-in-Publication Data
National Research Council. Transportation Research Board.

Design and performance of flexible pavements.

(Transportation research record, ISSN 0361–1981 ; 1095)
1. Pavements, Flexible—Design and construction.
2. Pavements, Flexible—Evaluation. I. National Research Council (U.S.). Transportation Research Board.
II. Series.
TE7.H5 no. 1095 380.5 s 87–7822
[TE270] [625.8]
ISBN 0–309–04115–5

TRANSPORTATION RESEARCH BOARD
National Research Council

ERRATA
TRB Publications
(through March 1989)

Special Report 218, Volume 1

In the keys to Figures 2-4 (page 30) and 3-1 (page 38), two of the definitions were transposed. The middle curve in Figure 2-4 is for male and female drivers, and the bottom curve is for female drivers. In Figure 3-1 the curve represents fatalities per 10,000 population, and the shaded bars represent thousands of fatalities. The correct figures are shown below:

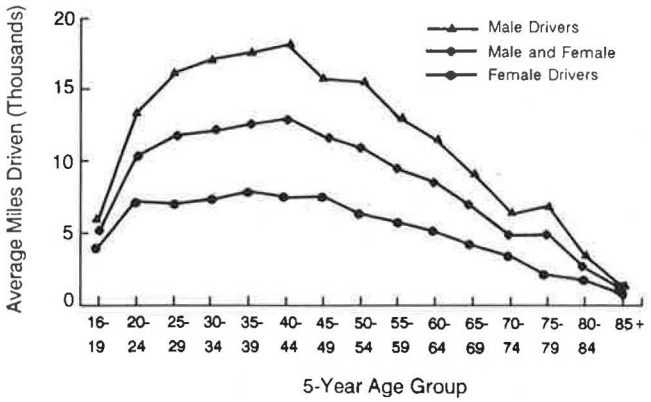

FIGURE 2-4

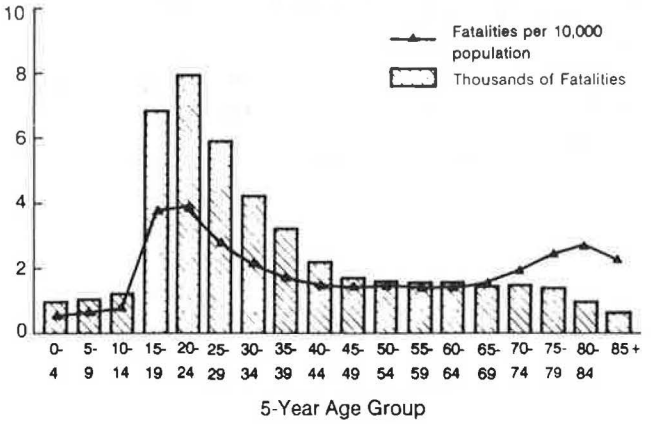

FIGURE 3-1

Transportation Research Record 1095

page 42

Equation 5 should read as follows:

$$\log_{10}(\varepsilon_{yy})_{ov} = -0.689 + 0.793 \log_{10}(\varepsilon_{yy}) - 0.041(H_{ov} + H_1)^{1/2} - 0.057(H_{ov})$$

Transportation Research Record 1106

Volume 2

page 225

The second sentence in the abstract should read as follows:

> In the past, a uniform set of geometric design standards for these types of roads was not available in Canada.

page 227

The last item in the bulleted list in column 1 should read as follows:

> One-lane, two-way resource development roads for ADTs up to 100 vpd.

pages 229–232

The figure captions should read as follows:

FIGURE 1	Cross-section elements for two-lane, low-volume earth and gravel roads.
FIGURE 2	Cross-section elements for two-lane, low-volume surfaced roads.
FIGURE 3	Cross-section elements for one-lane, two-way low-volume roads.
FIGURE 4	Cross-section elements for one-lane, one-way low-volume roads.
FIGURE 5	Roadway width versus design speeds of various road agencies (ADT < 50).
FIGURE 6	Roadway width versus design speeds of various road agencies (ADT 50 to 100).
FIGURE 7	Roadway width versus design speeds of various road agencies (ADT 100 to 150).
FIGURE 8	Roadway width versus design speeds of various road agencies (ADT 150 to 200).

Supplement

page 50

In the paper by Faiz and Fossberg, references 3 and 4 were transposed. The last two references in the paper should read as follows:

3. *Road Deterioration in Developing Countries.* Report 6968. Infrastructure Department, World Bank, Washington, D.C., Oct. 15, 1987.
4. M. Mason. *Axle Loading Study.* Internal report. Transportation, Water and Telecommunications Department, World Bank, Washington, D.C., 1981.

Transportation Research Record 1122

page 30

The last two columns in Table 2 are incorrect. The correct Table 2 is shown at the top of the next page.

TABLE 2 SITES WITH MERGING-RELATED ACCIDENTS

Site No.	Climbing Lane Length and AADT	Vertical Alignment	Horizontal Alignment	Sight Distance	Passing Ahead	Accidents[a] Total and Rate	Accidents[a] Merging-Related
1	0.13 mi	Up 8.5%	Tight curve	Restricted	Very	20	1
	3,400	No crest			Restricted	1,612[b]	#1[c]
2	0.73 mi	Up 6.0%	No curves	Excellent	Restricted	10	1
	9,725	No crest				282[b]	#2[c]
3	0.81 mi	Up 5.0%	After a curve	Good	Average	12	1
	9,725	Crest				364[b]	#3[c]
4	0.16 mi	Up 5.9%	Slight curve	Good	Restricted	17	5
	11,000	No crest				466[b]	#4–8[c]
5	0.22 mi	Up >5%	In middle of	Restricted	Restricted	6	1
	2,200	No crest	tight curve			747[b]	#9[c]
6	0.28 mi	Up >5%	In curve	Restricted	Very	4	2
	2,200	No crest			Restricted	498[b]	#10–11[c]

a - Accidents within ±0.10 mile of end of merging taper, 1980-84.

b - Accidents per 10^8 vehicle miles.

c - Numbers refer to accidents described in text.

Source: California Department of Transportation photolog, site plans, correspondence, TASAS, and (6).

page 34

The first sentence in the last paragraph in column 1 should read as follows:

For car speeds of 38 mph, truck speeds of 22 mph, and speeds of other slow vehicles of 26 mph, the following results are obtained.

Transportation Research Record 1131

The paper by Lacy and Pannee (pp. 99–106) was sponsored by the Committee on Engineering Fabrics.

Transportation Research Circular 330

Portions of the original publication were printed in an incorrect sequence. A revised photocopy of the circular is available on request from the Business Office, Transportation Research Board, 2101 Constitution Avenue, N.W., Washington, D.C. 20418 (telephone 202-334-3218).

NCHRP Synthesis of Highway Practice 138

page 4

The data in Table 2 are incorrect. The following table should be used in place of Table 2:

Speed (mph)	Speed (km/h)	Stopping Sight Distance (ft)	Stopping Sight Distance (m)
30	48	200	61
40	64	325	99
50	80	475	145
60	97	650	198
70	113	850	259

NCHRP Synthesis of Highway Practice 139

page 61

In reference 1, the date for "Accident Facts," published by the National Safety Council, should be 1986.

Transportation Research Record 1095

The **Transportation Research Record** series consists of collections of papers on a given subject. Most of the papers in a Transportation Research Record were originally prepared for presentation at a TRB Annual Meeting. All papers (both Annual Meeting papers and those submitted solely for publication) have been reviewed and accepted for publication by TRB's peer review process according to procedures approved by a Report Review Committee consisting of members of the National Academy of Sciences, the National Academy of Engineering, and the Institute of Medicine.

The views expressed in these papers are those of the authors and do not necessarily reflect those of the sponsoring committee, the Transportation Research Board, the National Research Council, or the sponsors of TRB activities.

Transportation Research Records are issued irregularly; approximately 50 are released each year. Each is classified according to the modes and subject areas dealt with in the individual papers it contains. TRB publications are available on direct order from TRB, or they may be obtained on a regular basis through organizational or individual affiliation with TRB. Affiliates or library subscribers are eligible for substantial discounts. For further information, write to the Transportation Research Board, National Research Council, 2101 Constitution Avenue, N.W., Washington, D.C. 20418.

Contents

A Computerized Analysis of Rutting Behavior of Flexible Pavement

DAVID L. ALLEN AND ROBERT C. DEEN

Rutting is one mode of failure in flexible pavements. Described herein are laboratory models that predict rutting in asphaltic concrete, dense-graded aggregate, and a subgrade soil. These models have been programmed to predict a rut depth for a particular pavement structure using a given set of traffic and environmental conditions. A number of rutting charts have been developed and an example is presented herein that can be used to estimate rutting in a particular structure after an assumed number of equivalent axle loads. Such charts can also be used for overlays on flexible and rigid pavements. A comparison is made between thickness designs using rutting and fatigue as failure criteria.

The behavior of asphalt-bound layers, unbound aggregate bases, and foundation soils (subgrades) may be affected by such variables as gradation, asphalt and moisture contents, type of aggregate, density, method of compaction, temperature, magnitude and frequency of loading, and duration of each load cycle. There are also other less significant variables. The complex interaction of all of these variables yields a composite behavior for a particular pavement structure that could become manifest in some form of distress or even complete "failure."

Flexible pavements are susceptible to rutting, but it is not well known where and to what extent rutting takes place within a pavement structure. Rutting is a result of the lateral distribution (generally approximated by a normal distribution) or scatter of wheel passes across the wheelpaths. A large percentage of wheel passes occur within relatively narrow paths on the pavement surface. It is the distribution of traffic that causes accumulated deformations to occur, producing ruts. If these ruts are to be estimated or predicted for design purposes, the behavior of the materials must be known or parameterized.

To determine where in the pavement structure and to what extent rutting occurs and to determine the factors that control rutting, a comprehensive laboratory testing program was performed. Various traffic and environmental parameters were controlled in the study; and from the data, mathematical models that described the rutting behavior of an asphaltic concrete, a dense-graded aggregate, and a subgrade soil were formulated. A traffic and a temperature model were also formulated to provide necessary input to the rutting models. These models have been collected and programmed in a computer program entitled PAVRUT. By using this program, an estimated rut depth can be calculated for any flexible pavement, assuming that the volume and characteristics of the traffic stream and the properties of the paving materials are known.

Kentucky Transportation Research Program, College of Engineering, University of Kentucky, Lexington, Ky. 40506-0043.

MODELS

Asphaltic Concrete Rutting Models

To predict accumulation of rutting in the field under repeated service loads, it was necessary to determine the susceptibility of an asphaltic concrete mixture to deformation. The mixture contained crushed limestone aggregate and was graded as shown in Figure 1. It contained 5.2 percent asphalt. Samples were compacted in a split mold that had a double plunger (top and bottom). The material was heated to 300°F (149°C), and the proper quantity of material was weighed into a heated mold. The material was compressed under a 5,000-lb (2273-kg) load until the proper height was obtained. The average temperature at the time of compaction was 280°F (138°C). The average height was 3.0 in. (76 mm) and the average diameter was 2.0 in. (51 mm). Twenty-seven unconfined repeated-load tests were performed on an asphaltic concrete base (asphalt cement grade was AC-20). The tests were run at three temperatures: 45°F (7°C), 77°F (25°C), and 100°F (38°C). Three vertical pressures were used at each temperature: 80 psi (551 kPa), 50 psi (345 kPa), and 20 psi (138 kPa). A detailed discussion of methodology, equipment, and analyses for those tests is given elsewhere *(1, 2)*.

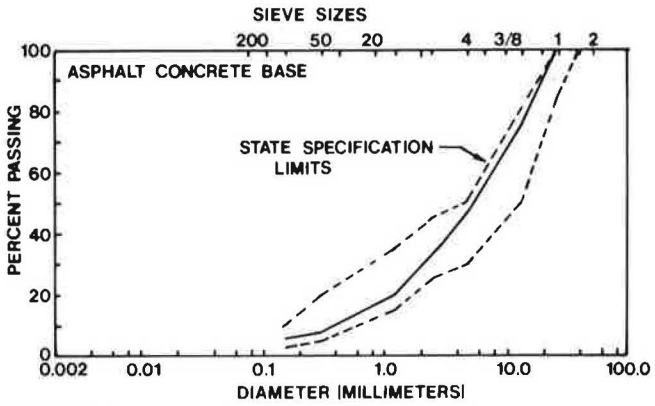

FIGURE 1 Gradation of asphalt concrete base.

Figure 2 is an example of the repeated-load data. A least-squares regression analysis of all data resulted in an equation that described plastic deformation (rutting) as a function of temperature, stress, and load repetitions:

$$\log \varepsilon_p = C_0 + C_1 (\log N) - C_2 (\log N)^2 + C_3 (\log N)^3 \quad (1)$$

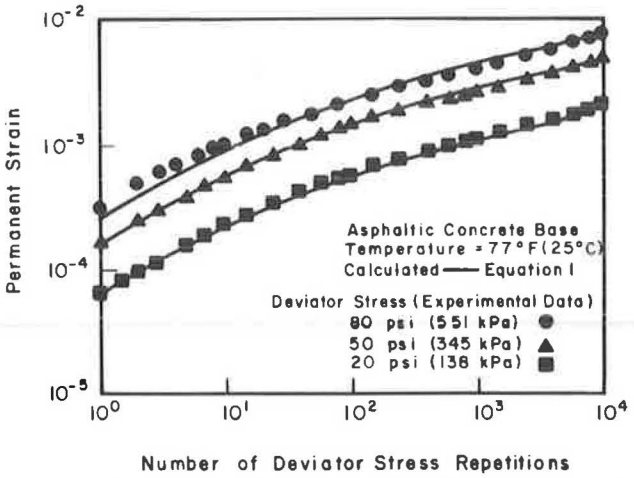

FIGURE 2 Permanent strain as a function of number of load cycles (asphaltic concrete).

where

ε_p = permanent strain,
N = number of stress repetitions,
C_3 = 0.00938,
C_2 = 0.10392,
C_1 = 0.63974,
C_0 = (−0.000663 T^2 + 0.1521 T − 13.304) + [(1.46 − 0.00572 T) (log σ_1)],
T = temperature (°F), and
σ_1 = stress (psi).

Dense-Graded Aggregate Rutting Model

The algorithm in this model also was developed from data obtained from a series of repeated-load tests on laboratory-compacted specimens of dense-graded aggregate. The dense-graded aggregate was crushed limestone. The gradation is shown in Figure 3. To prepare samples at various moisture contents, it was necessary to determine the moisture-density relationship according to AASHTO Standard T-180. The maximum dry density was 150 lb/ft^3 (2403 kg/m^3); optimum moisture content was 4.7 percent. The repeated-load tests were performed at moisture contents of 1.7, 3.6, and 5.3 percent. The specimen size was 6 in. (152 mm) in height and 2.8 in. (71.1 mm) in diameter. Confining pressures of 5 psi (34 kPa), 10 psi (69 kPa), and 15 psi (103 kPa) were used and deviator stresses of 10 psi (69 kPa), 20 psi (138 kPa), and 30 psi (207 kPa) were applied at each confining pressure. A total of 27 tests were run.

As in the case of asphaltic concrete, analysis of the repeated-load test data (an example is shown in Figure 4) resulted in a third-degree polynomial describing the plastic deformation as a function of stress level, confining pressure, moisture content, and load repetitions:

$$\log \varepsilon_p = C_0 + C_1 (\log N) + C_2 (\log N)^2 + C_3 (\log N)^3 \quad (2)$$

where

ε_p = permanent strain,
N = number of stress repetitions,
C3 = 0.0066 − 0.004 (log w),
C_2 = −0.142 + 0.092 (log w),
C_1 = 0.72
C_0 = [−4.41 + (0.173 + 0.003 w) (σ_1)] − [(0.00075 + 0.0029 w) (σ_3)],
w = moisture content (percent),
σ_1 = deviator stress (psi), and
σ_3 = confining pressure (psi).

Subgrade Rutting Model

As in the cases of asphaltic concrete and dense-graded aggregate, the algorithm in this model was developed from a series

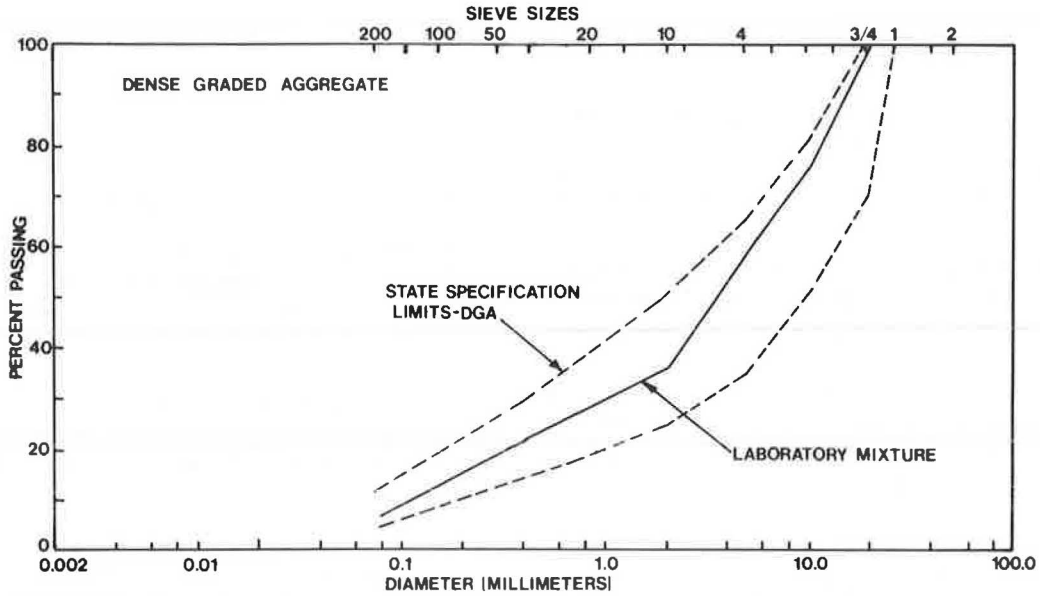

FIGURE 3 Gradation of dense-graded aggregate.

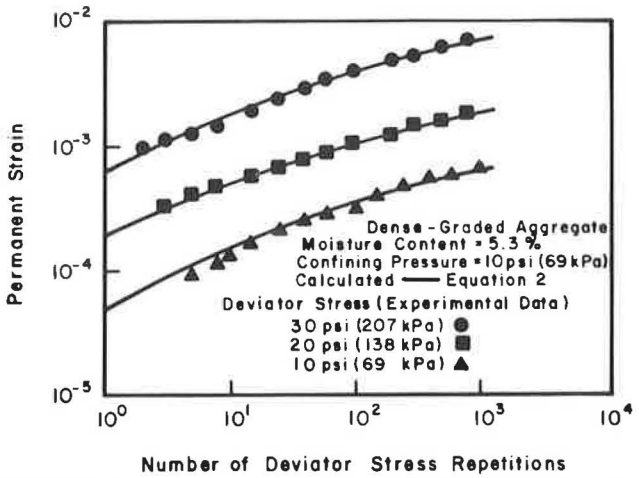

FIGURE 4 Permanent strain as a function of number of load cycles (dense-graded aggregate).

of repeated-load tests on laboratory-compacted soil specimens.

The gradation of the particular soil used in this study is shown in Figure 5. Results of the moisture-density test (AASHTO T-180) indicated a maximum dry density of 130.8 lb/ft^3 (2093 kg/m^3) at an optimum moisture content of 9.7 percent.

Two series of specimens were tested: one at 8.2 percent moisture and the other at 9.4 percent. Specimen size was 6 in. (152 mm) in height and 2.8 in. (71.1 mm) in diameter. Three confining pressures [5 psi (34 kPa), 10 psi (69 kPa), and 15 psi (103 kPa)] were used in each series. At least three specimens were tested at each confining pressure with deviator stresses of 2.5 psi (17 kPa), 5 psi (34 kPa), and 10 psi (69 kPa).

There was considerable scatter in the data, and results were not always repeatable. This was attributed largely to the high degree of variability of the material. An example of the repeated-load tests data is shown in Figure 6. Because of scatter, each curve in this figure is an average of two or more tests; and, for that reason, no data points are shown. A permanent deformation model was derived for the subgrade material using a linear-regression analysis on points taken from those average curves:

$$\log \varepsilon_p = C_0 + C_1 (\log N) + C_2 (\log N)^2 + C_3 (\log N)^3 \quad (3)$$

where

ε_p = permanent strain,
N = number of stress repetitions,
C_3 = 0.007 + 0.001 w,
C_2 = 0.018 w,
C_1 = $10^{(-1.1+0.1w)}$,
C_0 = $[(-6.5 + 0.38\ w) - (1.1 \log \sigma_3)] + (1.86 \log \sigma_1)$,
w = moisture content (percent),
σ_1 = deviator stress (psi), and
σ_3 = confining pressure (psi).

If desired, the subgrade rutting model may be used to calculate rutting as a function of California bearing ratio (CBR) rather than moisture content. The following relationship was developed from laboratory CBR tests on subgrade material at various moisture contents:

$$w = 10^{[0.8633 - 0.05645(\log_{10} CBR)]} \quad (4)$$

Equation 4 can be substituted for w in the previous equations when using CBR.

Temperature Model

This model is used to calculate the temperature of the asphaltic concrete at any depth for any typical hour of the year. This temperature is used to calculate strain in the asphalt concrete

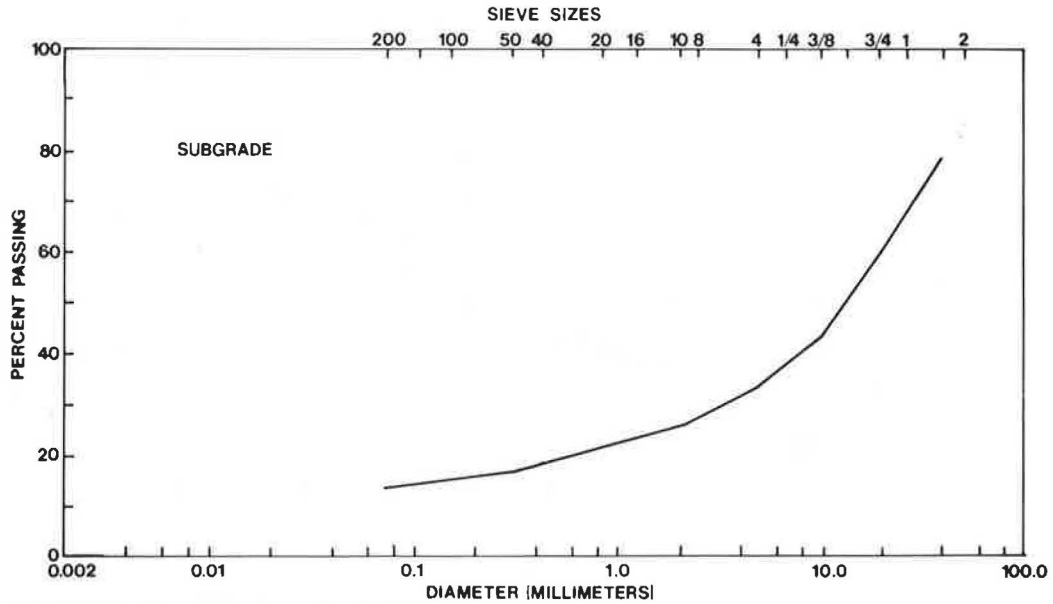

FIGURE 5 Gradation of subgrade soil.

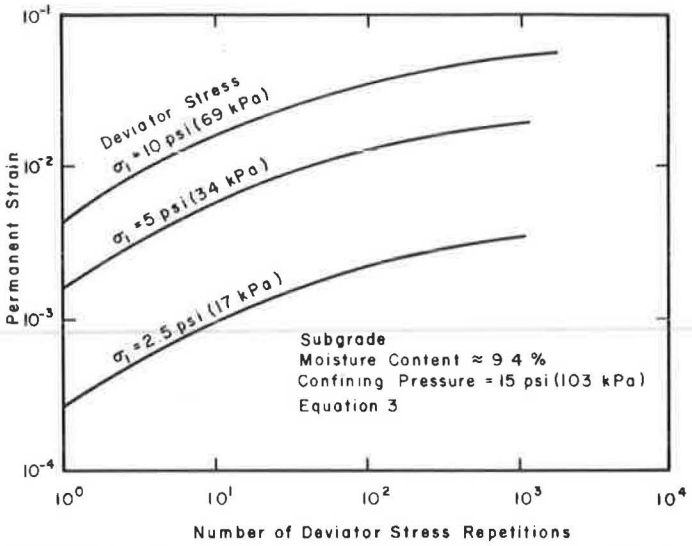

FIGURE 6 Permanent strain as a function of number of load cycles (subgrade).

and also to calculate the modulus of elasticity of the asphaltic concrete.

In 1969 Southgate and Deen *(3)* described an in-depth analysis of temperature-versus-depth data collected by Kallas *(4)* in 1964 and 1965 at The Asphalt Institute laboratory at College Park, Maryland. Charts similar to the one shown in Figure 7 were developed. In those charts (a total of 28), pavement temperature at some depth was plotted as a function of the pavement surface temperature plus the mean air temperature for the previous 5 days. Those relationships were developed by running a regression analysis on data from Kallas for most hours of the day (one chart for each hour).

To use information presented in Southgate and Deen's charts in the program, it was necessary to develop a mathematical model describing the relationship between the dependent variable (pavement temperature at some depth) and the independent variables (slope and zero intercept of the depth curves from all of Southgate and Deen's charts and pavement surface temperature plus the 5-day mean air-temperature history). As illustrated in Figure 7, the depth curves were straight lines; therefore, an equation of the following form should describe the relationship:

$$T = A + BX \quad (5)$$

where

T = temperature at some depth (°F),
A = zero intercept of depth curves,
B = slope of depth curves, and
X = pavement surface temperature plus 5-day mean air-temperature history (°F).

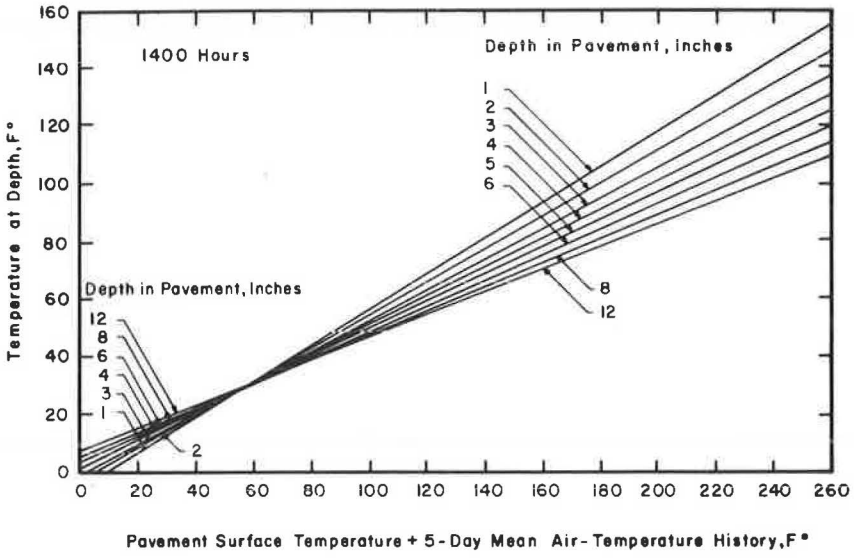

FIGURE 7 Pavement temperature at depth as a function of pavement surface temperature plus 5-day mean air-temperature history.

However, Variables A, B, and X are, in themselves, very complicated functions. As may be noted in Figure 7, Variables A and B are dependent on hour of the day and depth in the pavement. Variable X is dependent on month of the year and hour of the day.

To define Variables A and B, all values for A and B reported by Southgate and Deen were plotted as functions of hour and depth. Linear-regression analyses were performed, yielding functions that were fifth-degree polynomials in hour of the day and third-degree polynomials in depth in pavement. The following two equations describe Variables A and B:

$$A = (-0.8882061 - 5.409584\,H + 1.419966\,H^2 - 0.1436045\,H^3 + 0.006001302\,H^4 - 0.000087823\,H^5) + (-2.312872 + 3.643902\,H - 1.000187\,H^2 + 0.1082190\,H^3 - 0.004867211\,H^4 + 0.00007657193\,H^5)(D) + (0.3188233 - 0.4041188\,H + 0.1103354\,H^2 - 0.01201035\,H^3 + 0.0005488345\,H^4 - 0.000008829082\,H^5)(D)^2 + (-0.01064115 + 0.01438466\,H - 0.00390228\,H^2 + 0.00042378\,H^3 - 0.0000194274\,H^4 + 0.0000003144042\,H^5)(D)^3 \quad (6)$$

and

$$B = (0.5449503 + 0.01836149\,H - 0.01005689\,H^2 + 0.00157948\,H^3 - 0.00008601361\,H^4 + 0.000001517039\,H^5) + (-0.004002625 + 0.0112879\,H - 0.001222558\,H^2 - 0.0001705093\,H^3 + 0.00001952838\,H^4 - 0.0000004628811\,H^5)(D) + (0.0007371035 - 0.001401982\,H + 0.0002543963\,H^2 + 0.000001147628\,H^3 - 0.000001274846\,H^4 + 0.00000003690588\,H^5)(D)^2 + (-0.00007334696 + 0.00007449587\,H - 0.00001665841\,H^2 + 0.0000008755230\,H^3 + 0.00000000193508\,H^4 - 0.0000000006176451\,H^5)(D)^3 \quad (7)$$

where H is the hour of the day and D is the depth in the pavement (inches).

Variable X in Equation 5 also was defined from data reported by Southgate and Deen. Figure 8 shows the relationship between pavement surface temperature and hour of day, normalized to 132°F (the average temperature at 1300 hr for the month of July). A regression analysis on those data yielded the following "best-fit" equation:

$$T_n = -0.316 + 0.0814\,H + 0.0125\,H^2 + 0.00155\,H^3 + 0.0000230\,H^4 \quad (8)$$

where T_n is the normalized pavement surface temperature.

However, Equation 8 does not adequately describe the "linear" portion of the curve, from Hour 1 to Hour 6. Therefore, an additive correction factor (C_n), derived from a graphic solution, must be applied to Equation 8:

$$C_n = 10^{(-0.0757 - 0.0221\,H^2)} - 10^{(-2.96 + 0.058\,H^2)} \quad (9)$$

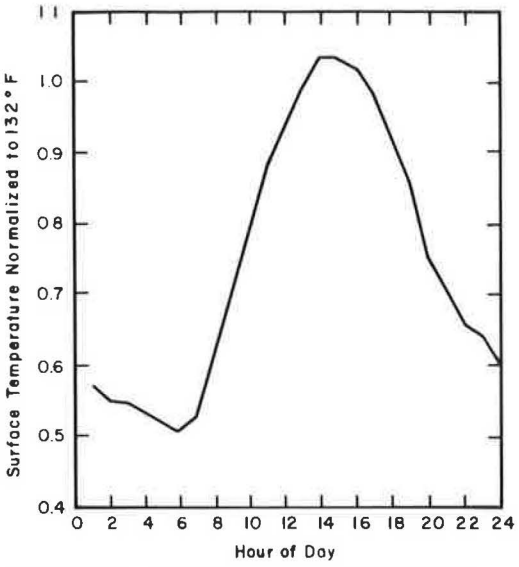

FIGURE 8 Pavement surface temperature normalized to 132°F (temperature at 1300 hr in July) as a function of hour of day *(1)*.

Combining Equations 8 and 9 gives the corrected pavement surface temperature in degrees Fahrenheit:

$$T_c = 132\,(T_n + C_n) \quad (10)$$

Equation 10 was based on temperatures for the month of July. Therefore, it must be corrected for each month. Figure 9, which was derived from Figure 22 of Southgate and Deen's report *(3)*, shows the relationship between normalized pavement surface temperature (°F) at 1300 hr and month of the year. As in Figure

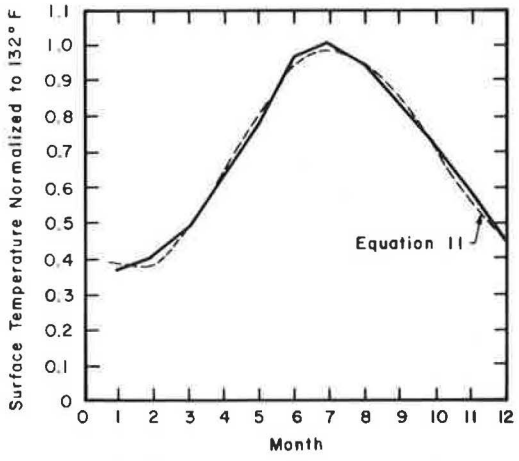

FIGURE 9 Pavement surface temperature normalized to 132°F (temperature at 1300 hr in July) as a function of month of year *(1)*.

8, the average pavement surface temperature at 1300 hr for the month of July (132°F) was set equal to 1.0. A regression analysis on that data gave the following result:

$$T_{nm} = 0.603192 - 0.35332\,M + 0.152582\,M^2 - 0.017904\,M^3 + 0.00062937\,M^4 \quad (11)$$

where T_{nm} is the normalized pavement surface temperature as a function of month and M is the month of the year (January = 1, December = 12).

Equation 10 can now be corrected for month of year:

$$ST = T_c \times T_{nm} \quad (12)$$

where ST is the pavement surface temperature for any month and hour of the year.

The 5-day mean air-temperature history is the last factor to be considered when defining Variable X in Equation 5. Figure 10 is a plot of the average daily temperature for each month, for the years 1970 through 1977. This was developed for locations

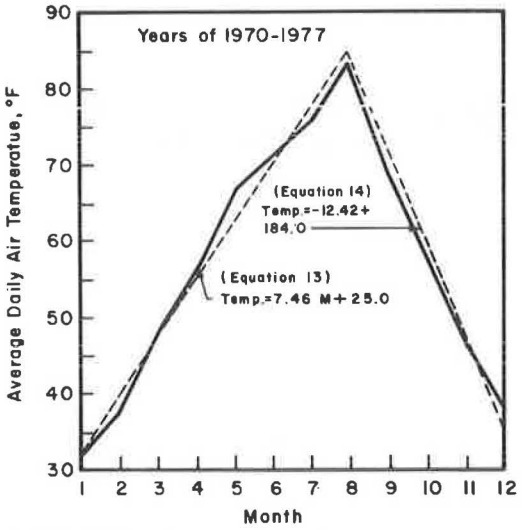

FIGURE 10 Average daily air temperature as a function of month of year.

with latitudes around 39 degrees North. Two linear "fits" were made to approximate the data. The first equation gives the mean daily temperature for the months of January through August:

$$T_{DA} = 7.46\ M + 25.0 \quad (13)$$

The second equation may be used to calculate the same variable for September through December:

$$T_{DA} = -12.42\ M + 184 \quad (14)$$

As noted earlier, Southgate and Deen's charts were based on the 5-day mean air-temperature history. However, in making the previous analysis, it was assumed that the average daily temperature of any 5-day period in the month would be reasonably close to the monthly mean. Although Southgate and Deen have shown that this is not entirely true, it appeared that the error introduced would not be significant (Figure 11). Variable X of Equation 5 has now been defined and can be written as

$$X = ST + T_{DA} \quad (15)$$

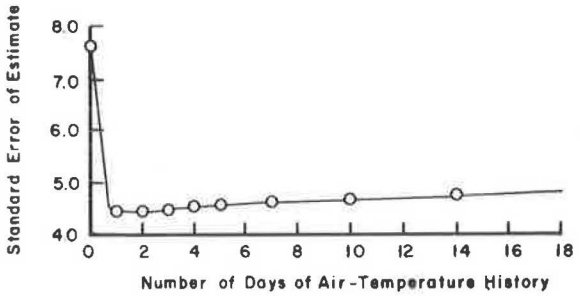

FIGURE 11 Standard error of estimate versus number of days of antecedent air temperatures for 6-in. depth at 1300 hr.

Modulus Models

The modulus of elasticity of asphaltic concrete was derived from Figure 19 of Southgate and Deen's report *(3)*. A regression analysis was performed on that data, yielding the following result:

$$\log E = 10.46 - 2.676 \log T \quad (16)$$

where E is the modulus of elasticity (psi) and T is the pavement temperature (°F) calculated from Equation 10.

The modulus calculated for dense-graded aggregate is actually a resilient modulus obtained from repeated-load tests. Definition of resilient modulus, how it was obtained, and the effects of confining pressure and moisture content on its magnitude are explained in detail elsewhere *(1)*. Again, regression analyses on the laboratory data gave the following equation for resilient modulus:

$$\log M_r = (5.4624 - 2.729 \log w) + (0.175 + 1.10 \log w)(\log \sigma_3) \quad (17)$$

where

M_r = resilient modulus (psi),
w = moisture content (percent), and
σ_3 = confining pressure (psi).

The equation describing the modulus of subgrade materials as a function of moisture content and confining pressure was developed from regression analyses of data obtained from resonant column tests on the material *(1)*:

$$\log E_r = 5.331 + 0.00070\ \sigma_3 + (0.11246 - 0.010060\ \sigma_3 + 0.000310\ \sigma_3^2)w - (0.02496 - 0.001880\ \sigma_3 + 0.00005490\ \sigma_3^2)w^2 \quad (18)$$

where E_r is the modulus of elasticity (psi) from the resonant column test. Moduli calculated with this model may be used to calculate stresses in the pavement structure.

Traffic Model

Traffic volumes by month and by hour of day for rural roads in Kentucky were reported by Herd et al. *(5)*. Figures 12 and 13

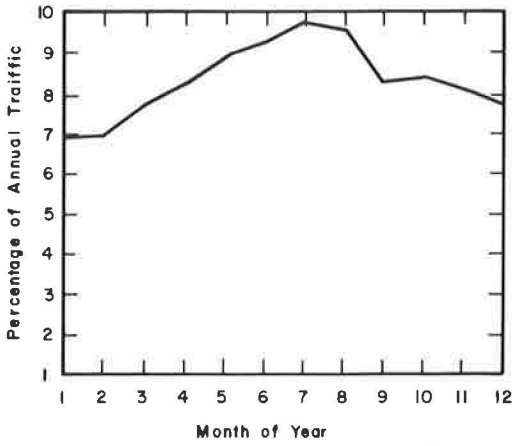

FIGURE 12 Percentage of annual traffic volume occurring in each month of the year.

were developed from their data. Figure 12 shows the percentage of total annual volume that occurs in each month, and Figure 13 illustrates the percentage of daily volume that occurs in any hour for a typical day. Although it is not entirely correct, for the sake of simplicity, it was assumed that the traffic pattern was the same for all days of any particular month.

To determine the volume for a particular hour of a particular month, it is necessary to multiply the percentage value from Figure 12 by the percentage value from Figure 13. This product is then multiplied by the number of days in a month (30 was assumed) and then by the annual volume.

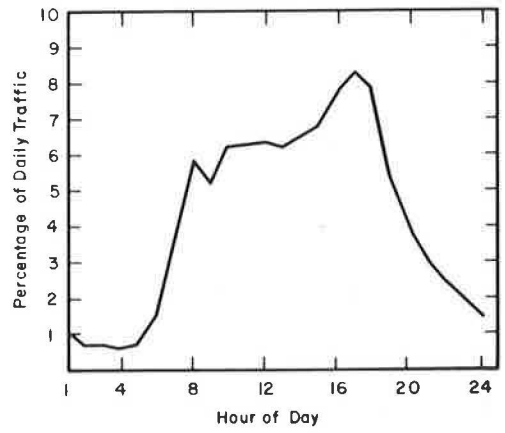

FIGURE 13 Percentage of daily traffic volume occurring in any hour of a typical day.

The total number of vehicles, however, is not the primary concern; the number of wheel passes is the major factor. To determine this, it was imperative to classify the traffic stream by types of vehicles. Traffic data for Kentucky indicated that approximately 20 percent of the traffic stream for rural roads was truck traffic. Furthermore, the same data showed that the average truck had 3.92 axles. Therefore, to obtain wheel passes, 80 percent of the hourly volume was multiplied by 2.0 (axles) for automobiles and 20 percent was multiplied by 3.92 (axles) for trucks to obtain the total number of wheel passes per hour.

All wheel passes do not occur at the same location on the pavement. It has been shown *(6)* that, in general, the distribution of wheel passes across any section of pavement approximates a normal distribution pattern (bell-shaped curve) or a sinusoidal function. This broadens the rut while reducing the depth. To account for such a pattern, the number of wheel passes was reduced to a number equal to the root mean square of the peak of the sinusoidal curve (0.707).

PROGRAM PAVRUT

All previously described models have been programmed as subroutines in PAVRUT.

There are 8,769 hr in a 365-day year. To be entirely correct, it would be necessary to calculate stresses, temperatures, and traffic volumes for each hour of the year; determine, from those calculations the amount of rutting in each layer for that particular hour; and, finally, sum all rutting values for 8,760 hr to obtain the total rut accumulated in 1 year. However, this would consume an extremely large amount of computer time. Therefore it was assumed that each month would have a "typical" day as far as traffic and temperature were concerned. Consequently, traffic and temperatures were determined for each hour of each typical day of the year. This means the program must cycle through each subroutine 288 times for each layer (12 typical days times 24 hr per day). In other words, to calculate rutting for one pavement, the program will cycle through most subroutines a total number of times equal to 288 multiplied by the number of layers.

The program will solve for rutting in a flexible pavement system that has up to 15 layers. However, the program requires a large amount of computer time, and the amount of time required increases rapidly with each additional layer to be analyzed.

Two classes of vehicles (such as automobiles and trucks) can be input for each problem with a different wheel load and tire pressure for each vehicle class. However, if only one class of vehicle is used, the program assumes that 20 percent of the annual volume is truck traffic.

It should be noted that the distribution of stresses in the pavement is calculated using layered elastic theory. A subroutine entitled COFE was used from the Chevron N-layer program to calculate stresses *(5)*.

An example output is shown in Figure 14. Each layer is identified. Layer thickness, magnitude of vertical compressive stress at the midpoint of the layer, depth of the midpoint of the layer, and moisture contents for dense-graded aggregate and subgrade are shown. In addition, the permanent deflection for each layer is printed. Finally, the total pavement deflection is printed.

To date only four field sites have been checked with estimated rut depths from the program. Figure 15 shows the results. There appears to be generally good agreement between measured and estimated rut depths, although in two cases the program slightly underestimated the rut depth.

```
**********************************************************************
*                                                                    *
*          10,000,000 EAL - RUN 21 - 20 10 18  CBR-7.5               *
*                                                                    *
**********************************************************************

LAYER NUMBER     1     ASPHALT CONCRETE
-----------------      LAYER THICKNESS        20.00
                       FIRST STRESS           22.60
                       ANSWER DEPTH           10.00
                       LAYER DEFLECTION    0.3098E 00

LAYER NUMBER     2     DENSE-GRADED AGGREGATE
-----------------      LAYER THICKNESS        10.00
                       FIRST STRESS            1.79
                       ANSWER DEPTH           25.00
                       MOISTURE CONTENT        3.00
                       LAYER DEFLECTION    0.3240E-01

LAYER NUMBER     3     SUBGRADE
-----------------      LAYER THICKNESS        18.00
                       FIRST STRESS            1.07
                       ANSWER DEPTH           39.00
                       MOISTURE CONTENT        7.00
                       LAYER DEFLECTION    0.1967E 00

TOTAL PAVEMENT DEFLECTION   0.5389E 00
```

FIGURE 14 Example printout.

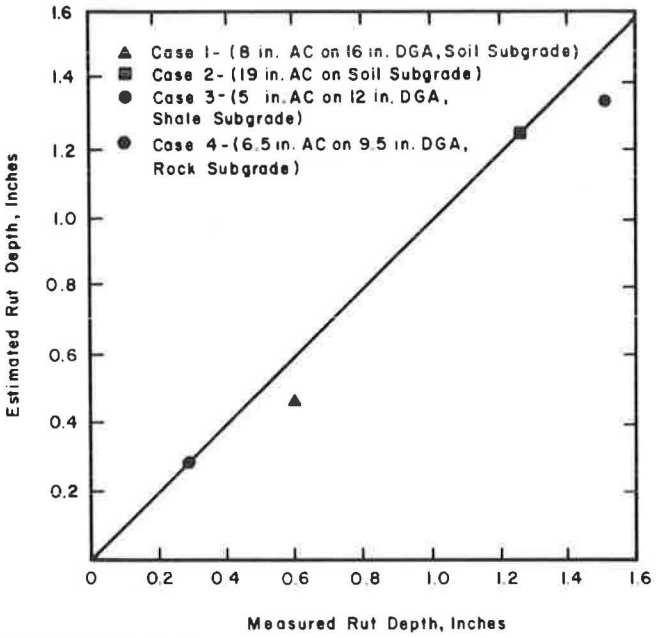

FIGURE 15 Estimated rut depths versus measured rut depths.

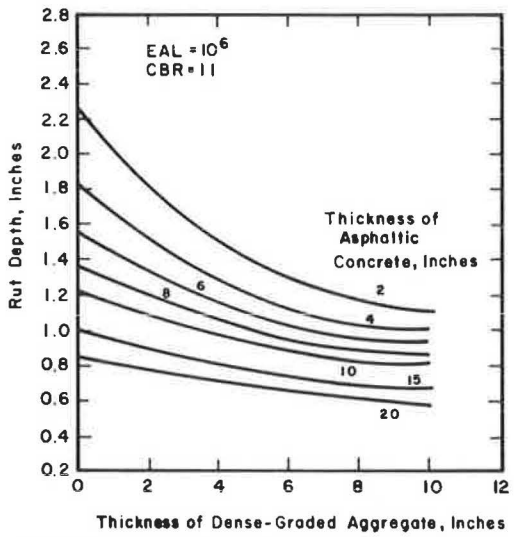

FIGURE 16 Rut depth chart.

EXAMPLE PROGRAM USES

The program may be used for any number of analyses, and three examples are given here. Figure 16 is a rut depth chart that was developed from the program. This chart permits a designer to estimate the amount of rutting for any particular pavement structure. Rutting also may be estimated for an in-service pavement. If the accumulated equivalent axle loads (EALs) are known, the remaining rutting life of a pavement may be estimated from such charts.

Figure 17 shows the relationship between rut depth and thickness of asphaltic concrete layers expressed as a percentage of total pavement thickness. All designs in Figure 17 are "equivalent" with respect to adequacy to resist failure by fatigue. As would be expected, CBR is quite influential in determining rut depth. Also, a somewhat surprising result, at EALs of 10^7, the more conventional designs of 33 or 50 percent asphaltic concrete thicknesses appear to be the better designs to minimize rutting. Although this hypothesis has not yet been tested extensively, it is suspected that the relationship shown in Figure 17 is related to the distribution of stresses in the pavement layers. Figure 18 shows a typical distribution of stresses with depth for a conventional design and for a full-depth design. Stresses decrease more rapidly in the asphaltic layers of

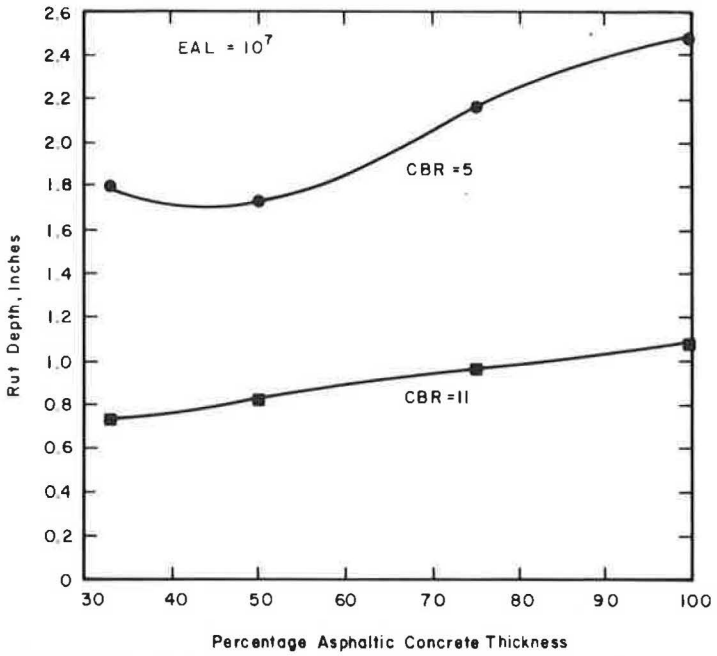

FIGURE 17 Rut depth as a function of the percentage of asphaltic concrete thickness.

the conventional design than in the more homogeneous full-depth design. This distribution tends to keep the higher stresses in the upper, stiffer layers of the conventional design. Stresses were calculated assuming linear elastic materials; therefore it is not clear how a nonlinear model of elasticity would affect the stress distribution and, consequently, the relationship shown in Figure 17.

In Kentucky, pavements are designed using fatigue as the failure criterion. However, rutting could, hypothetically, be used as a failure criterion. Figure 19 shows thickness design curves using a rut depth of 0.5 in. as the failure criterion. Up to 10^6 EALs, very thin pavements are required. However, from 10^6 to 10^7 EALs, the thickness required increases exponentially

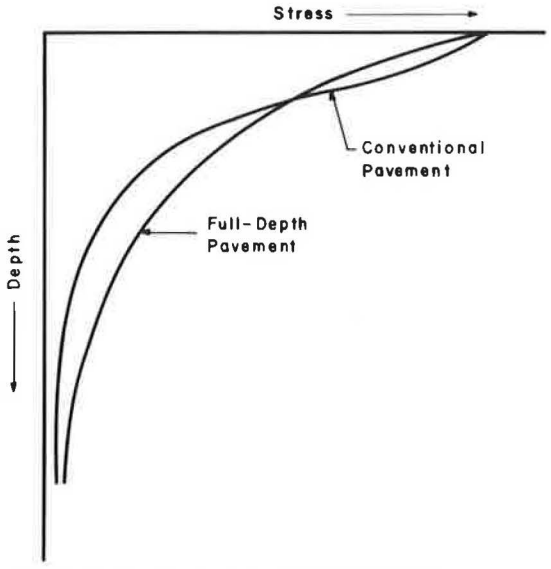

FIGURE 18 Typical stress distributions.

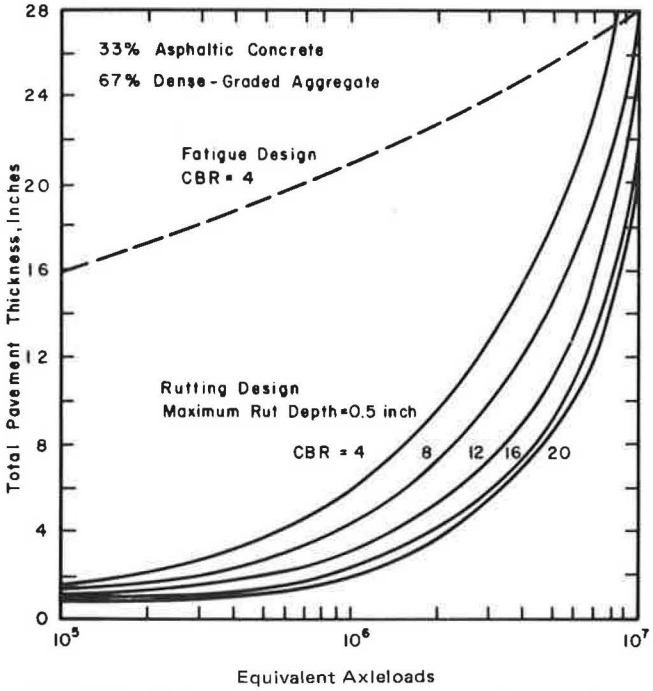

FIGURE 19 Thickness design curves for maximum rut depth of 0.5 in.

and becomes almost asymptotic at 10^7 EALs. From this it could be concluded that it is highly impractical to attempt to build a pavement thick enough to prevent a 0.5-in. rut depth for more than 10^7 EALs. For comparison, the thickness design curve presently used in Kentucky and based on the fatigue failure criterion is shown as the dashed line (for CBR = 4) in Figure 19. At an EAL of 8.4×10^6, the two failure criteria yield "equivalent" designs.

CONCLUSIONS

Based on a limited number of cases, the PAVRUT program appears to be reasonably accurate in predicting rut depths. Caution must be exercised in extrapolating the output to any flexible pavement because the models in the program are based on only one material.

Equivalent designs based on a fatigue failure criterion are not equivalent designs when using the rutting failure criterion.

In this study the more conventional designs (33 or 50 percent asphaltic concrete thickness) appear to function better from the standpoint of rutting than do full-depth asphaltic concrete pavements. Again, it must be emphasized that this conclusion is based on the behavior of only one material for each layer.

Rut depth charts developed from the PAVRUT program appear to be useful tools for determining the rutting potential of a particular flexible pavement structure. Such charts may be used to plan stage construction to minimize rutting and thus provide smoother pavements, which are also resistant to failure due to fatigue, for longer periods.

REFERENCES

1. D. L. Allen. *Determination of Rutting in Asphaltic Concrete Pavements: Field Instrumentation and Laboratory Characterizations.* Research Report 502. Division of Research, Kentucky Department of Transportation, Lexington, Aug. 1978.
2. D. L. Allen and R. C. Deen. Modulus and Damping of Asphaltic Concrete Using the Resonant Column. *Geotechnical Testing Journal*, ASTM, Vol. 3, No. 4, Dec. 1980.
3. H. F. Southgate and R. C. Deen. Temperature Distribution within Asphalt Pavements and Its Relationship to Pavement Deflection. In *Highway Research Record 291*, HRB, National Research Council, Washington, D.C., 1969, pp. 116–131.
4. B. F. Kallas. Asphalt Pavement Temperatures. In *Highway Research Record 150*, HRB, National Research Council, Washington, D.C., 1966, pp. 1–11.
5. D. R. Herd, K. R. Agent, and R. L. Rizenbergs. *Traffic Accidents: Day Versus Night.* Research Report 471. Division of Research, Kentucky Department of Transportation, Lexington, May 1977.
6. P. J. van der Loo. A Practical Approach to the Prediction of Rutting in Asphalt Pavements: The Shell Method. In *Transportation Research Record 616*, TRB, National Research Council, Washington, D.C., 1976, pp. 15–21.

Publication of this paper sponsored by Committee on Flexible Pavements.

ILLI-PAVE-Based Response Algorithms for Full-Depth Asphalt Concrete Flexible Pavements

M. GOMEZ-ACHECAR AND MARSHALL R. THOMPSON

In a mechanistic design procedure a structural model is used to predict pavement responses (stresses, strains, displacements). The ILLI-PAVE finite-element structural model considers nonlinear, stress-dependent resilient modulus material models and failure criteria for granular materials and fine-grained soils. Asphalt concrete (AC) is modeled as a linear elastic material. The computational techniques of the ILLI-PAVE computer program require a main-frame computer and are too costly, complex, and cumbersome to be used for routine design. To incorporate ILLI-PAVE structural model concepts into a mechanistic design concept, simplified response algorithms that reliably predict ILLI-PAVE responses for full-depth AC pavements are needed. A comprehensive ILLI-PAVE factorial study was conducted. The variables considered were thickness of asphalt concrete, asphalt concrete modulus, and subgrade resilient modulus. ILLI-PAVE-based response algorithms for full-depth AC pavements are presented for AC radial strain, surface deflection, subgrade deviator stress, subgrade vertical strain, and subgrade deflection. Additional algorithms relating AC radial strain and subgrade deviator stress ratio and surface deflection are also presented. The algorithms are sufficiently accurate for inclusion in "mechanistic" design procedures.

The various components of a mechanistic design procedure for full-depth asphalt concrete (AC) flexible pavements are shown in Figure 1. In this paper emphasis is placed on materials characterization, the structural model, and pavement response components. Concepts for a mechanistic design procedure based on the ILLI-PAVE finite-element structural model *(1)* and design algorithms developed from a comprehensive ILLI-PAVE data base *(2)* are presented. The subsequent development of a design procedure based on these concepts should include the consideration of climatic effects and the establishment of appropriate transfer functions.

Climatic effects (temperature, moisture, freeze-thaw) can be considered by quantifying their effects on material characteristics (resilient moduli and shear strength). Such considerations should be based on an extensive study of local climatic and soil conditions.

Transfer functions relating pavement response and pavement performance are not proposed. Typical transfer functions consider pavement responses related to subgrade permanent strain (subgrade resilient strain, subgrade stress, subgrade stress ratio) and AC fatigue (AC strain). Transfer functions for full-depth AC pavements are considered elsewhere *(2)*. Transfer functions should be developed on the basis of consideration of the paving materials, soils, climate, and so forth relevant to local conditions. Laboratory testing information and field performance data are essential inputs to "calibrating" a transfer function.

Department of Civil Engineering, University of Illinois at Urbana-Champaign, Urbana, Ill. 61801.

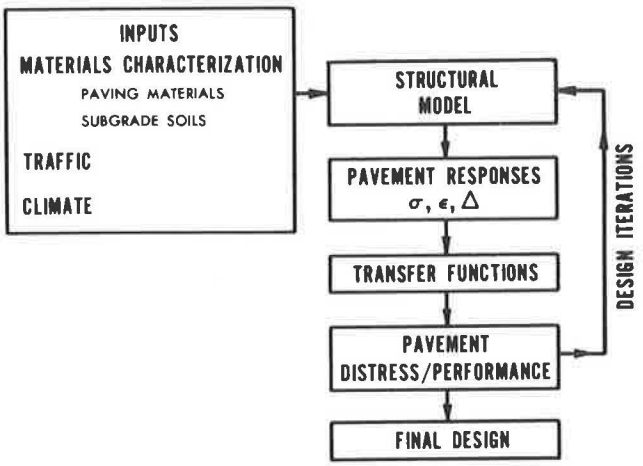

FIGURE 1 Components of a mechanistic design procedure.

Transfer functions are an important part of a total mechanistic design procedure. Transfer functions appropriate for use with the ILLI-PAVE procedure are not necessarily compatible with linear elastic (or other) analysis procedures.

The analyses and algorithms presented in this paper are only for 18-kip single axle load conditions. Mixed traffic should be converted to equivalent 18-kip single axle loads when the ILLI-PAVE procedure is incorporated in a comprehensive design procedure.

ILLI-PAVE

In ILLI-PAVE *(1)* the pavement is considered an axisymmetric solid of revolution. Nonlinear, stress-dependent resilient modulus material models and failure criteria for granular materials and fine-grained soils *(1, 3, 4)* are incorporated in the ILLI-PAVE finite-element model. The principal stresses in the granular material and fine-grained soil layers are modified at the end of each iteration so that they do not exceed the strength of the materials as defined by the Mohr-Coulomb theory of failure.

Studies that compare measured and ILLI-PAVE-predicted load-deformation responses reported by Raad and Figueroa *(1)*, Suddath and Thompson *(5)*, Traylor *(6)*, Hoffman and Thompson *(7)*, Gomez and Thompson *(2)*, and Elliott and Thompson *(8)* yielded favorable results. The ILLI-PAVE approach has been successfully used in developing a flexible

highway pavement overlay design procedure based on nondestructive testing data analyses *(9)* as well as mechanistic thickness design procedures for secondary road flexible pavements *(10)* and soil-lime layers *(11)*. Gomez and Thompson *(2)* and Elliott and Thompson *(8)* successfully used ILLI-PAVE procedures to analyze the pavement responses and predict the performance of the AC + bituminous-treated granular base sections (the "Base Type Studies") and the Loop 4 flexible pavement sections of the AASHO Road Test.

The computational techniques of the ILLI-PAVE computer program (currently a main-frame computer is required) are too costly, complex, and cumbersome to be used for routine design. Simplified analysis algorithms that reliably predict ILLI-PAVE response solutions for full-depth asphalt concrete pavements have been developed *(2)* to incorporate ILLI-PAVE structural model concepts in a mechanistic design concept. The algorithms can be easily programmed for inexpensive calculator or personal computer applications.

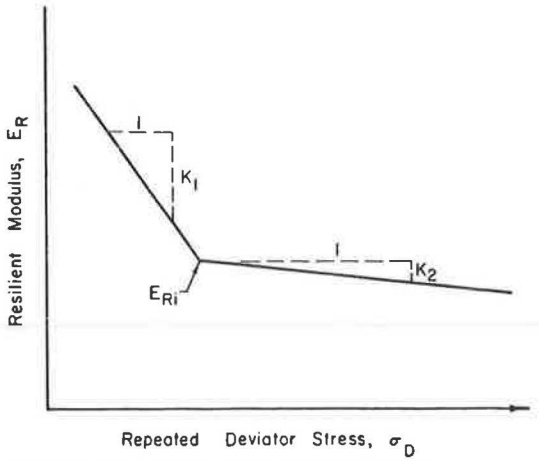

FIGURE 2 Arithmetic model for stress-dependent resilient behavior of fine-grained soils.

SOILS AND MATERIAL CHARACTERIZATION

General

The resilient behavior of a soil or material is an important property for pavement analysis and design. A commonly used measure of response is the resilient modulus defined by

$$E_R = \sigma_D/\varepsilon_r$$

where

E_R = resilient modulus,
σ_D = repeated deviator stress, and
ε_r = recoverable axial strain.

Repeated unconfined compression or triaxial testing procedures are often used to evaluate the resilient moduli of fine-grained soils and granular materials. Resilient moduli are stress dependent: fine-grained soils experience resilient modulus decreases with increasing stress, and granular materials stiffen with increasing stress level. Because unbound granular materials are not used in full-depth AC pavements, only fine-grained soils are further discussed.

Fine-Grained Soils

Two stress-dependent behavior models (arithmetic and semi-log) have been proposed for describing the stress softening behavior of fine-grained soils. The arithmetic model is shown in Figures 2 and 3. Extensive resilient laboratory testing, nondestructive pavement testing, and pavement analysis and design studies at the University of Illinois have indicated that the arithmetic model (Figure 2) is adequate for flexible pavement analysis and design activities.

In the arithmetic model, the value of the resilient modulus at the breakpoint in the bilinear curve (E_{Ri} in Figure 2), is a good indicator of a soil's resilient behavior. The slope values (K_1 and K_2) display less variability and influence pavement structural response to a smaller degree than E_{Ri}. Thompson and Robnett *(12)* simplified developed procedures for estimating the resilient behavior of fine-grained soils based on soil classification, soil properties, and moisture content.

Four fine-grained subgrade types (very soft, soft, medium, and stiff) are included in this study. Pertinent subgrade properties and characteristics are given in Table 1. Resilient modulus-repeated deviator stress level relations used in the ILLI-PAVE model are shown in Figure 4.

Asphalt Concrete

A constant linear resilient modulus is used to represent the AC layer. AC modulus-temperature relations must be considered in selecting modulus values. Procedures for establishing AC modulus-pavement temperature relations are presented in The Asphalt Institute *(13)* and SHELL *(14)* design procedures. The AC modulus values selected for this study are consistent with the range of AC moduli and temperatures expected to be encountered in Illinois. The modulus values and other properties used in the analyses are given in Table 1.

DEVELOPMENT OF DATA BASE

All ILLI-PAVE analyses were based on a 9,000-lb circular load (80-psi pressure) as a representation of one dual-wheel of the standard 18-kip (18,000-lb) single axle load. The ILLI-PAVE data base *(2)* included information for 96 pavement configurations. AC thicknesses were 4, 6, 9, 12, 15, and 16 in. These thicknesses are representative of a broad range of typical flexible pavement designs. Four levels of subgrade moduli/strength (stiff, medium, soft, and very soft) and four levels of AC modulus (2,000, 1,000, 500, and 200 ksi) were evaluated for each AC thickness. The ILLI-PAVE response data are presented elsewhere *(2)*.

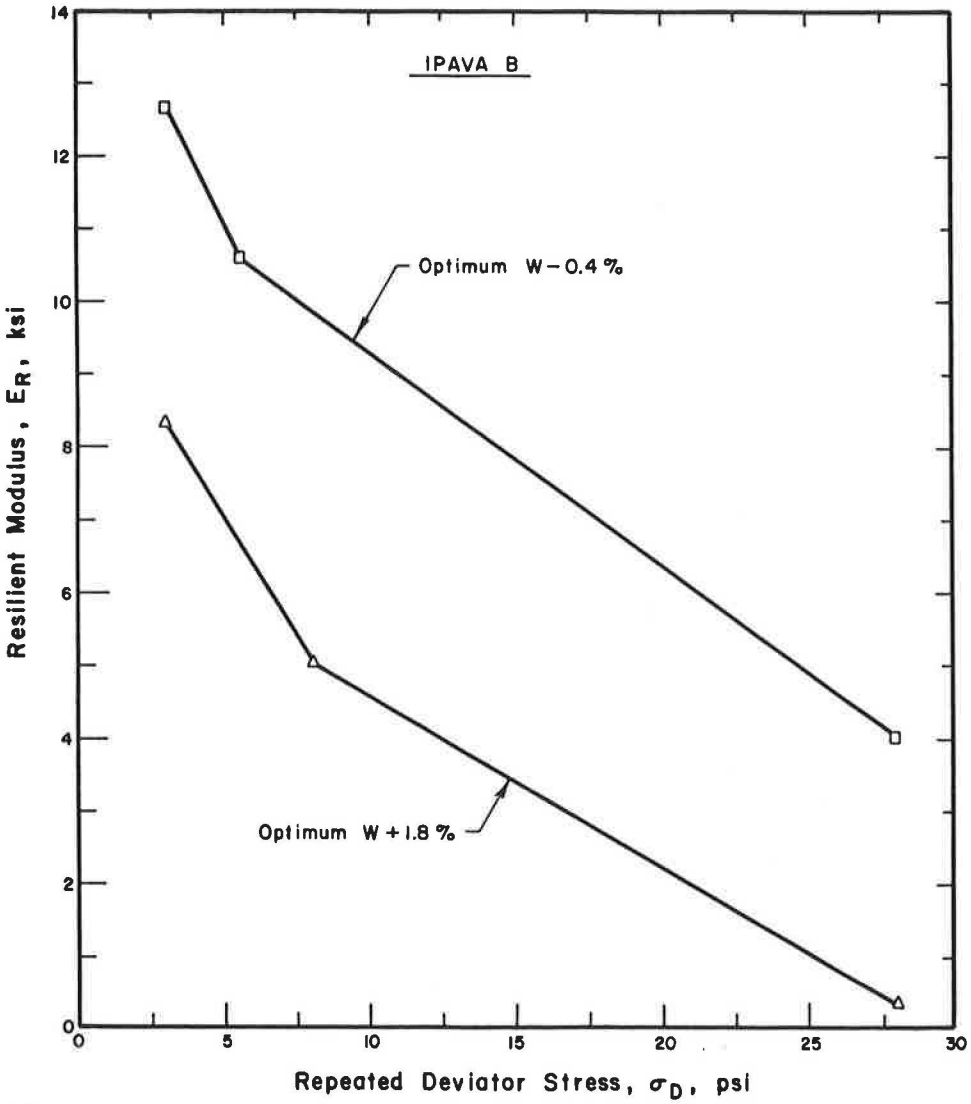

FIGURE 3 Typical stress-dependent resilient behavior of a fine-grained soil [AASHTO A-7-6(36)].

TABLE 1 ILLI-PAVE MATERIAL PROPERTIES

		ASPHALT CONCRETE				SUBGRADE			
	UNITS	VERY HARD	HARD	MEDIUM	LOW	STIFF	MEDIUM	SOFT	VERY SOFT
Unit Weight	psf	145.00	145.00	145.00	145.00	125.00	120.00	115.00	110.00
Lateral Pressure Coeff. at Rest		0.20	0.50	0.67	0.80	0.82	0.82	0.82	0.82
Poisson's Ratio		0.30	0.35	0.40	0.46	0.45	0.45	0.45	0.45
Unconfined Compress. Strength (qu)	psi					32.80	22.85	12.90	6.21
Deviator Stress:									
Upper Limit	psi					32.80	22.85	12.90	6.21
Lower Limit	psi					2.00	2.00	2.00	2.00
Resilient Modulus:									
E_{Ri}	ksi					12.34	7.68	3.02	1.00
E-failure	ksi					7.605	4.716	1.827	1.00
E-Const. Modulus	ksi	2000	1000	500	200				
Friction Angle	deg.					0.0	0.0	0.0	0.0
Cohesion	psi					16.40	11.425	6.45	3.105

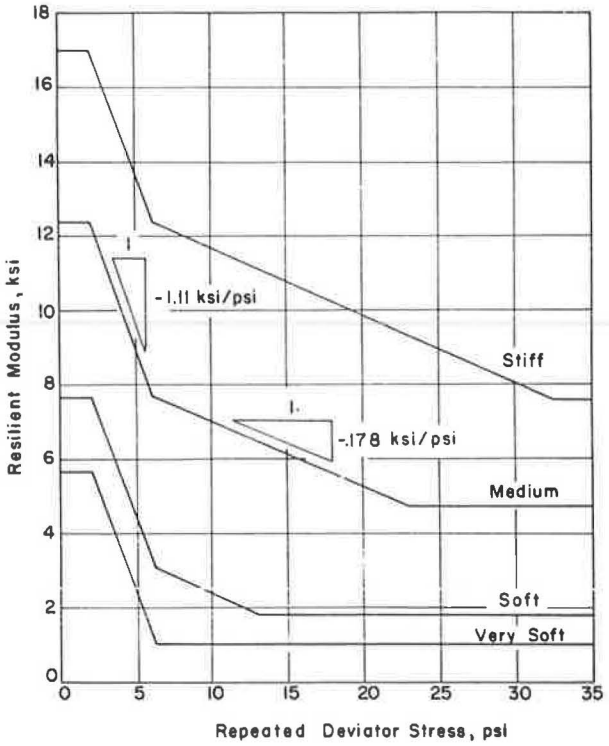

FIGURE 4 Resilient modulus-deviator stress relations for ILLI-PAVE subgrades.

DEVELOPMENT OF DESIGN ALGORITHM

The design algorithms were developed using the SPSS stepwise regression program *(15)*. The regression equation is developed in a series of steps by entering the independent (prediction parameters) variables one at a time. At each step the variable entered is the one that makes the greatest improvement in the prediction of the dependent variable (pavement response parameter). The pavement factors included in the analyses as independent variables were (*a*) AC thickness, (*b*) AC modulus, and (*c*) subgrade E_{Ri}.

Algorithms for predicting the following pavement responses were established.

1. AC radial strain at the bottom of the AC surface layer,
2. Subgrade deviator stress,
3. Surface deflection,
4. Subgrade deflection, and
5. Subgrade vertical strain.

These responses are those generally used in various transfer functions (Figure 1) that relate pavement response to pavement performance. Additional algorithms that relate AC radial strain and subgrade stress ratio (subgrade deviator stress/unconfined compressive strength) to surface deflection were also developed.

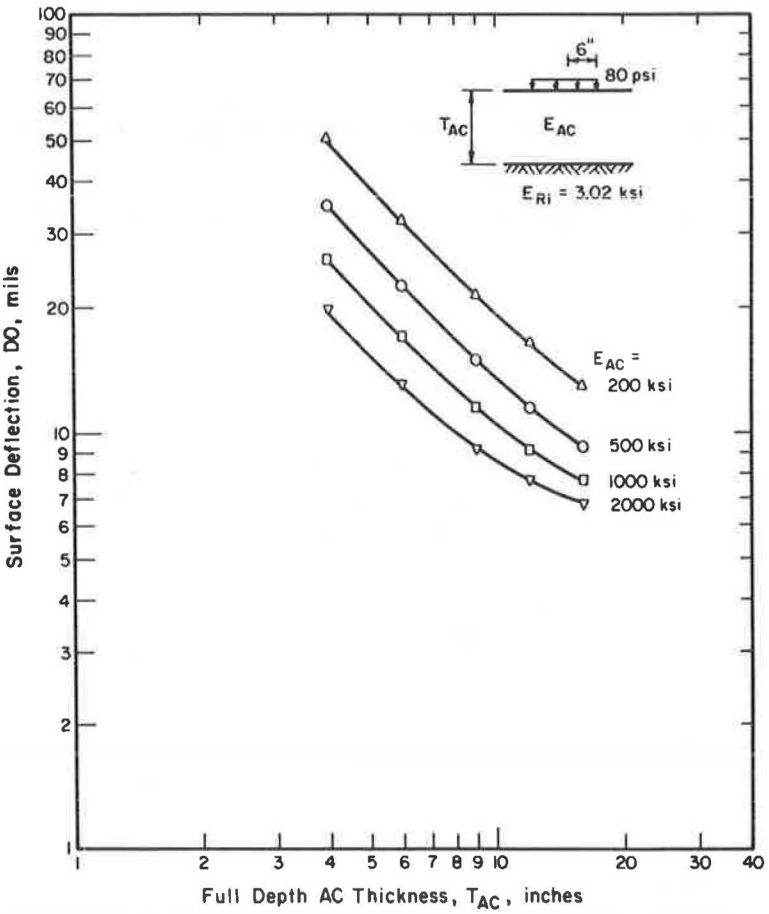

FIGURE 5 Relationship between surface deflection (at R = 0.0 from load) and thickness of the asphalt concrete (T_{AC}) for a soft subgrade.

Algorithms that relate to AC rutting were not developed. It is intended that rut development within the AC portion of the pavement system be controlled by the proper selection of materials, mix design, and construction control.

The algorithms for predicting ILLI-PAVE pavement structural responses are as follows.

Asphalt strain

$$\text{Log } \varepsilon_{AC} = 5.746 - 1.589 \text{ Log } T_{AC} - 0.774 \text{ Log } E_{AC} - 0.097 \text{ Log } E_{Ri}$$

$R^2 = 0.967$ SEE = 0.083

Subgrade deviator stress

$$\text{Log DEV} = 2.744 - 1.138 \text{ Log } T_{AC} - 0.515 \text{ Log } E_{AC} + 0.289 \text{ Log } E_{Ri}$$

$R^2 = 0.976$ SEE = 0.053

Surface deflection

$$\text{Log DO} = 3.135 - 0.895 \text{ Log } T_{AC} - 0.359 \text{ Log } E_{AC} - 0.287 \text{ Log } E_{Ri}$$

$R^2 = 0.984$ SEE = 0.033

Subgrade deflection

$$\text{Log DSUB} = 3.090 - 0.979 \text{ Log } T_{AC} - 0.321 \text{ Log } E_{AC} - 0.306 \text{ Log } E_{Ri}$$

$R^2 = 0.983$ SEE = 0.037

Subgrade vertical strain

$$\text{Log } \varepsilon_z = 4.022 - 1.680 \text{ Log } T_{AC} - 0.667 \text{ Log } E_{AC} - 0.165 \text{ Log } E_{Ri}$$

$R^2 = 0.944$ SEE = 0.110

Asphalt strain-surface deflection

$$\text{Log } \varepsilon_{AC} = 1.53 \text{ Log DO} + 0.319$$

Subgrade stress ratio-surface deflection

$$\text{Log S} = 1.28 \text{ Log DO} - 2.21$$

$R^2 = 0.81$ SEE = 0.08

where

T_{AC} = asphalt concrete thickness (in.),
E_{AC} = asphalt concrete modulus (ksi),

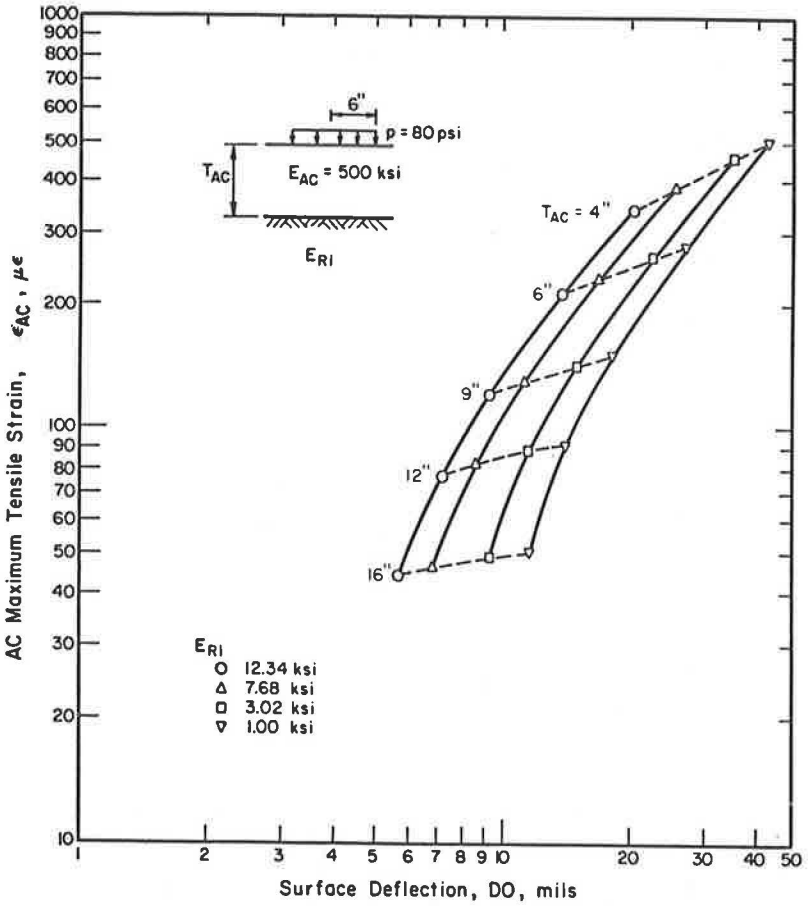

FIGURE 6 Relationship between maximum radial tensile strain at the bottom of AC and surface deflection for an AC modulus of 500 ksi.

E_{Ri} = subgrade modulus (see Figure 2) (ksi),
ε_{AC} = asphalt concrete radial tensile strain (microstrain),
DEV = subgrade deviator stress, $\sigma_1 - \sigma_3$ (psi),
DO = surface deflection (mils),
DSUB = subgrade deflection (mils),
ε_z = subgrade vertical strain ($\times 10^{-4}$),
S = subgrade stress ratio (subgrade deviator stress/unconfined compressive strength),
R^2 = coefficient of determination,
R = correlation coefficient, and
SEE = standard error of estimate.

The various statistical parameters show that the algorithms are excellent. Indeed, the standard error of estimate (SEE) is generally within the accuracy of the ILLI-PAVE model itself as determined by comparing the results of ILLI-PAVE analyses made using differing element mesh configurations.

The algorithms should not be used to solve for any of the independent variables. It might be tempting to use the surface deflection design algorithm as a pavement analysis tool to solve for or back-calculate the subgrade resilient modulus. The general practice of using regression equations in this manner is not correct and can lead to unnecessary errors. The appropriate approach is to develop separate regression equations using each desired "unknown" parameter as the dependent variable.

TYPICAL BEHAVIOR OF FULL-DEPTH AC PAVEMENT

Typical ILLI-PAVE outputs and relations are shown in the following figures:

Figure 5 shows the relationship between deflection at the surface (DO) and thickness of the asphalt concrete (T_{AC}) for a subgrade (E_{Ri}) of 3.02 ksi. There is a strong correlation between the deflection at the surface, the thickness of the asphalt concrete, and the resilient modulus of the subgrade. DO decreases with an increase in T_{AC} and E_{AC} for a given E_{Ri}.

Surface deflection (DO) is related to the maximum tensile strain at the bottom of the asphalt concrete (ε_{AC}). DO and ε_{AC} relations are shown in Figures 6 and 7. Figure 6 is for a constant modulus of asphalt concrete (E_{AC}), and Figure 7 is for a constant E_{Ri}.

Subgrade stress ratio (S), defined as the ratio of the deviator stress (σ_d) to the unconfined compressive strength (q_u) was also related to surface deflection (DO). Figure 8 shows such a relationship suggesting good correlation.

SUMMARY

ILLI-PAVE-based design algorithms for full-depth asphalt concrete flexible pavements are presented. The algorithms are

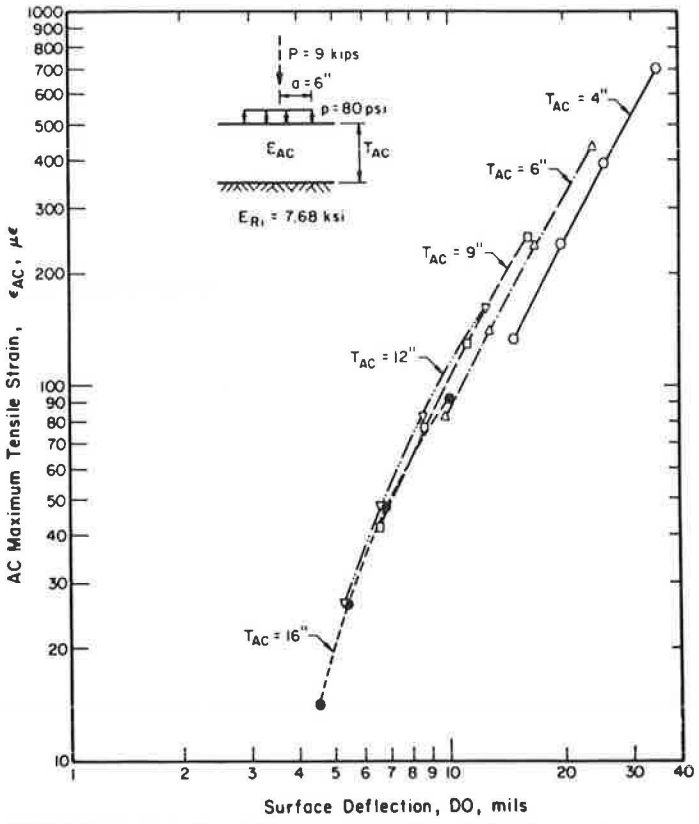

FIGURE 7 Relationship between surface deflection and the maximum radial tensile strain at bottom of AC for a medium subgrade (E_{AC} is variable from 200 to 2,000 ksi).

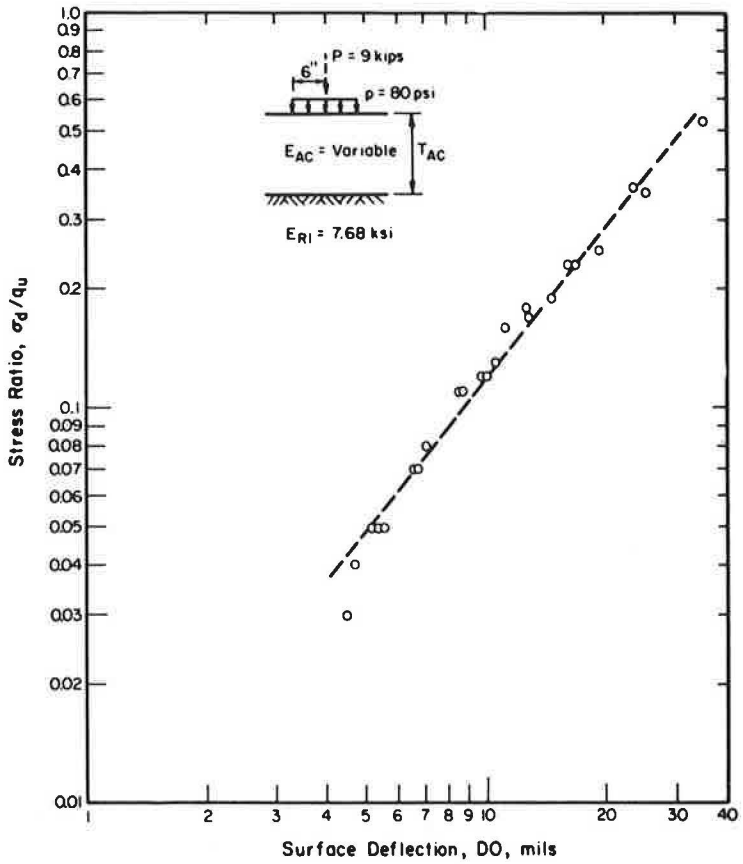

FIGURE 8 Variation of stress ratio as a function of surface deflection for a 7.68-ksi subgrade modulus.

sufficiently accurate for inclusion in mechanistic design procedures. Pertinent design algorithm inputs are AC thickness, AC modulus, and subgrade E_{Ri}. The algorithms should not be extrapolated beyond the range of variables considered in the ILLI-PAVE data base unless check runs are conducted with ILLI-PAVE to determine the validity of the algorithms in the area of extrapolation.

Factors that relate to climate, traffic, and transfer functions for local conditions must be appropriately evaluated and included in the development of a complete mechanistic-based design procedure.

ACKNOWLEDGMENT

This paper is based on the results of Project IHR–510—Mechanistic Evaluation of Illinois Flexible Pavement Design Procedures. IHR–510 was sponsored by the Division of Highways of the Illinois Department of Transportation and the Federal Highway Administration of the U.S. Department of Transportation.

REFERENCES

1. L. Raad and J. L. Figueroa. Load Response of Transportation Support Systems. *Transportation Engineering Journal of ASCE*, Vol. 106, No. TE1, Jan. 1980, pp. 111–130.
2. M. Gomez and M. R. Thompson. *Mechanistic Design Concepts for Full-Depth Asphalt Concrete Pavements.* Civil Engineering Studies, Transportation Engineering Series 41. University of Illinois at Urbana-Champaign, Aug. 1984.
3. J. L. Figueroa. *Resilient Based Flexible Pavement Design Procedures for Secondary Roads.* Ph.D. dissertation. Department of Civil Engineering, University of Illinois, Urbana, 1979.
4. M. S. Hoffman and M. R. Thompson. *Mechanistic Interpretation of Nondestructive Pavement Testing Deflections.* Civil Engineering Studies, Transportation Engineering Series 32. University of Illinois at Urbana-Champaign, June 1981.
5. L. P. Suddath and M. R. Thompson. *Load-Deflection Behavior of Lime-Stabilized Layers.* Technical Report M-118. U.S. Army Construction Engineering Research Laboratory, Champaign, Ill., 1975.
6. M. R. Traylor. *Nondestructive Testing of Flexible Pavements.* Ph.D. dissertation. Department of Civil Engineering, University of Illinois, Urbana, 1979.
7. M. S. Hoffman and M. R. Thompson. *Nondestructive Testing of Flexible Pavements—Field Testing Program Summary.* Civil Engineering Studies, Transportation Engineering Series 31. University of Illinois at Urbana-Champaign, June 1981.
8. R. P. Elliott and M. R. Thompson. *Mechanistic Design Concepts for Conventional Flexible Pavements.* Civil Engineering Studies, Transportation Engineering Series 42. University of Illinois at Urbana-Champaign, 1984.
9. M. R. Thompson. *Concepts for Developing a Nondestructive Based Asphalt Concrete Overlay Thickness Design Procedure.* Civil Engineering Studies, Transportation Engineering Series 34. University of Illinois at Urbana-Champaign, June 1982.
10. J. L. Figueroa and M. R. Thompson. Simplified Structural Analyses of Flexible Pavement for Secondary Roads Based on ILLI-PAVE. In *Transportation Research Record 766*, TRB, National Research Council, Washington, D.C., 1980, pp. 5–10.

11. M. R. Thompson and J. L. Figueroa. Mechanistic Thickness-Design Procedure for Soil-Lime Layers. In *Transportation Research Record 754*, TRB, National Research Council, Washington, D.C., 1980, pp. 32–36.
12. M. R. Thompson and Q. L. Robnett. Resilient Properties of Subgrade Soils. *Transportation Engineering Journal of ASCE*, Vol. 105, No. TE1, Jan. 1979, pp. 71–89.
13. *Research and Development of the Asphalt Institute's Thickness Design Manual (MS-1)*. 9th ed. Research Report 82-2. The Asphalt Institute, College Park, Md., 1982.
14. *Shell Pavement Design Manual*. Shell International Petroleum Company Limited, London, England, 1978.
15. *Statistical Package for Social Sciences*. 2nd ed. McGraw-Hill Book Company, New York, 1975.

Publication of this paper sponsored by Committee on Flexible Pavements.

Evaluation and Verification of the VESYS–3–A Structural Design System for Two Test Sites in Nebraska

ROY V. SNEDDON

VESYS–3–A, a mechanistic design system for asphalt pavements, was field verified for three pavement sections at two test sites in Nebraska. Predictions of present serviceability index (PSI) were in good agreement with field measurements for a 20-year-old three-layer pavement located near Elmwood, Nebraska. Field-measured PSI-values for an 8-in. full-depth pavement also agreed with predictions for the study period. Rut depth estimates from the model were small and were in general agreement with field measurements. Cracking estimates were poor and tended to underestimate the time required to develop observable fatigue cracking in the field. Asphalt, base course, and subgrade materials were tested in a 4.0-in.-diameter modified triaxial cell. Dynamic conditioning and rest periods were used to simulate service conditions. Indirect tensile tests of asphalt gave creep compliances and permanent strain parameters similar to those reported in the literature. Indirect tensile test fatigue characterization greatly underestimated pavement fatigue life compared with wheel-tracking test data and back-calculated AASHO Road Test data. Incremental creep tests of unbound materials tended to underestimate permanent strain parameters.

Research efforts in mechanistic design of asphalt concrete pavements have resulted in two computer simulation programs, the FHWA VESYS–3–A and an NCHRP program called PDMAP *(1)*. PDMAP does not appear to have found wide acceptance in either the academic community or at the state DOT level at this time (1985). These programs model the pavement structural system as either linearly elastic or linearly viscoelastic layers composed of materials that have probabilistic characterizations. Traffic volume can vary over time and axle load distributions within the traffic can be simulated. The effect of environmental changes is accounted for by defining temperature "seasons" during which material properties can be changed. The output of a typical pavement simulation run includes the following types of information: *(a)* stresses and strains in the pavement, *(b)* pavement deflections, *(c)* estimates of fatigue cracking, *(d)* rut depths, *(e)* roughness, and *(f)* present serviceability index (PSI).

Rationally, such software tools are attractive for pavement management, design, and rehabilitation. Their actual use in a state highway department or DOT, however, must await successful field testing and verification. Field verification of earlier versions of the VESYS model by the state of Utah and other agencies *(2-4)* has produced encouraging results.

In general, pavement materials have been characterized in accordance with methods described by Kenis *(5)* or ASTM *(6)*. The indirect tensile test *(7, 8)* of asphalt has been used in some cases and has the advantages of simplicity and ease of fabrication of test specimens.

The objectives of this study are *(a)* to report the results of

Department of Civil Engineering, University of Nebraska-Lincoln, Lincoln, Nebr. 68588-0531.

field verification of VESYS–3–A for three test sections located in east central Nebraska and *(b)* to describe methods of materials characterization using the indirect tensile test and the triaxial test both of which were performed wholly within a 4.0-in.-diameter triaxial cell.

FIELD VERIFICATION

Test Sections

Three test sections at two different sites were selected by the Nebraska Department of Roads for field verification of the predictive capabilities of VESYS–3–A using criteria developed by the state of Utah *(2)*. These two test sites contain pavement cross sections that are typical of much of the secondary road system in Nebraska. The 3.0-in. pavement section at Site 1 is of special interest because it is representative of thousands of miles of rural Nebraska pavements. Current AASHTO design procedures indicate that such thin sections should perform poorly; however, state experience indicates relatively good performance.

Site 1, called Elmwood-Manley, is a short spur that connects the town of Elmwood and NE–50. Site 2 is located on NE–14 north of Central City, Nebraska. The geographic locations of these sites are indicated by the circular insets in Figure 1.

Site 1 contains two pavement sections, a 3.0-in. section between Mileposts 3 and 7 and a 5.0-in. section between Mileposts 8 and 10. The surficial soil is typically Marshall silty clay loam, an AASHTO A–7–6 soil. These soils mantle the gently rolling farmland typical of this area except near a few creeks and ditches where the soils are of fairly recent alluvial origin. The subgrade is considered well drained and is probably not affected by the groundwater table. A considerable log of performance data is available for this site. Construction was completed in the fall of 1962.

Site 2 is a full-depth asphalt section 8.0 in. thick. The surficial soils are typically of the Lex series and represent poorly drained soils of the bottomland near the Platte River. Their AASHTO classifications are A–6 and A–7. Significantly fewer performance data are available for this site. The pavement was completed in the fall of 1975.

Model Calibration

Austin Research Engineers (ARE) *(9)* was able to develop a good fit between the pavement simulation and data for field performance of I–80N near Snowville, Utah *(2)*; however, asphalt and unbound material property data differed from the original laboratory data. These changes involved a 50 percent reduction in creep compliance in the asphalt as well as 20 percent reductions for the base course and subgrade. Back-calculated fatigue data based on the AASHO Road Test *(9)* replaced Utah's laboratory data. Finally, pavement temperatures were significantly higher than those based on mean ambient temperatures at Snowville corrected for the effect of pavement heating *(10, 11)*.

Pavement material properties determined using the procedures described in the section entitled Materials Characterization required some adjustment to achieve reasonable correlations with field performance. The permanent deformation variable (GNU) was increased to be consistent with values reported by others, and AASHO back-calculated fatigue factors (K_1 and K_2) were also used. To weight the effects of daytime traffic more heavily, mean monthly ambient temperatures were increased 10°F before pavement temperature was determined. A similar approach was used by Thower *(12)*. Early simulation runs predicted fatigue failures in the 3.0-in. pavement in 2 years, a time completely inconsistent with field experience. Therefore the ZCRACK depth was changed from 3.0 to 2.30 in. thus reducing the values of radial strain used in predicting fatigue failure. These adjustments were made to obtain good predictions of PSI and resulted in generally satisfactory performance of the model in predicting cracking and rut depth as described later. The final values for all input variables for each test section as they were input to the model can be found elsewhere *(13)*.

Results

PSI is the principal tool used in determining need for rehabilitation of asphalt pavements in Nebraska and thus the primary basis on which satisfactory model performance was judged. Pavement evaluations are principally based on road meter data

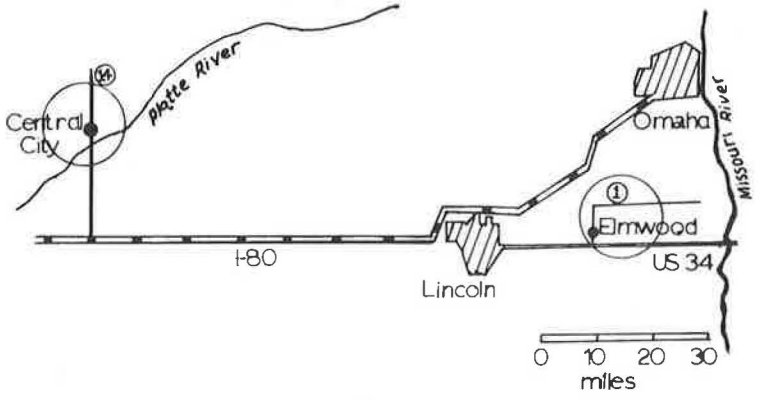

FIGURE 1 Location of test sections.

supplemented by rut depth measurements and crack surveys. Predicted PSI as a function of time is plotted for each test section in Figures 2–4. A band representing the 95 percent confidence level of the predictions is also shown as an aid to interpretation. Plotted on these same figures are mean PSI values based on field measurements. One standard deviation of the field data is plotted as a vertical line above and below a data point. Good correlation between the model and field data is indicated in all cases. The "kink" in the model prediction for Site 1, which occurs in 1974, corresponds to rapid increases in predicted fatigue cracking and appears to match field behavior.

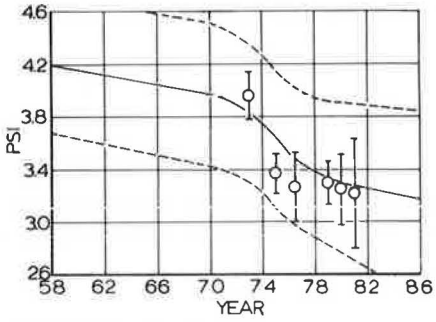

FIGURE 2 Predicted and measured PSI, Elmwood 3-in. section.

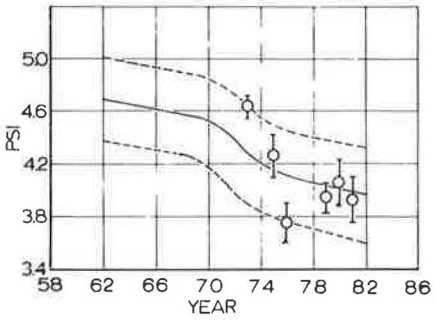

FIGURE 3 Predicted and measured PSI, Elmwood 5-in. section.

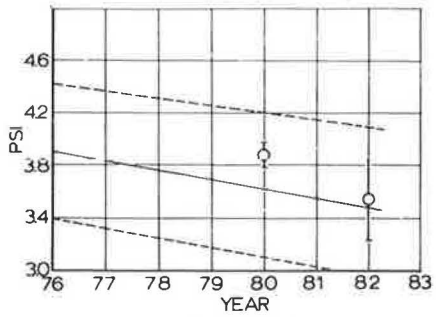

FIGURE 4 Predicted and measured PSI, Central City.

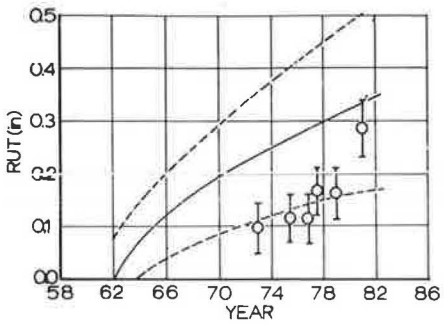

FIGURE 5 Predicted and measured rut depth, Elmwood 3-in. section.

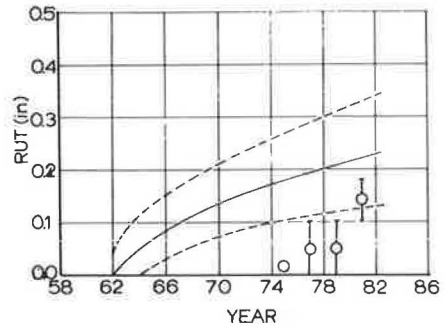

FIGURE 6 Predicted and measured rut depth, Elmwood 5-in. section.

Rut depth predictions are plotted in Figures 5–7 together with the 95 percent confidence level band. Measured rut depths and their standard deviations are plotted for comparison. The model generally overpredicts rut depth when input data are chosen to "best fit" PSI. It should be noted that, with the exception of data for Site 1 in 1981, rather crude techniques are used to measure rut depth. Because both the measured and the predicted rut depths are small, however, the model predictions are considered reasonable. It is possible to further improve the model's performance by slight adjustments of GNU and α, which control the accumulation of the plastic strain developed after each axle load.

Previous attempts at field verification of the predicted extent of fatigue cracking have generally been poor. The results shown plotted in Figures 8–10 are slightly better. Using ZCRACK = 2.30 improved the prediction for the 3.0-in. pavement at Site 1. The predicted values are reasonable; however, the 5.0-in. section is poor. No cracking is predicted by the model for Central City and very little was found; however, because only 7 years of simulation and field experience are involved at Central City, no definitive conclusion can be drawn.

Field cracking estimates are difficult to make. During site inspections many areas thought to be uncracked were found to be cracked when examined with a magnifying glass. Verification of cracking suffers from model, laboratory-testing, and field-measuring deficiencies. Laboratory testing exhibits the single greatest deficiency.

CHARACTERIZATION OF MATERIALS

Practical implementation of mechanistic design in a state DOT requires significant simplification and speedup of materials-testing procedures. The repeated load, indirect tensile test

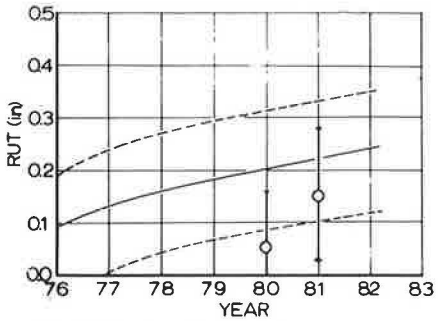

FIGURE 7 Predicted and measured rut depth, Central City.

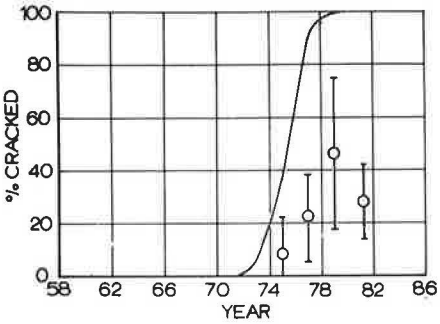

FIGURE 8 Predicted and measured cracking, Elmwood 3-in. section.

(7, 8, 14) using Marshall test specimens was selected for characterization of bituminous mixtures. It represents a good compromise between simplicity and incorporation of field loading conditions. Marshall samples were tested in a modified 4.0-in.-diameter triaxial cell that also acted as a temperature-controlled bath (±0.2°F) during testing. The 8.0-in. × 4.0-in.-diameter samples of the base course and subgrade were tested in the same cell. A pneumatic servo-controlled loading system was used for all materials testing *(13)*.

Pretest Dynamic Conditioning of Asphalt Samples

The use of static creep compliance data in field verification of VESYS has been questioned. Predicted field cracking and rutting are often much larger than predicted by the model *(2, 15)*. During sensitivity analysis ARE *(15)* suggested and

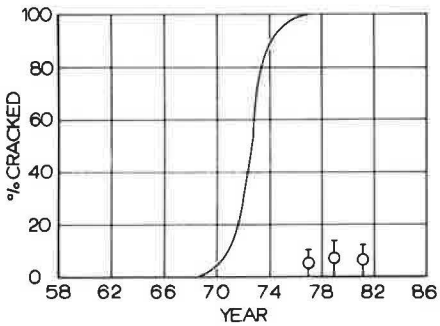

FIGURE 9 Predicted and measured cracking, Elmwood 5-in. section.

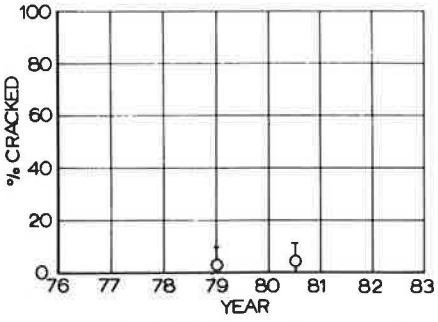

FIGURE 10 Predicted and measured cracking, Central City.

verified that dynamic conditioning before the static creep test would decrease creep compliance and thus improve these predictions. Furthermore, the inverse of creep compliance after conditioning was found to approximate the resilient modulus when the loading time was between 50 and 100 msec.

Another example of the need for conditioning is the test results from VESYS–3–A. Utah test data *(2)* for I–80N (Snowville) were used for initial familiarization runs with the model. Snowville climatological data for the study period were used to obtain pavement temperature estimates. Model predictions greatly overestimated measured rut depths and fatigue cracking. In a subsequent familiarization run, results were significantly improved when creep compliances of the asphalt were reduced 50 percent. ARE calibrations of VESYS–3 *(9)* produced good comparisons with field measurements. However, ARE departed significantly from the laboratory data reported by Utah as well as from Snowville climatological data. These results indicate the importance of conditioning when using laboratory test data as well as the potential of the model to predict field performance.

A conditioning effect was found for two Marshall specimens formed from Nebraska Type-B mix. The dynamic moduli for the two tests were 250,000 and 500,000 psi, an increase from 100,000 psi. The values of dynamic modulus for the conditioned specimens were consistent with values reported in the literature *(15)*.

Rest periods increase fatigue life up to a ratio of rest period to load duration of 10 *(16)*. Therefore the dynamic conditioning adopted for testing sought to incorporate this finding. The load duration used was 50 msec, which represents the integrated effects of truck speed and truck length. However, the respone of the pneumatic controller was such that the rest period-to-load duration ratio obtained experimentally was only 9. Typically, 15,000 cycles of haversine conditioning load with a 50-msec load duration and a 450-msec rest period were used.

Measurement of Creep Compliance

In a viscoelastic material at constant stress, strains increase over time at a decreasing rate. Therefore creep compliance can be considered the inverse of Young's modulus at various times of loading (t). Using this definition, creep compliance of a Marshall sample can be shown to be given by *(13)*

$$D(t) = C \cdot Y(t)/P \quad (1)$$

where

$Y(t)$ = vertical deformation at time t,
P = vertical load,
C = 0.693 when $\nu = 0.0$, and
C = 0.698 when $\nu = 0.5$.

Before they were tested all samples were sealed in microcrystalline wax to prevent climatic conditioning *(17)*. A sample was then conditioned with 15,000 cycles of 100-lb haversine loading at a temperature of 70°F. The sample was then held at a constant small seating load and brought to the final test temperature before creep compliance was measured. Samples were tested at 100°F, 70°F, and 50°F using 1,000-sec square-wave pulse loads of 33, 100, and 300 lb, respectively, in accordance with generally accepted procedures *(1, 6, 9)*.

Permanent Deformation Properties

An alternative to dynamic testing for the determination of permanent deformation properties *(5, 18–21)* is an incremental static creep test. The creep test procedure offers the potential for multiple tests on a single sample at different temperatures as well as reduced testing times; it was therefore used in this study.

Specimens were dynamically conditioned at 70°F before the incremental static creep test. After conditioning, samples were brought to the specified test temperature and a square-wave pulse was applied and held for 100 msec. The load was then removed and the permanent horizontal and vertical deformations were recorded after 2 min of rebound. This same process was repeated for load duration times of 1 sec and 10 sec. The 100-sec and 1,000-sec tests were given 4 min of rebound before the plastic deformation was recorded. Data from the incremental creep test were reduced in accordance with procedures given elsewhere *(13, 18, 19)*.

Fatigue Properties

Laboratory fatigue tests have been used to estimate the fatigue life of asphalt pavement in several studies *(2, 8, 15, 16)*. However, in general the predicted fatigue life greatly underestimates the measured field performance. Various reasons have been suggested for the observed differences [e.g., *(a)* failure to include the effect of rest periods *(16; 22,* p.176; *23)*; *(b)* lateral distributions of wheel loadings across the pavement *(16, 23, 24, 25)*; *(c)* inappropriate testing technique for the application such as controlled stress, controlled strain *(16)*; *(d)* time required for crack propagation *(26, 27)*; *(e)* temperature effects *(12, 16)*; and *(f)* convergence problems in the mathematical model *(28)*].

Wheel-loading tests *(25)* and a reevaluation of the AASHO Road Test fatigue data *(15, 29)* have also been used in drawing these conclusions. Finn *(30)* indicated that it was necessary to adjust laboratory constant strain fatigue data 10- to 13-fold to achieve correlation with AASHO Road Test fatigue data. Brown and Pell *(31)* suggest a fatigue design curve displaced from the laboratory curve that gives fatigue lives 20 times laboratory values determined from controlled stress tests.

Using Dijk's work *(16, 26)*, multipliers of fatigue life to account for these affects are rest periods (6 to 10X), lateral distribution of wheel loads (2.5X), and time required for crack propagation (3 to 5X). Therefore adjustments ranging from 45 to 125X are possible. Ullitdz *(27)* allowed a factor of 100 for the effect of rest periods and the time for crack propagation.

The samples used in fatigue tests were conditioned at the fatigue test temperature and at load levels that would have a neglible effect on expected fatigue life. However, the ratio of rest period to load duration was maintained at 9 as in creep testing. Response time of the loading system limited the maximum loads that could be applied in 50 msec for various load shapes. To obtain the maximum dynamic loads, square-wave loading was used rather than haversine loading. This difference in load mode should have a minimal effect on fatigue life.

Laboratory results from the indirect tensile test *(3, 8)* are typically expressed in terms of tensile strain at the center of the sample after 200 load cycles. In the fatigue test series, 200 cycles were counted after 15,000 cycles of conditioning load were applied. The tensile strain was estimated from the resilient modulus measured at 200 cycles using an assumed value of Poisson's ratio of 0.4 based on the work of Vila and Terrel *(17)*.

Simulation Requirements of Unbound Materials

The dynamic properties of unbound materials (i.e., base course and subgrade soil) used in a simulation of the as-built pavement system are influenced by the following factors: *(a)* thixotropy, *(b)* method of compaction, *(c)* confining pressure, *(d)* magnitude of applied stress difference, *(e)* long-term in situ unit weight and water content, *(f)* intrinsic properties such as granulometry and plasticity, and *(g)* as-constructed variability. Therefore, in developing methods for materials characterization, each factor should be considered in a rational way during sample preparation and testing.

Seed et al. *(32)* tested AASHO Road Test subgrade soils using field cores and laboratory-compacted samples. The effects of thixotropy were removed after 40,000 cycles of loading. Modulus of resilience also stabilized after 200 load repetitions and remained essentially constant up to 100,000 cycles of loading. Resilient moduli measured on field-compacted cores taken from untrafficked loops and laboratory kneading-compacted samples compared favorably. Samples from the trafficked loops also agreed well, but the resilient strains were less than for kneading-compacted samples.

Confining pressures within the pavement section are produced by superposition of the lateral components of overburden and axle loads. Typical triaxial confining pressures used are 3.0 psi for subgrade soil and 8 to 10 psi for base course materials *(2, 5)*.

The stress difference (deviator stress) produced by axle loads decreases with depth through the pavement section and depends to some degree on the stiffness of the overlying materials. A precise determination of the amount requires a com-

puter model of the pavement and the surface loading. This can be readily done using VESYS. However, typical values suggested are 20.0 psi for base course and 6.0 psi for subgrade soil.

Chu et al. *(33)* suggested allowing laboratory-prepared samples to come to equilibrium with a simulated in situ water table. This procedure reproduces normal ambient moisture conditions rather than the much more severe soaking or saturated conditions sometimes advocated.

Subgrade materials selected for testing should represent the range of possible plasticity and grain size distributions in the study area. This will provide a range of material responses and thus bound the simulation. Because VESYS requires the expected mean and variance of as-built material responses, Kenis *(5)* suggests building in variability during sample compaction.

Preparation, Conditioning, and Testing of Samples

Samples 8.0 × 4.0 in. in diameter were prepared by kneading compaction to moisture contents and dry unit weights representative of field-measured, as-constructed, dry unit weights and water contents and their standard deviations. Field water table conditions were produced in some of the samples tested following the procedure of Chu et al. *(33)*. The rest of the samples were tested in an as-compacted condition.

The effects of thixotropy were removed by conditioning all samples with 50,000 cycles of haversine stress equal to the test stresses given in Table 1. After conditioning, creep compliance was determined following the procedures suggested by Kenis *(5)*. An incremental static creep test *(5, 18)* was used to determine α and GNU, the permanent deformation properties.

TABLE 1 TRIAXIAL TEST STRESSES FOR UNBOUND MATERIALS

Sample Type	Confining Stress (psi)	Conditioning Stress (psi)	Stress Difference (psi)
Subgrade	3.0	6.0	6.0
Base course	10.0	20.0	20.0
	8.0	20.0	20.0

Test Results

Asphalt creep compliances for Elmwood and Central City together with those for AASHO Test Section 266 and I–80N in Utah are given in Table 2. The values of D(t) obtained for conditioned asphalt samples from Elmwood and Central City are quite similar to those found by others *(2, 14)*. However, the AASHO data were determined using dynamically conditioned triaxial samples. The Utah tests were on unconditioned samples using the indirect tensile test. Compliances for the unbound materials are quite similar in all cases.

Table 3 gives a comparison of α- and GNU-values determined in the study and those found by others. Test results for Elmwood using incremental creep tests on conditioned, indirect tensile samples compare well with those of the repeated load tests reported for tests when the number of cycles of loading is less than 100,000. The Brampton test for 300,000 to 700,000 cycles is significantly different. The increase in GNU and, to a lesser degree, in α is significant. This has been reported *(14)* and was the basis for adjusting these values by ARE. Increasing them alters the VESYS model response. Rut

TABLE 2 COMPARATIVE CREEP COMPLIANCES OF BOUND AND UNBOUND MATERIALS ($psi^{-1} \times 10^{-5}$)

Source	Load Duration (sec) 0.001	0.01	0.10	1.0	10.0	100.0
Asphalt						
AASHO No. 266	0.065	0.12	0.33	0.80	1.50	2.60
Utah I–80N	–	0.38	0.54	0.78	1.09	1.61
Elmwood	0.21	0.34	0.55	0.90	1.45	2.30
Central City	0.021	0.095	0.18	0.36	0.70	1.40
Subgrade and Base Course						
AASHO No. 266						
Base	–	3.30	–			
Subgrade	–	14.0	–			
Utah I–80N						
Base	–	13.7	–			
Subgrade	–	7.32	–			
Elmwood						
Base	–	3.60	–			
Subgrade	–	3.70	–			
Central City subgrade	–	3.03	–			

Note: Dashes = data not applicable.

TABLE 3 COMPARATIVE PERMANENT DEFORMATION PARAMETERS α AND GNU FOR BOUND AND UNBOUND MATERIALS

Source	Material	Test Type	α	GNU
Asphalt				
AASHO No. 266 *(15)*	Cores	RLT	0.67	0.16
Brampton *(15)*	–	RLT		
10,000–30,000 cycles			0.61	0.076
300,000–700,000 cycles			0.90	0.51
Utah I–80N *(2)*	6.5% asphalt/gravel	RLT	0.52	0.064
Elmwood	4% asphalt/gravel	IT–IC	0.576	0.048
Subgrade and Base Course				
AASHO No. 266 *(15)*	Base course	RLT	0.93	2.65
	Subgrade	RLT	0.63 to 1.0	<0.1
I–80N Utah *(2)*	Base course	RLT	0.743	0.065
	Subgrade	RLT	0.635	0.040
Elmwood	Base course	T–IC	0.593	0.0004
	Subgrade	T–IC	0.479	0.0031
Central City	Subgrade	T–IC	0.459	0.0026

Note: RLT = repeated load triaxial, IT–IC = indirect tensile incremental creep, T–IC = triaxial incremental creep, and dash = data not available.

depths increase during the early years, but the rate of increase is less at later times, which improves the model's long-term predictive capacity although short-term rut depths are overestimated. Short-term overestimates of rut depth are also shown in Figures 5–7. GNU-values for the unbound Elmwood and Central City base course and subgrades are approximately one order of magnitude too small. These samples were all dynamically conditioned before testing, which significantly reduces the incremental strains observed at load times less than 100 sec. This substantially decreases GNU because it is initial strain dependent.

Interpretation of the fatigue characterizations (K_1 and K_2) given in Table 4 is much less clear. The Elmwood data are similar to Pell's data for a rotating beam test. K_1 is much smaller than the back-calculated AASHO data that are considered to represent a low fatigue life mix. The wheel-tracking data that are thought to best represent actual field performance have large values of K_1. Strains in the Elmwood samples were estimated at 200 cycles using dynamic modulus values. This probably contributed to a substantial reduction in K_1. Adedimila and Kennedy *(8)* used static moduli in their fatigue strength characterizations based on indirect tensile tests. The effect of crack propagation time is only included in the wheel-tracking tests. In conclusion, present laboratory tests are indicative of mix quality but do not appear to provide reasonable parameters for the VESYS model.

CONCLUSIONS

VESYS–3–A predicted PSI in three pavements with good agreement between field-measured values and model predictions when the depth of cracking (ZCRACK) was reduced. A comparison of field-measured rut depths and the simulation from the model is reasonable. Rut depths estimated early in the pavement's life exceeded measured values. Fatigue-cracking estimates were in fair agreement with field data. However, the AASHO Road Test back-calculated values of K_1 and K_2 can be used on an interim basis for Nebraska Type-B mixes.

Ambient temperatures were increased 10°F before pavement temperatures were estimated in order to weight daylight traffic's contribution to pavement damage more heavily. The sensitivity of the model to pavement temperature suggests the need for a data base of pavement temperatures in Nebraska.

Although satisfactory model predictions resulted from using Nebraska's W–4 tables for the three test sites evaluated, these data should be improved. The VESYS–3–A damage models are extremely sensitive to the heavier axle loads in the traffic load distribution.

The materials characterized had creep compliances in agreement with values found in the literature. Plastic strain characterizations α and GNU were reasonable for the asphalt tested. The values of GNU were too small for the base course and subgrade soils tested. Dynamic conditioning possibly reduced the initial plastic strains thus decreasing GNU. Fatigue factor K_1 was somewhat smaller than expected, possibly because of the small strains computed when the dynamic modulus was used to estimate the strain after 200 load cycles. Wheel-tracking test data or AASHO-estimated fatigue values should be used in the VESYS–3–A model in the interim.

Characterization of Nebraska pavement materials requires additional research effort to enlarge the data base. α and GNU for unbound materials from incremental static creep tests require further evaluation to improve GNU data. Repeated-load creep tests may be required. The indirect tensile fatigue test is not expected to provide good VESYS–3–A input data but can be used rationally to improve mix design.

TABLE 4 COMPARATIVE FATIGUE VALUES (K_1 AND K_2) FOR DIFFERENT TESTING METHODS

Source	Material	Test Type	K_1 STRNCOEF	K_2 STRNEXP
Shell *(25)*	California medium crushed aggregate	WTT	8.8×10^{-4}	2.64
ARE *(15)*	AASHO Road Test	Back-calculation	6.18×10^{-13}	5.00
Washington	AC	BF	6.52×10^{-5}	2.50
Monismith in Adedimila and Kennedy *(8)*[a]	40–50 penetration asphalt/granite	BF	1.03×10^{-10}	4.01
Utah I–80N, Anderson et al. *(2)*	6.5% asphalt/gravel	IT	0.349	1.55
Pell *(8)*[b]	7.7% asphalt	RB	2.5×10^{-17}	5.8
ARE *(8)*[c]	6% asphalt	IT	9.3×10^{-11}	3.49
Elmwood	4% 100–120 penetration/gravel	IT	1.16×10^{-18}	5.81

Note: WTT = wheel tracking, BF = beam flexure, RB = rotating beam, and IT = indirect tensile.

[a]68°F.
[b]50°F.
[c]75°F.

ACKNOWLEDGMENT

This study has been made possible by a grant from the FHWA, U.S. Department of Transportation, and the Nebraska Department of Roads. The author is grateful to Donald Swing and Robert Wedner of the Department of Roads for their interest in and encouragement of the project. Personnel from the department provided all field measurements and site samples. The Engineering Research Center of the College of Engineering and the University of Nebraska Computer Network provided equipment and computational support for the project.

REFERENCES

1. F. N. Finn, W. J. Kenis, and H. A. Smith. Mechanistic Structural Subsystems for Asphalt Concrete Pavement Design and Management. In *Transportation Research Record 602*, TRB, National Research Council, Washington, D.C., 1977, pp. 17–23.
2. D. I. Anderson, D. E. Peterson, J. C. McBride, and L. W. Shepherd. *Field Verification and Implementation of the VESYS IIM Structural Subsystem in Utah*. Report FHWA–RD–78–510. FHWA, U.S. Department of Transportation, Feb. 1978.
3. J. Sharma, L. L. Smith, and B. E. Ruth. Implementation and Verification of Flexible Pavement Design Methodology. *Proc., 4th International Conference on Structural Design of Asphalt Pavements*, University of Michigan, Ann Arbor, 1977, pp. 175–185.
4. M. G. Sharma, W. J. Kenis, T. D. Larson, and W. L. Gramling. Evaluation of Flexible Pavement Design Methodology Based Upon Field Observations at PSU Test Track. *Proc., 4th International Conference on Structural Design of Asphalt Pavements*, University of Michigan, Ann Arbor, 1977, pp. 158–174.
5. W. J. Kenis. *Predictive Design Procedures, VESYS Users Manual—An interim Design Method for Flexible Pavements Using the VESYS Structural Subsystem*. Report FHWA–RD–77–154. FHWA, U.S. Department of Transportation, Jan. 1978, pp. 1–128.
6. *Test Procedures for Characterizing Dynamic Stress-Strain Properties of Pavement Materials*. ASTM Special Report 162. ASTM, Philadelphia, Pa., 1975, 140 pp.
7. G. Gonzalez, T. Kennedy, and J. Anagnos. *Evaluation of Resilient Elastic Characteristics of Asphalt Mixtures Using the Indirect Tensile Test*. Research Report 183–6. Center for Highway Research, The University of Texas at Austin, Nov. 1975.
8. A. S. Adedimila and T. W. Kennedy. *Fatigue and Resilient Characteristics of Asphalt Mixtures by Repeated-Load Indirect Tensile Test*. Research Report 183–5. Center for Highway Research, The University of Texas at Austin, Aug. 1975.
9. J. B. Rauhut and P. R. Jordahl. *Effects on Flexible Highways of Increased Legal Vehicle Weight Limits Using VESYS IIM*. Report FHWA–RD–77–116. FHWA, U.S. Department of Transportation, Jan. 1978.
10. A. L. Straub, H. N. Schenck, and F. E. Przybycun. Bituminous Pavement Temperatures Related to Climate. In *Highway Research Record 256*, HRB, National Research Council, Washington, D.C., 1968, pp. 53–77.
11. B. J. Kallas. Asphalt Pavement Temperatures. In *Highway Research Record 150*, HRB, National Research Council, Washington, D.C., 1956, pp. 1–11.
12. E. N. Thower. *A Parametric Study of a Fatigue Prediction Model for Bituminous Road Pavements*. Report 892. Transportation and Road Research Laboratory, Crowthorne, Berkshire, England, 1979.
13. R. V. Sneddon, *Evaluation and Verification of the VESYS–3–A Structural Design System for Two Test Sites in Nebraska*. Study 79–2. Nebraska Department of Roads, Lincoln, 1982, pp. 1–55.
14. K. Wallace and C. L. Monismith. Diametral Modulus Testing on Nonlinear Pavement Materials. *Proc., AAPT*, Vol. 44, 1980, pp. 633–649.
15. J. B. Rauhut, J. C. O'Quin, and W. R. Hudson. *Sensitivity Analysis of FHWA Structural Model VESYS II*. Report FHWA–RD–76–23. FHWA, U.S. Department of Transportation, Vol. 1, May 1976.
16. W. Van Dijk and W. Visser. The Energy Approach to Fatigue Design. *Proc., AAPT*, Vol. 46, 1977, pp. 1–37.
17. J. M. Villa and R. L. Terrel. Influence of Accelerated Climatic Conditioning on Split Tension Deformations of Asphalt Concrete. *Proc., AAPT*, Vol. 44, 1975, pp. 119–142.
18. J. S. Lai and W. L. Hufferd. Predicting Permanent Deformation of Asphalt Concrete from Creep Tests. In *Transportation Research Record 616*, TRB, National Research Council, Washington, D.C., 1976, pp. 41–43.
19. W. J. Kenis and M. G. Sharma. Rut Depth Procedures for Permanent Deformation in Asphalt Pavements. In *Transportation Research Record 616*, TRB, National Research Council, Washington, D.C., 1976, pp. 28–30.
20. S. R. Brown and M. S. Snaith. The Permanent Deformation Characteristics of a Dense Bitumen Macadam Subjected to Repeated Loading. *Proc., AAPT*, Vol. 43, 1974, pp. 224–252.
21. P. J. van de Loo. Practical Approach to the Prediction of Rutting in Asphalt Pavements: The Shell Method. In *Transportation Research Record 616*, TRB, National Research Council, Washington, D.C., 1976, pp. 15–21.
22. B. E. Ruth and G. K. Olson. Creep Effects on Fatigue Testing of Asphalt Concrete. *Proc., AAPT*, Vol. 46, 1977.

23. L. Francken. Fatigue Performance of a Bituminous Road Mix Under Realistic Test Conditions. In *Transportation Research Record 712*, TRB, National Research Council, Washington, D.C., 1979, pp. 30–37.
24. J. Verstraeten, J. E. Romain, and V. Ververka. The Belgian Road Test Road Research Center's Overall Approach to Asphalt Pavement Structural Design. *Proc., 4th International Conference on Structural Design of Asphalt Pavements,* University of Michigan, Ann Arbor, 1977, pp. 298–324.
25. A. I. M. Classen, J. M. Edwards, P. Sommer, and P. Uge. Asphalt Pavement Design: The Shell Method. *Proc., 4th International Conference on Structural Design of Asphalt Pavements*, University of Michigan, Ann Arbor, 1977, pp. 39–74.
26. W. Van Dijk. Practical Fatigue Characterizations of Bituminous Mixes. *Proc., AAPT,* Vol. 44, 1975, pp. 38–68.
27. P. Ullitdz. A Fundamental Method for Prediction of Roughness and Cracking of Pavements. *Proc., AAPT,* Vol. 48, 1979, pp. 557–586.
28. J. B. Rauhut, W. J. Kenis, and W. R. Hudson. Improved Techniques for Prediction of Fatigue Life for Asphalt Concrete Pavements. In *Transportation Research Record 602*, TRB, National Research Council, Washington, D.C., 1976, pp. 27–32.
29. R. I. Kingham. Failure Criteria Developed from AASHO Road Test Data. *Proc., 3rd International Conference on the Structural Design of Asphalt Pavements,* London, England, Vol. 1, 1972, pp. 656–669.
30. F. N. Finn. Discussion of the Energy Approach to Fatigue Design by W. Van Dijk and W. Visser (*Proc., AAPT*, Vol. 46, 1977, pp. 1–37). *Proc., AAPT,* Vol. 46, 1977, p. 38.
31. F. S. Brown and P. S. Pell. A Fundamental Structural Design Procedure for Flexible Pavements. *Proc., 3rd International Conference on the Structural Design of Asphalt Pavements,* London, England, Vol. 1, 1972, pp. 369–381.
32. H. B. Seed, C. K. Chan, and C. E. Lee. Resilience Characteristics of Subgrade Soils and Their Relation to Fatigue Failures in Asphalt Pavements, *Proc., 1st International Conference on Structural Design of Asphalt Pavements,* University of Michigan, Ann Arbor, Vol. 1, 1962, pp. 611–636.
33. T. Y. Chu, W. K. Humphries, and S. N. Chen. A Study of Subgrade Moisture Conditions in Connection with Design of Flexible Pavement Structures. *Proc., 3rd International Conference on Structural Design of Flexible Pavement Structures,* London, England, Vol. 1, 1972, pp. 53–66.

Publication of this paper sponsored by Committee on Flexible Pavements.

Thickness Design for Flexible Pavement: A Probabilistic Approach

K. P. GEORGE AND S. HUSAIN

The thickness design procedure presented in this paper makes use of the concepts of limiting subgrade strain to control permanent deformation and limiting tensile strain in the asphalt layer (or limiting tensile stress in the cement-treated layer, if applicable) to control fatigue cracking. The input variables such as traffic load, ambient temperature, and subgrade resilient modulus are considered stochastic. The design nomographs incorporate reliability in design (50, 65, 80, and 95 percent), which is a unique feature of the method adopted here. Design nomographs are prepared for structural sections that consist of an asphalt concrete surface and a base of the designer's choice (asphalt treated, dense-graded aggregate, or cement treated) placed directly on the subgrade. A rational method for selecting asphalt grade is an integral part of the design procedure. The asphalt selection criteria dictate the use of relatively low-stiffness bituminous mixtures in cold climates and high-stiffness mixtures in hot climates. The region-to-region modulus variation, however, is accounted for by the judicious use of a multiplying factor that would transform the nomograph thickness to the "true" design value. To assess the reasonableness of the proposed procedure, the design thickness has been compared with that of the revised AASHO guide and with the Thickness Design Manual (MS–1) of the Asphalt Institute.

Department of Civil Engineering, The University of Mississippi, University, Miss. 38677.

The concept of structural design of asphalt pavements that employs mechanistic models and uses the fundamental properties of the pavement materials is no longer new to pavement technologists. The mechanistic concept of pavement analysis has become a powerful tool for researchers and is being increasingly recognized by design engineers as well.

Fatigue cracking and subsequent loss of performance, permanent deformation, and low-temperature cracking in pavement systems are topics of major concern. Fatigue cracking in asphaltic or granular-base pavement is attributed to the development of tensile strains that, when repeatedly applied,

cause distress that is manifested by cracks. Fatigue cracking in pavements with a cement-treated base is due to either excessive tensile stress in the base layer or tensile strain in the asphaltic surface. However, rutting results from excessive vertical strains at the subgrade level and plastic deformation in pavement layers whereas low-temperature cracking is the result of the stiffening effect on the asphaltic surface. The magnitude of these responses (stresses and strains) is influenced by vehicular load and environmental conditions. Although these and other causal factors are stochastic in nature, only a few studies *(1-3)* in the last few years have dealt with the problem of pavement analysis and design from a probabilistic point of view. None of the studies, however, has produced design curves or nomographs that incorporate reliability in design. The recently published Asphalt Institute manual *(4)* incorporates the mechanistic approach as well as other currently acceptable research. The stochastic nature of the design factors, however, has not been fully implemented in the design. The manual simply recommends the use of percentile values in selecting the design subgrade resilient modulus.

A complete set of design curves must include pavements that incorporate a minimum of three types of bases: asphalt-treated base (ATB), conventional or dense-graded granular (aggregate) base (DGA), and stabilized base such as cement-treated base (CTB). That the cement-treated base is not included in the design charts is considered to be a drawback of the Asphalt Institute manual *(4)*.

The goal of this study is to develop a probability-based design algorithm that accounts for inherent uncertainties in the design parameters. Traffic load, temperature, and subgrade support (moduli) value are the main parameters that exhibit randomness. The analysis also accounts for uncertainty associated with application of the Palmgren-Miner (PM) rule *(5)*. Employing the probabilistic algorithm the researchers have prepared a set of design charts that incorporate a range of reliability levels for three types of bases: asphalt-treated base, dense-graded aggregate, and cement-treated base. The design curves are made versatile by including asphalt selection criteria proposed by Basma and George *(6)*.

PROBABILISTIC STRUCTURAL MODEL

A simplified structural design entails three basic variables: subgrade support, expressed in terms of resilient modulus; traffic applications or life; and thickness of the pavement structure. The design approach proposed herein attempts to predict the thickness of the pavement, given the other two inputs. A combination of mechanistic and empirical procedures is used in developing the design model. It consists, primarily, of three interactive submodels: *(a)* primary structural response model, *(b)* life prediction model, and *(c)* cumulative damage model.

Primary Response Model

The primary response model, employing the BISAR program, determines such response variables as stress, strain, and deflection at prescribed positions of the pavement, which, in turn, is modeled as a layered elastic system. Wheel loads, ambient temperature (which influences the stiffness modulus of asphalt concrete), subgrade resilient modulus, and structural number (SN) (as defined by the AASHO Road Test) are the parameters considered to have the most influence on the response variables and, in turn, pavement life. In formulating the model, therefore, a complete factorial experiment is designed, a partial listing of which is given in Figure 1. The formulation in the ensuing sections is similar to that of George and Nair *(1)*. The design factors include structural number (SN), modulus of resilience (M_r), air temperature (T), and wheel loads (L). The dimensions of the factorial designs are $5 \times 3 \times 12 \times 5$; that is, 5 levels of SN exist in combination with 3 levels of subgrade modulus value, and each of these 15 combinations is analyzed for 12 levels of air temperature; finally, each of these 80 combinations is subjected to 5 levels of wheel load. Tire pressures are varied with wheel loads: 9,000-lb (40-kN), 8,000-lb (36-kN), and 6,000-lb (27-kN) dual wheel loads with 80 psi (552 kPa) and the remaining loads, 4,000-lb (18-kN) and 2,000-lb (9-kN) single wheel, are at 70 and 30 psi (482 and 207 kPa), respectively.

The layer thickness (derived from SN), subgrade resilient

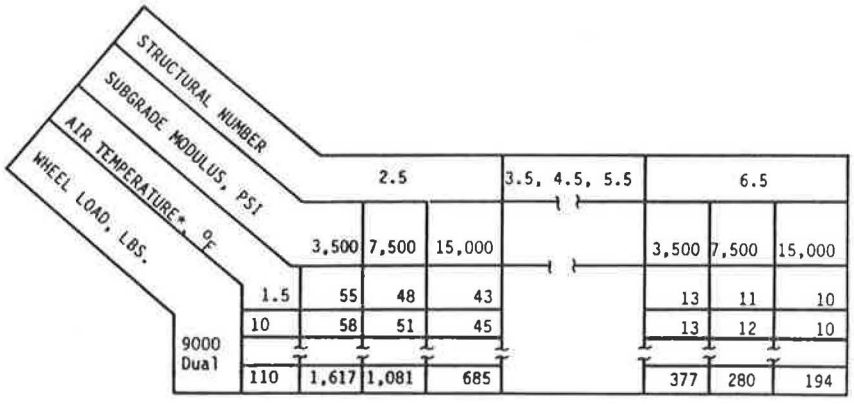

* 1.5 °F, 10 °F to 110 °F in steps of 10°
1 lb = 4.448 N
1 psi = 6.895 kPa

FIGURE 1 Primary response (tensile strain in base layer in microstrains) of a few designs for 9,000-lb (40-kN) dual wheel load, complete design includes 8,000-lb (36-kN) and 6,000-lb (27-kN) dual wheel and 4,000-lb (18-kN) and 2,000-lb (9-kN) single wheel.

modulus, and wheel loads are direct inputs into the BISAR program. Temperature enters into the analysis as it affects the stress-strain response of bituminous concrete in the surface layer and in the base layer, when applicable. The temperature-dependent moduli are derived in two steps as described herein. First, the temperatures of both layers in the model are estimated from the air temperature employing the following empirical relationship *(7)*:

Layer 1

$$T_p = T_a [1 + (3/h_1 + 12)] - (102/h_1 + 12) + 6$$

Layer 2

$$T_p = T_a [1 + (3/3h_1 + h_2 + 12)] - (102/3h_1 + h_2 + 12) + 6 \quad (1)$$

where

T_p = pavement temperature;
T_a = air temperature; and
h_1, h_2 = thickness of surface layer, base layer.

Second, the layer temperature determined in Equation 1, in conjunction with the temperature-modulus relationship for asphalt concrete, as graphed in Figure 2, determines the moduli of the layers at the specified T_a. Poisson's ratio is assumed to be 0.3, 0.35 (or 0.25 for CTB), and 0.45 for surface, base, and subgrade, respectively.

Life Prediction Models

As discussed in the previous section, the pavement response variables are computed by the BISAR program whereas pavement lives, determined by design criteria, are estimated by employing empirical relationships.

The design criteria to be used in computing design life are an important consideration. In this research, wheel loads are deemed to produce two strains and a stress that are believed critical for design purposes:

1. The horizontal tensile strain (ε_t) on the underside of the lowest bituminous layer,
2. The vertical compressive strain (ε_c) at the top of the subgrade layer, and
3. The horizontal tensile stress (σ_t) on the underside of CTB only.

If the horizontal tensile strain or the horizontal tensile stress in CTB, if applicable, is excessive, fatigue cracking of the corresponding layer will result. If the vertical compressive strain is excessive, permanent deformation will result, causing, in turn, rutting of the surface.

There is general agreement among researchers about the determinants of fatigue cracking in asphalt concrete pavements. The cycles to fatigue failure are largely dependent on the maximum tensile strain that is repeatedly experienced by the asphalt concrete layer and other secondary factors such as mix stiffness. For this study, the cycles to failure are postulated to be of the following form, as proposed by Finn et al. *(9)*.

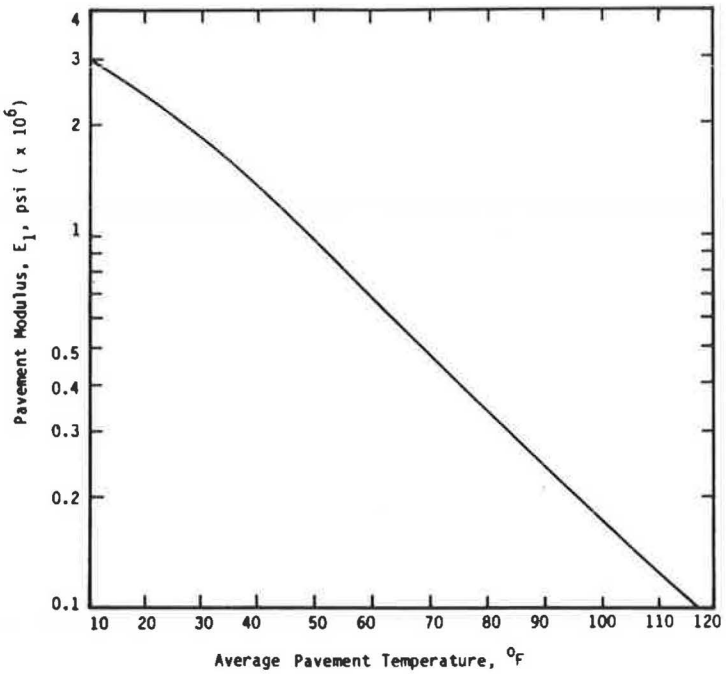

1 psi = 6.894 kPa
°F = 1.8°C + 32

FIGURE 2 Modulus-temperature relationship of asphalt concrete *(8)*.

Equation 2 was derived allowing for 45 percent fatigue cracking in the wheel paths.

$$N_f = 18.4(C) \times 4.325 \times 10^{-3} (\varepsilon_t)^{-3.29} (|E^*|)^{-0.854} \quad (2)$$

where

N_f = number of 18-kip (80-kN) equivalent single axle loads (ESALs) before (fatigue) failure occurs,
ε_t = tensile strain in asphalt layer (in./in. or mm/mm),
$|E^*|$ = asphalt mixture stiffness modulus (psi or kPa), and
C = function of air voids (V_v) and asphalt volume (V_b).

Like the fatigue life equation, the vertical compressive strain criterion is related to number of load applications by an equation of the form

$$N_f = a\,(1/\varepsilon_c)^b \quad (3)$$

where ε_c is the vertical compressive strain in μ in./in. (μ mm/mm) at subgrade surface and a, b are fitting coefficients; a = 3.0212×10^{15} and b = 3.571, respectively, as proposed by Brown *(10)*.

A tensile stress criterion for cement-treated base is believed to be relevant and preferred to the tensile strain criterion. This conclusion is reached after an in-depth study of the two criteria and after confirmation that the strain criterion is highly conservative in that it predicts significantly shorter life for CTB *(11)*. The fatigue equation that follows is attributable to Scott *(12)*:

$$\sigma_t = 94.4 - 4.71 \log N_f \quad (4)$$

where σ_t is the initial flexural stress.

The life (N_f) of the 900 pavement models is calculated by employing either Equation 2 or Equation 3 for ATB and DGA pavements and Equation 2, 3, or 4 for CTB pavement. In each case, two or three lives, as applicable, are obtained, one for each critical response value; the smallest of the two or three is used in subsequent calculations. With N_f as the dependent variable and L, T, M_r, and SN of Table 1 as independent variables, multiple regression models are formulated: for brevity, only one equation for ATB is included here:

$$N_f = 24144.210\, SN^{-3.803} L^{24.137}\, T^{-2.372} \exp(0.279SN) \exp(12.600\, L - 1128\, L^2 + 0.041\, L^3) \exp[1422\,(\ln T)^2 - 0.270\,(\ln T)^3] \exp[-2.270 \cdot 10^{-9} M_r^2 + 5.048 \cdot 10^{-13} M_r^2 T^2 + 0.037(\ln M_r L)^2] \quad (5)$$

where

L = wheel load in kips (4.448 kN),
T = temperature in degrees Fahrenheit (32 + 1.8°C), and
M_r = subgrade resilient modulus in psi (6.895 kPa).

Cumulative Damage Model

Employing the functional relationship among N_f and L, T, M_r, and SN and the joint probability density function of random variables L, T, and M_r [$f_{L,T,M_r}(l,t,m)$], expectation of $1/N_f$ is, by definition,

$$E[1/N_f] = \int \int_{-\infty}^{\infty} \int \{1/[N_f(L,T,M_r,SN)]\} f_{(L,T,M_r)}(l,t,m)\, dl\, dt\, dm \quad (6)$$

where E [ ] stands for the expected value (mean) of the random variable.

According to the PM rule, if N_f is deterministic, $1/N_f$ represents the "unit damage." Expected value of $1/N_f$ is simply the unit damage induced in a pavement of average structural number by a single load application of mean magnitude at average conditions of temperature and subgrade support.

The most widely used failure criterion of variable-stress fatigue is the Palmgren-Miner hypothesis of linear damage accumulation. As indicated before, both fatigue and rutting are considered to be potential distresses that detract from serviceability. For want of a better model, the PM rule is presumed to govern the accumulated rutting damage also. The cumulative damage (Δ), in accordance with the PM hypothesis, is

$$\Delta = \sum_k \sum_j \sum_i (n_{ijk}/N_{f\,ijk}) \quad (7)$$

TABLE 1 DESIGN PARAMETERS

Design Factor	Probability Distribution Chart	Parameters of Probability Distribution
Critical damage (D)	Lognormal	$\mu_D = 1.0$; $C_D = 0.5$
Cumulative damage, (Δ)	Lognormal	μ_Δ = 1.00, 0.80, 0.56 and 0.40 from Figure 3; $C_\Delta = 0.67$
Traffic	Shifted exponential (Figure 4)	$\lambda = 0.45$ kip^{-1}, $l = 1.0$
Air temperature	Two-parameter Weibull (Figure 5)	Characteristic value = 70°F, slope = 3.5
Subgrade modulus	Lognormal	μ_{M_r} = 3,000, 100,000, 20,000, and 30,000 psi; $C_{M_r} = 0.2$

Note: 1 kip = 4,448 kN, 1°F = 1.8°C + 32, and 1 psi = 6.895 kPa.

where

Δ = cumulative fatigue damage;
n_{ijk} = the predicted number of applications of strain range ε_{ijk} (stress range σ_{ijk}, if applicable);
N_f = number of load applications (before failure) of strain range ε_{ijk} (stress range σ_{ijk}, if applicable); and
i, j, and k = discrete values of load (L), temperature (T), and subgrade resilient modulus (M_r), respectively.

Because ε or σ, if applicable, is a continuous variable, the expression for damage can be expressed in an integral form. The expected number of load cycles [$n(\varepsilon)$] in the load range (l, $l + \Delta l$) applied when the pavement temperature is in the range (t, t + Δt) and subgrade resilient modulus in the interval (m, m + Δm) can be expressed as

$$n(\varepsilon) = N'_f f_{L,T,M_r} (l,t,m)\, \Delta l\, \Delta t\, \Delta m \quad (8)$$

where N'_f is the expected number of mixed traffic load cycles before failure. Assuming probabilistic independence among L, T, and M_r, Equation 8 can be rearranged, and, when substituted in Equation 7, an expression for expected cumulative damage (μ_Δ) will result:

$$\mu_\Delta = N'_f f_L(l)\, f_t(t) f_{M_r}(m) dl\, dt\, dm / N_f(L,T,M_r,SN) \quad (9)$$

It is instructive to rewrite Equation 9 in the following manner:

$$\mu_\Delta = N'_f f(SN)\, E_{M_r}\left(E_T\left\{E_L\left[1/N_f(L,T,M_r)\right]\right\}\right)$$

$$= N'_f f(SN)\, E(1/N_f) \quad (10)$$

where f(SN) is a function of SN.

For a given pavement of known structural number, Equation 10 provides for the expected value of cumulative damage as a product of the expected value of damage for a single load cycle, referred to as "unit damage" and the expected number of load applications for failure.

Reliability-Based Design

By using Equation 9, expected cumulative damage (μ_Δ) can be solved, provided that the probability density functions of random variables L, T, and M_r are known. Because of the uncertainties in predicting fatigue damage, fatigue life can be estimated with only a certain reliability (confidence) level. For example, a fatigue life estimated with a reliability level of 95 percent implies that there is at least a 95 percent chance that the pavement will not show the specified amount of fatigue cracking before it reaches its estimated fatigue life.

Before a reliability level can be specified, the probability distribution of Δ needs to be known. Significant experimental evidence has been presented in the literature that indicates that the distribution of fatigue lives at a particular stress level is lognormal *(13, 14)*. If N_f is a random variable lognormally distributed by virtue of Equation 7, Δ is also lognormally distributed, $\Delta = LN(\mu_\Delta, \sigma_\Delta)$.

As has been demonstrated experimentally by many investigators, the critical damage at failure (D) is not always close to 1.00 but assumes a wide distribution of values *(15)*. For many materials, this variation appears to follow lognormal distribution, $D = LN(\mu_D, \sigma_D)$. Because both Δ and D are random variables, reliability (R) can be defined as the event ($\Delta < D$). That is,

$$R = P(\Delta < D) \quad (11)$$

A closed-form expression of μ_Δ in terms of C_Δ and R is given herein. Various stops of its derivation can be seen elsewhere *(1)*.

$$\mu\Delta = \exp\{(1/2)\, ln(1 + C_\Delta^2) - 0.1116 - \phi^{-1}(R)\,[ln(1 + C_\Delta^2) + 0.2231]^{1/2}\} \quad (12)$$

where ϕ is the standard normal variate.

A graphic representation of Equation 12 is shown in Figure 3. Equation 12, in conjunction with Equation 9, renders an explicit solution for the fatigue life (N) of a pavement of given SN; these steps constitute a pavement analysis. Alternatively, a design will entail solving the two equations for SN.

Probability Density Functions for Input Variables

Solving for Equation 9 requires probability distribution functions for wheel load, ambient temperature, and subgrade mod-

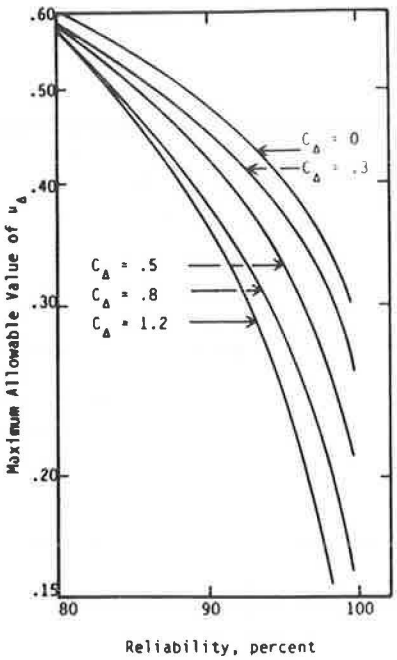

FIGURE 3 Maximum allowable μ_Δ as a function of R and C_Δ; μ_D = 1, C_D = 0.5 *(1)*.

ulus. The development of appropriate probability distributions may vary somewhat, depending on availability of data. The authors, however, outline what they believe to be a viable approach.

The wheel load distribution is derived using the Mississippi truck weight data of 1977 and 1980. Passenger cars are excluded from the data. The cumulative truck weight data, along with the "best fit" cumulative distribution function, are shown in Figure 4. A shifted exponential distribution fits the data best with $\lambda = 0.45$ kip^{-1}.

The temperature distribution is obtained from the daily temperature of a station located in University (northern Mississippi), which is considered to have temperatures representative of the southeastern United States. The 2-year data showed a tendency toward air temperature distributed according to a two-parameter Weibull distribution with characteristic value and slope of distribution of 70°F and 3.5, respectively (Figure 5).

The wide fluctuation of the subgrade moduli, for such reasons as temperature or moisture changes or both, must be accounted for by prescribing a probability density function. The subgrade support value data of the AASHO Road Test, when plotted on an annual basis, give rise to a lognormal distribution *(1)*. In view of the direct relationship between subgrade support value and subgrade resilient modulus, a lognormal distribution for the latter may be postulated as well, LN[4500, 900].

Design Charts

When Equation 9 is integrated after the proper substitutions have been made for the probability density functions and N_f expression as in Equation 5, an expression for μ_Δ is obtained for ATB. Similar expressions for DGA and CTB have been obtained; however, they are not reported in this paper. For easy reference, the parameters related to the probability density functions used in those computations are given in Table 1.

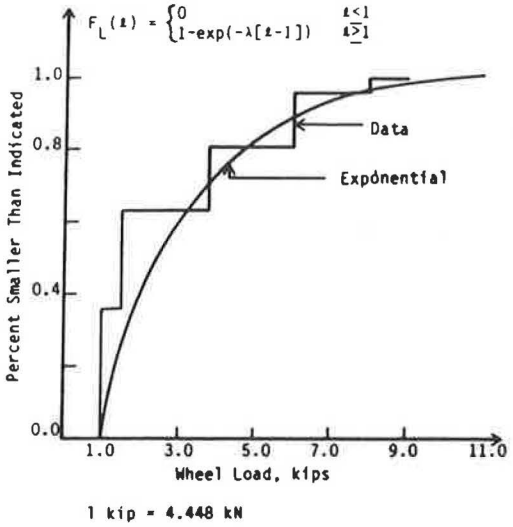

FIGURE 4 Cumulative distribution function of wheel loads, trucks only (shifted exponential with $\lambda = 0.45$ kip^{-1}) *(1)*.

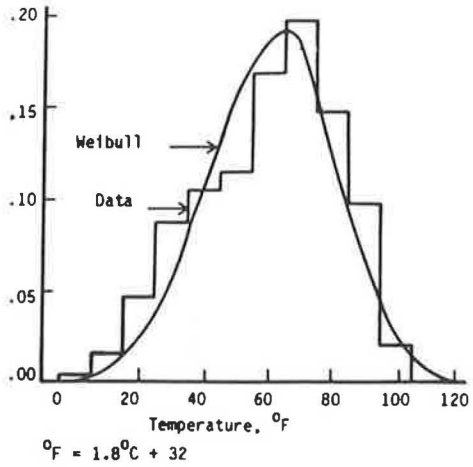

FIGURE 5 Relative frequency of temperature data compared with the theoretical distribution (Weibull with scale parameter 70°F and slope 3.5) *(1)*.

When an appropriate value of μ_Δ has been selected, depending on the desired confidence as in Figure 3, it is a simple procedure to derive and graph explicit relations among the three variables, traffic load repetitions (N_f'), asphalt concrete thickness included in the structural number, and the resilient modulus (M_r). Figures 6 and 7 are illustrative of these charts, for ATB and DGA, respectively. Note that the mixed traffic N_f' needs to be converted into 18-kip (80-kN) ESAL (using AASHO equivalency factors) before the graphs are plotted. A complete set of charts for ATB, DGA, and CTB can be seen in Husain *(16)*. The thickness values shown represent the thicknesses required to satisfy the tensile strain and compressive strain criteria for ATB and DGA pavement and all three of the criteria for CTB pavement.

EFFECT OF TEMPERATURE ON ASPHALT THICKNESS

Selection of Asphalt Grade for Mix Design

To account for the effect of temperature on asphalt mixture, it is customary to specify softer-grade asphalt in colder climates to reduce low-temperature thermal cracking and harder-grade asphalt in warmer climates to reduce rutting. On the basis of earlier work of Von Quintus et al. *(17)*, Basma and George *(6)* developed nomographs to help select asphalt grade such that both thermal cracking [not more than 35 ft/1,000 ft^2 (115 m/1000 m^2)] and rutting [not more than 0.5 in. (12.5 mm)] requirements would be met. Basma and George, employing the nomographs and such weather data as the mean annual air temperature and monthly mean air temperature for some 175 typical stations across the United States, prepared an asphalt selection map identifying five zones commensurate with five grades of asphalt (Figure 8). This map offers a simple procedure for selecting the asphalt grade appropriate to the temperature regime of an area. Asphalt selection using this map is in good agreement with that of the Asphalt Institute *(4)*. For

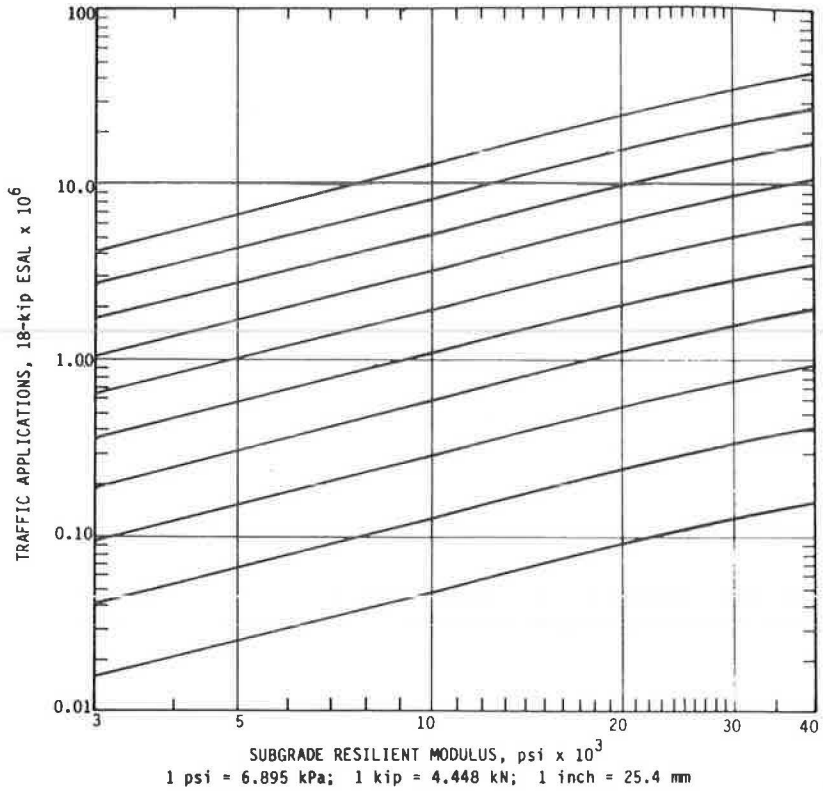

FIGURE 6 Design chart for asphalt-treated base (80 percent confidence level).

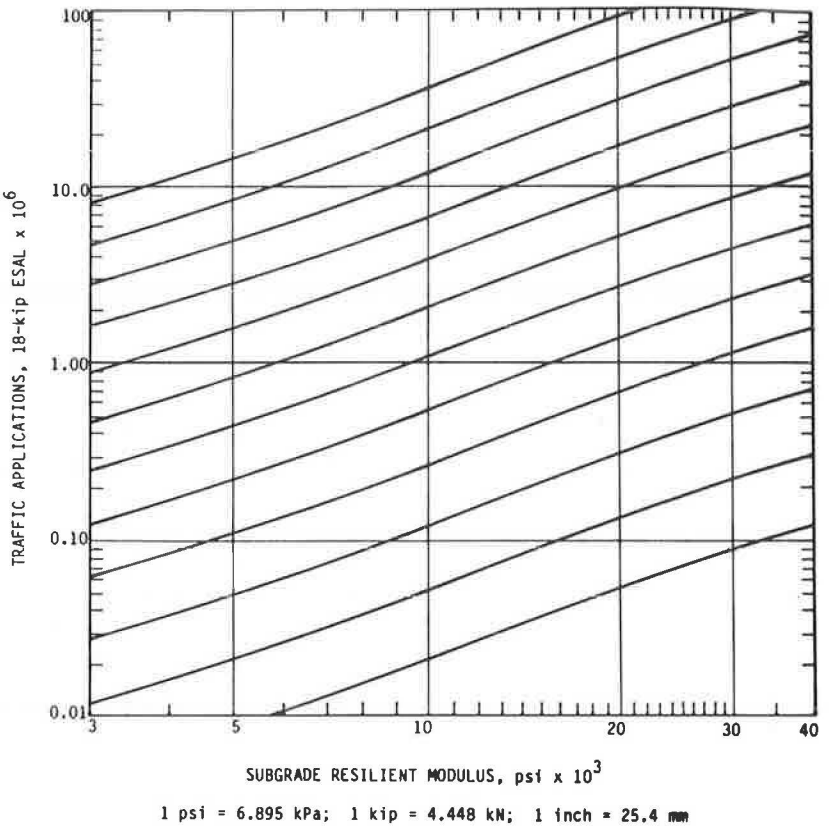

FIGURE 7 Design chart for dense-graded aggregate base 8 in. thick (80 percent confidence level).

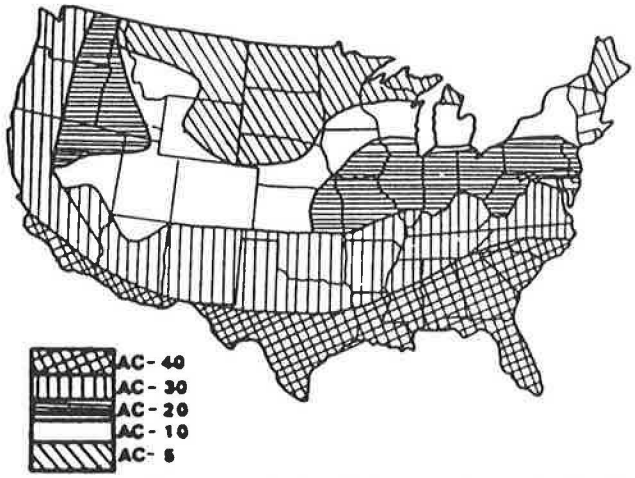

FIGURE 8 Recommended asphalt concrete grades for the United States.

example, the Chicago area with a mean annual air temperature of 50°F (10°C) calls for an asphalt grade of from AC–10 to AC–20 by both methods (Figure 8 and *4*, Table VI-1).

AC Thickness Influenced by Asphalt Grade

The question of the effect of asphalt grade on AC thickness now arises. That is, is AC–5 bituminous concrete required for the northern climate as effective (fatigue resistant) as, say, AC–40 mix mandated for the southern climate? To offer an explanation of this dilemma, Basma and George, employing the asphalt selection criteria, prescribed specific asphalt grades for each climatic zone. The "effective moduli" that correspond to various asphalt grades are also reported in the study (Table 2).

Effective modulus is defined as the weighted mean asphalt concrete modulus (weighted with respect to fatigue) *(17)*. Interestingly enough, the effective modulus, as given in Table 2, exhibited little variation within a zone, even with the different asphalt grades specified in Figure 8. The data clearly show that

TABLE 2 EFFECTIVE MODULI AND ASPHALT GRADES

Zone	Asphalt Grade	Effective Modulus (psi x 10^5)
Wet no-freeze	AC-40	8.40
Wet freeze and thaw	AC-30	5.30
Wet freeze	AC-20	4.42
	AC-10	4.43
	AC-5	4.27
Dry no-freeze	AC-40	4.90
Dry freeze and thaw	AC-30	3.30
Dry freeze	AC-5	2.50
	AC-10	2.40
	AC-30	2.90

1 psi = 6.895 kPa

the prevailing climate of the region stipulates the asphalt grade and therefore determines the asphalt concrete modulus. For example, the effective modulus in a wet no-freeze region may be three times as large as that in a dry freeze region. How this fluctuation affects thickness design is discussed next.

Basma and George studied this problem and defined what is known as modulus factor *(MF)* (ratio of structural layer coefficient evaluated at the reference modulus of 500,000 psi or 72.5 $\times$ 10^3 kPa to that at an arbitrary modulus). Because the layer coefficient and thickness required are related (through structural number), *MF* could be interpreted as a thickness adjustment factor *(TAF)* that accounts for the modulus fluctuations from region to region. When *MF*- or *TAF*-values of this previous study are plotted against the respective moduli, a definite trend is noted in their variations (Figure 9).

Whether or not this relationship is valid is investigated in the present research effort by repeatedly calculating the thickness nomographs, similar to Figures 6 and 7, using a range of effective moduli above and below the reference modulus of 500,000 psi (72.5 $\times$ 10^3 kPa). Note that a modulus of 500,000 psi (72.5 $\times$ 10^3 kPa) is used to prepare the nomographs in Figures 6 and 7. The moduli inputs for the calculations are ascertained from temperature distributions (mean and variance) employing Figure 2. For each temperature distribution, two moduli are calculated: a "simple" mean and a "derived" mean *(18)*. The two sets of moduli are subsequently used to calculate asphalt layer thicknesses. Again, the thickness adjustment factors (ratio of thickness of AC for 500,000 psi or 72.5 $\times$ 10^3 kPa to that for another modulus) are plotted against the respective moduli. That the *TAF*-versus-moduli relationship of the present study is in good agreement with that of the previous study attests to the validity of the *TAF* concept. A trend line comprising the two sets of data is shown by a solid line in Figure 9.

The thickness adjustment factor is proposed as a multiplier that would transform the calculated thickness values (from the nomograph) to the "true" design value. Asphalt concrete surfacing needs to be thicker in regions where the *TAF* is greater than 1 than it does in regions where the *TAF* is less than 1. The writers propose that *TAF* be used as an adjustment factor to account for the modulus variation. That is, when the projected modulus of a region is different from 500,000 psi (72.5 $\times$ 10^3 kPa), the nomographed thickness values should be adjusted employing the *TAF*. *TAF* will be greater than 1 when the effective modulus for the region is below the reference value of 500,000 psi and smaller than 1 when the effective modulus is above the reference value. The use of *TAF* is illustrated in the example problems.

SUMMARY

The design procedure presented in this paper is believed to have successfully incorporated both mechanistic and empirical state-of-the-art information in a viable design methodology. A major improvement in this procedure is the incorporation of structural performance characteristics. Structural performance refers to fatigue cracking and surface rutting. A unique aspect of this design algorithm is that it accounts for variabilities or uncertainties, or both, that are inherent in the design parameters: traffic load, ambient temperature, and subgrade support

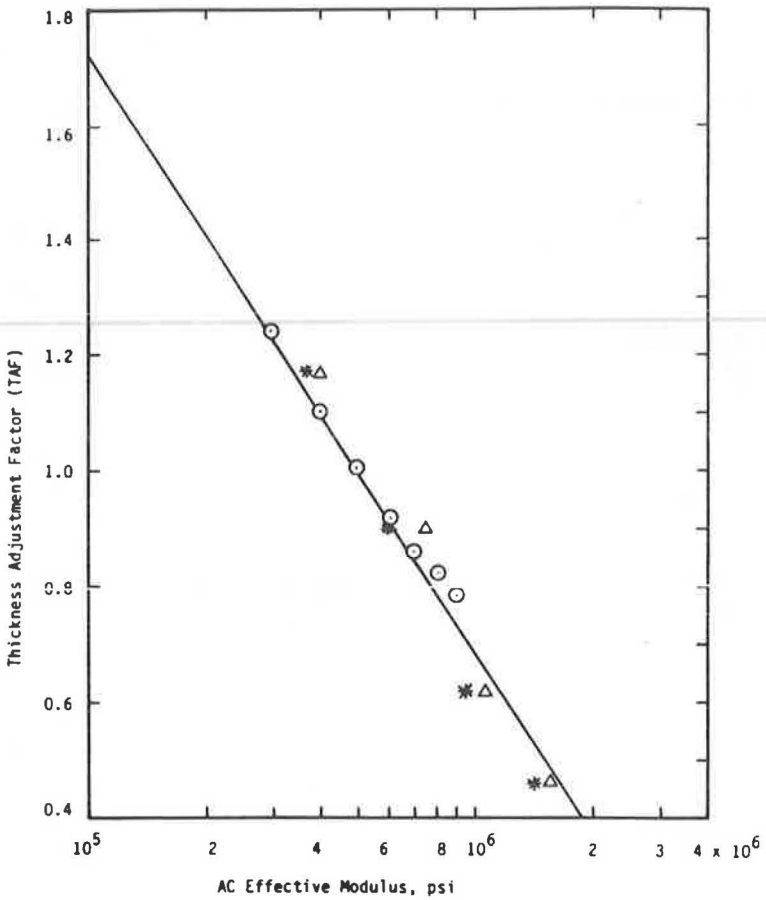

1 psi = 6.895 kPa

FIGURE 9 Thickness adjustment factor related to asphalt effective modulus.

TABLE 3 DATA REQUIRED FOR THICKNESS DESIGN

Item	Example 1	Example 2
Mean Air Temperature	45 °F (7 °C)	60 °F (20 °C)
Climatic Zone	Dry freeze	Wet freeze/thaw
Asphalt-Cement Grade	AC-5	A-30
Effective Modulus	2.5 x 10^5 psi (17.2 x 10^5 kPa)	5.3 x 10^5 psi (5.8 x 10^5kPa)
Mean Subgrade Modulus	11 x 10^3 psi (1.6 x 10^3 kPa)	9 x 10^3 psi (1.3 x 10^3 kPa)
AASHO Asphalt Layer Coefficient	0.44	0.44
AASHO CTB Layer Coefficient	0.23	0.23
AASHO DGA Layer Coefficient	0.14	0.14
AASHO Regional FActor	3.0	2.0
Design Traffice	7.5 x 10^6 18-kip	7.5 x 10^6 18-kip
Reliability Level	80 percent	80 percent
Terminal PSI	2.5	2.5

°F = 1.8°C + 32
1 kip = 4.448 kN

TABLE 4 COMPARISON WITH OTHER METHODS

Location	No. of 18-kip ESALs	Thickness of Asphalt Concrete (in.)		
		Probabilistic Fatigue Design, 80% Reliability	Asphalt Institute (4)	AASHO (19)
Huron, S.D.				
RF = 3.0				
E_S = 11,000 psi	7.5×10^6	15.0	13.3	9.6
Oxford, Miss.				
RF = 2.0				
E_S = 9,000 psi	7.5×10^6	11.7	13.0	9.3

Note: 1 psi = 6.895 kPa and 1 in. = 25.4 mm.

conditions. Because the design incorporates reliability in design, the engineer, if he wishes, can exercise a wide range of reliability options commensurate with the functional classification of the pavement. Design nomographs for two types of base materials, ATB and DGA, are included in this paper; a complete set of nomographs for four different reliability levels, however, can be found elsewhere *(16)*.

A rational method for selecting asphalt grade is presented as an integral part of the design procedure. When implementing this criterion for the entire nation, it becomes clear that the desired bituminous mix for each climatic region (six in all) exhibits a unique effective modulus. The region-to-region modulus variation, however, is accounted for by the use of the thickness adjustment factor (multiplying factor) that would transform the nomograph value (of thickness) to the "true" design value.

The example problems presented in the following subsections illustrate the entire procedure, including the use of the thickness adjustment factor. The data required for the thickness design, along with other information for both examples, are given in Table 3.

Example 1: Huron, South Dakota

Enter Figure 6 with design traffic 7.5×10^6 18-kip ESAL and subgrade modulus 11,000 psi (1.6×10^3 kPa) and obtain the asphalt layer thickness 11.5 in. (292 mm) for standard conditions. Because Figure 6 is prepared by using asphalt modulus 5×10^5 psi (7.25×10^3 kPa), the thickness obtained from this figure should be corrected for the asphalt grade, selected for local conditions. From Figure 9, read the TAF = 1.3 corresponding to asphalt concrete modulus 2.5×10^5 psi (36.3×10^3 kPa). Multiply the thickness obtained previously by *TAF* to get the design asphalt thickness, 1.3 × 11.5 in. = 15.0 in. (381 mm). The design asphalt thickness determined from the present method is compared with thickness obtained from Asphalt Institute *(4)* and AASHO *(19)* methods.

Example 2: Oxford, Mississippi

With design traffic 7.5×10^6 18-kip ESAL and subgrade modulus 9×10^3 psi (1.3×10^3 kPa), the required thickness of asphalt concrete for standard conditions, from Figure 6, is 12.0 in. (305 mm). Enter Figure 8 and obtain *TAF* = 0.97 corresponding to 5.30×10^5 psi (76.8×10^3 kPa) effective asphalt concrete modulus. Thus the design asphalt concrete thickness is 0.97 × 12.0 in. = 11.7 in. (297 mm).

The asphalt concrete thickness calculated using the present method is compared with those of the Asphalt Institute (AI) as well as the AASHO Interim Guide (Table 4). The present method results in the greatest thickness of the three for colder regions (for example, South Dakota) and intermediate thickness for warmer regions (for example, Mississippi). That the proposed method, unlike the AI and the AASHO methods, accounts for the stiffness modulus of the asphalt mix is the reason for the greater thickness for the colder region and the relatively smaller thickness for the warmer region. Note that according to the AASHO method the pavement is consistently underdesigned for both warmer and colder regions.

The asphalt thicknesses derived from the three methods, for a range of traffic (Mississippi), are shown in Figure 10. In accordance with the proposed method, for the range of traffic

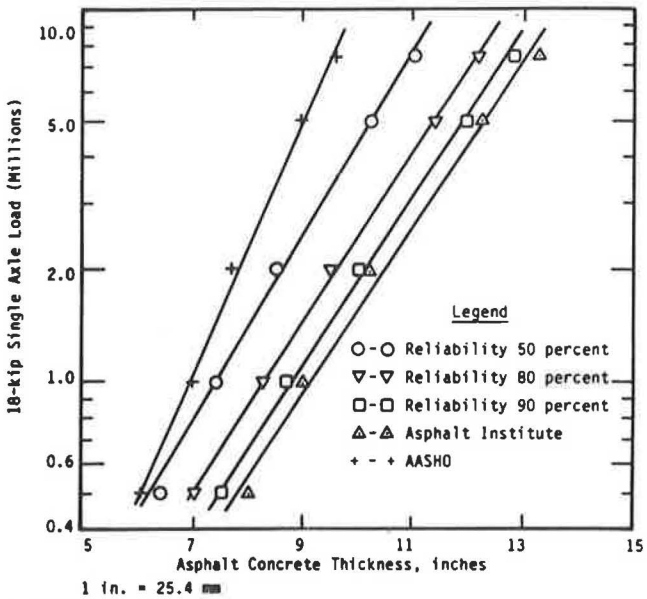

FIGURE 10 Comparison of asphalt concrete design thickness from various methods for subgrade resilient modulus 9,000 psi (1.3×10^3 kPa) for a warm region (Mississippi), effective modulus 5.3×10^5 psi (5.8×10^3 kPa).

levels considered and for all three of the reliability levels, the required thicknesses lie between those required by AI and AASHO methods.

These examples reaffirm the conclusion that the proposed design procedure is sound with respect to the use of mechanistic methods, probabilistic consideration of variables, and, finally, asphalt grade selection.

ACKNOWLEDGMENTS

This paper is a part of the study titled "Overlay Design and Reflection Cracking Study for Flexible Pavements," sponsored by the Mississippi Highway Department and the U.S. Department of Transportation, Federal Highway Administration. The authors wish to acknowledge the Shell-Laboratorium for their permission to use the BISAR program.

REFERENCES

1. K. P. George and S. K. Nair. Probabilistic Fatigue Design for Flexible Pavements. *Proc., Fifth International Conference on the Structural Design of Asphalt Pavements*, The Netherlands, 1982.
2. W. J. Kenis. Predictive Design Procedures—A Design Method for Flexible Pavements Using the VESYS Structural Subsystem. *Proc., Fourth International Conference on the Structural Design of Asphalt Pavements*, The University of Michigan, Ann Arbor, 1977.
3. R. B. Kulkarni. Probabilistic Prediction of Pavement Distress Models. *Proc., Third International Conference on Applications of Statistics and Probability in Soil and Structural Engineering*, Sydney, Australia, 1979.
4. *Thickness Design—Asphalt Pavements for Highways and Streets.* MS–1. The Asphalt Institute, College Park, Md., 1981.
5. M. A. Miner. Cumulative Damage in Fatigue. *Transactions of the ASME*, Vol. 67, 1945.
6. A. A. Basma and K. P. George. Environmental Factors in Flexible Pavement Design. In *Transportation Research Record 954*, TRB, National Research Council, Washington, D.C., 1984, pp. 52–58.
7. D. Hwang and M. W. Witezak. *Program DAMA: User's Manual.* University of Maryland, College Park, 1979.
8. K. Majidzadeh and J. Ilves. *Flexible Pavement Overlay Design.* Report GHWA/RD–81/032. Federal Highway Administration, Vol. 1., 1981.
9. F. N. Finn, C. Saraf, R. Kulkarni, K. Nair, W. Smith, and A. Abdullah. The Use of Distress Prediction Subsystems for the Design of Pavement Structure. *Proc., Fourth International Conference on the Structural Design of Asphalt Pavements,* The University of Michigan, Ann Arbor, 1977.
10. S. F. Brown, J. M. Brunton, and P. S. Pell. The Development and Implementation of Analytical Pavement Design for British Conditions. *Proc., Fifth International Conference on the Structural Design of Asphalt Pavements,* Delft University, Delft, The Netherlands, 1982, pp. 3–16.
11. K. P. George. *Material Parameters for Pavement Design Using AASHO Interim Guide.* Final Report. The University of Mississippi, University, 1981.
12. J. L. M. Scott. Flexural Stress-Strain Characteristics of Saskatchewan Soil-Cement. Technical Report 23. Saskatchewan Department of Highway, Saskatoon, 1974.
13. P. S. Pell and I. F. Taylor. Asphaltic Road Materials in Fatigue. *Proc., Association of Asphalt Paving Technologists*, Vol. 38, 1969.
14. C. L. Monismith et al. *Asphalt Mixture Behavior in Repeated Flexure.* Report 705. Institute of Transportation and Traffic Engineering, University of California, Irvine, 1972.
15. P. H. Wirsching and J. T. P. Yao. A Probabilistic Design Approach Using the Palmgren-Miner Hypothesis. *Proc., National Structural Engineering Conference,* ASCE, Vol. 1, 1976.
16. S. Husain. *Evaluation of Flexible Pavement and Overlay Design.* Ph.D. dissertation. The University of Mississippi, University, 1985.
17. H. L. Von Quintus, F. N. Finn, W. R. Hudson, and F. L. Roberts. *Flexible and Composite Structures for Premium Pavements,* Vol. 2: *Design Manual.* FHWAH–RD–80. FHWA, U.S. Department of Transportation, 1980.
18. J. R. Benjamin and C. A. Cornell. *Probability Statistics and Decision for Civil Engineer.* McGraw-Hill Book Company, New York, 1970.
19. *AASHO Interim Guide 1972.* AASHO, Washington, D.C., 1972.

Publication of this paper sponsored by Committee on Flexible Pavements.

The opinions, findings, and conclusions expressed in this paper are those of the authors and not necessarily those of the Mississippi State Highway Department or the Federal Highway Administration. This paper does not constitute a standard, specification, or regulation.

Development of a Simplified Mechanistic Pavement Evaluation and Overlay Design Procedure for Flexible Pavements

EMMANUEL FERNANDO, DAVID LUHR, AND DAVID ANDERSON

A simplified mechanistic pavement evaluation and overlay design procedure is presented. The procedure assumes a three-layer model of a pavement structure and requires falling-weight sensor deflections for estimating remaining life and required overlay thickness. Linear elastic layered theory was used to develop strain-versus-deflection relationships for direct calculation of pavement strains from measured falling-weight deflections. This is believed to be a simpler and more straightforward approach than the back-calculation of layer moduli from measured surface deflections and the subsequent calculation of stresses or strains, or both, using elastic layered theory. To develop the strain-deflection relationships, the multilayer linear elastic program BISAR was used in a large factorial study. The program was modified for implementation on a microcomputer, thus making the factorial study feasible. Strain-versus-deflection relationships were developed for asphalt tensile and subgrade compressive strains. Pavement performance predictions that were calculated using strains from the deflection relationships were compared with those from deflection basin–fitting algorithms, using theoretically generated deflection data as well as field data. Relationships for designing overlay thicknesses were developed by evaluating the variation in pavement strains due to the addition of an overlay. The simplified mechanistic pavement evaluation and overlay design procedure presented can be readily implemented on a microcomputer, unlike other mechanistic procedures that require more computer resources.

The existing U.S. highway network represents a major investment in public transportation by state and federal agencies. Many of today's highways were constructed during the road-building boom of the 1950s and 1960s. Consequently, many of these roads are nearing or past the end of their design lives and are in need of major rehabilitation. Because of the increasing cost of new highway construction, and because of the need for protecting the investment made in the existing road network, pavement maintenance and rehabilitation have become a major concern of state and federal agencies.

The most widely used means of pavement rehabilitation is the design and construction of overlays. The design of overlays varies among highway agencies, depending on local conditions and experience. In general, current design practices range from empirical procedures that use limiting deflection criteria to more mechanistic procedures that consider stresses and strains in the pavement structure. Procedures that use limiting deflection criteria are considerably simpler and easier to implement; however, because these design relationships are based on local conditions and experience, they cannot be used with different materials, or in other regions, without extensive correlations.

In contrast, the more mechanistic procedures are more comprehensive and can be used for a much wider range of conditions because the design is based on a mechanistic analysis of the pavement structure and the material properties of the various pavement layers. The material properties (i.e., layer moduli) are typically determined by fitting deflection basin measurements or from laboratory testing of samples taken from the pavement sections being considered. Of the two methods, deflection basin fitting, using linear elastic layered theory, is probably the more widely used procedure for in situ determination of pavement properties. It is a nondestructive test procedure and is comparatively simpler than the laboratory determination of layer moduli. The resilient moduli are required in existing mechanistic design procedures for the purpose of determining the pavement response parameters (e.g., asphalt tensile strain, subgrade compressive strain) used in estimating the remaining life of an existing pavement structure.

In this paper, a simpler approach for flexible pavement evaluation and overlay design is presented. Instead of using measured surface deflections to estimate the layer moduli, the measured deflections are used to estimate the strains directly. This approach was used in the development of the flexible pavement evaluation procedure presented herein.

METHODOLOGY FOR DEVELOPING AN EVALUATION PROCEDURE FOR FLEXIBLE PAVEMENTS

In the development of this pavement evaluation procedure, the three-layer model shown in Figure 1 was assumed to represent

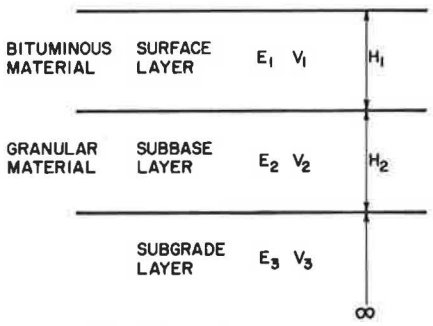

FIGURE 1 Three-layer pavement model used in the development of strain-versus-deflection relationships.

Pennsylvania Transportation Institute, Pennsylvania State University, University Park, Pa. 16802.

the pavement structure. A three-layer model was selected instead of a four-layer model because it represents typical pavement conditions in Pennsylvania. Existing rational overlay design procedures, such as those developed by Shell *(1)* and Resources International, Inc. (RII) *(2)*, also use a three-layer representation of the pavement structure.

The assumptions of linear elastic layered theory were assumed to be valid. In addition, it was assumed that surface deflections are obtained using the falling-weight deflectometer at a load level of 9,000 lb. A design single axle load of 18 kips is used in the procedure. Consequently, corrections for stress dependency of unbound pavement materials are not necessary if falling-weight deflection measurements are taken at a load level of 9,000 lb. This simplifies the pavement evaluation procedure and makes practical use of the capability of the falling-weight deflectometer to provide a wide range of loadings.

A large factorial study was undertaken to develop relationships between strains and surface deflections. Specifically, equations were developed for estimating the tensile strain at the bottom of the existing asphalt layer and the compressive strain at the top of the subgrade. These two types of strains are used as criteria in several existing performance models *(1-4)*.

The factorial study used the three-layer model shown in Figure 1. To simplify the analysis, fixed values for the Poisson's ratios of the various layers were assumed. Specifically, the Poisson's ratios for the bituminous surface layer, the subbase, and the subgrade were assumed to be 0.30, 0.40, and 0.45, respectively. Consequently, there were five factors in the factorial design: *(a)* asphalt surface modulus, *(b)* subbase modulus, *(c)* subgrade modulus, *(d)* asphalt surface thickness, and *(e)* subbase thickness. Four different levels for each factor were assumed (Table 1). The levels fall within the normal range of values expected for each factor under actual field conditions. The resulting factorial design consisted of 4^5, or 1,024, possible combinations of moduli and thicknesses. For each of these combinations, the multilayer elastic BISAR program developed by Shell *(5)* was used to calculate surface displacements due to the falling-weight load of 9,000 lb applied through a circular plate of 5.9-in. radius.

The full factorial design established for the study is large, and under ordinary circumstances it would not have been practical to evaluate pavement response for all of the 1,024 combinations of moduli and thicknesses included in the factorial. Instead, only a fractional factorial would have been evaluated. It was, however, feasible to evaluate the full factorial for this project because the researchers modified the program, BISAR, to run on an IBM PC/XT microcomputer.

Theoretical surface displacements were determined at seven different positions, corresponding to the seven sensors of the falling-weight deflectometer (FWD). The spacing between sensors was assumed to be 1 ft. The theoretical displacements calculated by BISAR for the falling-weight loading conditions were compared with actual falling-weight deflections taken at the Pavement Durability Research Facility of the Pennsylvania Transportation Institute. The objective of the comparison was to verify whether the actual measured deflections were within the range of the theoretical deflections generated by BISAR. It was found that measured deflections for Sensors 4 through 7 were out of the range of the corresponding theoretical sensor deflections, which were larger in magnitude. Consequently, a new factorial design was established that contained higher levels of subgrade moduli. The levels selected were 5,000, 20,000, 35,000, 50,000, and 65,000 psi, respectively, and were established from an examination of back-calculated subgrade moduli using measured field deflections. Levels for the other factors were left unchanged. Consequently, the second factorial consisted of $4^4 \times 5$, or 1,280, possible combinations of moduli and thicknesses. Measured FWD deflections were again compared with the new set of theoretical deflections and were found to be within range.

The displacements calculated by BISAR for the FWD loading conditions, and for the combinations of layer moduli and thicknesses included in the first and second factorials, were subsequently correlated with computed strain values associated with an 18-kip load to establish strain-versus-deflection relationships. The program BISAR was used to compute strains for all possible combinations of moduli and thicknesses included in both factorials. The strains calculated were the tensile strain at the bottom of the bituminous surface layer and the compressive strain at the top of the subgrade.

The 18-kip single axle load was assumed to be transmitted to the pavement through a pair of dual wheels, each of which carried 4,500 lb. Tires were assumed to be inflated to a pressure of 100 psi, and the tires of each dual wheel were assumed to be separated by 13.1 in. For simplicity in the analysis, only strains directly under one tire of the 18-kip single axle design load were considered.

TABLE 1 THICKNESS AND MODULUS VALUES USED IN THE FACTORIAL STUDY

Layer	Thickness (in.)	Modulus (psi)	
Surface	1.0, 4.0, 7.0, 10.0	100,000	450,000
		800,000	1,150,000
Subbase	3.0, 7.0, 11.0, 15.0	10,000	30,000
		50,000	70,000
Subgrade	infinite	3,000	8,000
		13,000	18,000

Values of Poisson's ratio used for the surface, subbase and subgrade were 0.30, 0.40, and 0.45 respectively.

STRAIN-DEFLECTION RELATIONSHIPS DEVELOPED FROM THE FACTORIAL STUDY

The method of least squares was used to establish relationships between theoretical strains due to an 18-kip axle load and FWD surface deflections. Through regression analysis of the data generated from the factorial study, the following relationships for estimating strains from measured surface deflections were developed:

$$\log_{10}[\varepsilon_{yy}/\log_{10}(H_1+1)] = -2.261 - 0.944\log_{10}(W_1 - W_2) + 1.947\log_{10}[(W_1 - W_3)/W_2] + 0.175(W_1{*}H_2) + 0.926\log_{10}(W_1{*}W_2) \quad (1)$$

$R^2 = 0.915$, SEE = 0.141, N = 2,256 observations

$$\log_{10}(\varepsilon_{zz}) = -0.054 + 1.941\log_{10}(W_1 - W_2) - 2.004\log_{10}[(W_1 - W_3)/W_2] - 1.465\log_{10}(H_1 + H_2) - 0.136(H_2)^{1/2} + 0.725\log_{10}(W_1{*}H_2) + 0.285(W_1{*}H_1)^{1/2} - 0.910\log_{10}(W_1{*}W_2) \quad (2)$$

$R^2 = 0.963$, SEE = 0.084, N = 2,304 observations

where

- ε_{yy} = tensile strain at the bottom of the bituminous surface layer,
- ε_{zz} = compressive strain at the top of the subgrade,
- W_i = deflection at the ith sensor of the FWD (in.),
- H_1 = thickness of the existing bituminous surface layer (in.),
- H_2 = thickness of existing subbase (in.),
- R^2 = coefficient of determination, and
- SEE = standard error of the estimate.

In the formulation of Equations 1 and 2, analyses of residuals were used to verify model assumptions concerning linearity, independence of error terms, and homogeneity of variance. In addition, correlations between independent variables were examined to prevent problems associated with multicollinearity. These steps were taken to ensure that the relationships established were statistically sound and robust.

Figure 2, which is a plot of the predicted versus the theoretical asphalt tensile strains, shows good agreement between the predicted and theoretical values for most of the 2,256 observations used to develop Equation 1. However, there are also several cases in which the agreement is not good. For these cases, an effort was made to establish possible reasons for the poor agreement between predicted and theoretical values. Combinations of layer moduli and thicknesses, for which the absolute values of the residuals were greater than twice the standard error of the estimate, were examined to determine if there was any consistent pattern among the various combinations. No consistent patterns were found, nor did the combinations represent unrealistic cases. Consequently, the observations for which there was poor agreement between predicted and theoretical values were not deleted from the data set used to develop the relationship for estimating asphalt tensile strain. It should be mentioned that these observations for which the residuals were larger represent only a small percentage of the total number of observations used to develop the equation.

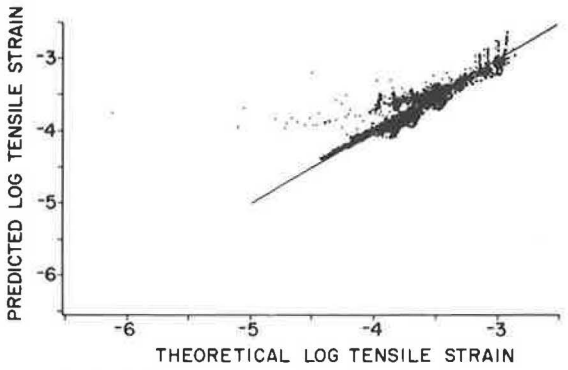

FIGURE 2 Comparison of predicted and theoretical asphalt tensile strains.

Figure 3 shows the accuracy of the predictions of subgrade compressive strain from Equation 2. In the figure the logarithms of predicted and theoretical compressive strains are compared. To illustrate better the accuracy of the predictions, a histogram of the ratios of the residuals to the standard error of the estimate is shown in Figure 4. It can be seen that a majority of the residuals (about 90 percent of the total number of observations) are within one standard error of the estimate, which is 0.084 for Equation 2. The antilog of this number is 1.21, which indicates that the percentage difference between predicted and theoretical compressive strains would be within 21 percent for most of the 2,304 observations used to develop the equation. In addition, Figure 4 shows that approximately 48 percent of the total number of residuals are actually within one-half of the standard error of the estimate.

The preceding discussion indicates that the relationships established in this paper can be used, with a reasonable degree of confidence, for estimating asphalt tensile and subgrade compressive strains directly from measured deflection basin indices and existing layer thicknesses.

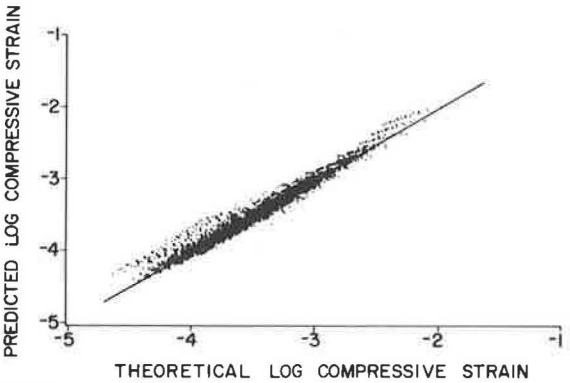

FIGURE 3 Comparison of the logarithms of predicted and theoretical subgrade compressive strains.

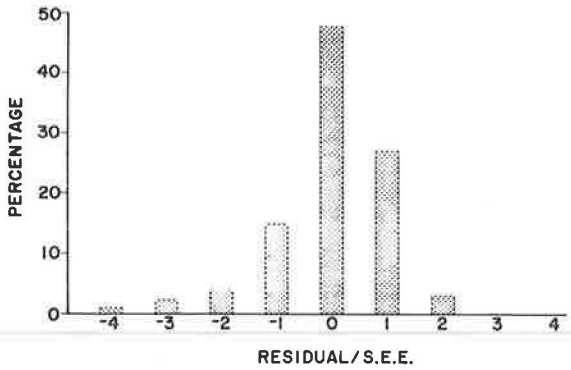

FIGURE 4 Histogram of the ratios of the residuals to the standard error of the estimate for Equation 2.

COMPARISON OF STRAIN-VERSUS-DEFLECTION AND DEFLECTION BASIN–FITTING METHODOLOGIES

To evaluate the equations developed, 15 combinations of layer moduli and thicknesses were randomly generated (Table 2), and the program BISAR was used to calculate theoretical FWD pavement deflections and strains due to an 18-kip axle load for each combination. The theoretical deflections generated were used in the strain-versus-deflection relationships (Equations 1 and 2) to estimate the asphalt tensile and subgrade compressive strains due to an 18-kip load.

The deflections obtained were also used as inputs to two overlay design procedures that use the deflection basin–fitting methodology for pavement evaluation. These two procedures are OAF, developed by RII for FHWA *(2)*, and FPEDD1, developed by Uddin at the University of Texas at Austin *(6)*. Using the theoretical FWD deflections, these two procedures back-calculated the known theoretical layer moduli (Table 2). The program BISAR was used with the back-calculated layer moduli from each procedure to calculate the asphalt tensile and subgrade compressive strains due to an 18-kip axle load. Performance prediction estimates were then generated using the calculated strain values. In connection with this, the tensile strains were used with the ARE fatigue equation *(3)*, and the subgrade strains were used with the performance model developed by Luhr et al. *(4)*. These two performance equations are defined, respectively, as follows:

$$W_{18} = 9.73 \times 10^{-15} (1/\varepsilon_t)^{5.16} \quad (3)$$

$$\log_{10} N_X = 2.15122 - 597.662 (\varepsilon_{SG}) - 1.32967 (\log_{10} \varepsilon_{SG}) + \log_{10} [(PSI_i - TSI)/(4.2 - 1.5)]^{1/2} \quad (4)$$

where

W_{18} = weighted 18-kip applications before Class-2 cracking,
ε_t = tensile strain at the bottom of the asphalt surface layer,
$\log_{10} N_X$ = $\log_{10}$ of allowable applications of axle load X,
ε_{SG} = subgrade compressive strain due to axle load X,

TABLE 2 COMBINATIONS OF LAYER MODULI AND THICKNESSES USED IN THE EVALUATION OF STRAIN-DEFLECTION RELATIONSHIPS

	Layer Moduli (psi)			Thickness (in.)	
	Surface	Subbase	Subgrade	Surface	Subbase
1)	411,200	29,200	12,000	2.0	3.0
2)	733,200	31,600	15,450	4.0	7.0
3)	871,200	45,400	6,600	5.0	3.0
4)	120,000	33,000	13,400	4.5	11.0
5)	220,000	62,200	10,000	7.5	6.0
6)	190,400	44,000	14,000	3.0	5.0
7)	246,000	18,500	9,000	2.5	4.0
8)	798,000	20,000	6,000	7.5	3.5
9)	430,000	63,000	4,500	5.5	7.0
10)	227,000	29,000	7,000	7.0	11.0
11)	328,000	64,000	18,000	7.0	7.0
12)	457,000	26,000	10,000	6.5	3.0
13)	540,000	33,000	11,000	4.0	15.0
14)	160,000	20,000	12,000	2.0	3.0
15)	108,000	18,000	15,000	4.5	3.0

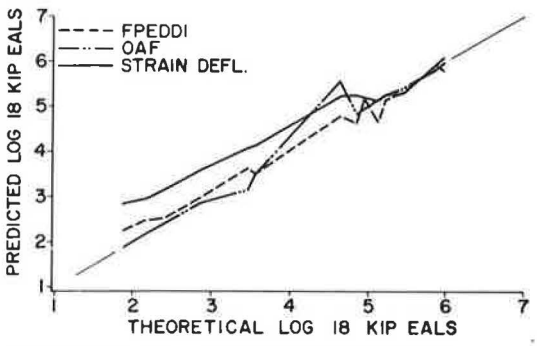

FIGURE 5 Comparison of predicted and theoretical pavement performance based on asphalt tensile strain.

PSI_i = initial PSI of pavement, and
TSI = terminal serviceability index.

Figures 5 and 6 show comparisons of the performance predictions using the theoretical strains with the predictions using the strains from programs OAF, FPEDD1, and the strain-versus-deflection relationships. In general, the performance predictions from the deflection basin–fitting procedures match more closely the predictions generated from the theoretical strains than those generated from the simplified strain-versus-deflection procedure. In most cases, the performance predictions from the simplified procedure are higher than the theoretical number of 18-kip equivalent axle loads (EALs) to failure. However, in all cases the differences in performance estimates among the various procedures are within one order of magnitude, and for a normal range of traffic expected in the field (e.g., 100,000 to 10,000,000 18-kip EALs) the performance estimates from both methodologies tend to compare more favorably. Thus the strain-deflection methodology presented herein does yield reasonable results compared with theoretical pavement response. It should also be noted that, for some combinations of layer moduli and thicknesses, unrealistic estimates of fatigue life (i.e., less than 1,000 18-kip EALs) are obtained from the theoretical tensile strains. The unrealistically low performance estimates occurred for hypothetical pavement sections with low asphalt modulus or thin layer thickness. For these cases, however, the strain-versus-deflection methodology yielded higher performance estimates.

Field-measured FWD deflections taken from eight different pavement sections at the Pennsylvania Transportation Research Facility were also used with the strain-versus-deflection relationships. The field-measured deflections were entered into programs OAF and FPEDD1, and the back-calculated layer moduli generated were used in a linear elastic layered analysis to predict strains in the pavement sections. Performance estimates for the various sections were subsequently calculated using the predicted strains, as was done in the preceding theoretical analysis. In addition, performance estimates were obtained using resilient modulus values determined from laboratory tests performed on the field materials. Consequently, performance estimates were calculated using the strain values determined from *(a)* the strain-versus-deflection relationships (Equations 1 and 2), *(b)* the back-calculated layer moduli from programs OAF and FPEDD1, and *(c)* modulus data determined in the laboratory. The calculated performance estimates for each section are plotted in Figure 7 (based on asphalt strain) and Figure 8 (based on subgrade strain).

It can be observed that, for the eight sections included in the analysis, performance estimates based on tensile strain, and determined from the basin-fitting procedures, and the asphalt strain-versus-deflection relationship are in better agreement than are those calculated using laboratory-determined moduli. Thus performance evaluation using the simplified procedure

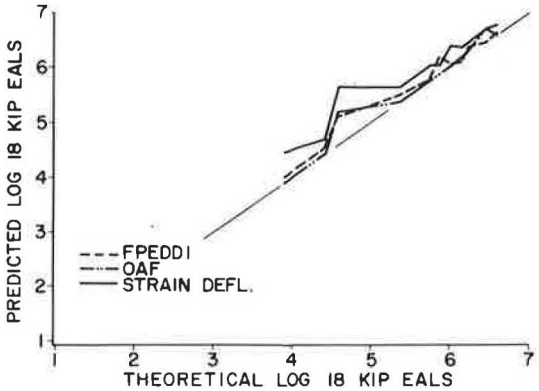

FIGURE 6 Comparison of predicted and theoretical pavement performance based on subgrade compressive strain.

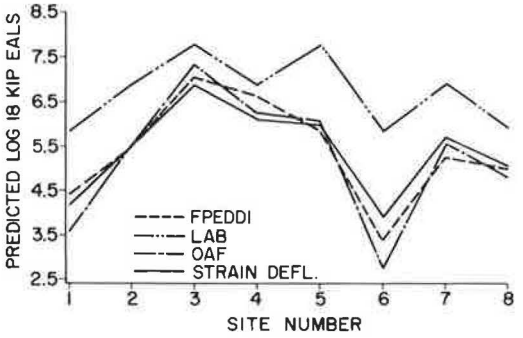

FIGURE 7 Comparison of pavement performance estimates based on asphalt tensile strain using field data.

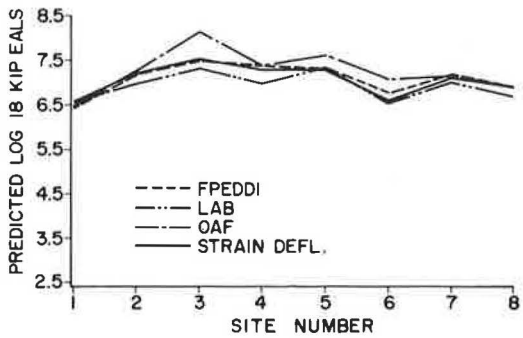

FIGURE 8 Comparison of pavement performance estimates based on subgrade compressive strain using field data.

yields results that are comparable to those obtained from procedures that back-calculate layer moduli from measured deflections. However, on the basis of the field performance of the various sections, the performance estimates calculated using laboratory-determined moduli are more realistic. This may be because the model used to estimate performance from asphalt tensile strains was calibrated using laboratory-determined moduli, the values of which may be quite different from those obtained using field deflection measurements.

Figure 8 shows a comparison of the performance predictions based on subgrade compressive strain. In contrast with the results presented previously, the performance predictions based on subgrade compressive strain show a relatively smaller amount of variation among the various sections and the procedures used to estimate pavement performance. In all cases, the differences are within an order of magnitude. Thus, for the sections included in the analysis, performance estimates based on subgrade compressive strain appear to be more stable and less sensitive to the procedure used to estimate pavement strains.

DEVELOPMENT OF A THICKNESS DESIGN PROCEDURE FOR FLEXIBLE PAVEMENT OVERLAYS

The strain-versus-deflection relationships allow for a simpler determination of remaining pavement life and permit the practical use of deflection measurements in a network-level pavement management system for screening pavements that are in need of overlays. However, a procedure for determining actual overlay thicknesses is also required. In the development of the simplified mechanistic pavement evaluation and overlay design procedure, linear elastic layered theory was used to develop the thickness design procedure for overlays. In the formulation of the method, the overlay was assumed to be an additional layer placed on top of the existing three-layer pavement (Figure 1), and the overlaid pavement is assumed to be represented by a four-layer model.

The required overlay thickness is based on the reduction in strains that results from the application of an overlay. The reduced strains are used to calculate pavement life after an overlay. In the development of the procedure, the strains after an overlay (four-layer model) were correlated with the strains before the overlay (three-layer model) and the overlay thickness.

To establish the equations for strains after an overlay, the factorial designs were modified to take into account the additional overlay layer. The additional factors were the modulus and the thickness of the overlay. The Poisson's ratio of this layer was assumed to be constant at 0.30.

Three levels for the overlay thickness were selected: 1, 3, and 5 in. These levels represent a typical range of overlay thicknesses found in practice. The overlay modulus was set at one typical value because, if several levels for the overlay modulus were selected, use of the overlay design procedure would require that the overlay modulus be known by the user. The value selected was 450,000 psi. With the addition of overlay thickness as a factor at three levels and overlay modulus as a factor at only one level, the size of each factorial established previously was increased threefold. In the analysis, the levels of the factors in the original factorials were retained, and the only modifications made were *(a)* inclusion of overlay thickness as a factor having three different levels and *(b)* inclusion of overlay design modulus as a factor set at just one level.

The program BISAR was then used to calculate strains for each combination of moduli and thicknesses in both factorials. Strains were also calculated at the top of the subgrade and at the bottom of the original bituminous surface layer. The computed values represent the strains due to an 18-kip load after the placement of an overlay. By the method of least squares, these values were subsequently correlated with the corresponding strains before the overlay and the overlay thickness. The relationships developed for estimating the tensile and compressive strains of a pavement after an overlay are given by Equations 5 and 6:

$$\log_{10}(\varepsilon_{yy})_{ov} = -0.689 + 0.793 \log_{10}(\varepsilon_{yy}) - 0.041 (H_{ov})^{1/2} + H_1 - 0.057 (H_{ov}) \quad (5)$$

R^2 = 96.63 percent, SEE = 0.057, N = 6,180 observations

$$\log_{10}(\varepsilon_{zz})_{ov} = -0.359 + 0.870 \log_{10}(\varepsilon_{zz}) - 0.051 (H_{ov}) - 0.109 [(H_{ov} + H_1)/H_1]^{1/2} \quad (6)$$

R^2 = 97.34 percent, SEE = 0.062, N = 6,912 observations

where

$(\varepsilon_{yy})_{ov}$ = tensile strain at the bottom of the original bituminous surface layer after an overlay,
$(\varepsilon_{zz})_{ov}$ = compressive strain at the top of the subgrade after an overlay,
ε_{yy} = tensile strain at the bottom of the original bituminous surface layer before an overlay,
ε_{zz} = compressive strain at the top of the subgrade before an overlay,
H_{ov} = overlay thickness (in.), and
H_1 = thickness of the original bituminous surface layer (in.).

Predicted and theoretical strain values are compared in Figures 9 and 10 to show the accuracy of the estimates resulting

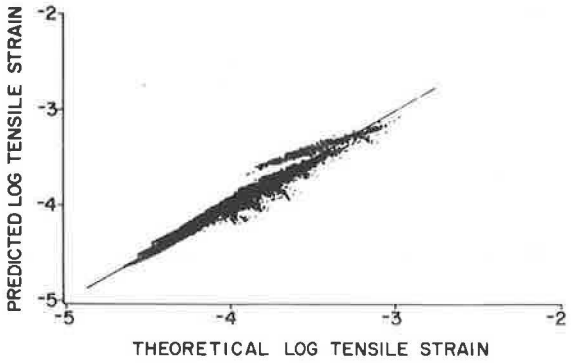

FIGURE 9 Comparison of predicted and theoretical log tensile strains after an overlay.

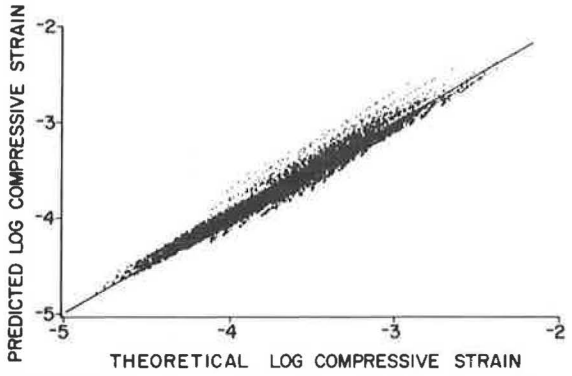

FIGURE 10 Comparison of predicted and theoretical log compressive strains after an overlay.

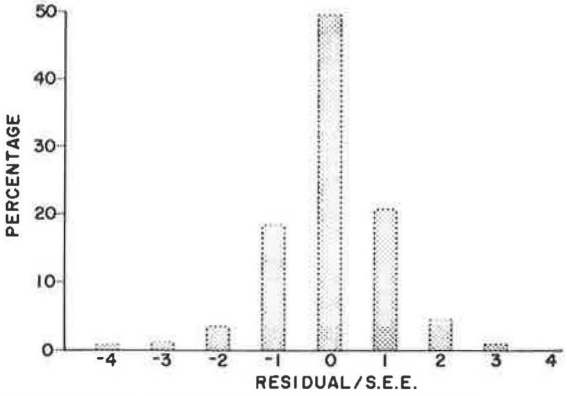

FIGURE 12 Histogram of the ratios of the residuals to the standard error of the estimate for Equation 6.

from Equations 5 and 6. In addition, histograms of the ratios of residuals to the standard error of the estimate for each equation are shown in Figures 11 and 12. As indicated in Figures 9 and 11, the equation for tensile strain after an overlay produces reasonably good estimates. In particular, Figure 11 shows that most of the differences between the predicted and the theoretical logarithms of the tensile strains after an overlay are within one standard error of the estimate, which is equal to 0.057 for Equation 5. Because the antilog of this number is 1.14, the difference between most of the predicted and theoretical strains is within 14 percent. About 50 percent of the 6,180 residuals included in Figure 11 are actually within one-half of the standard error of the estimate for the equation. Figures 10 and 12 likewise show reasonable agreement between the compressive strains predicted by Equation 6 and the theoretical strains. In particular, Figure 12 indicates that most of the differences between the predicted and the theoretical logarithms of the compressive strains after an overlay are within one standard error of the estimate, which is 0.062 for Equation 6. The antilog of this number is 1.15, which indicates that the differences between most of the predicted and actual strains are within 15 percent. Figure 12 also shows that about 50 percent of the 6,912 residuals from the regression analysis of subgrade compressive strain are actually within just one-half of the standard error of the estimate.

Equations 5 and 6, therefore, provide a means for determining the required overlay thicknesses based on either an asphalt tensile strain or a subgrade compressive strain criterion. The thickness design procedure is iterative: trial overlay thickness values are assumed until the strains computed after an overlay yield satisfactory estimates of design life from performance equations based on either of the aforementioned strain criteria.

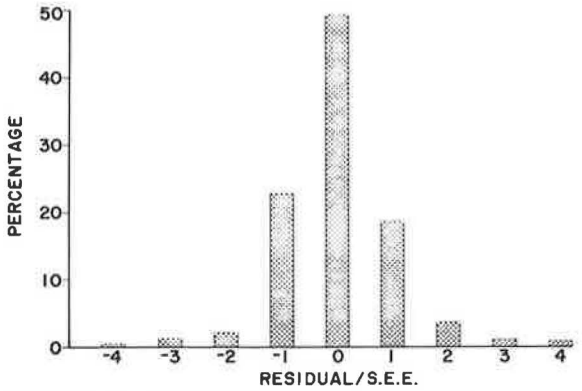

FIGURE 11 Histogram of the ratios of the residuals to the standard error of the estimate for Equation 5.

SUMMARY AND CONCLUSIONS

A simplified mechanistic pavement evaluation and overlay design procedure has been presented. In the development of the procedure, the concept of estimating pavement strains directly from measured surface deflections was introduced. The findings from the study indicate that the prediction of strains directly from measured surface deflections is a viable approach to the performance evaluation of flexible pavements. The procedure is much simpler than existing mechanistic design methods that back-calculate layer moduli from measured surface deflections and subsequently calculate from elastic layer theory the performance-related response parameters (e.g., asphalt tensile strain, subgrade compressive strain). The simplified procedure does not require iterative basin fitting or use of elastic layer programs that require considerable computer capabilities and time. The simplified procedure can be implemented on a small microcomputer *(7)* and requires little time to execute.

There may be occasions when knowledge of the in situ layer moduli is necessary. However, for routine pavement performance evaluation, application of the simplified procedure shows great promise. The method allows for the practical use of surface deflection measurements in a network-level pavement management system for screening pavements in need of rehabilitation.

Strain-versus-deflection relationships were developed for estimating asphalt tensile and subgrade compressive strains directly from measured deflections. Most performance equations available today are based on one of these two strain criteria. The strain-deflection equations were developed assuming linear elastic layered theory, and the relationships are applicable for estimating strains from surface deflection measurements taken with the FWD at a load level of 9,000 lb. The

primary reason for selecting this load level is that, if designs are based on 18-kip EALs, then corrections for stress dependency of unbound pavement materials need not be considered.

Comparison of performance estimates from both strain-deflection and deflection basin–fitting methodologies were made using theoretically generated deflection data and field-measured data. The results from field data included in the analysis indicate that performance predictions based on tensile strain, and calculated using laboratory-determined moduli, are more realistic than those obtained from the back-calculation procedures and the asphalt strain-versus-deflection relationship. The reason may be that the model used to estimate performance from asphalt tensile strain was calibrated using laboratory-determined moduli, the values of which may be quite different from those obtained using field deflection measurements. However, a better agreement was observed among the performance predictions based on subgrade strain. The results of the analysis therefore indicate that performance estimates based on subgrade strain are more stable and less sensitive to the procedure used to analyze the pavement. In addition, comparisons of performance estimates calculated from theoretically generated deflection data indicate that the strain-deflection relationships yield results that compare reasonably with performance predictions from existing deflection basin–fitting algorithms.

ACKNOWLEDGMENT

This paper is based on a project sponsored by the Pennsylvania Department of Transportation and the U.S. Department of Transportation, Federal Highway Administration.

REFERENCES

1. A. I. M. Claessen and R. Ditmarsch. Pavement Evaluation and Overlay Design—The Shell Method. *Proc., 4th International Conference on the Structural Design of Asphalt Pavements*, University of Michigan, Ann Arbor, 1977, Vol. 1, pp. 649–662.
2. K. Majidzadeh and G. V. Ilves. *Flexible Pavement Overlay Design Procedures*, Vol. 1: *Evaluation Modification of the Design Methods*. Final Report FHWA/RD–81/032. Resource International, Inc., New York; FHWA, U.S. Department of Transportation, Aug. 1981.
3. Austin Research Engineers. *Asphalt Concrete Overlays of Flexible Pavements*, Vol 1: *Development of New Design Criteria*. Report FHWA–RD–75–75. FHWA, U.S. Department of Transportation, 1975.
4. D. R. Luhr, B. F. McCullough, and A. Pelzner. Simplified Rational Pavement Design Procedure for Low-Volume Roads. In *Transportation Research Record 898*, TRB, National Research Council, Washington, D.C., 1983, pp. 202–206.
5. D. L. De Jong, M. G. F. Peutz, and A. R. Korswagen. *Computer Program BISAR*. External Report. Koninklijke/Shell-Laboratorium, Amsterdam, The Netherlands, 1973.
6. W. Uddin. *A Structural Evaluation Methodology for Pavements Based on Dynamic Deflections*. Ph.D. dissertation. The University of Texas at Austin, 1984.
7. E. G. Fernando, D. R. Luhr, and D. A. Anderson. *Development of an Overlay Design Procedure for Flexible Pavements*. PaDOT Research Project 82–11, PTI Report 8416. Pennsylvania Transportation Institute, Pennsylvania State University, University Park, Vol. 2, 1984.

Publication of this paper sponsored by Committee on Flexible Pavements.

On Predicting Pavement Surface Distress with Empirical Models of Failure Times

WILLIAM D. O. PATERSON AND ANDREW D. CHESHER

A statistical procedure that overcomes common difficulties in the development of distress models from empirical data is described and applied in an example. The time at which cracking or raveling appears in bituminous pavements is influenced by both trafficking and weathering and varies across pavements, even under nominally identical conditions. Also, any data set that represents a uniform sample of roads of all ages in a network over a given time period will typically include some unobserved (or "censored") events, that is pavements on which distress began either before or after the observation "window." The method applies failure-time theory, using maximum likelihood methods so that censored data can be included to prevent statistical bias in the predictions. The variability of failure times is represented by a Weibull distribution because that is considered the most appropriate for the concurrent mechanisms of fatigue and weathering and is flexible in shape. An example application of the procedure to a major analysis of Brazilian condition data shows that it permitted the use of a much wider data base than would otherwise be possible and produced important results that quantify strong effects of weathering and variability.

The initiation of surfacing distress such as cracking or raveling marks a significant stage in the deterioration of a pavement. From this point, the rate of deterioration usually accelerates at a rate that varies with traffic, pavement, and climatic conditions. The economic consequences of this are expressed through the secondary impact of surfacing distress on road roughness, which has a significant influence on vehicle operating costs *(1)*.

The timing of periodic maintenance to control the deterioration is thus largely dependent on the time of initiation of distress. Hence the prediction of that time is an important component of pavement management systems and models for the economic evaluation of road maintenance policies and pricing policies. That distress does not occur instantaneously over the entire length of roads under like conditions is also important because the needs for maintenance expenditure are thereby spread over time. Considerable attention was therefore devoted to the modeling of pavement distress from field data in recent World Bank studies *(1,2)*, and in particular to the joint effects of traffic and aging because these influence the allocation of road damage costs between users and society.

The procedure described is a statistical method for estimating empirical prediction models from pavement condition data. The method, based on failure-time theory, incorporates the stochastic variations of pavement behavior and represents the concurrent effects of traffic-related fatigue and time-related aging, which can vary considerably from region to region. The method was developed because the variability evident in real pavement data and the fact that the time of appearance of distress usually cannot be observed on all sections within a finite study period were hindering the analysis of cracking and raveling data from a major United Nations Development Program road costs study in Brazil *(3)*.

One example from the World Bank's analysis of this study *(2)* is given to illustrate the procedure, and guidance is given on its application to other regions.

W. D. O. Paterson, Transportation Department, The World Bank, 1818 H St., N.W., Washington, D.C. 20433. A. D. Chesher, Department of Economics, University of Bristol, Bristol, England.

TRAFFIC AND AGE-RELATED MECHANISMS

Traffic-related cracking occurs through fatigue of bituminous surfacing materials under repeated wheel-load applications. The occurrence of failure, here defined as the first visible crack, is commonly expressed in terms of the cumulative number of load applications and is related to the tensile strains induced in the surfacing under the spectrum of mixed wheel loadings and to the material properties, primarily mixture stiffness and the volume of bituminous binder, by the following general expression:

$$N_f = K \cdot \varepsilon_t^{-n} \quad (1)$$

where

N_f = number of repetitions of load in flexure under strain control to the initiation of fatigue cracking;
ε_t = maximum horizontal tensile strain; and
K, n = estimated constants (values vary with materials and test conditions, but typically n increases from 3 to 7 as the material stiffness increases from soft to stiff or brittle).

The strains induced in the surfacing depend primarily on the tire contact pressure (and on wheel load in the case of thick surfacings), the thickness and stiffness of the surfacing layer, and the stiffness of the underlying pavement. Laboratory testing has indicated considerable stochastic variation in failure lives, which range typically over an order of magnitude or by a factor of three each side of the mean, under controlled conditions.

Due to exposure to air, a bituminous binder hardens over time primarily by oxidation, which consequently reduces the

fatigue life of the surfacing material. The rate at which this occurs depends on the oxidation resistance of the binder, which varies with the chemical composition and source of crude; on temperature; and on the film thickness, which determines the length of the oxidation path *(4)*. Hardening rates therefore vary with binder source, climate, and material design. Dickinson *(4)* has observed that cracking usually occurs when a binder reaches a critical viscosity at which the binder can no longer sustain the low strain levels associated with daily thermal movements and fracture occurs. By that stage the surfacing is typically 9 years old although, depending on the composition of the binder, the age may range between 6 and 15 years. This cracking by "aging" usually takes the form of irregular or "map" cracking with a spacing greater than 0.5 m and is likely to progress rapidly over the full area of surface. Raveling can also occur at this viscosity through fracture of the binder film on individual particles.

Thus the interaction of oxidation with traffic-related fatigue advances the time at which fracture occurs in all bituminous-surfaced pavements. This interactive effect may be depicted conceptually as is done in Figure 1. The fatigue life of the surfacing (in logarithm of load repetitions), shown by Curve A for the exposed surface and Curve B for the underside, decreases as the surfacing ages due to oxidation. Curve A is initially highest because lower strains are induced at the surface, but oxidation reduces the life at the exposed surface more rapidly than at the underside, as shown. Under high traffic volumes, shown as Curve C, traffic-related fatigue causes cracking first (at 4.5 years in the example), and, depending on the relative disposition of Curves A and B, initiation of cracking may occur either at the surface (as shown) or at the underside. Under very low traffic volumes, or on stiff pavements, Curve C may be lower than Curve D so that initial fracture may be attributable primarily to the age-related mechanism.

The relative influences of traffic and aging are therefore likely to vary considerably across pavements that have different surfacings, materials, and traffic and also across climates, because these factors influence the relative position of the functions shown. Empirical models must represent such interaction and be adaptable, through parameterization or calibration, to other conditions.

FAILURE-TIME THEORY

Concepts

The initiation of distress such as cracking is a discrete but highly variable event. That is, cracking will occur at different times at various locations along a nominally homogeneous road. The first of these times is termed the initiation of cracking. Another pavement of nominally identical properties and traffic will have initiation at a different time (T_i), where i indexes the pavement section.

The time (T_i) or age of the surfacing at "failure" (here defined as the appearance of distress) thus varies in the real world, even under nominally identical conditions. This can be represented by a probability density function [f(t)] as shown by a hypothetical example in Figure 2. In the function drawn, the first crack is unlikely to appear within "A" years of surfacing construction and is nearly certain to appear before the surfacing is "B" years old. On about one-half of all identical pavements, the first crack is likely to have appeared within "C" years. The probability or chance that the pavement will not have cracked by a certain age is represented by the survivor function [$\bar{F}(t)$] in Figure 2*b*. The location of the functions along the time axis and their shapes can be expected to depend on the properties of the pavement and the intensity of traffic and loading stresses to which it is subjected.

In some instances, when modeling fatigue cracking, it may be desirable to use cumulative traffic (for example the log-

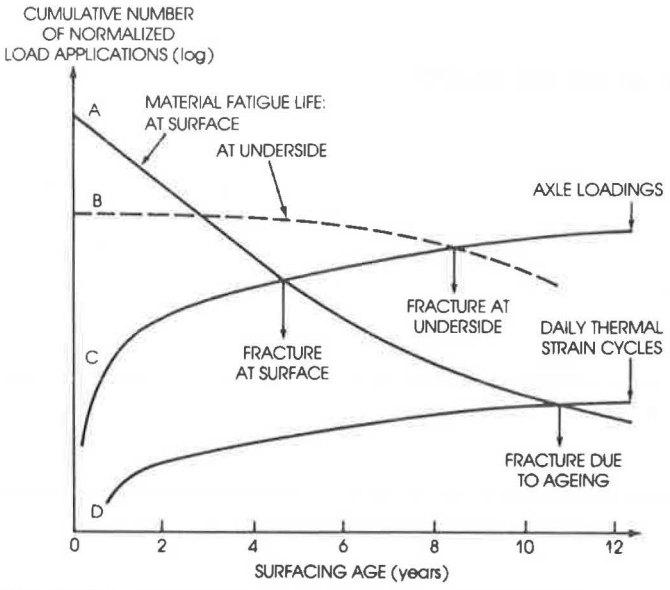

FIGURE 1 Interaction between traffic-related and aging-related fatigue that causes cracking in bituminous surfacings.

arithm of cumulative equivalent standard axles) in place of chronological time, but the modeling principles are similar for both cases. In general, time is the most convenient unit for planning models and is used in the argument that follows.

Because data collection surveys are typically of limited duration, in addition to the considerable variability in failure times, there is the difficulty of unobserved failure events in a typical set of pavement condition data. Among a uniform cross section of pavements with a range of different ages, strengths, and traffic loadings, some of the pavements will have already been cracked on the first survey date, some will begin to crack during the survey period, and on others cracking will begin

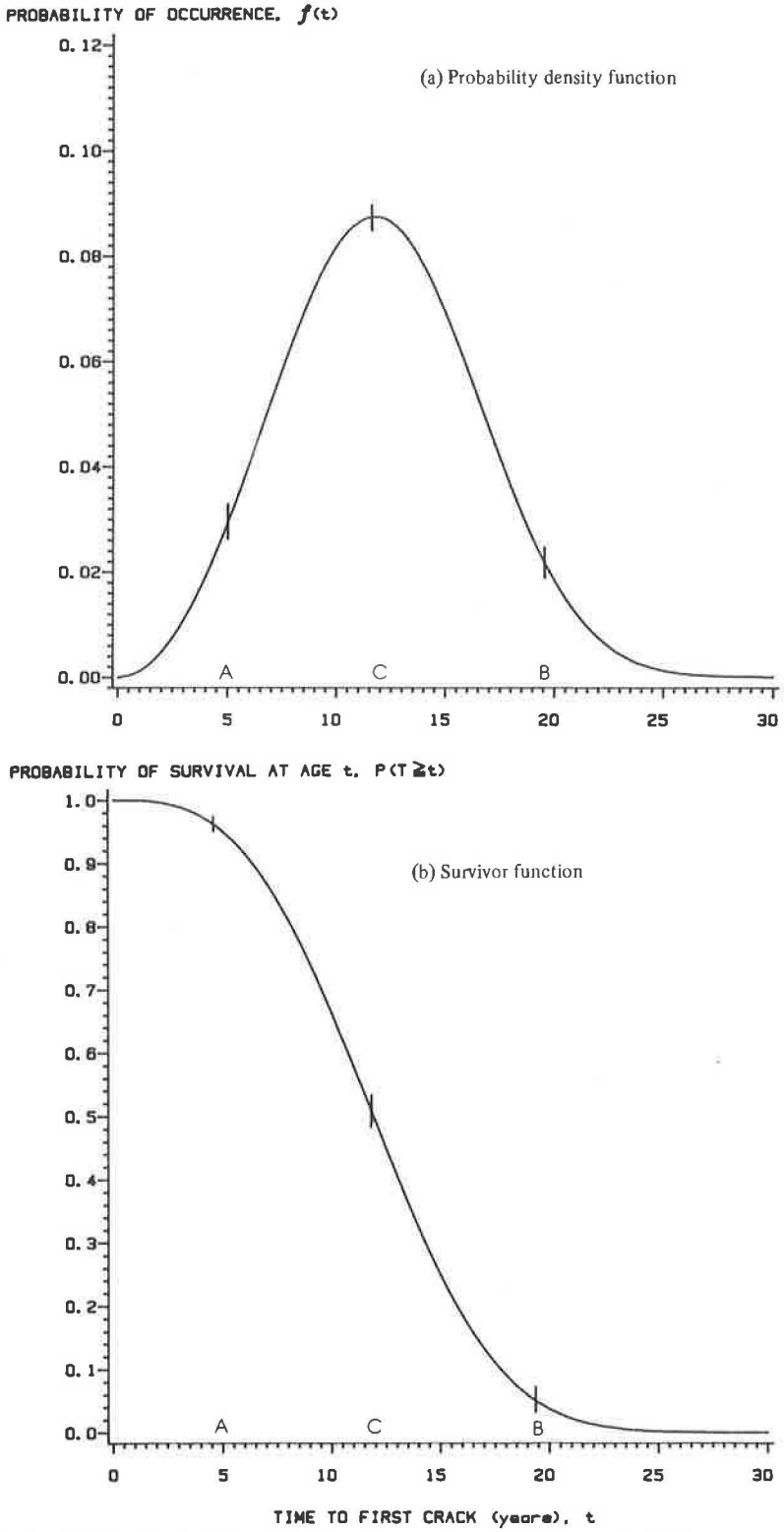

FIGURE 2 Variability of failure times represented by probability density and survivor functions of time to first distress.

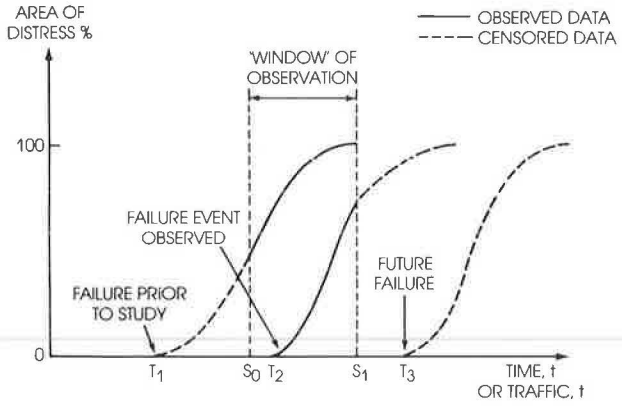

FIGURE 3 Unobserved or censored data on distress initiation and progression: example of three pavement sections with prior, observed, and future failure events, respectively.

only after the end of the survey, as shown in Figure 3. If only the cracking initiation events observed during the survey were included in a statistical analysis, important information about the stochastic and mechanistic properties of the phenomenon coming from the "before" and "after" events might be excluded and thus cause a bias in the model. These latter events, known as "censored data," can be of vital importance particularly in representing long-life pavements in an analysis.

Both features, stochastic variations and censored data, were addressed by developing an estimation procedure based on the principles of failure-time analysis, originally developed to study the reliability of industrial components. The procedure uses the statistical method of maximum likelihood estimation to exploit both censored and uncensored data, as described in the following section, and a flexible distribution that enables the variability of failure times to be determined by the data, as outlined in the succeeding section.

Censored Data: Maximum Likelihood Estimation

T is defined as the time from construction of a section of surfacing to failure, where T is a random variable indexed by i, a section identifier to indicate that the distribution of T depends on section characteristics. The term "failure" is used to describe the first appearance of the mode of pavement distress that is of interest, for example, narrow cracking, wide cracking, or raveling.

T is regarded as a continuous nonnegative random variable and its probability density function is denoted by f(t), its distribution function by F(t), and its survivor function by $\bar{F}(t) = P(T > t) = 1 - F(t)$ (see Figure 2).

Suppose a road section is selected at random, initially observed S_0 years after surfacing, and finally observed $S_1 > S_0$ years after surfacing. One and only one of the following events may be observed:

- $T < S_0$: failure occurred before the road was observed. In this case define $D_1 = 1$, otherwise define $D_1 = 0$.
- $S_0 \leq T \leq S_1$: failure occurred while the road was observed. In this case define $D_2 = 1$, otherwise define $D_2 = 0$. Let z be the observed value of T.
- $S_1 < T$: failure occurred after the road was observed. In this case define $D_3 = 1$, otherwise define $D_3 = 0$.

Let

$$t = S_0 \text{ if } D_1 = 1,$$
$$= z \text{ if } D_2 = 1, \text{ and}$$
$$= S_1 \text{ if } D_3 = 1.$$

By selecting a road at random, values are obtained for D_1, D_2, D_3, and t.

To exploit data on all sections it is necessary to develop a maximum likelihood estimator. Accordingly, consider the joint probability–probability density function of the discrete D_1, D_2, and D_3 and the continuous t.

Standard probability theory gives D_1, D_2, and D_3 as multinomially distributed with $P(D_1 = 1) = F(S_0)$, $P(D_2 = 1) = F(S_1) - F(S_0)$, and $P(D_3 = 1) = \bar{F}(S_1)$. Conditional on $D_1 = 1$ or $D_3 = 1$, t is either S_0 or S_1 with probability 1 in each case. Conditional on $D_2 = 1$, t has the truncated probability density function $f(t)/[F(S_1) - F(S_0)]$. Multiplying marginal and conditional probabilities gives

$$P(D_1 \cap D_2 \cap D_3 \cap t) = F(S_0)^{D_1} \; f(t)^{D_2} \; \bar{F}(S_1)^{D_3}$$
$$= F(t)^{D_1} \; f(t)^{D_2} \; \bar{F}(t)^{D_3} \qquad (2)$$

Now write f(t) as a conditional failure time probability density function, depending on section characteristics x and parameters θ. Then

$$P(D_1 \cap D_2 \cap D_3 \cap t \mid x, \theta) = F(t \mid x, \theta)^{D_1} \; f(t \mid x, \theta)^{D_2} \; \bar{F}(T \mid x, \theta)^{D_3} \qquad (3)$$

Estimation of θ can be achieved by calculating the maximum likelihood estimator. Index t and x by i, which distinguishes sections. Then the probability–probability density function of the observed D_i's, t_i's $\boldsymbol{D}$, and $\boldsymbol{t}$, given the x's, $\boldsymbol{x}$, and θ, is

$$P(\boldsymbol{D} \cap \boldsymbol{t} \mid \boldsymbol{x}, \theta) = \prod_{i=1}^{n} F(t_i \mid x_i, \theta)^{D_{1i}} \; f(t_i \mid x_i, \theta)^{D_{2i}} \; \bar{F}(t_i \mid x_i, \theta)^{D_{3i}} \qquad (4)$$

By taking logs, Equation 5, the log-likelihood function, is obtained. The maximum likelihood estimator ($\hat{\theta}$) is that value of θ which maximizes Equation 5. $\hat{\theta}$ must be obtained using numerical methods. Under fairly general conditions $\hat{\theta}$ is consistent and efficient. The variance-covariance matrix of $\hat{\theta}$ is estimated by minus the inverse of the Hessian of Equation 5 at $\theta = \hat{\theta}$. See Rao *(5)* or Theil *(6)* for further details of the properties of $\hat{\theta}$.

$$L(\theta \mid \boldsymbol{D}, \boldsymbol{t}, \boldsymbol{x}) = \sum_{i=1}^{n} \{D_{1i} \log F(t_i \mid x_i, \theta) + D_{2i} \log f(t_i \mid x_i, \theta) + D_{3i} \log \bar{F}(t_i \mid x_i, \theta)\} \qquad (5)$$

The log-likelihood function of Equation 5 is maximized by

some variant of the Newton-Raphson procedure. A program was developed that maximizes Equation 5 either by Newton-Raphson as modified by Berndt et al. *(7)* or by steepest ascent.

The Berndt et al. modification of the Newton-Raphson procedure makes use of the identity:

$$E(n^{-1}\delta^2 L/\delta\theta\delta\theta') = -E[n^{-1}(\delta L/\delta\theta)(\delta L/\delta\theta')] \quad (6)$$

so that the matrix of second derivatives

$$E(\delta^2 L/\delta\theta\delta\theta')$$

is estimated by the approximation

$$-n^{-1}\sum_{i=1}^{n}(\delta L_i/\delta\theta)(\delta L_i/\delta\theta')$$

where $(\delta L_i/\delta\theta)$ is the ith term in the summation

$$(\delta L/\delta\theta) = \sum_{i=1}^{n}(\delta L_i/\delta\theta).$$

The program uses analytic expressions for first derivatives of the log-likelihood function. At the termination of the optimization the Hessian associated with the log-likelihood function is calculated by differencing the analytic first derivative vector. Eigenvalues are calculated to check on the definiteness of the Hessian and the Hessian is then inverted to obtain estimates of asymptotic variances and covariances of estimated coefficients. Various predictions are provided for each observation so that the equivalent of residuals can be examined. The program will calculate asymptotic confidence intervals around predictions and provide various graph plots if required.

Asymptotic confidence intervals for expected failure times are provided by exploiting the local large sample linearity of the expression for expected failure time given pavement characteristics and computing the asymptotic variance of the resulting linear approximation; 1.96 times the square root of this variance is then added to and subtracted from the predicted expected failure time to give the required interval.

Starting values for the parameters are provided automatically, but there is provision for using a manual start if required. The program is written in SAS's matrix procedure *(8)*.

Variability of Failure Times

The underlying variation of failure times was assumed in the failure-time model to follow a Weibull distribution [for which general statistical results may be found in Chapter 20, Vol. 1 of Johnson and Kotz *(9)*]. A log normal distribution is also available in the program, but the Weibull distribution was considered the most representative of the joint mechanisms of fatigue and aging for the following reasons.

The time to failure of a section is the first failure to occur among all individual elements of the surfacing, where each fails at a time following some probability law, as shown in Figure 4*a*. The Weibull distribution, a Type-3 extreme value distribution, is suitable for determining the minimum (or limiting distribution) of a series of minima (that is the failure times).

The mechanisms of fatigue under traffic and oxidation, which reduce the available fatigue life, work concurrently, and

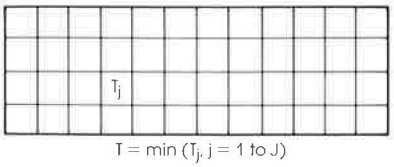

(a) Cracking initiation in a nominally homogeneous section represented by elements over which pavement properties are randomly distributed. Failure occurs at the minimum of the failure times of all elements

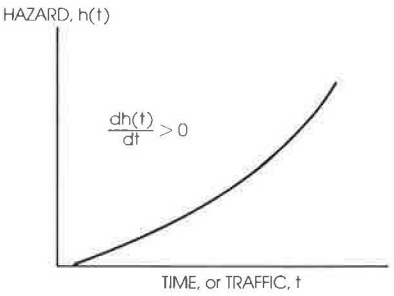

(b) Fatigue is a hazard which increases monotonically with time or with cumulative number of axle transits (we expect $\beta > 0$)

FIGURE 4 Two hypotheses on the probability of occurrence of crack initiation that indicate a Weibull distribution of failure times.

thus the probability of cracking occurring in the surfacing is expected to increase as the pavement ages. For example, the chances that a pavement will crack in its 15th year, if it has not already cracked by that time, are considered greater than the chances of its cracking in, say, the previous year. This can be described as an increasing "hazard" of cracking. The hazard function [h(t)], a concept used in reliability theory, is proportional to the probability that failure will occur in a short time interval at time t given that it has not occurred previously. It is defined by

$$h(t) = [f(t)/1 - F(t)] = [f(t)/\bar{F}(t)] \quad (7)$$

where

$f(t)$ = probability density function associated with T;
$F(t)$ = probability distribution function, = $P(T \leq t)$; and
$\bar{F}(t)$ = $P(T \geq t)$.

To model fatigue, therefore, the hazard is expected to be an increasing function of time as shown in Figure 4*b*. When the hazard is specified by

$$h(t) = \alpha^{-\beta} t^{\beta-1} \quad \alpha, t \geq 0 \text{ and } \beta > 1 \quad (8)$$

the probability distribution function is defined by

$$F(t) = 1 - \exp[-(1/\beta)\alpha^{-\beta} t^{\beta}] \quad (9)$$

where

α = function of the variables causing failure,

β = curvature of hazard function, and
t = time (or cumulative traffic).

This is the distribution function associated with a Weibull distribution, describing a positively skewed distribution over the nonnegative real axis. The expected, or mean, time to failure [E(T)] is given by

$$E(T) = \alpha B(\beta) \quad (10)$$

where $B(\beta)$ is a constant function of β given by

$$B(\beta) = \beta^{(1-\beta)}/\beta\ \Gamma(1/\beta)$$

and selected values for $B(\beta)$ are as given in Table 1.

The selection of the type of distribution is important because results are sensitive to it when many of the data have censored values. The Weibull distribution appears to be appropriate for representing the variability of failures for the two conceptual reasons just outlined. It also is flexible because it describes a family of skewed curves for different values of β and α that appear to be realistic for pavement data, as shown in Figure 5. The β parameter determines the shape of the distribution, which becomes narrower as β increases. The α parameter is a scaling function that locates the distribution along the time axis. Because both the β and α parameter values are estimated from the observed data, and neither is fixed, the Weibull model is particularly adaptable to actual circumstances.

The objective of the estimation is not only to determine the average time to failure and its distribution but also to estimate how the expected time to failure depends on pavement and traffic characteristics. These are represented in the α parameter of the model that must be nonnegative. Although other forms could be used, α here was defined by the vector

$$\alpha = \exp [X' \gamma]$$
$$= \exp (\gamma_0 + \gamma_1 x_1 + \gamma_2 x_2 + \gamma_3 x_3 \ldots) \quad (11)$$

where γ is the vector of coefficients γ_i and X is the vector of parameters (pavement strength, traffic flow, etc.).

Given various pavement, traffic, and environmental parameters (x_i), the model estimates the coefficients (γ_i) and the shape parameter (β), which is assumed constant for all pavements within the data set.

The mean time to failure [E(T) from Equation 10] can be used directly in road deterioration predictions in the same way as the mean time from a deterministic model. In practice, the prediction of the expected time to failure took the following simple form:

$$E(T) = B(\beta) \exp [\gamma_0 + \gamma_1 x_1 + \gamma_2 x_2 \ldots] \quad (12)$$

The probability with which failure might occur at some time other than the expected time derives from the value of β, shown for example in the family of probability functions generated by different values of β in Figure 5. At low values of β, say below 2.5, the distributions tend to be widely dispersed and highly skewed with more than half of the observations having values less than the mean but with a number of very late failures. At high values of β, the distributions tend to be more concentrated and centered about the mean.

In general, the failure time (T_p) associated with any probability, $p = P[T \leq T_p]$, can be related directly to the mean E(T) by

$$T_p = K(p) \cdot E(T) \quad (13)$$

where $K(p) = [-\beta\ ln(1-p)]^{1/\beta}/B(\beta) \cdot K(p)$ is thus a constant function of β, and values for selected values of probability p are given in Table 1. For example, the median time [M(T)] and lower quartile time [$T_{0.25}$] to failure are given by

$$M(T) = K(0.5)\ E(T) \quad (14a)$$

$$T_{0.25} = K(0.25)\ E(T) \quad (14b)$$

TABLE 1 CONSTANTS DESCRIBING A WEIBULL DISTRIBUTION OF FAILURE TIMES: FUNCTION B AND FACTORS K(p) OF EXPECTED FAILURE TIME E(T) FOR SELECTED PROBABILITIES (p) AND VALUES OF β

BETA	B	SIQF	K05	K10	K25	K50	K75	K90	K95
1.0	1.000	0.549	0.051	0.105	0.288	0.693	1.386	2.303	2.996
1.5	1.183	0.447	0.153	0.247	0.483	0.868	1.377	1.932	2.302
2.0	1.253	0.362	0.256	0.366	0.605	0.939	1.329	1.712	1.953
2.5	1.280	0.300	0.344	0.458	0.685	0.973	1.284	1.573	1.748
3.0	1.288	0.255	0.416	0.529	0.739	0.991	1.249	1.479	1.614
3.5	1.287	0.221	0.476	0.584	0.779	1.001	1.220	1.410	1.521
4.0	1.282	0.195	0.525	0.629	0.808	1.007	1.197	1.359	1.451
4.5	1.275	0.174	0.566	0.665	0.831	1.010	1.178	1.319	1.398
5.0	1.267	0.157	0.601	0.694	0.849	1.012	1.163	1.287	1.356
6.0	1.251	0.131	0.657	0.741	0.876	1.014	1.138	1.239	1.294
7.0	1.235	0.113	0.699	0.775	0.895	1.014	1.120	1.204	1.250
8.0	1.221	0.099	0.733	0.801	0.909	1.014	1.106	1.179	1.218
9.0	1.209	0.088	0.759	0.822	0.919	1.014	1.095	1.159	1.193
10.0	1.198	0.079	0.781	0.839	0.928	1.013	1.086	1.143	1.173
15.0	1.157	0.053	0.850	0.891	0.953	1.011	1.058	1.095	1.114
20.0	1.131	0.039	0.885	0.918	0.965	1.009	1.044	1.071	1.085
25.0	1.113	0.032	0.908	0.934	0.972	1.007	1.035	1.057	1.068
30.0	1.100	0.026	0.923	0.945	0.977	1.006	1.030	1.047	1.056

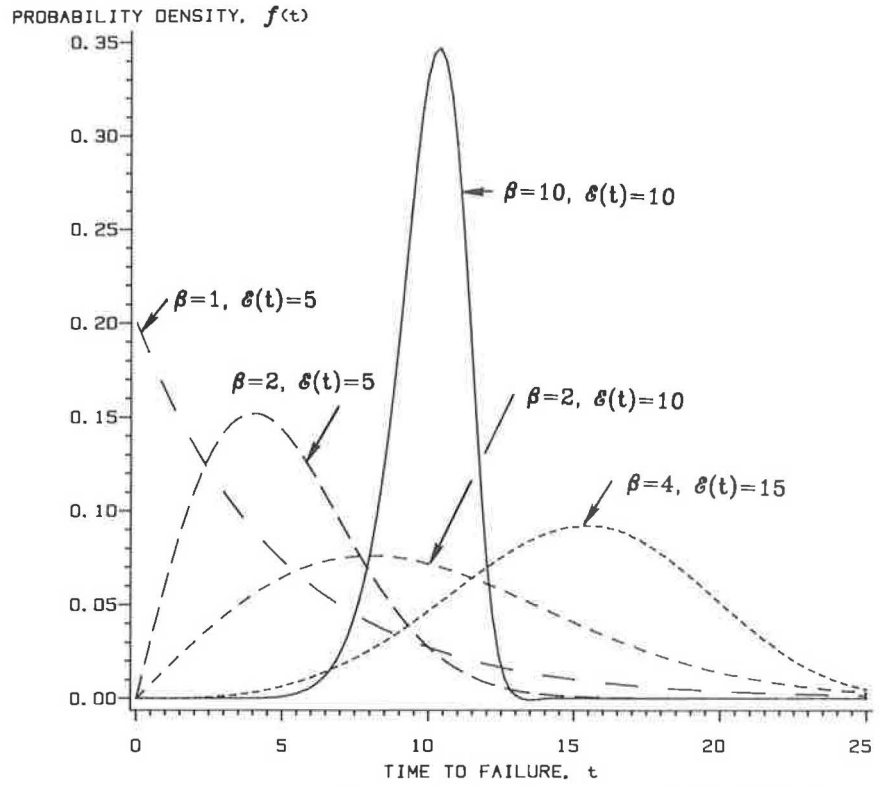

FIGURE 5 Family of probability density functions represented by Weibull distribution of time to failure.

For practical purposes, the width of dispersion is most simply described by the spread of time between two specific probabilities, usually the quartiles. For convenience the semi-interquartile factor (SIQF) is defined to represent the age range between 25 percent and 75 percent failure probabilities, that is the range within which about 50 percent of the pavements may be expected to fail [i.e., (1 ± SIQF) E(T)] where

$$\text{SIQF} = (1/2)\,[K(0.75) - K(0.25)] \qquad (15)$$

Goodness of Fit

The goodness of fit of probabilistic models requires special interpretation because two components are present: the probability of failure occurring by the estimated time and the error of estimate.

First, note that whereas the traditional measures of goodness of fit indicate what proportion of the variation in the dependent variable can be accounted for by variation in the independent variables, in the failure-time models there is an upper bound on this proportion. In principle, the exact time to failure is not predictable because the failure time is a random variable with distributed, positive values; thus R^2 and similar measures can never approach unity. The model explains the variation of failure times that can be attributed to pavement and traffic characteristics, but further than that the influence of chance ensures that 100 identical pavements will crack at 100 different times. No model explains the latter variation, but the Weibull model predicts that it exists and estimates the shape of its distribution through the β parameter. This is typified by the SIQF defined in Equation 15.

Second, the value of log-likelihood (LL) that is maximized in the estimation is not a dimensionless proportion like R^2; its value varies with the magnitude of the dependent variable and with the number of observations, so that it is meaningless to compare LL-values across models or groups of models (except where identical sets of dependent variables are involved). When the dependent variable is of a fixed dimension, it is useful to define an average log-likelihood (LL divided by the number of observations) as a normalized measure of goodness of fit across models having different numbers of observations within the same data set.

Third, because the model used here is not a linear regression model there is no obvious equivalent of the conventionally reported "standard error." To assess the predictive power of the model, confidence intervals (with asymptotic validity) around predicted expected failure times were calculated as described earlier. Because the size of the interval depends in part on the error of estimate of the parameter coefficient, it also varies with the values of the pavement parameters. Thus the intervals do not form a locus of the expected time to failure but instead form loci of the explanatory parameters. As a practical measure, it is possible to compute an "average confidence interval," which is the arithmetic average of the estimated 95th percentile confidence intervals of all observations expressed in units of the dependent variable, for example, ± 1.2 years. Although this is not a precise statistic, it provides a meaningful estimate of the intervals to be expected given the observed ranges of explanatory variables.

Finally, assessing the adequacy of models for censored data remains an open research question, which has recently been addressed by Chesher et al. *(10)*, for example. Future applications of the procedure should consider these developments. In this instance the three practical measures noted previously were used:

- Goodness of fit: average log-likelihood value (for internal best fit for given data set and dependent variable);
- Predictive power: average 95th percentile confidence intervals (average for given data set); and
- Stochastic variation: SIQF; for example, a value of SIQF = 0.36 for $\beta = 2.0$ indicates a fairly wide dispersion, and a value of 0.09 for $\beta = 10$ indicates a very narrow dispersion (meaning that like roads will fail at very similar times).

PRACTICAL APPLICATION

Initiation of Cracking in Surface Treatments

To illustrate the application of the procedure, the empirical estimation of cracking initiation in double surface treatment (DST) (or chip seal) surfacings from data collected in the Brazil Road Costs Study *(3)* is used. The method was applied extensively in analysis of these data as described in full for this and other surface types in Paterson *(2)*; these models have been incorporated in the World Bank Highway Design and Maintenance Model *(1)* for economic evaluation of highway projects and policies.

Observations of initiation of cracking were taken from time-series pavement condition survey data over a 5-year period on 36 independent test sections with original DST surfacings selected within a factorial experimental matrix of traffic volume, surfacing age, base type, and vertical geometry. Initiation of cracking was defined by the occurrence of crocodile cracking of 1 to 3 mm width covering not more than 5 and not less than 0.5 percent of the surfacing area of a subsection. Of the total 102 subsection observations, there were 72 independent traffic-section combinations. The chip seal DST generally had a 14- to 19-mm stone size in the first seal and a 7- to 10-mm size in the second seal. Other characteristics are given in Table 2.

As might be expected for a representative sample of a road network in any given time "window," the actual event of cracking initiation was observed on only 35 of the 102 subsections; 10 had cracked earlier, and the remainder were still uncracked at the date of the last survey. Conventional least squares estimation techniques would therefore have had to exclude two-thirds of the data and operate on only the observed events, whereas all observations could be used in the failure-time estimation procedure.

The surfacing lives observed in the study are shown in Figure 6; symbols are used to indicate whether the initiation occurred before, during, or after the study. The symbol "0" indicates that initiation occurred earlier than, that is below, the point indicated; the symbol "❑" indicates an observed initiation; and the symbol "+" indicates that the initiation occurred later than, that is above, the point indicated. A general tendency for the surfacing life to decrease as the annual volume of traffic loading increases can be seen in Figure 6*a*, although there are a number of exceptions and in particular one group of observations has lives longer than 17 years. When the life is expressed in classical fatigue terms of the cumulative number of 80-kN equivalent single axle loads (ESALs) to cracking initiation, as shown in Figure 6*b*, it can be seen that shorter lives are usually associated with higher pavement deflections, but again there are several exceptions and considerable scatter.

Model estimations were made on the data using the failure-time procedure. When time to failure was used as the dependent variable, traffic effects were represented by the rate of trafficking (that is the annual volume per lane) normalized to the average rate over the first 8 years of service in order to avoid the collinearity that occurs between age and traffic volume due to annual traffic growth (old pavements usually carry a higher volume now than when they were new). When cumulative ESALs to failure was the dependent variable, the rate of aging was represented by the inverse of traffic flow (e.g., years per million axles). Benkelman beam deflection, modified structural number, base type and California bearing

TABLE 2 DATA CHARACTERISTICS OF CRACKING INITIATION IN SURFACE TREATMENT SURFACINGS IN BRAZIL ROAD COSTS STUDY

Parameter	Units	Range of Values
Surfacing age	Year	2.7-21
Cumulative loading	Million ESALs/lane	0.005-5.16
Traffic volume (two way)	Vehicles/day	100-2,300
Traffic loading	Million ESALs/lane/year	0.001-0.24
Deflection (Benkelman 80 kN)	mm	0.26-2.02
Modified structural no.		2.93-5.15
Base course CBR	%	32-143
Resilient modulus of surfacing at 30°C (4/36)	GPa	1.6-2.7
No. of sections		36
No. of subsections		102
No. with prior cracking		10
No. observed to crack		35
No. with future cracking		57

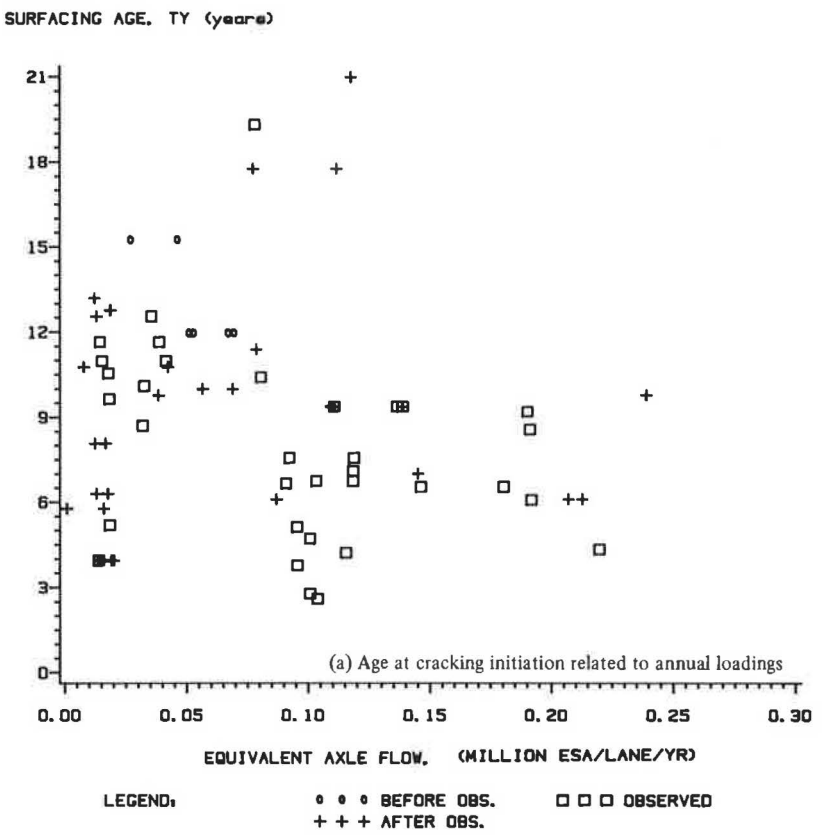

(a) Age at cracking initiation related to annual loadings

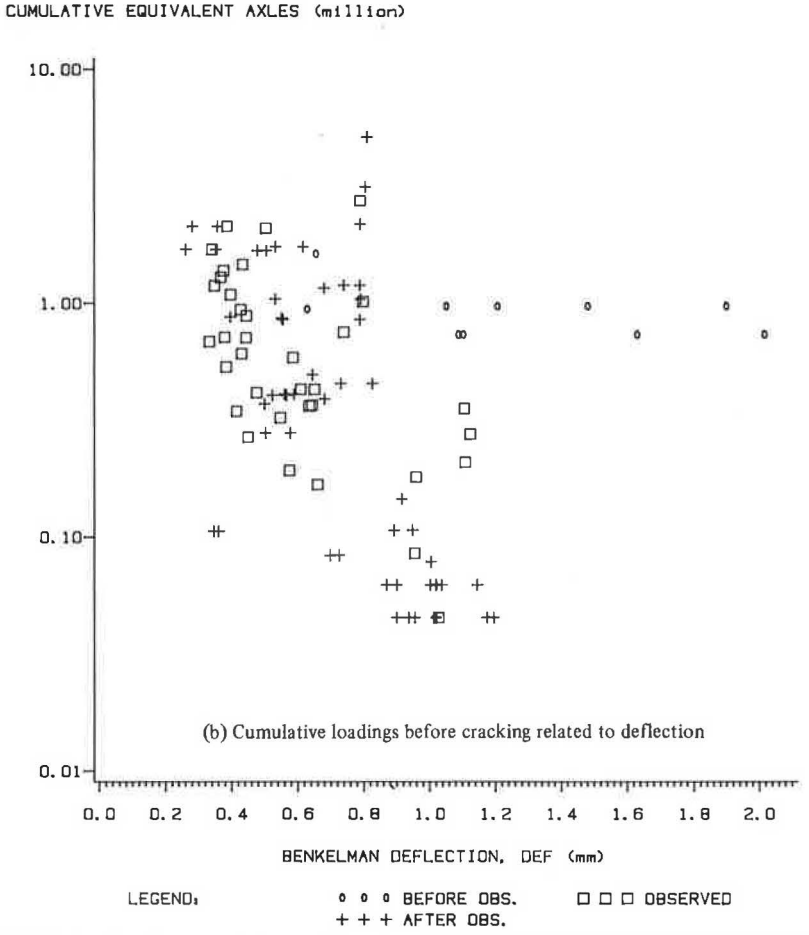

(b) Cumulative loadings before cracking related to deflection

FIGURE 6 Observed lives of double surface treatment surfacings in Brazil as functions of traffic and pavement deflection.

ratio (CBR), construction quality, monthly rainfall, traffic volume (with and without load effects given by ESALs), and surfacing thickness were used as explanatory variables.

The selection of the final models was based on the best statistical fit, as defined by the maximum log-likelihood value and minimum interquartile probability range, and on whether the predictions were reasonable over the range of estimation and beyond. The two with widest application are as follows:

1. $E(T) = 13.2 \exp [-24.3 (1 + CQ) YE2/SNC^2]$ (16)

SIQF = 0.295
Average 95 percent confidence interval = 1.73 years
Average maximum likelihood = –1.27
$\beta = 2.54$

2. $E(T) = 13.6 \exp [-3.19 (1 + CQ) YE2 DEF]$ (17)

SIQF = 0.305
Average 95 percent confidence interval = 1.73 years
Average maximum likelihood = –1.27
$\beta = 2.47$

where

- E(T) = expected age of surfacing at initiation of narrow crocodile cracking (1 to 3 mm in width), in years;
- YE2 = annual volume of equivalent 80-kN single axles computed with a relative damage power of 2, in million ESALs per lane per year;
- SNC = modified structural number of pavement strength including subgrade contribution [see Paterson *(2)*];
- DEF = pavement surface deflection by Benkelman beam under 80-kN axle load, in mm; and
- CQ = construction quality factor (= 0 for good quality, = 1 when original construction was faulty).

The goodness of fit of the prediction for Model 1, shown in Figure 7, is reasonable but not excellent, reflecting both the large amount of stochastic variation that is observed under real conditions and the difficulties in explaining all of the diverse contributory factors that cause cracking in thin surfacings by practicable measures. The surfacing lives predicted by Equation 16 for a range of pavement strengths and traffic loadings are shown in Figure 8. This shows that the life decreases as the traffic-loading volume increases but at a rate that decreases as the pavement strength (or stiffness) increases. The focal point at an age of 13.2 years represents the effect of aging and oxidation under very low-volume traffic. This point is likely to vary from region to region with the various factors that influence the oxidation rate of the binder, as mentioned earlier.

The variability of cracking failure times due to chance, that is, most of the variance that could not be explained by physical parameters, amounted to a distribution in which half of the

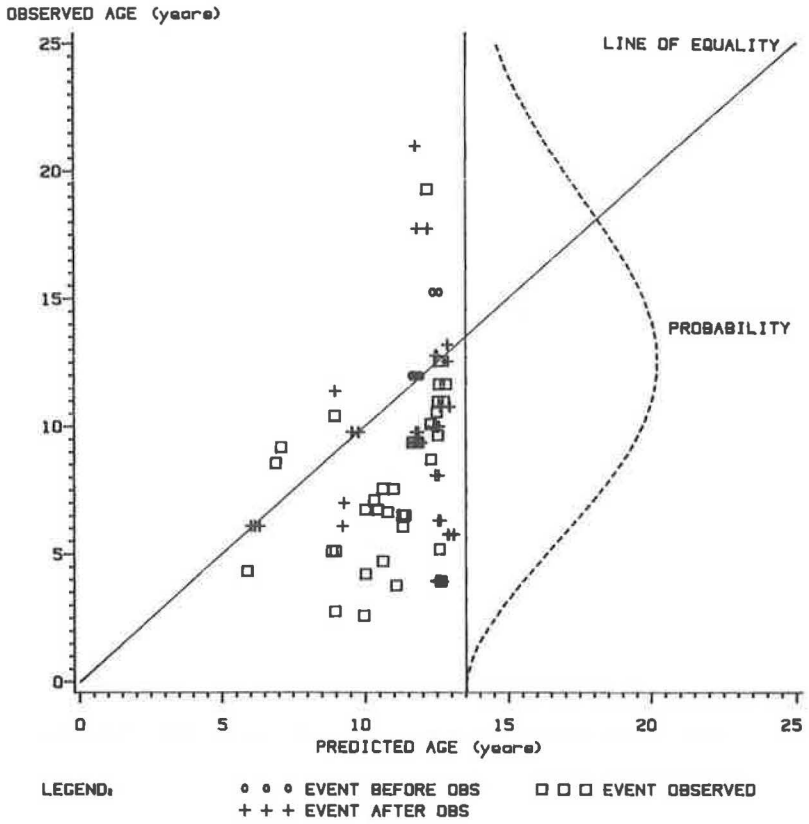

FIGURE 7 Goodness of fit of prediction model for initiation of all cracking for Brazilian data: double surface treatment surfacings on granular base pavements.

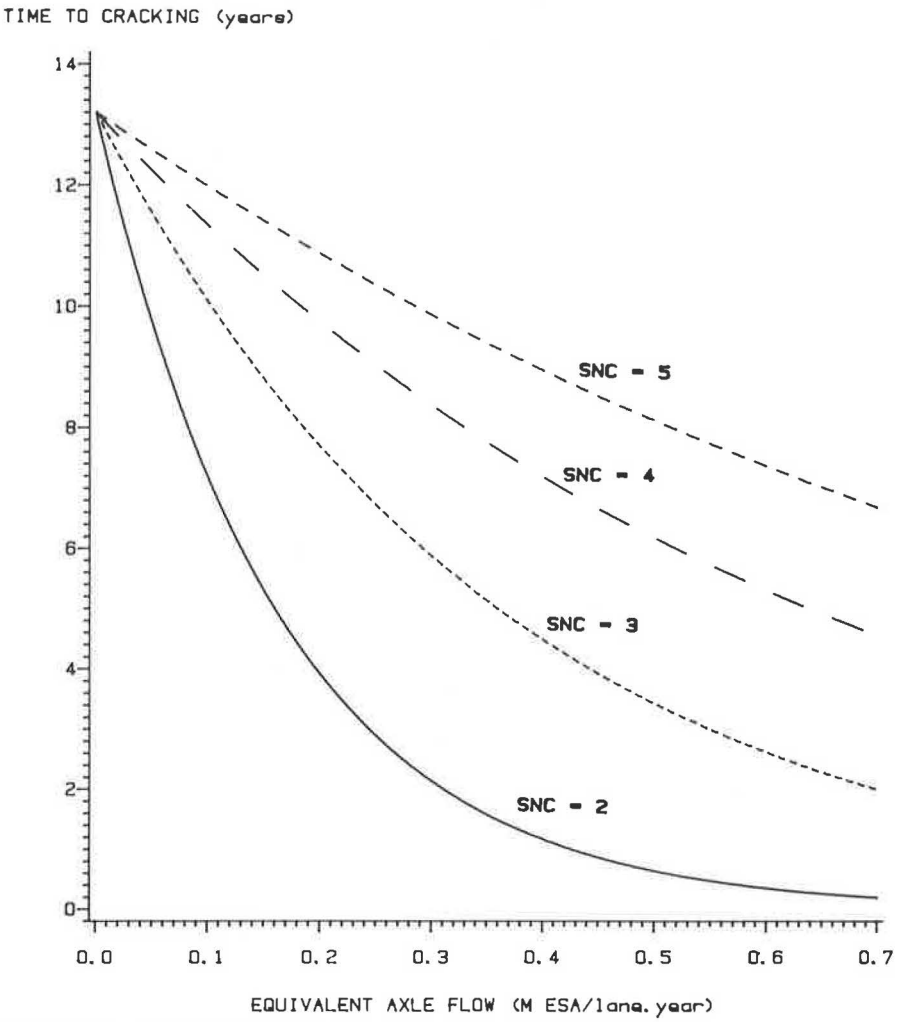

FIGURE 8 Predictions of crack initiation for pavements with original double surface treatment surfacings and granular base in nonfreezing climates.

pavements would fail within ±30 percent of the mean or expected time of failure and the remainder would crack either sooner or later than that range of time. This underlying variability found in the data is shown by the bell curve in Figure 7. This curve is large and graphically illustrates why the empirical analysis of performance data is so difficult.

Calibration or Adaptation of a Model

In a region for which a large, well-structured data set is not available to permit an original estimation of cracking models, it is desirable to calibrate a model such as the present one to satisfy the specific material and climatic conditions of that particular region. In the case presented here, calibration is most effectively achieved by assuming, as a first approximation, that the coefficients of the traffic and pavement parameters are correctly estimated because the function represents an underlying physical mechanism and that it is the aging and oxidation function that most needs to be adapted to local conditions.

On this assumption, calibration can be achieved by assessing the average life of a sample of low-volume pavements in the region and computing an adjustment factor equal to the ratio of the observed low-volume road life ($\bar{T}_L$) to 13.2 years:

$$E(T)' = K_c\, E(T) \tag{18}$$

where

$E(T)'$ = calibrated estimate of failure time for local conditions,
K_c = local adjustment factor = $\bar{T}_L/13.2$, and
$\bar{T}_L$ = average observed age at failure of local surfacings under low traffic volumes.

CONCLUSION

The development of this procedure, based on the principles of failure-time theory, has provided the statistical means for analyzing surface distress data from pavement performance studies or pavement condition data bases with greatly increased scope. Unobserved cracking events (i.e., censored data) that occur outside the period of data collection are taken into account by

the procedure and thus a statistical bias in the results, which might occur were they ignored, is prevented. The underlying variability of failure times due to chance rather than physical properties is quantified by the procedure and the example given shows that the variability can be quite large for cracking failure times. The Weibull distribution chosen for this purpose is highly adapatable to real data and appears to be particularly appropriate to the increasing chance of cracking that occurs as a result of the concurrent effects of fatigue and oxidation.

Although the exposition and example refer to oxidation and aging as the primary time-related mechanism, which was appropriate for the tropical climate of the example application, the model principles apply equally to other time-related environmental mechanisms such as cold-temperature cracking, shrinkage cracking, and so forth.

REFERENCES

1. T. Watanatada, C. G. Harral, W. D. O. Paterson, A. Dhareshwar, A. Bhandari, and K. Tsunokawa. *The Highway Design and Maintenance Model.* 2 Vols. The World Bank, Washington, D.C., 1987, forthcoming.
2. W. D. O. Paterson. *Road Deterioration and Maintenance Effects: Models for Planning and Management.* The World Bank, Washington, D.C., 1987, forthcoming.
3. *Research on the Interrelationships Between Costs of Highway Construction, Maintenance and Utilization (PICR).* Final Report, 12 Vol. Empresa Brasileira de Planejamento de Transportes (GEIPOT), Brasilia, Brazil, 1982.
4. E. J. Dickinson. *Bituminous Roads in Australia.* Australian Road Research Board, Melbourne, Australia, 1984.
5. C. R. Rao. *Linear Statistical Inference and Its Applications.* 2nd ed. John Wiley and Sons, Inc., New York, 1973.
6. H. Theil. *Principles of Econometrics.* John Wiley and Sons, Inc., New York, 1971.
7. E. K. Berndt et al. Estimation and Inference in Nonlinear Structural Models. *Annals of Economic & Social Measurement*, Vol. 3, 1974, pp. 653–665.
8. *SAS Users Guide.* SAS Institute, Inc., Cary, N.C., 1979.
9. N. L. Johnson and S. Kotz. *Continuous Univariate Distributions.* Houghton Mifflin Co., Boston, Vol. 1, 1970.
10. A. D. Chesher, T. Lancaster, and M. Irish. On Detecting the Failure of Distributional Assumptions. Presented at 1985 Summer Workshop of the Econometric Society, Paris, France (forthcoming in Annales de l'Institut National de la Statistique et des Etudes Economiques).

Publication of this paper sponsored by Committee on Flexible Pavements.

Response and Performance of Alternate Launch and Recovery Surfaces that Contain Layers of Stabilized Material

ROBERT R. COSTIGAN AND MARSHALL R. THOMPSON

The purpose of this study was to validate a mechanistic approach to the design and evaluation of alternate launch and recovery surfaces (ALRS) that contain layers of stabilized material. Validation was achieved by relating predicted first-pass structural response parameters to observed performance of field-test items. Eight two-layer rigid pavement test items and one three-layer rigid pavement test item were constructed of cement aggregate mixture layers. Items were subjected to simulated channelized F–4 main gear traffic using a load cart. Moduli of layers of stabilized material were back-calculated from falling weight deflectometer load-deflection data. First-pass predicted structural response was determined using stress-dependent finite element computer programs. The test items were thin by conventional design standards and had predicted first-pass stress ratios greater than one in the stabilized-material layers. Transfer functions were developed to relate predicted first-pass crack tensile stress to passes to functional failure. Major conclusions include *(a)* the mechanistic approach to the design and analysis of ALRS containing stabilized-material layers is valid; *(b)* critical pavement response affecting performance occurs at transverse shrinkage cracks; *(c)* performance is dominated by the thickness of the stabilized layer; and *(d)* ALRS containing stabilized materials require a wearing course on the surface of the stabilized layer to prevent tire abrasion and environmental deterioration.

The U.S. Air Force Engineering and Services Laboratory, Tyndall Air Force Base, Florida, conducts research and development to increase the readiness and survivability of tactical fighter air bases. An effective means of increasing survivability and ensuring that aircraft operations can resume almost immediately after an air attack is the construction of alternate launch and recovery surfaces (ALRS). ALRS are constructed in peacetime for immediate availability after an air attack. Increased surface redundancy greatly complicates the enemy's targeting problems and reduces the probability of achieving a total airfield closure.

Operational plans call for ALRS to be used only in wartime. ALRS must safely support only a few hundred fighter aircraft sorties so the traffic levels will be much less than for normal airfield pavements. The feasibility of the ALRS concept depends on pavements that are inexpensive to build, reliable, and easy to inspect and maintain.

R. R. Costigan, Air Force Engineering and Services Center, Tyndall Air Force Base, Fla. 32403. M. R. Thompson, Department of Civil Engineering, University of Illinois at Urbana-Champaign, Urbana, Ill. 61801.

MECHANISTIC DESIGN

Thompson et al. *(1)* demonstrated the feasibility of a mechanistic design approach for ALRS containing layers of stabilized material. Properties of stabilized material, structural modeling and behavior concepts, and environmental factors were considered in this system. Because ALRS are low-traffic-volume-to-failure airfield pavements, a research program was undertaken to supplement airfield pavement performance data for these low traffic levels. Validation of the mechanistic design concept required relating predicted first-pass structural response parameters (stress, strain, and deflection) with observed field performance of ALRS containing stabilized-material layers at low traffic levels to failure.

FIELD-TEST ITEMS

Eleven 30-ft-long by 12-ft-wide test items (Figures 1 and 2) were constructed at the Waterways Experiment Station (WES), Vicksburg, Mississippi in 1983 *(2)*. The 11 test items were built in two 12-ft-wide lanes. Each lane was excavated 4 ft below grade into the in situ lean clay (CH) at the site.

The CH soil used for the 48-in. subgrade layer was placed in the excavation in 6-in. lifts and compacted to the density required to produce a desired 5 to 6 California bearing ratio (CBR). The subgrade as constructed was quite uniform among the items with field CBRs from 4.4 to 6.5 measured at 0-, 6-, and 12-in. depths and moduli of subgrade reaction (k) from 96 to 121 psi/in.

Items 1 through 8 were cement aggregate mixture (CAM) layer pavements of different strengths and thicknesses. A poorly graded gravelly clayey sand (classified SP–SC) was used for the CAM. The CAM was field mixed offsite on a mixing pad and then placed with a paver in 5- to 6-in. lifts. Difficulties were experienced in compacting the CAM to the desired density on the soft subgrade. Laboratory CE55 maximum dry density with 5 percent cement was 137 pcf at 6 percent optimum moisture content. However, field dry densities were only 117 pcf. Item 11 was similar except that it was surfaced with a 1-in. asphalt concrete wearing course.

CAM cement content and thickness design values for the test items are shown in Figure 2. Design thicknesses were selected to produce functional and structural failures from a few passes to more than 1,000 passes. The constructed thicknesses differed slightly from the design values and constructed thicknesses were used in all structural analyses. Coefficients of variation for constructed thickness ranged from 1.3 to 7.0 percent.

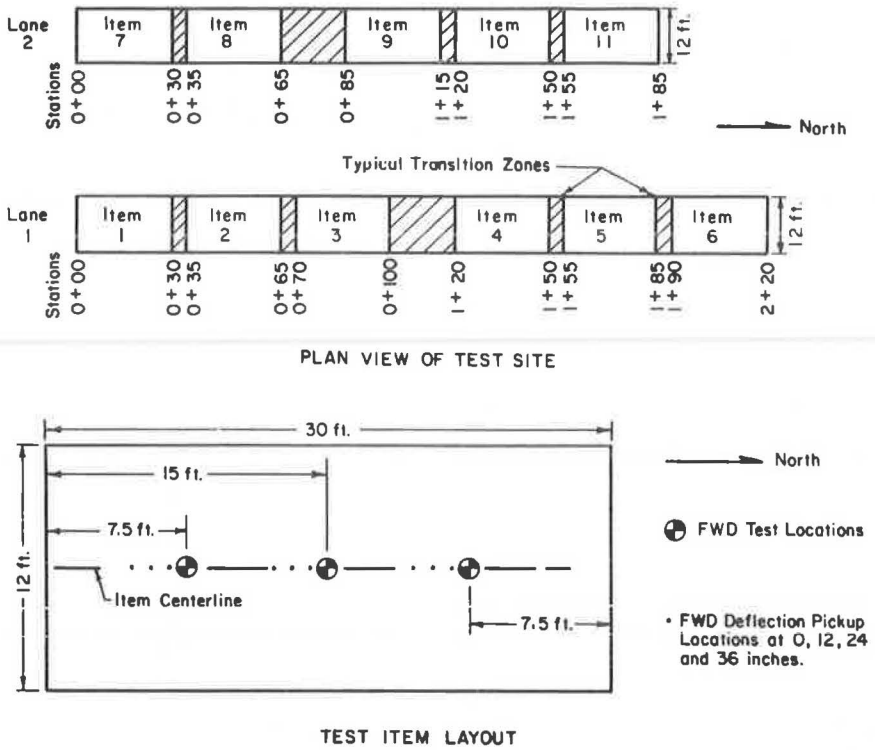

FIGURE 1 ALRS test site layout.

Simulated F–4 aircraft taxi traffic was applied in a single channelized lane down the center of the items using a load cart fitted with an F–4 main gear tire loaded to 27,000 lb and pressurized to 265 psi. Traffic was applied until structural failure or 1,000 passes, whichever occurred first.

Two inverted pavement test items, 9 and 10, were also built. These had a 1-in. asphalt concrete wearing course, 4 in. of crushed limestone base course, and 12 in. of either lime-stabilized clay (Item 9) or CAM (Item 10) subbase course. Discussion of the response and performance of the inverted pavement test items is not included in this paper but may be found elsewhere *(3)*.

FALLING WEIGHT DEFLECTOMETER

Falling weight deflectometer (FWD) nondestructive testing load-deflection measurements were obtained at item quarter points before, during, and after load cart traffic. The FWD applied an impulse load of 9,000 or 15,000 lb to the pavement

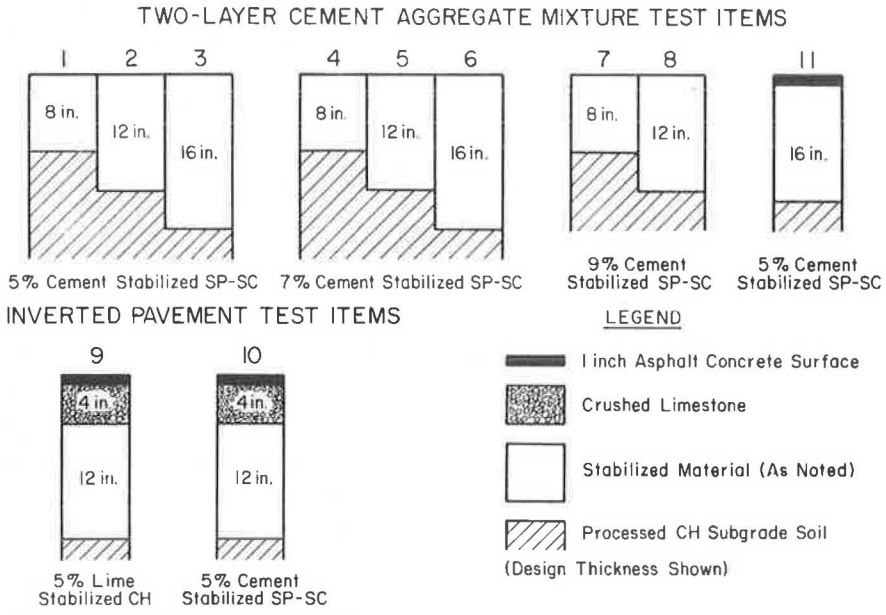

FIGURE 2 Description of test items.

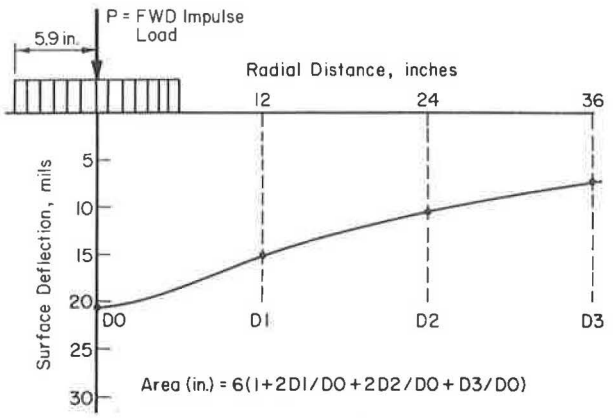

FIGURE 3 FWD deflection basin.

surface through an 11.8-in.-diameter plate. Surface deflections were recorded at the center of the load and at radial distances of 12, 24, and 36 in., denoted D0, D1, D2, and D3, respectively (Figure 3).

CRACK LOAD TRANSFER EFFICIENCY

Load transfer efficiency (LTE) of selected transverse shrinkage cracks was measured before and during trafficking. LTE varied from 25 to 77 percent with most between 30 and 35 percent. LTE is a deflection-based measure of the crack shear transfer efficiency. The FWD load plate was placed tangent to the crack and deflections were recorded on each side of the crack in the immediate vicinity of the load. LTE is then determined by

$$LTE = (\Delta_u/\Delta_1)100 \quad (1)$$

where

LTE = load transfer efficiency, percent;
Δ_u = crack deflection of unloaded slab; and
Δ_1 = crack deflection of the loaded slab.

When no load transfer exists across the crack, the LTE is zero.

COMPUTER MODELS USED IN ANALYSIS

Two finite element computer programs were used in the analysis of the FWD load-deflection data and in the prediction of first-pass structural response:

- ILLI–PAVE, a stress-dependent multilayer axisymmetrical solid structural model for single wheel loads *(4)* and
- ILLI–SLAB, a two-dimensional, multislab rigid pavement model that considers joints and cracks *(5)*.

CHARACTERIZATION OF MATERIALS

Subgrade

Repeated-load unconfined compression tests were performed on specimens prepared from tube samples of in-place CH subgrade. An extensive ILLI–PAVE analytical study was conducted to determine the uniformity of the processed CH subgrade between test items. Study results showed the item average subgrade resilient modulus response for all of the test items could be replaced by the grand average of all of the subgrade samples with only an approximate 2 percent difference in calculated structural response parameters. In all remaining ILLI–PAVE analysis concerning these test items, the grand average ALRS subgrade was used to represent the processed CH subgrade. Resilient modulus–deviator stress relations for the processed and in situ subgrades are shown in Figure 4.

Unconfined compression tests were performed on the subgrade tube samples following resilient modulus testing. Unconfined compressive strength (q_u) was taken at 5 percent total axial strain and ranged from 20 to 31 psi.

Asphalt Concrete

The modulus of the asphalt concrete wearing course in Item 11 was estimated at 700 ksi based on the 50°F field temperature during the traffic tests.

Cement Aggregate Mixture

If all the test item structural variables are known except the modulus of the CAM layer, it can be back-calculated from the FWD deflection data. This was accomplished by modeling the known properties of the test items in the ILLI–PAVE structural model. The modulus of the CAM layer was varied until the ILLI–PAVE–predicted deflection basin matched the field FWD deflection basin.

Figure 5 shows that the D0 deflection for a given load and subgrade is primarily influenced by the modulus of the CAM layer whereas the D3 deflection is largely influenced by the subgrade modulus. If the predicted deflections match the FWD deflections, both the rigid CAM layer and the subgrade are being accurately modeled. Figure 6 shows the FWD deflection basin for Item 8 and ILLI–PAVE–predicted deflection basins for various CAM layer moduli. When the deflection basins are matched, the back-calculated CAM modulus is approximately 400 ksi. The nearly exact match of the D3 deflection indicates that the subgrade was properly modeled.

The back-calculated modulus was an "effective" layer modulus because the presence of minute cracks and irregularities in the stabilized layer affect FWD deflections. A study was conducted to determine the accuracy required of the back-calculated CAM modulus for use in structural analysis. The sensitivity of tensile stress and strain at the bottom of the CAM layer to large variations in the CAM layer modulus is shown in Figures 7 and 8. The degree of accuracy obtained by the back-calculation procedure for the CAM layer modulus is satisfactory to accurately calculate the structural response parameters that affect item performance.

Accurate assessment of the individual and combined effects of CAM strength and thickness on performance requires a good measure of field strength. CAM strength is affected by soil properties, mixing efficiency, cement content, moisture, curing conditions, and density. A laboratory strength study was con-

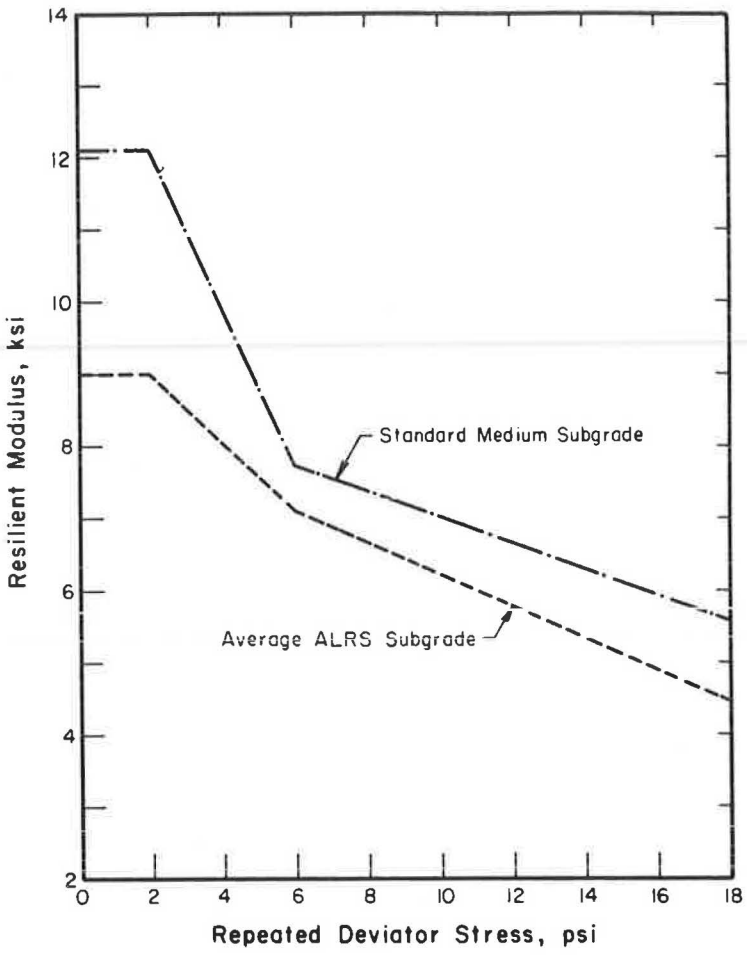

Description	E_{ri}	K_1	K_2
Average ALRS Subgrade	7.07	-0.48	-0.22
Standard Medium Subgrade	7.68	-1.11	-0.18

FIGURE 4 Subgrade models for back-calculation procedure.

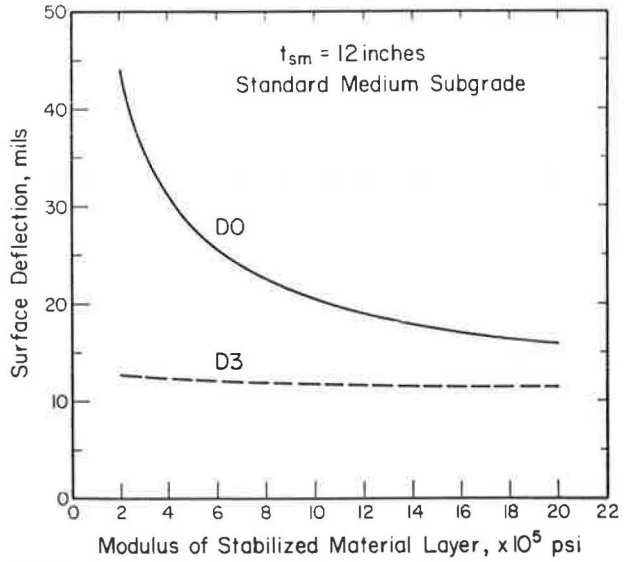

FIGURE 5 Effect of stabilized-material layer modulus on D0 and D3. Deflection in test items, ILLI–PAVE model *(1)*.

ducted on the CAM to determine the effects of density, cement content, and curing on strength *(3)*.

CAM field flexural (tensile) strength was estimated from the laboratory strength study results. To account for the inefficiencies of field mixing compared with laboratory mixing, a field-mixing efficiency (field strength/laboratory strength) of 0.65 was selected for the ALRS field test *(6-8)*. Flexural strength is approximately 20 to 30 percent of unconfined compressive strength *(7)*. For the CAM material, flexural strength was estimated at 22 percent of the unconfined compressive strength. Estimated field flexural strengths for the various CAM layers are given in Table 1.

PHASES OF ITEM PERFORMANCE

Item cracking and deflection measurements under traffic indicate performance of the items can be divided into three general phases (Figure 9):

- Phase 1 begins with the initial condition of the pavement

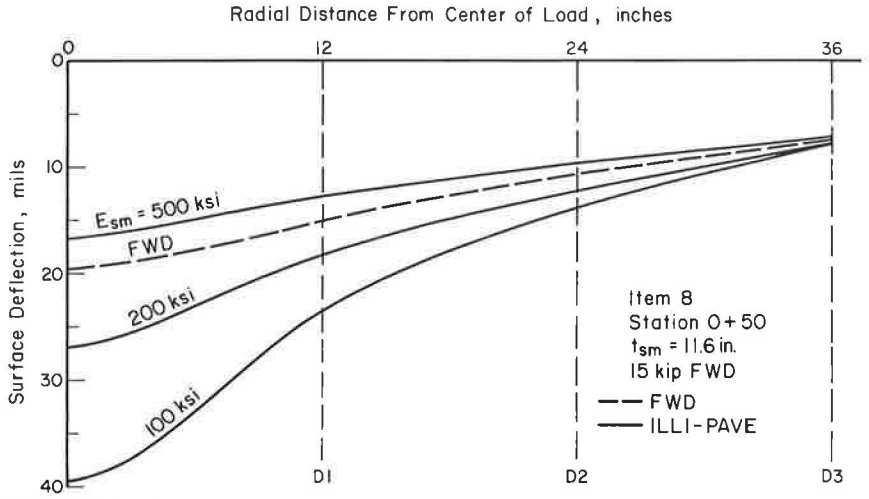

FIGURE 6 Comparison of FWD and predicted ILLI–PAVE deflection basins.

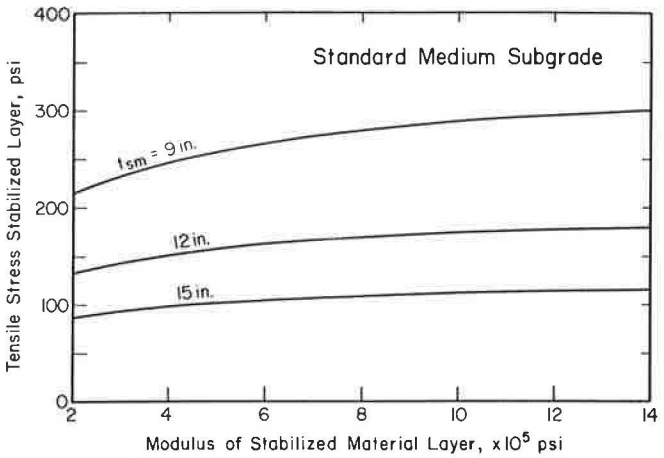

FIGURE 7 Effect of modulus and thickness of the stabilized layer *(1)*.

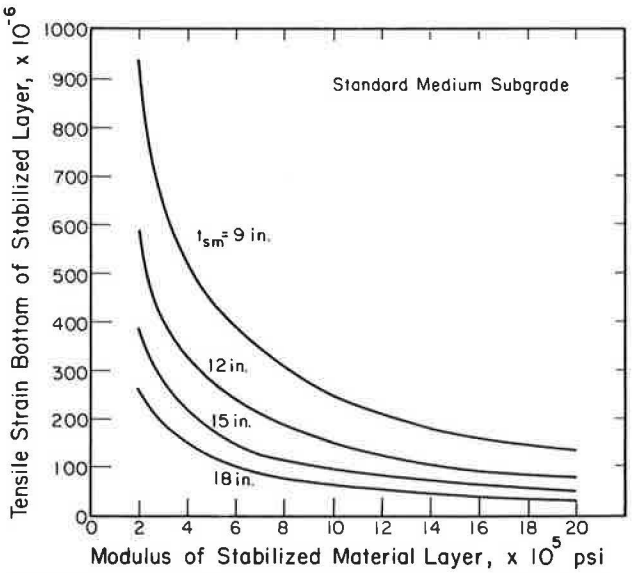

FIGURE 8 Effect of stabilized-material layer modulus and thickness on tensile strain in stabilized layer *(1)*.

and ends with the development of load-related longitudinal cracks along the edges of the channelized traffic lane. These cracks usually start at a transverse shrinkage crack and propagate longitudinally from the transverse crack.

- Phase 2 includes continued lengthening and "working" of the load-related longitudinal cracks.
- Phase 3 begins with the development of transverse ladder cracks in the traffic lane and ends with the tire punching through the CAM layer into the subgrade.

The type of cracking observed in the ALRS field test was also noted in cement-stabilized pavements subjected to channelized traffic *(9)*.

DISCUSSION OF PHASES OF PERFORMANCE

Phase 1

The predicted F–4 first-pass crack flexural (tensile) stress (acting parallel to the transverse shrinkage crack) at the bottom of the CAM layer exceeded the estimated field flexural strength in all items (discussed in detail later). A longitudinal crack on the underside of the CAM layer at the center of the traffic lane formed on the first pass of the F–4 load cart (Figure 10). Continued traffic caused the crack to propagate up into the CAM layer. This longitudinal crack reduced the stiffness of the CAM layer in the traffic lane and resulted in increased pass deflections and permanent deformations of the subgrade.

Phase 2

Continued traffic propagated the longitudinal crack on the underside of the CAM layer. Increased pass deflection caused a decrease in the radius of curvature and an increase in the tensile stress on the surface of the CAM layer at the edges of the traffic lane producing additional longitudinal cracks (Figure 11). As the surface longitudinal cracks propagated down into the CAM layer, the flexural stress at the bottom of the CAM layer acting

TABLE 1 ESTIMATED CAM FIELD FLEXURAL STRENGTH

Item	Percent Cement	Dry Density (pcf)	Predicted Lab. Unconf. Comp. Strength (psi)	Estimated Field Flexural Strength(1) (psi)
1	5	112.6	241	35
2	5	118.2	455	65
3	5	118.9	475	68
4	7	-----	----	---
5	7	120.7	857	123
6	7	125.8	990	142
7	9	113.2	615	88
8	9	127.3	1111	159
10	5	120.0	500	72
11	5	118.2	455	65

(1) $f_b = UCS_{lab} \times 0.65 \times 0.22$.

parallel to the transverse shrinkage crack was reduced. This can be explained by the transverse distance between the longitudinal surface cracks at the edges of the traffic lane being too short to produce large flexural action in this direction. The area within the traffic lane begins to act as a long thin slab bounded on the ends by the transverse shrinkage cracks and on the sides by the longitudinal surface cracks at the traffic lane edges.

Phase 3

With the development of the surface longitudinal cracks, subgrade deviator stress greatly increases and increased permanent deformation occurs in the subgrade with further traffic applications. The LTE across the longitudinal surface cracks decreases, and continued traffic effects further increases in the subgrade deviator stress. The critical stress in the CAM layer now shifts from parallel to the transverse shrinkage crack to parallel to the traffic direction. The flexural (tensile) stress parallel to the short axis (transverse) is now quite small in comparison with the longitudinal axis. The stress levels at the bottom and top of the CAM layer parallel to the long axis of the traffic lane are approximately equal to the flexural strength. This causes transverse ladder cracks to form in the traffic lane (Figure 12). The effective "slab" size is now only slightly larger than the area of the tire. Critical stress conditions now shift from the rigid stabilized-material layer to the subgrade. When the subgrade shear stress increases, further traffic applications effect large subgrade displacements and permanent deformations, and the tire ultimately punches through the CAM layer into the subgrade.

The longitudinal cracks on the underside of the CAM layer probably developed on the first pass because the predicted stress ratio at the transverse shrinkage crack exceeded one. The rate of crack propagation observed in the CAM layer was related to the resilient and permanent behavior of the subgrade. Softer subgrades with larger resilient deflections and permanent deformations for the same CAM stress ratio displayed faster crack propagation and earlier functional failure.

Crack propagation and subgrade permanent deformation in

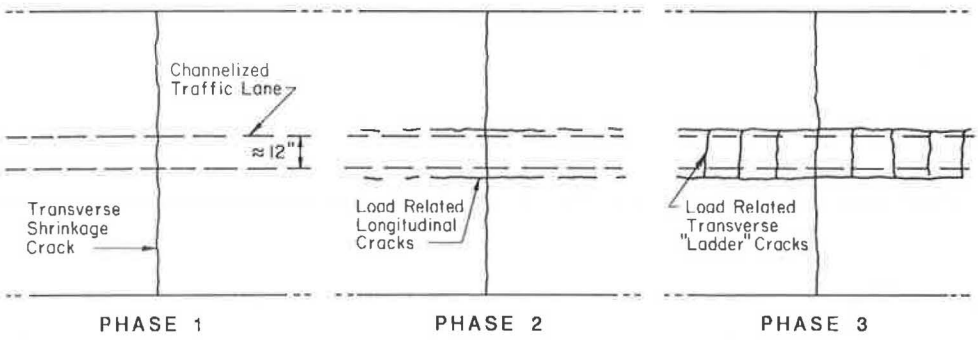

FIGURE 9 Phases of performance.

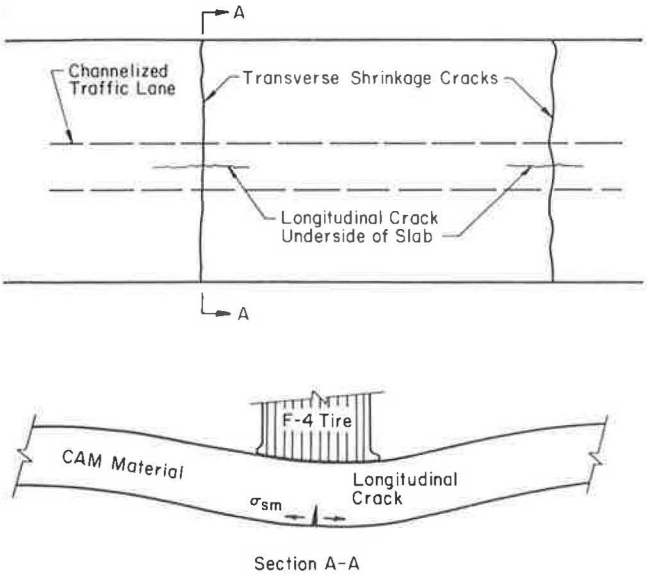

FIGURE 10 Cracking in Phase 1 of item performance.

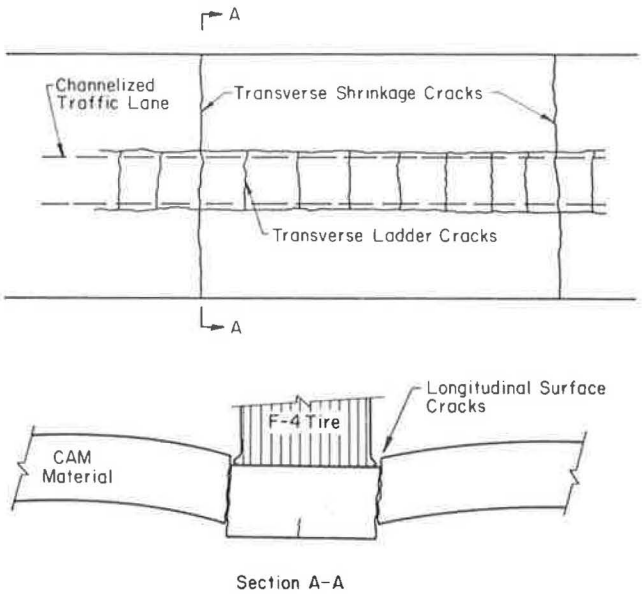

FIGURE 12 Cracking in Phase 3 of item performance.

the ALRS test pavements with a stress ratio greater than one are a complex relationship among thickness, modulus, and strength of the CAM; crack LTE; and the subgrade strength and modulus. After the longitudinal crack on the underside of the CAM layer has formed, the pavement structure cannot be accurately modeled. The mechanistic approach is primarily applicable to an intact slab without cracking.

The type and severity of cracking influence traffic lane surface deflections (Figure 13). During Phase 1, pass deflection is relatively constant and permanent deformation accumulates slowly. During Phase 2, deflection slowly increases with each pass, but, in Phase 3, it increases dramatically until failure occurs. Cumulative permanent deformation continues to increase during Phase 2 and large increases occur during Phase 3.

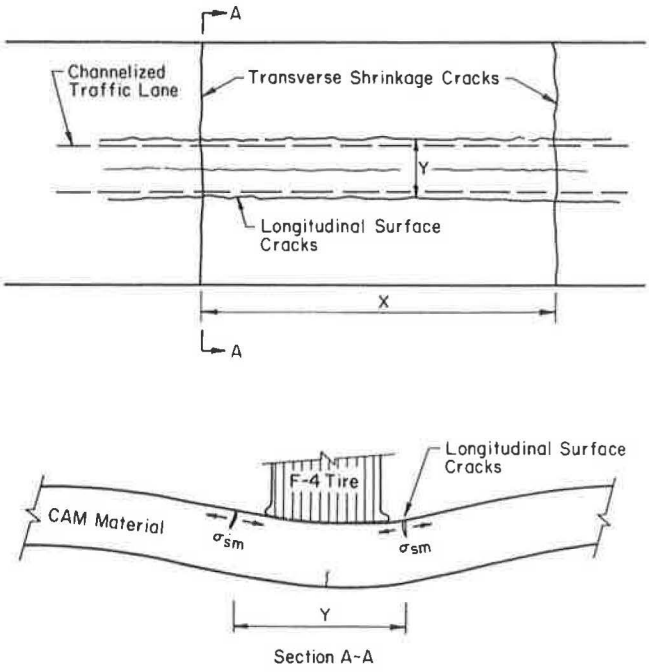

FIGURE 11 Cracking in Phase 2 of item performance.

STRUCTURAL AND FUNCTIONAL FAILURE

Performance is the measure of how well a pavement fulfills its intended purpose. Functional failure of the pavement is reached when it can no longer meet the requirements of the user (i.e., when the pavement causes handling problems for the pilot or causes damage to the aircraft). Structural failure is defined as the collapse of the pavement structure or the breakdown of one or more of the pavement components to the extent that the pavement is not capable of carrying the imposed loads.

If environmentally related distress does not occur (as in this field test), surface roughness accumulation is a function of traffic-induced distress. If the rigid stabilized-material layer remains intact, pavement deflections are stable and the degree of surface roughness is acceptable. Major surface roughness occurs when the slab-type behavior of the intact stabilized-material layer breaks down due to severe cracking.

Extensive research has been conducted *(10–13)* on aircraft-pavement interaction. Recent field and model studies on the response of the F–4 to various forms of surface roughness indicate the need for a relatively smooth surface *(14)*. These "general smoothness criteria" served as a guideline in estimating the passes to functional failure for the two-layer test items (Table 2).

FIRST-PASS CRACK STRUCTURAL RESPONSE

A high-strength and high-modulus stabilized-material layer displays "slab-type" behavior. Most rational analyses of pavement behavior concerning cementitious materials have shown that flexural (tensile) stress is the critical factor affecting initiation and early propagation of load-related cracks *(15)*.

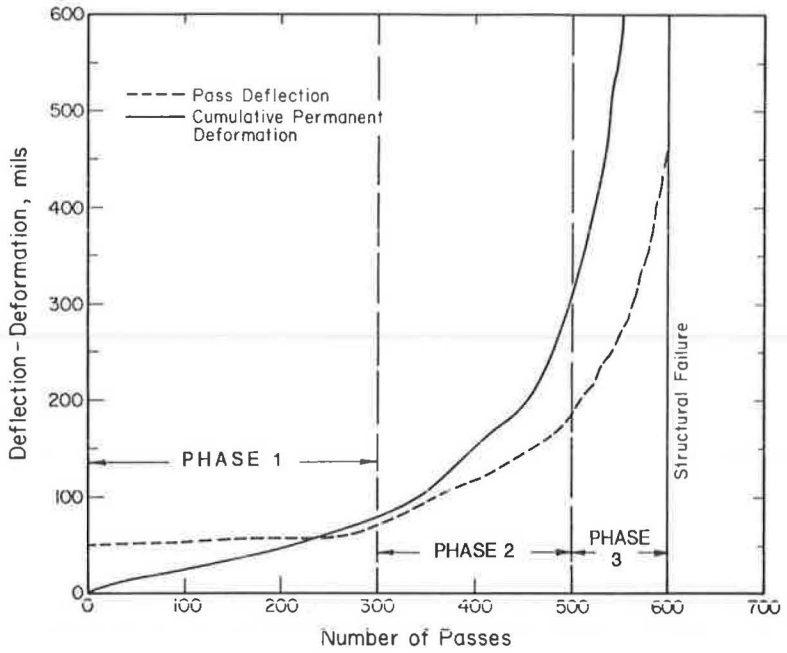

FIGURE 13 Typical pass deflection and cumulative permanent deformation.

The maximum flexural (tensile) stress occurs when the load is adjacent to a crack *(6, 16, 17)*. This stress is at the bottom of the stabilized-material layer and acts parallel to the crack. Researchers have reported this "crack" stress to be 40 to 50 percent greater than the interior load flexural (tensile) stress *(1)*. This increased stress may be characterized as a load placement effect factor (LPEF) and defined as

$$LPEF = \sigma_{crack}/\sigma_{interior} \quad (2)$$

where

σ_{crack} = flexural stress in the stabilized layer when the load is at a crack for a specific LTE and
$\sigma_{interior}$ = flexural stress in the stabilized layer for an interior load condition.

The maximum value for the LPEF occurs for the free edge condition. Westergaard's new equations for stresses in concrete

TABLE 2 F-4 PASSES TO FUNCTIONAL FAILURE AND STRUCTURAL FAILURE

Item	Description	Failure Location	Passes To: Functional Failure	Passes To: Structural Failure
1	8.4 in. CAM (5% cement)	0+16	30	48
2	12.4 in. CAM (5% cement)	0+59	500	650
3	16.6 in. CAM (5% cement)	0+84(1)	1000	1000+
4	7.6 in. CAM (7% cement)	1+35	1	6
5	10.9 in. CAM (7% cement)	1+77.5	110	127
6	16.6 in. CAM (7% cement)	2+09.5(1)	1000+	1000+
7	8.0 in. CAM (9% cement)	0+06.8	65	82
8	10.7 in. CAM (9% cement)	0+42.5	520	550
11	1.5 in. Asphalt Concrete 10.0 in. CAM (5% cement)	1+77.5	500	636

(1) Probable failure location if trafficked beyond 1000 passes.

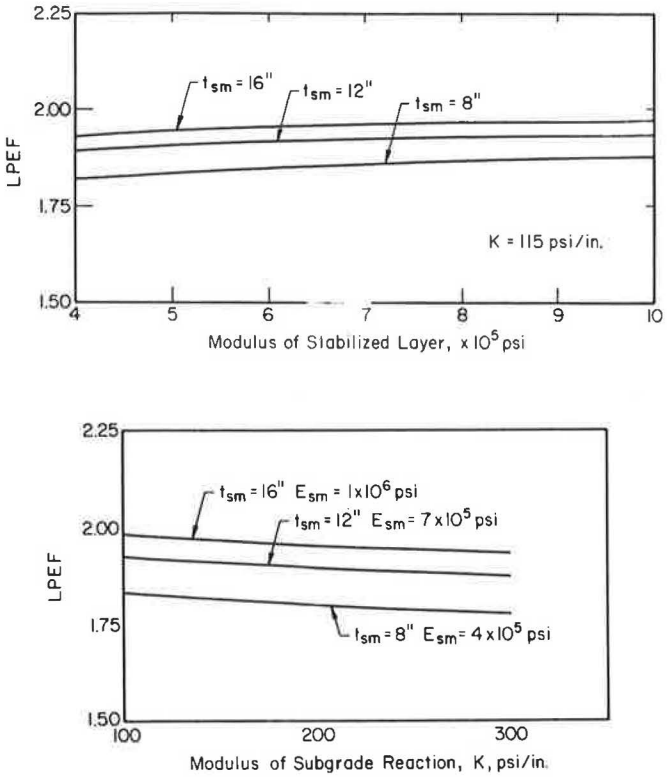

FIGURE 14 Effect of slab modulus, thickness, and subgrade support on LPEF, 27 kips, 265 psi (Westergaard's 1947 equations).

airfield pavements *(18)* indicate that LPEF approaches 1.8 for 8-in.-thick slabs and 2.0 for 16-in. slabs. Large variations in subgrade support and slab modulus have little effect on the LPEF (Figure 14).

To determine the effect of LTE on the LPEF, an ILLI–SLAB study was conducted. Figure 15 shows LPEF as a function of thickness and LTE. Note that the upper limit for LPEF approaches that calculated by Westergaard's equations. The

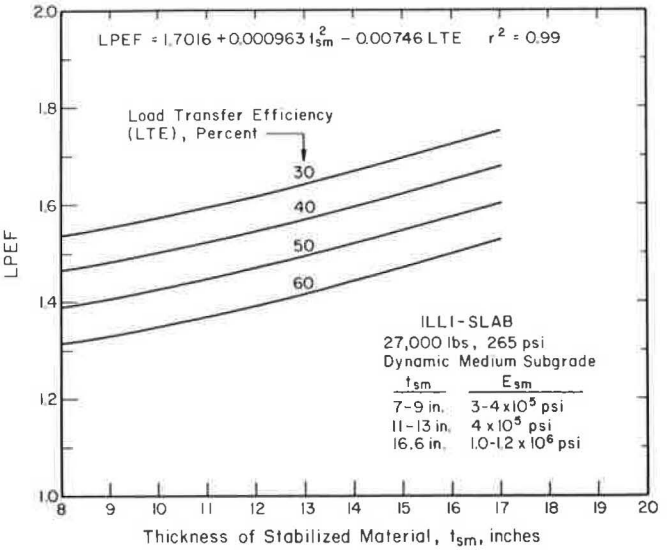

FIGURE 15 LPEF.

flexural (tensile) stress in the stabilized layer at a crack, σ_{crack}, with partial load transfer is estimated by the equation:

$$\sigma_{crack} = \sigma_{interior} \times LPEF \quad (3)$$

where

$\sigma_{interior}$ = interior flexural stress calculated by ILLI–PAVE and
LPEF = load placement effects factor for a specific LTE determined from Figure 15.

Table 3 gives the predicted first-pass structural response for an F–4 interior load of 27 kips and 265 psi tire pressure for the various test items. The flexural stress near the crack compared with the interior flexural stress is related to the thickness of the CAM layer and the LTE of the crack by the load placement effect factor (LPEF) in Figure 15. Table 4 gives the predicted first-pass crack flexural (tensile) stress at the bottom of the CAM layer.

FIRST-PASS STRESS RATIO AND PERFORMANCE

Predicted transverse crack stress ratios (tensile stress/flexural strength) in the CAM layer for the first pass of the F–4 are given in Table 5. Field flexural strength was estimated using the results of the laboratory strength study and field density data.

Larsen and Nussbaum *(19)* noted a 26 percent coefficient of variation (standard deviation/mean) for the flexural strength of cemented materials. Predicted stress ratios should reflect this variability. Figure 16 shows the range of the predicted first-pass crack stress ratio in the CAM layer using a 25 percent strength variability. The passes to functional failure for the items are also shown in this figure.

PREDICTED F–4 FIRST-PASS CRACK RESPONSE

CAM layer thickness had the largest effect on the structural response of the two-layer items. The thicker items had smaller surface deflections, larger deflection basin areas, smaller CAM flexural stress and stress ratios, smaller CAM flexural strain and strain ratios, and smaller subgrade deviator stress and shear stress ratios. When the variability of the back-calculated CAM modulus and strength are considered, both 16-in. items had predicted first-pass crack CAM stress and strain ratios near 1.

EFFECT OF THICKNESS, MODULUS, AND STRENGTH ON STRESS RATIO

An ILLI–PAVE study was conducted using the F–4 main gear loading to determine the combination of slab thickness, slab modulus, and slab strength for a predicted crack stress ratio in the stabilized-material layer large than 1. The standard medium subgrade was selected with a 30 percent LTE across the CAM

TABLE 3 ILLI-PAVE STRUCTURAL RESPONSE TO INTERIOR F-4 LOAD (27 KIPS, 265 PSI), ITEMS 1 THROUGH 8 AND 11

Information and Structural Response	Item								
	1	2	3	4	5	6	7	8	11
Station	0+16	0+59	0+84	1+35	1+77	2+09	0+07	0+42	1+77
Stabilized Material									
Thickness, inches	8.4	12.4	16.6	7.6	10.9	16.6	8.0	10.7	10.0
Modulus, ksi	300	400	1000	25	400	1200	400	400	300
Surface Deflection Basin									
D0 at R = 0 inches, mils	52.05	30.97	16.91	202	34.95	15.99	47.44	35.58	33.19
D1 at R = 12 inches, mils	35.77	22.88	14.27	67.8	25.72	13.78	33.79	26.16	24.45
D2 at R = 24 inches, mils	22.89	17.30	12.81	24.6	18.69	12.55	22.21	18.89	18.02
D3 at R = 36 inches, mils	13.95	12.92	11.62	9.8	13.27	11.54	13.94	13.32	13.11
Area, inches	21.13	24.06	29.34	11.78	23.52	30.09	21.93	23.44	23.73
Stabilized Material (Bottom of Layer)									
Radial Tensile Stress, psi	258	148	95	130	184	97	295	190	140
Radial Tensile Strain, microstrain	752	336	86	5255	422	72	689	436	427
Subgrade (Top of Layer)									
Normal Stress, psi	17.6	9.3	4.6	59.7	10.9	4.3	16.3	11.2	10.3
Shear Stress, psi	5.67	2.92	1.08	13.80	3.50	0.96	5.14	3.59	3.46
Deviator Stress, psi	11.38	5.84	2.17	27.60	6.98	1.91	10.24	7.20	6.93
Shear Stress Ratio (τ/c)	0.37	0.20	0.07	1.00	0.30	0.07	0.36	0.30	0.32

Note: Item 11 has 1.5 inch asphalt concrete wearing course at the surface (modulus of 700 ksi).

transverse shrinkage cracks. The flexural strength was estimated using the relationship:

$$f_b = 0.22(E_{sm}/1200) \quad (4)$$

where f_b is flexural strength in psi and E_{sm} is modulus in psi.

Crack tensile stress was estimated by increasing the interior load stress by the LPEF in Figure 15.

The results of the study are shown in Figure 17. One combination that produces a stress ratio of 1 is

f_b = 137 psi,
E_{sm} = 7.5×10^5 psi, and
t_{sm} = 16.6 in.

This combination is quite close to Item 6, which had a predicted first-pass crack stress ratio of 1.1. Although the unconfined compressive strength of cement-stabilized granular materials can be greater than 2,000 psi, a typical value is approximately 1,000 psi. This equates to an estimated flexural strength of 220 psi and an estimated modulus of elasticity of 1.2

TABLE 4 PREDICTED F–4 FIRST-PASS FLEXURAL (TENSILE) STRESS, BOTTOM OF CAM STABILIZED LAYER

Item	Thickness (in.)	ILLI-PAVE Tensile Stress Bottom of CAM Layer (psi)	First Pass Crack LTE (percent)	Load Placement Effect Factor	Predicted Crack Tensile Stress Bottom of Stabilized Layer (psi)
1	8.4	258	77	1.19	307
2	12.4	148	45	1.50	222
3	16.6	95	38	1.68	160
4	7.6	Subgrade Shear Failure First Pass of F-4 Load Cart			
5	10.9	184	50	1.50	276
6	16.6	97	45	1.64	158
7	8.0	295	62	1.32	389
8	10.7	190	(1)	1.00	190
11	10.0	140	90	1.10	154

(1) No transverse shrinkage crack; interior loading condition used.

TABLE 5 PREDICTED F–4 FIRST-PASS CRACK STRESS RATIO, BOTTOM OF CAM MATERIAL LAYER

Item	Station	Predicted Crack[1] Flexural Stress Stabilized layer (psi)	Estimated Mean[2] Flexural Strength (psi)	Predicted First Pass Stress Ratio
1	0+16	307	35	8.77
2	0+59	222	65	3.42
3	0+84	160	68	2.35
4	1+35	---	---	-----
5	1+77.5	276	123	2.24
6	2+09.5	158	142	1.11
7	0+06.8	389	88	4.42
8	0+42.6	190	159	1.20
11	1+77.5	154	65	2.37

(1) Table 4.
(2) Table 1.

$\times 10^6$ psi. From Figure 17 a minimum of 13.6 in. of stabilized material would be required for a first-pass predicted crack stress ratio of 1 or less.

TRANSFER FUNCTION

All of the predicted F–4 first-pass stress ratios in the CAM layers of the ALRS test items exceeded 1. By definition, a stress ratio cannot exceed 1 because the limiting stress is the strength of the material. A stress ratio less than 1 is a realistic measure of the stress level in a material compared with its strength and is useful in fatigue analysis.

Stress ratios greater than 1 are only useful as "quantitative indicators of performance" and not as absolute values. These quantitative indicators of performance are useful in comparing performance among ALRS test items with stress ratios greater than 1. Transfer functions developed for stress ratios greater

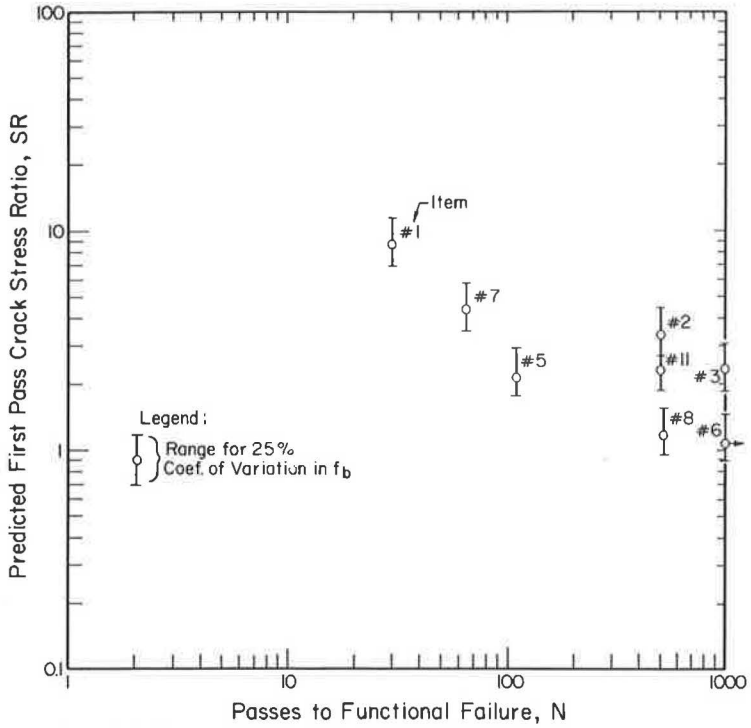

FIGURE 16 Item performance and predicted first-pass crack stress ratio in CAM layer.

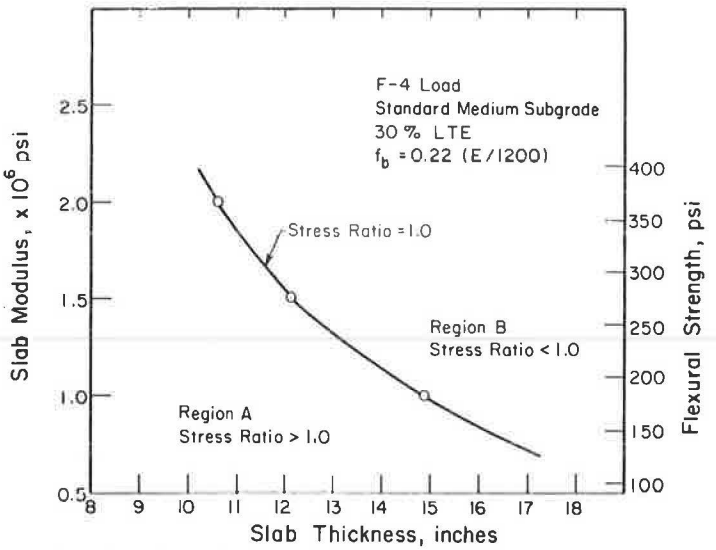

FIGURE 17 Combinations of slab modulus, strength, and thickness for crack stress ratio of 1.

than 1 reflect crack propagation rates after crack initiation, and those for stress ratios less than 1 relate to crack initiation. These "crack propagation" stress ratio transfer functions are more relevant for analysis than for design.

Many factors influence the rate of crack propagation in the CAM layer for stress ratios greater than 1 and large variability in performance at a given stress ratio should be expected. A transfer function based on the results of the ALRS field test should be conservative to reflect this variability.

Figure 18 shows a recommended transfer function relating passes to functional failure and the predicted first-pass crack stress ratio in the CAM layer. The form of the transfer function is

$$SR = 4.54N^{-0.2054} \quad (5)$$

where SR is the crack stress ratio in the stabilized-material layer and N is passes to functional failure.

The upper bound of the stress ratio for one pass is approximately 4.54. The performance of the two-layer ALRS test

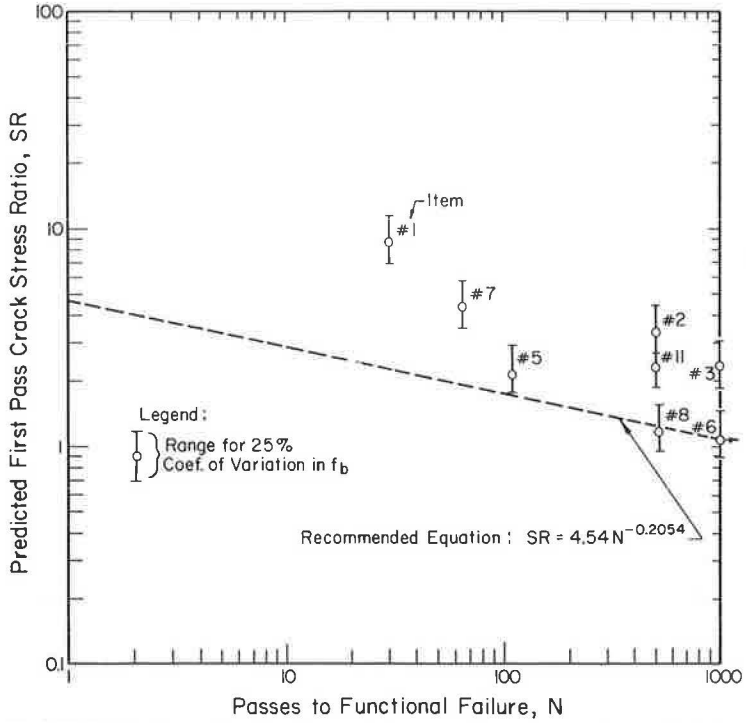

FIGURE 18 Transfer function relating performance and predicted first-pass crack stress ratio in CAM layer.

items falls above this transfer function as shown in Figure 18. Notice that the 16-in. items have stress ratios near 1 at 1,000 passes.

CONCLUSIONS

These conclusions are pertinent to both the design and the evaluation of ALRS containing stabilized-material layers for fighter aircraft with single tire main gears. The processes of design and evaluation are similar and include many of the same steps. In both, a mechanistic analysis of the resulting pavement structure is performed to determine the response parameters of interest (stress, strain, and deflection). These are then used to predict performance through appropriate transfer functions.

1. The mechanistic approach to the design and analysis of ALRS containing stabilized-material layers is valid. Important pavement section parameters that affect response and performance can be identified and performance can be predicted using appropriate transfer functions.
2. Critical pavement response affecting performance occurs at a transverse shrinkage crack. A crack load transfer efficiency (LTE) of 30 percent was typical of ALRS test section conditions. Increasing the interior load flexural (tensile) stress in the stabilized-material layer by 50 percent is a good estimate of the crack tensile stress for a 30 percent LTE.
3. Postcracking performance is dominated by the thickness of the stabilized-material layer. Strength of the stabilized material for pavements with a predicted stress ratio greater than 1 does not have a major effect on performance.
4. ALRS design for passes to functional failure of 1,000 or fewer should be based on an intact slab analysis and the predicted first-pass crack stress ratio should be limited to less than 1. The relationship among thickness, modulus, strength, LTE, and subgrade strength in partly cracked stabilized-material layers is too complex to model.
5. Conservative transfer functions for the prevailing subgrade conditions were developed to relate predicted first-pass crack stress to pavement performance. The transfer functions developed are more applicable to analysis of ALRS than to design. The transfer functions may not be applicable for a "range" of subgrade strength conditions.
6. ALRS containing cement-stabilized materials require a wearing course on the surface of the stabilized material to prevent tire abrasion. The wearing course need not provide additional load-carrying capability.

ACKNOWLEDGMENTS

This paper was prepared by the Department of Civil Engineering, University of Illinois at Urbana-Champaign, under contract to the Air Force Engineering and Services Center, Engineering and Services Laboratory, Tyndall Air Force Base, Florida.

REFERENCES

1. M. R. Thompson et al. *Development of a Preliminary ALRS Stabilization Material Pavement Analysis System (SPAS).* Technical Report ESL–TR–83–84. U.S. Air Force Engineering and Services Center, Tyndall Air Force Base, Fla., Aug. 1984.
2. C. R. Styron. *Performance Data For F–4 Load Cart Operations on Alternate Launch and Recovery Surfaces.* Technical Report ESL–TR–83–46. U.S. Air Force Engineering and Services Center, Tyndall Air Force Base, Fla., July 1984.
3. R. R. Costigan and M. R. Thompson. *Response and Performance of Alternate Launch and Recovery Surfaces Containing Stabilized-Material Layers.* Technical Report ESL–TR–84–25. U.S. Air Force Engineering and Services Center, Tyndall Air Force Base, Fla., Jan. 1985.
4. L. Raad and J. L. Figueroa. Load Response of Transportation Support Systems. *Transportation Engineering Journal,* ASCE, Vol. 106, No. TE1, Jan. 1980.
5. M. R. Thompson, A. M. Ioannides, J. M. Fischer, and E. J. Barenberg. *Development of a Stress-Dependent Finite Element Slab Model.* Report AFOSR–TR–83–1061. Air Force Office of Scientific Research, Bowling Air Force Base, Washington, D.C., 1983.
6. J. K. Mitchell, P. Dzwilewski, and C. L. Monismith. *Behavior of Stabilized Soils Under Repeated Loading,* Report 6: *A Summary Report with a Suggested Structural Pavement Design Procedure.* Contract Report 3–145. U.S. Army Engineers Waterways Experiment Station, Vicksburg, Miss., 1974.
7. M. R. Thompson and B. J. Dempsey. *Durability Testing of Stabilized Materials.* Final Report UILU–ENG–74–2010. Engineering Experiment Station, University of Illinois, Urbana, June 1974.
8. *Bulletin 292: Soil Stabilization with Portland Cement.* HRB, National Research Council, Washington, D.C., 1961.
9. M. C. Wang and W. P. Kilareski. Behavior and Performance of Aggregate-Cement Pavements. In *Transportation Research Record 725,* TRB, National Research Council, Washington, D.C., 1979, pp. 67–74.
10. A. P. Berens and R. Newman. *Analysis for the Determination of Significant Characteristics of Runway Roughness.* Technical Report AFFDL–TR–73–109. Air Force Flight Dynamics Laboratory, Wright-Patterson Air Force Base, Ohio, Nov. 1973.
11. P. N. Sonnenburg. *Analysis of Airfield Roughness Criteria.* Technical Report FAA–RD–75–110. FAA, U.S. Department of Transportation, Nov. 1976.
12. A. G. Gerardi. *Digital Simulation of Flexible Aircraft Response to Symmetrical and Asymmetrical Runway Roughness.* AFFDL–TR–77–37. Air Force Flight Dynamics Laboratory, Wright-Patterson Air Force Base, Ohio, Aug. 1977.
13. A. G. Gerardi. Dynamic Response of Aircraft to Pavement Unevenness. In *Special Report 175: Research in Airport Pavements,* TRB, National Research Council, Washington, D.C., 1978, pp. 91–96.
14. *Rapid Runway Repair Interim Planning Guidance.* Engineering and Services Laboratory, Air Force Engineering and Services Center, Tyndall Air Force Base, Fla., Dec. 1981.
15. M. W. Witczak. *Pavement Performance Models, Repeated Load Fracture of Pavement Systems.* Contract Report S–76–15. U.S. Army Engineer Waterways Experiment Station, Vicksburg, Miss., Vol. I, Aug. 1976.
16. E. Otte. Analysis of a Cracked Pavement Base Layer. In *Transportation Research Record 725,* TRB, National Research Council, Washington, D.C., 1979, pp. 45–51.
17. E. Otte, P. F. Savage, and C. L. Monismith. Structural Design of Cemented Pavement Layers. *Transportation Engineering Journal,* ASCE, Vol. 108, No. TE4, July 1982.
18. H. M. Westergaard. New Formulas for Stresses in Concrete Pavements of Airfields. *Transactions of American Society of Civil Engineers,* May 1947.
19. T. J. Larsen and P. J. Nussbaum. *Fatigue of Soil-Cement.* Bulletin D119. Portland Cement Association, Research and Development Laboratories Development Department, Skokie, Ill., 1967.

Publication of this paper sponsored by Committee on Flexible Pavements.

The contents do not necessarily reflect the official views or policies of the U.S. Air Force. This paper does not constitute a standard, specification, or regulation.

DISCUSSION

ANASTASIOS M. IOANNIDES
Visiting Research Associate, University of Illinois, Urbana.

Among other useful information, the authors present an interesting approach to the determination of the load placement effect factor (LPEF). This would allow the maximum bending stress in a slab due to edge loading (σ_e) to be estimated, given the corresponding stress developing under interior loading (σ_i). The need to determine LPEF stems from two simple observations:

- The edge stress is generally higher than the interior stress and is therefore more critical for design purposes and
- The edge stress is much more difficult, if not impossible, to determine using the commonly available analytical and numerical engineering tools for several situations of practical interest.

Inspection of the Westergaard (dense liquid) solutions, and recent results obtained by the writer using several computerized procedures employing the elastic solid model *(1)*, have led to the following conclusion:

Independent of the individual values of the parameters entering into the analysis, the value of the ratio (σ_e/σ_i), or LPEF, is solely a function of the ratio of the size of the loaded area to the radius of relative stiffness [e.g., (a/l), (a/l_e), (c/l), (c/l_e)] where

a = radius of circular loaded area,
c = side length of square loaded area,
l = radius of relative stiffness (dense liquid), and
l_e = radius of relative stiffness (elastic solid).

This assertion derives from the fact that both both σ_e and σ_i, expressed in a nondimensional form ($\sigma h^2/P$) where

σ = bending stress (σ_e or σ_i),
h = thickness of slab, and
P = total applied loads,

are themselves uniquely defined by the load size ratio, independent of the individual values of a, l, l_e, h, P, and so forth for typical values of the Poisson ratio for the slab.

Figure 19 shows the variation of (σ_e/σ_i) with the load size ratio obtained using the closed-form (infinite slab) solutions for the dense liquid and elastic solid foundations. The dense liquid solutions are obtained using Westergaard's equations. For the elastic solid, Losberg's equation was used for the interior bending stress *(2)*. The edge stress was obtained using H51ES *(1)*, a computerized version of a chart by Pickett et al. *(3)*. In a previous paper *(4)*, the writer showed that of the dense liquid solutions presented by Westergaard, only the "new equation" is analytically correct. The corresponding curve in Figure 19 is a concise way of presenting all of the curves in Figure 14 of the authors. Figure 19 also indicates that, in the range of loaded area sizes commonly encountered in practice, the elastic solid ratio of (σ_e/σ_i) is generally about 25 percent smaller than the corresponding dense liquid (new equation) value.

The curves in Figure 19 show the variation of the LPEF for the case of an infinite slab. The authors note that for a dense liquid foundation "the upper limit for LPEF approaches that calculated by Westergaard's equations." Thus smaller slabs may be expected to give lower values of LPEF. This is further demonstrated by the slab size investigations conducted by the writer for both the dense liquid and elastic solid subgrades *(1, 4, 5)*. The (L/l) or

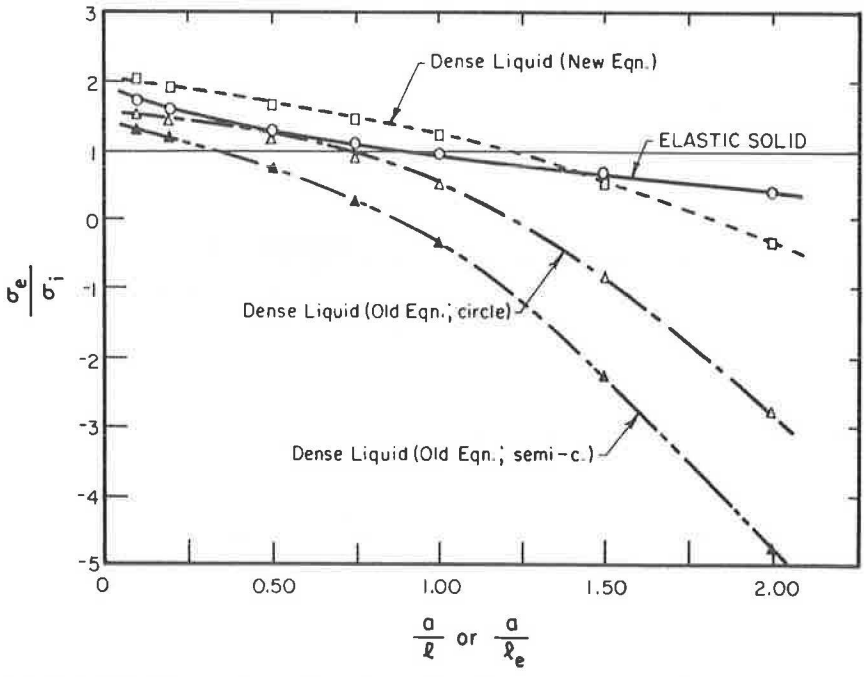

FIGURE 19 Comparison of maximum bending stresses under interior and edge loads.

(L/l_e) requirement for the development of the infinite-slab interior stress has been found to be about 3.0 to 3.5. The corresponding value for the edge stress is considerably higher, at about 5.0. This will lead to a lower value of (σ_e/σ_i) or LPEF than indicated in Figure 19 for slabs the length (L) of which is shorter than 5.0 times the radius of relative stiffness. The value of LPEF of 1.4 to 1.5, recommended by Thompson et al. *(6)* and other investigators, probably refers to such shorter (or cracked) slabs.

The relatively high values of LPEF indicated in Figure 19 are only valid within a narrow region at the plate edge. For typical loaded area sizes, the bending stress under an edge load may be expected to decrease to that due to interior loading within a distance of about one-half the radius of relative stiffness away from the edge.

In Figure 15, for the case of an F–4 aircraft load, the authors used ILLI–SLAB to derive the following equation for LPEF (dense liquid):

$$\text{LPEF} = 1.7016 + 0.000963\ h^2 - 0.00746\ \text{LTE} \qquad (6)$$

where LTE denotes the load transfer efficiency at the slab joints. Equation 6, given in Figure 15, accounts for the effect of load transfer, but it is only applicable to the case it was derived for because the major factor of (a/*l*) does not enter it explicitly. To compare Equation 6 with the results in Figure 19, one of the cases analyzed by the authors may be considered. Let

$E = 7 \times 10^5$ psi,
$h = 12$ in.,
$a = 5.7$ in.,
$\text{LTE} = 0$,
$k = 200$ psi/in., and
$p = 265$ psi.

For this system, $l = 27.3$ in. and $(a/l) = 0.21$. Equation 6 gives LPEF = 1.84 compared with LPEF = 1.92 obtained from Figure 19. Thus the authors' expression slightly underestimates the infinite-slab LPEF.

In view of no better alternative, the authors recommended that in situ edge stress be estimated from the interior stress calculated using ILLI–PAVE and Equation 6. The writer proposes the solid curve in Figure 19 as an improved choice for the determination of LPEF in such a calculation. This will avoid the introduction of any discrepancies between the layered elastic theory in ILLI–PAVE and the plate theory on which both Equation 6 and Figure 19 are based. The validity of this proposition has recently been reinforced by results obtained using two- and three-dimensional finite element computer programs *(7)*.

REFERENCES

1. A. M. Ioannides. *Analysis of Slabs-On-Grade for a Variety of Loading and Support Conditions*. Ph.D. dissertation. University of Illinois, Urbana, 1984.
2. A. Losberg. *Structurally Reinforced Concrete Pavements*. Doktorsavhandlingar Vid Chalmers Tekniska Hogskola, Goteborg, Sweden, 1960.
3. G. Pickett and S. Badaruddin. Influence Chart for Bending of a Semi-Infinite Pavement Slab. *Proc., 9th International Congress on Applied Mechanics,* Université de Bruxelles, Vol. 6, 1957.
4. A. M. Ioannides, M. R. Thompson, and E. J. Barenberg. Westergaard Solutions Reconsidered. In *Transportation Research Record 1043,* TRB, National Research Council, Washington, D.C., 1985, pp. 13–23.
5. A. M. Ioannides, M. R. Thompson, and E. J. Barenberg. Finite Element Analysis of Slabs-On-Grade Using a Variety of Support Models. *Proc., Third International Conference on Concrete Pavement Design and Rehabilitation,* Purdue University, Lafayette, Ind., April 1985.
6. M. R. Thompson et al. *Development of a Preliminary ALRS Stabilization Material Pavement Analysis System (SPAS)*. Technical Report ESL–TR–83–84. U.S. Air Force Engineering and Services Center, Tyndall Air Force Base, Fla., Aug. 1984.
7. A. M. Ioannides. Recent Findings Using Advanced Analysis Methods for Slabs-On-Grade. Presented to the Committee on Rigid Pavements at the 65th Annual Meeting of the Transportation Research Board, Washington, D.C., Jan. 1986.

Effects of Truck Tire Contact Pressure Distribution on the Design of Flexible Pavements: A Three-Dimensional Finite Element Approach

HSIEN H. CHEN, KURT M. MARSHEK, AND CHHOTE L. SARAF

The objective of the study reported in this paper was to investigate the effect of high inflation pressure and heavy axle load on asphalt-concrete pavement performance by using a three-dimensional finite element model instead of an elastic layer model, which is commonly used for pavement design. The flexible pavement finite element analysis was conducted with both an experimental nonuniform pressure model and a uniform pressure model as input to the program TEXGAP–3D. The results show that *(a)* the uniform pressure model overestimated the increase in tensile strain at the bottom of the surface for overinflated tires and underestimated the increase in tensile strain at the bottom of the surface for overloaded tires, *(b)* both high inflation pressure and heavy load caused a high increase in tensile strain at the bottom of the surface and a significant reduction of the pavement fatigue damage life, and *(c)* the axle load (not the inflation pressure) had a major influence on the subgrade rutting life.

A previous investigation *(1)*, which used a nonuniform concentric circular pressure model, has presented results that show the effect of high inflation pressures and heavy loads on the critical tensile strain at the bottom of the surface course and the compressive strain at the top of the subgrade. This model was obtained by dividing the experimental tire-pavement contact pressure distribution (along the tire contact width at the center of the tire imprint) into 14 different pressure regions. The pressure in each region was averaged and the radial distance was adjusted so that the total load from the nonuniform concentric circular pressure model was equal in magnitude to the tire axle load. However, experimental results show that the shoulder regions of a truck tire produce two strips of high pressure that can dominate the whole contact pressure distribution. Compared with the experimental tire contact pressure distribution, neither the uniform pressure model nor the nonuniform concentric circular pressure model appears appropriate as input for a pavement stress analysis. Note that the uniform pressure model assumed the contact pressure to be uniform over the circular (or square) imprint area and equal in magnitude to the tire inflation pressure.

The main objective of this paper is to investigate the effects of high inflation pressure and heavy load on stress on and damage to asphalt-concrete pavement by using a three-dimensional finite element model (i.e., experimental tire-pavement contact pressure distribution) instead of the nonuniform circular pressure model.

There are several general-purpose finite element computer programs available that can be used to analyze pavement performance. For the three-dimensional contact pressure model, the computer program TEXGAP–3D was selected in this study to predict the performance of flexible pavements under various inflation pressures and truck tire axle loads.

H. H. Chen and K. M. Marshek, Mechanical Engineering Department, The University of Texas at Austin, Austin, Tex. 78712. C. L. Saraf, Center for Transportation Research, The University of Texas at Austin, Austin, Tex. 78712.

DESCRIPTION OF PROGRAM TEXGAP–3D

The TEXGAP–3D (Texas Grain Analysis Program) is a linear elastic, static, finite element code for the analysis of a three-dimensional continuum structure and as such is not a general-purpose code because it does not contain other element types (e.g., beam, plate, and shell elements). The element library includes quadratic, isoparametic 20-node bricks; 15-node triangular prisms; and 10-node tetrahedrons. Material models include isotropic, orthotropic, and anisotropic. Permissible loadings and boundary conditions include pressure and traction on a surface, sliding and clamped surfaces, and prescribed nodal point forces or displacements.

PAVEMENT MODEL

The pavement selected for analysis is typical of that used on Texas farm-to-market roads and the behavior of the pavement structure is assumed to be linear elastic and homogeneous. The modulus of elasticity, Poisson's ratio, and layer thickness of each layer are as follows:

Surface	
Thickness	1.5, 2.0, 3.0, and 4.0 in.
Surface modulus	400 ksi
Poisson's ratio	0.35
Base	
Thickness	8 in.
Base modulus	60 ksi
Poisson's ratio	0.40
Subgrade	
Thickness	169 in.
Subgrade modulus	6 ksi
Poisson's ratio	0.45

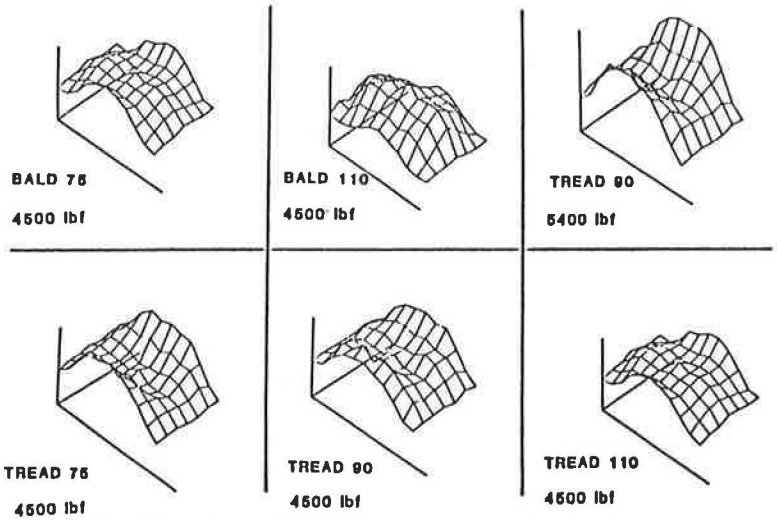

FIGURE 1 Experimental tire contact pressure distributions for various inflation pressures and axle loads.

PRESSURE DISTRIBUTION MODEL FOR TEXGAP–3D

The three-dimensional experimental truck tire contact pressure distributions for various tire inflation pressures (75, 90, and 110 psi) and axle loads (4,500 and 5,400 lbf) are shown in Figure 1. The pressure distribution model for an inflation pressure of 75 psi and an axle load of 4,500 lbf is given in Table 1. The pressure distributions input to TEXGAP–3D for the six cases studied in this paper are given elsewhere *(1)*. Because the contact pressure distributions are quite symmetric along the tire centerline, only one-quarter of the tire-pavement interaction was analyzed to minimize computer costs. The three-dimensional finite element model ($9 \times 6 \times 4$) consists of 216 solid brick elements. The element size was smallest within the contact pressure region as shown in the lower left corner of Figure 2. The pressure loading consists of 6×3 elements. Each element corresponds to an individual uniform contact pressure within the corresponding cell region. The bottom of the subgrade was assumed to be rigid.

EFFECT OF TIRE PRESSURE ON TENSILE STRAIN AT THE BOTTOM OF THE SURFACE

To demonstrate the accuracy of the TEXGAP–3D finite element model, results were compared with those of the layer program ELSYM5 for a uniform circular pressure model. Figure 3 shows the comparison of the three-dimensional uniform pressure model TEXGAP–3D and the uniform circular pressure model ELSYM5 for tensile strain at the bottom of the surface with various surface thicknesses (note that U designates uniform pressure model employing TEXGAP–3D and L designates the results from layer program ELSYM5). There is a close correspondence between the results from the two models. The increase of inflation pressure from 75 to 110 psi results in an approximate 102-microstrain (1 microstrain = 1×10^{-6} in./in.) increase at the bottom of a 1.5-in.-thick surface pavement. For the thicker surface pavements, the effect of the tire-pavement contact pressure distribution on surface tensile strain becomes less significant.

Figure 4 shows a comparison of the experimental non-

TABLE 1 EXPERIMENTAL TIRE CONTACT PRESSURE DISTRIBUTION MODEL FOR TEXGAP–3D

Along-Tire Contact Length (in.)	Along-Tire Contact Width (in.)											
	0	0.43	1.08	1.61	2.15	3.23	4.2	5.16	6.24	6.78	7.31	8.0	8.4
0	46	59	50	33	58	63	58	62	16	67	73	52	
1.47	112	96	64	35	65	59	52	68	44	59	98	124	
2.83	134	98	98	0	45	50	46	55	15	92	98	138	
4.25	133	101	71	36	63	60	55	55	17	87	97	125	
5.67	113	100	74	34	60	49	48	74	46	56	94	111	
7.09	66	62	59	17	54	34	50	58	25	65	66	57	
8.5													

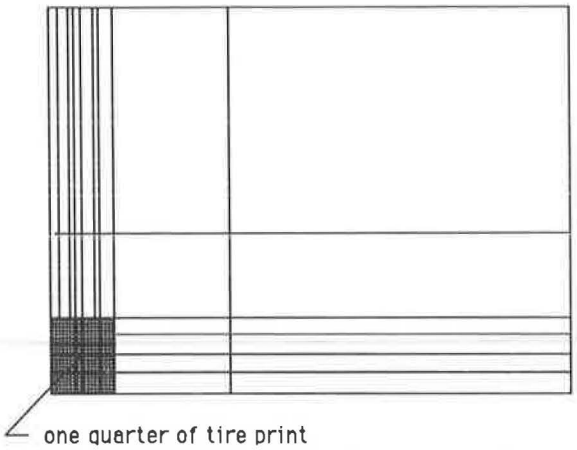

FIGURE 2 Grid formulation at the surface of the asphalt-concrete pavement (5 ft long by 5 ft wide).

uniform pressure model (T7545. T11045) and the uniform pressure model (U7545, U11045) for tensile strain at the bottom of the surface with various surface thicknesses (T designates the treaded-tire experimental contact pressure model). With a 47 percent increase in the inflation pressure (for the same axle load), the uniform pressure model predicts a 62 percent increase in the surface tensile strain at the bottom of the 1.5-in.-thick pavement, whereas the experimental model yields a 33 percent increase in the surface tensile strain. The uniform pressure model overestimates the reduction of contact area with an increased inflation pressure (for the same axle load) from 75 to 110 psi. For example, with the 47 percent increase in tire inflation pressure, the uniform pressure model will produce a 32 percent decrease in contact area compared with a measured 9 percent decrease in truck tire gross contact area.

For the 2-in.-thick surface pavement, the effect of increased

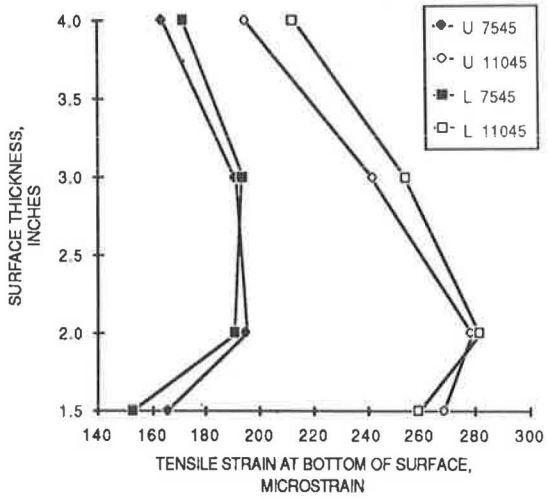

FIGURE 3 Effect of pressure distribution model on critical tensile strain at the bottom of the surface. U and L, respectively, represent the analysis obtained using TEXGAP–3D and ELSYM5, and the values 7545 and 11045 are for a tire loaded at 4,500 lbf with inflation pressures of 75 and 110 psi, respectively.

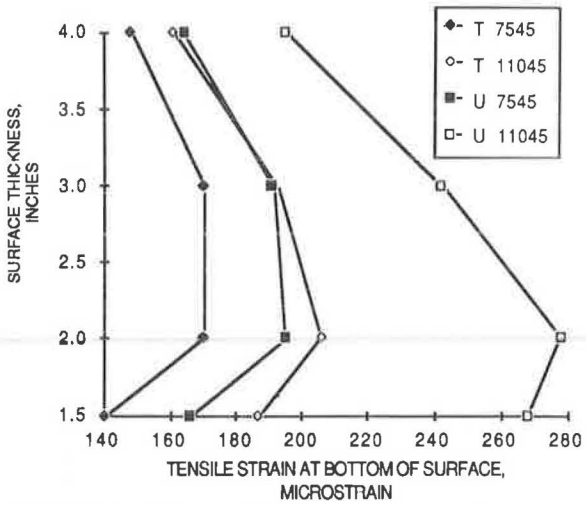

FIGURE 4 Effect of inflation pressure on the critical tensile strain at the bottom of the surface. T designates a treaded tire with a nonuniform (experimental) pressure model, and U designates a uniform pressure model. The values 7545 and 11045 represent, respectively, a tire loaded at 4,500 lbf with inflation pressures of 75 and 110 psi.

inflation pressure on the surface tensile strain along the tire transverse direction is shown in Figure 5. At a distance of 6 in. from the tire centerline, inflation pressure will have no significant effect on surface tensile strain.

EFFECT OF AXLE LOAD ON TENSILE STRAIN AT THE BOTTOM OF THE SURFACE

Figure 6 shows the effect of tire axle load on critical tensile strain for surface thickness of from 1.5 to 4.0 in. for both the nonuniform experimental pressure model and the uniform pres-

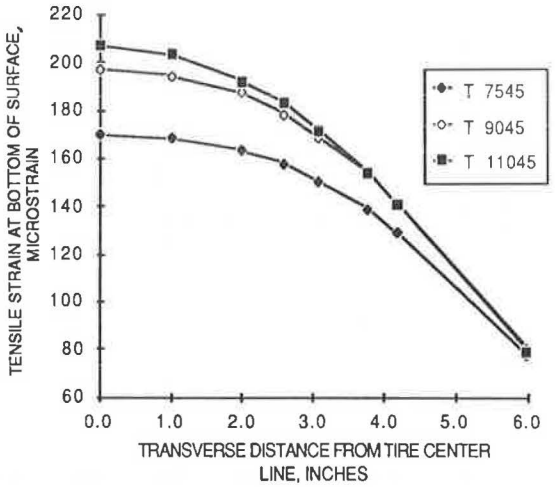

FIGURE 5 Effect of inflation pressure on the tensile strain contour at the bottom of a 2-in.-thick surface pavement. T designates a treaded tire; the values 7545, 9045, and 11045 represent, respectively, a tire loaded at 4,500 lbf with inflation pressures of 75, 90, and 110 psi.

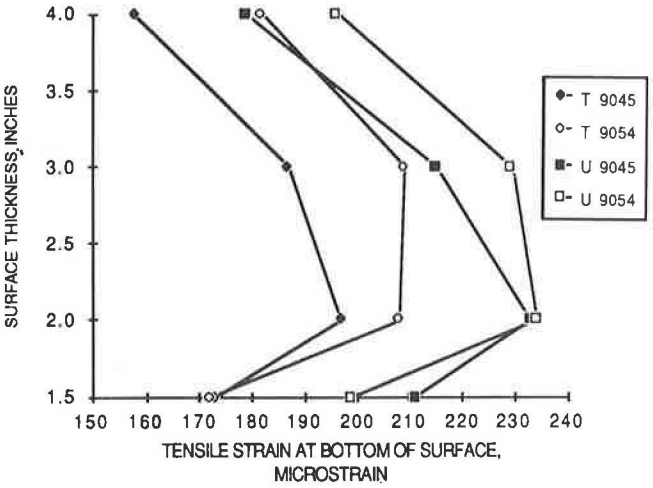

FIGURE 6 Effect of axle load on tensile strain at the bottom of the surface. T designates a treaded tire with nonuniform (experimental) pressure model, and U designates a uniform pressure model. The values 9045 and 9054 represent, respectively, a 90-psi tire inflation pressure with loads of 4,500 and 5,400 lbf.

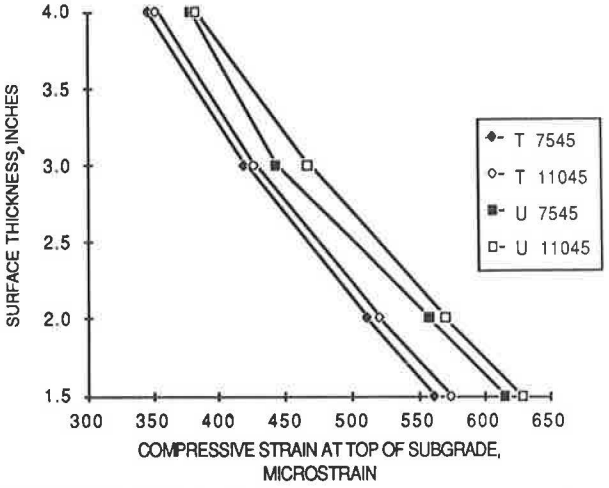

FIGURE 8 Effect of inflation pressure on compressive strain at the top of the subgrade. T designates a treaded tire with a nonuniform (experimental) pressure model, and U designates a uniform pressure model. The values 7545 and 11045 represent, respectively, a tire loaded at 4,500 lbf with inflation pressures of 75 and 110 psi.

sure model. The results from the uniform pressure model are conservative in comparison with those of the experimental model for various surface thicknesses. As anticipated, the overloaded tire consistently produces the highest strains. For a 4.0-in.-thick surface pavement and a 20 percent increase in the axle load (for the same tire inflation pressure), the uniform pressure model results in a 10 percent increase in the surface tensile strain compared with a 15 percent increase for the experimental pressure model. The uniform pressure model overestimates the increase of the contact area and therefore produces a smaller increase in surface tensile strain.

Figure 7 shows the tensile strain developed at the bottom of the 2-in.-thick surface course by the application of a 4,500-lbf load and a 5,400-lbf load (20 percent overload) to the treaded tire at the 90-psi–rated inflation pressure. The overloaded tire consistently produces a higher tensile strain even at a distance of 6.0 in. from the tire centerline.

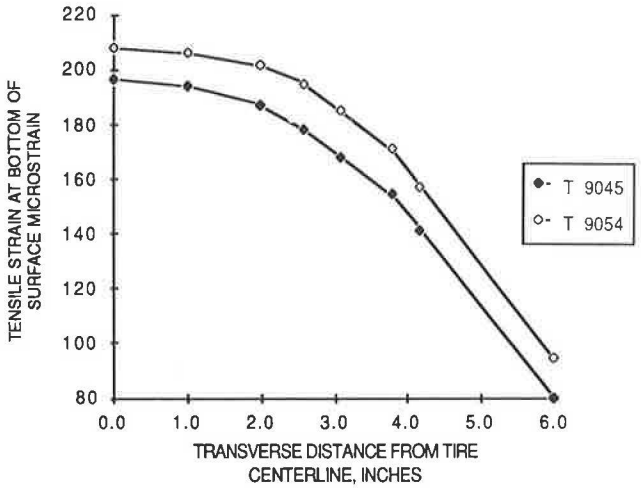

FIGURE 7 Effect of axle load on tensile strain at the bottom of a 2-in.-thick surface pavement. T designates a treaded tire, and the values 9045 and 9054 represent, respectively, a 90-psi tire inflation pressure with loads of 4,500 and 5,400 lbf.

EFFECT OF TIRE PRESSURE ON SUBGRADE COMPRESSIVE STRAIN

Figure 8 shows that a 47 percent increase in inflation pressure (for the same axle load) produces less than a 2 percent increase in the compressive strain developed at the top of the subgrade for both the uniform pressure model and the nonuniform experimental pressure model. The uniform pressure model consistently overestimates the subgrade compressive strain except for thick surface pavements.

EFFECT OF AXLE LOAD ON SUBGRADE COMPRESSIVE STRAIN

Figure 9 shows that the axle load has a significant effect on the compressive strains at the top of the subgrade for both the uniform pressure model and the nonuniform pressure model. The figure shows that a 20 percent increase in axle load (for the same inflation pressure) produces approximately a 20 percent increase in the critical subgrade compressive strain for both models. However, the uniform pressure model consistently overestimated the subgrade compressive strain (compared with the strain obtained by the nonuniform pressure model) for the range of surface thicknesses shown.

PAVEMENT DAMAGE

The two primary pavement distress conditions addressed in this analysis are fatigue and rutting. Fatigue cracks may develop if

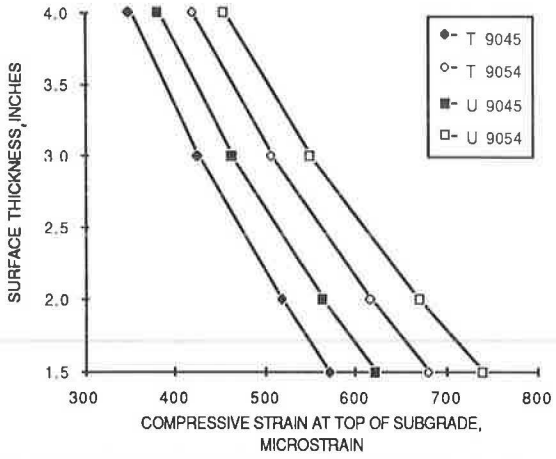

FIGURE 9 Effect of axle load on compressive strain at the top of the subgrade. T designates a treaded tire with a nonuniform (experimental) pressure model, and U designates a uniform pressure model. The values 9045 and 9054 represent, respectiveiy, a 90-psi tire inflation pressure with loads of 4,500 and 5,400 lbf.

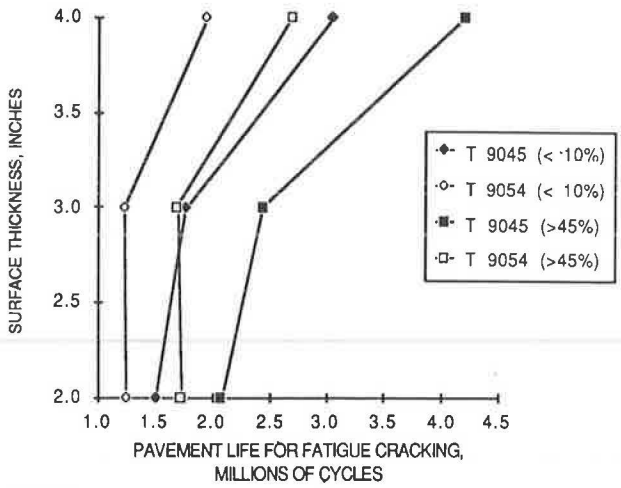

FIGURE 11 Effect of axle load on pavement fatigue damage life. T designates a treaded tire, and the values 9045 and 9054 represent, respectively, a 90-psi tire inflation pressure with loads of 4,500 and 5,400 lbf.

the tensile strain at the bottom of the asphalt layer is excessive. Rutting, the permanent deformation that leads to loss of surface shape, may occur if the compressive strain at the top of the subgrade is excessive.

FATIGUE-CRACKING DAMAGE

Flexible pavement fatigue is manifested by the appearance of alligator cracking in the wheelpaths and is caused by excessive tensile stresses and strains at the bottom of the asphalt-concrete surface layer. The tensile strains that have been computed using TEXGAP–3D at the bottom of the asphalt-concrete surface are used to approximate the number of 18-kip axle load applications until Class 2 cracking occurs. Class 2 cracking is defined as the appearance of alligator cracking. Class 3 cracking is defined as the progression of alligator cracking to severe spalling. A pavement surface that has Class 2 cracking is assumed to have failed in fatigue.

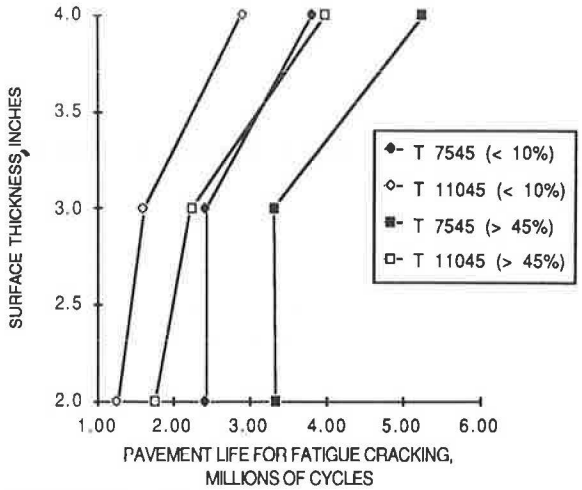

FIGURE 10 Effect of inflation pressure on pavement fatigue damage life. T designates a treaded tire, and the values 7545 and 11045 represent, respectively, a tire loaded at 4,500 lbf with inflation pressures of 75 and 110 psi.

Predictions of the number of loads (N_f) necessary to cause fatigue failure have been developed in the literature. Such predictions are based on laboratory tests, with little correlation to field experience to account for the relaxation times between traffic loads and the resulting differences in crack propagation rates. A literature survey showed that the number of wheel loads required to initiate fatigue distress is on the order of 13 to 18 times that predicted by constant stress laboratory tests *(2)*.

A field fatigue distress model was developed by Finn et al. *(2)* for two levels of cracking: *(a)* cracking less than or equal to 10 percent of the wheelpath area and *(b)* cracking equal to or greater than 45 percent of the wheelpath area. These equations are

$$\log N_f (\leq 10\%) = 15.947 - 3.291 \log \varepsilon_t - 0.854 \log E^* \quad (1)$$

$$\log N_f (\geq 45\%) = 16.086 - 3.291 \log \varepsilon_t - 0.854 \log E^* \quad (2)$$

where

N_f = the number of loads of constant stress necessary to cause fatigue cracking,
ε_t = the initial tensile microstrain at the bottom of the surface, and
E^* = the complex modulus of the asphalt-concrete surface (ksi).

The number of loads of constant stress necessary to cause fatigue cracking can be obtained by substituting the computed tensile strain from finite element program TEXGAP–3D into Equations 1 and 2 for either the 10 percent cracking model or the 45 percent cracking model. Figure 10 shows the effect of

TABLE 2 TENSILE STRAIN AT THE BOTTOM OF THE SURFACE AND CORRESPONDING FATIGUE LIFE FOR VARIOUS SURFACE THICKNESSES, INFLATION PRESSURES, AND AXLE LOADS

	Tensile Strain at Bottom of Surface (10^{-1} in./in.) for Surface Thickness of (in.)			10% Fatigue-Cracking Model (million cycles) for Surface Thickness of (in.)			45% Fatigue-Cracking Model (million cycles) for Surface Thickness of (in.)		
	2.0	3.0	4.0	2.0	3.0	4.0	2.0	3.0	4.0
T7545	170.0	170.4	148.1	2.42	2.40	3.82	3.34	3.31	5.26
T11045	206.5	192.3	161	1.27	1.62	2.90	1.76	2.23	3.99
T9045	196.5	187	158.4	1.51	1.77	3.06	2.07	2.44	4.21
T9054	208	208.9	181.6	1.25	1.23	1.95	1.72	1.69	2.69
U7545	194.6	191.1	163.8	1.55	1.65	2.74	2.14	2.27	3.77
U11045	277.8	242	194.5	0.48	0.76	1.56	0.66	1.04	2.14
U9045	232.6	214.8	178.6	0.864	1.12	2.06	1.19	1.55	2.84
U9054	233.6	228.8	196.5	0.85	0.91	1.50	1.17	1.26	2.07

Note: T designates a treaded tire, with a nonuniform (experimental) pressure model, and U designates a uniform model. The last two digits (45 and 54) stand for 4,500 lbf and 5,400 lbf, respectively, and the numbers 75, 90, and 110 represent inflation pressures of 75, 90, and 110 psi, respectively.

increasing tire inflation pressure on fatigue damage life for various surface thicknesses. Pavement life improves with thicker pavement. For the 2-in.-thick surface pavement, a 47 percent increase in the tire inflation pressure (for the same axle load) results in a 33 percent increase in the surface tensile strain and therefore in a 48 percent reduction of pavement life for the 10 percent fatigue-cracking model and the 45 percent fatigue-cracking model. Figure 11 shows the effect of truck tire overload on the pavement fatigue life for various surface thicknesses (2 to 4 in.). For a 4-in. surface pavement, a 20 percent increase in axle load (for the same tire inflation pressure) will cause a 36 percent reduction in pavement life for both fatigue-cracking models. The tensile strains at the bottom of the surface and the corresponding number of constant stress cycles (N_f) necessary to cause either 10 or 45 percent fatigue cracking are given in Table 2 for various surface thicknesses, inflation pressures, and axle loads.

RUTTING

Rutting in the wheelpaths results from high compressive strains and permanent deformation in one or more pavement layers, influenced by truck tire axle load, layer properties, environment, and number of traffic loadings. Analysis of the AASHO Road Test showed that lateral movement of material in the subbase accounted for most of the rutting observed *(3)*.

To minimize surface rutting, Shell Company engineers used results from the AASHO Road Test to develop a compressive strain criteria equation *(4)*:

$$W_{18} = 6.15 \times 10^{17} (1/\varepsilon_c)^{4.0} \quad (3)$$

where ε_c is the compressive microstrain at the top of the subgrade, and W_{18} is the number of weighted 18-kip axle loads before excessive permanent deformation.

Figure 12 shows the effect of increasing the axle load on the subgrade rutting damage life for various surface thicknesses. A 20 percent increase in axle load (for the same inflation pressure) will result in a 19 percent increase in subgrade compressive strain and a 50 percent reduction in pavement life. The subgrade compressive strains and the corresponding rutting life are given in Table 3 for various surface thicknesses, inflation pressures, and tire axle loads.

CONCLUDING REMARKS

The effects of high inflation pressure and heavy load on asphalt-concrete pavement stresses, strains, and the corresponding pavement damage life were analyzed using the three-dimensional finite element tire-pavement contact pressure model rather than the uniform circular pressure model or the nonuniform concentric circular pressure model.

The computation time for a single run on TEXGAP–3D (216 brick elements) was approximately 18 min, corresponding to $80 per case, compared with a 2.5-sec execution time using the layer program ELSYM5.

Table 4 gives a comparison of the three-dimensional finite element model (uniform or nonuniform pressure distribution) and ELSYM5. On the basis of the limited number of tire contact pressure distributions and pavements studied, it can be

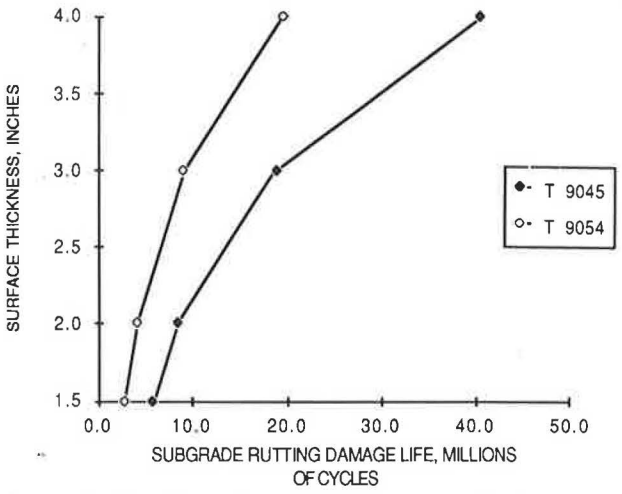

FIGURE 12 Effect of axle load on pavement subgrade rutting damage life. T designates a treaded tire, and the values 9045 and 9054 represent, respectively, a 90-psi tire inflation pressure with loads of 4,500 and 5,400 lbf.

TABLE 3 COMPRESSIVE STRAIN AT THE TOP OF THE SUBGRADE AND THE CORRESPONDING PAVEMENT DAMAGE LIFE FOR VARIOUS SURFACE THICKNESSES, INFLATION PRESSURES, AND AXLE LOADS

	Compressive Strain at Top of Subgrade ($\times 10^{-6}$ in./in.) for Surface Thickness of (in.)				Million Load Cycles Before Excessive Deformation (rutting) for Surface Thickness of (in.)			
	1.5	2.0	3.0	4.0	1.5	2.0	3.0	4.0
T7545	562.8	510.8	419.6	347.2	6.13	9.03	19.8	42.3
T11045	575.3	521.4	427.2	352.6	5.61	8.32	18.5	39.8
T9045	571	518	424.7	351	5.78	8.54	18.9	40.5
T9054	681	618.3	508	420.4	2.86	4.21	9.23	19.7

TABLE 4 COMPARISON OF VARIOUS MODELS FOR TENSILE STRAIN AND SUBGRADE COMPRESSIVE STRAIN

	47% Increase in Tire Inflation Pressure			20% Increase in Truck Tire Axle Load		
	Nonuniform	Uniform	ELSYM5	Nonuniform	Uniform	ELSYM5
Tensile strain at bottom of surface (% increase)	33	62	69	15	10	8
Subgrade compressive strain (% increase)	2	2	5	19	19	17

concluded that the uniform pressure model overestimates the tensile strain at the bottom of the surface for either underinflated or overinflated tires. The uniform pressure model will predict a higher percentage increase in tensile strain than will the nonuniform experimental pressure model. However, with the same percentage increase in truck tire axle load, the uniform pressure model will underestimate the percentage increase in the surface tensile strain.

Inflation pressure will have less than a 2 percent effect on the compressive strains at the top of the subgrade for either the uniform pressure model or the nonuniform pressure model. Therefore inflation pressure is an insignificant factor in subgrade rutting.

Axle load has a significant effect on subgrade compressive strain and corresponding subgrade rutting life. A 20 percent increase in the axle load results in a 19 percent increase in the subgrade compressive strain and an approximately 50 percent reduction of pavement life.

ACKNOWLEDGMENTS

The authors are pleased to acknowledge the combined efforts and support of the Center for Transportation Research and the Mechanical Engineering Department at the University of Texas at Austin and the Texas State Department of Highways and Public Transportation, in cooperation with the Federal Highway Administration, U.S. Department of Transportation.

REFERENCES

1. K. M. Marshek, W. R. Hudson, H. H. Chen, C. Saraf, and R. B. Connell. *Effect of Truck Tire Inflation Pressure and Axle Load on Pavement Performance.* Research Report 386–2F. Center for Transportation Research, The University of Texas at Austin, 1985.
2. F. Finn et al. The Use of Distress Prediction Subsystems for the Design of Pavement Structures. *Proc., 4th International Conference on the Structural Design of Asphalt Pavements,* University of Michigan, Ann Arbor, Aug. 1977.
3. *Special Report 61E: The AASHO Road Test: Report 5—Pavement Research.* HRB, National Research Council, Washington, D.C., 1962.
4. *Shell Pavement Design Manual.* Shell International Petroleum Company Limited, London, England, 1978.

Publication of this paper sponsored by Committee on Flexible Pavements.

Effect of Layer Slippage on Performance of Asphalt-Concrete Pavements

M. Y. SHAHIN, K. KIRCHNER, E. W. BLACKMON, AND HISAO TOMITA

Stresses and strains that result from aircraft loading in an asphalt-concrete pavement section were computed by layered elastic theory. A fatigue model was used to estimate the life of the pavement. Variations in interlayer slippage, layer thickness, asphalt stiffness, and pavement loading were shown to affect the life of the pavement. Layer slippage generates large tensile strains at the bottom of the slipped layer. Asphalt at either side of the slipped interface distorts in different directions, which propagates the layer slippage and further destroys the bond between the layers. Under vertical loading in a pavement in which slippage has occurred, increasing the thickness of the slipped overlay decreases the fatigue life of the pavement until a thickness of 6 in. is reached. High asphalt stiffness of thin overlays reduces the fatigue life of the pavement. Horizontal tangential loads cause the location of the maximum tensile strain in the pavement to shift to behind the wheel at the top of the overlay. If slippage has occurred, the horizontal load must be completely withstood by the top slipped layer. This leads to crescent cracks in slipped overlays. The effect is smaller in stiffer layers. The influence of overlay thickness is minor in this case. A pavement in which interlayer slippage has occurred should be repaired by removing the slipped overlay and replacing it with a well-bonded overlay. Overlaying a second time requires a very large overlay to keep the tensile strains in the slipped overlay small.

Slippage between pavement layers changes the stress distribution within a pavement section, overstressing areas in the pavement and reducing performance. This paper provides the results of a study of interlayer slippage of airfield pavements. Stresses and strains in a pavement section that result from aircraft loading were computed by layered elastic theory. A fatigue model was used to estimate the life of the pavement. Variations in interlayer slippage, layer thickness, asphalt stiffness, and pavement loading were shown to affect the life of the pavement.

The pavement section used, shown in Figure 1, was designed for a DC–9 aircraft assuming a fairly weak subgrade [California bearing ratio (CBR) = 5]. The pavement was designed using FAA Advisory Circular 150/5320–6C, *Airport Pavement Design and Evaluation (1)*. A 2-in. asphalt-concrete overlay was added and assumed to slip by varying amounts over the original asphalt layer.

M. Y. Shahin, K. Kirchner, and E. W. Blackmon, U.S. Army Construction Engineering Research Laboratory, P.O. Box 4005, Champaign, Ill. 61820–1305. H. Tomita, FAA, U.S. Department of Transportation, APM–740, 800 Independence Avenue, S.W., Washington, D.C. 20591.

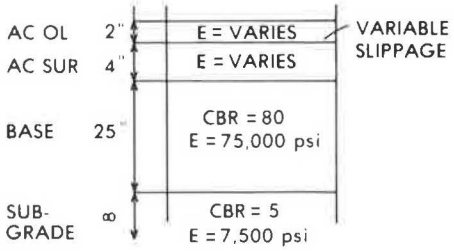

FIGURE 1 Pavement section and properties.

COMPUTER MODEL

To model the stresses, strains, and displacements in the asphalt-concrete pavement, the Shell Research computer program Bitumen Structures Analysis in Roads (BISAR) *(2)* was used. This program uses elastic layer theory to analyze multilayered systems subjected to vertical and horizontal multiple loadings. BISAR allows varying degrees of slippage between the layers by considering the relative displacement of the layers to be proportional to the shear stress transferred across the layer interface. The degree of slippage that can be modeled ranges from no slippage to frictionless (complete) slippage. The ability of BISAR to model the slipped layer condition with both horizontal and vertical loads made this program attractive for investigating interlayer slippage.

FATIGUE MODEL

A representative fatigue model that would take varying asphalt stiffnesses into consideration was desired. Two fatigue models, the French Shell model *(3)* and the Way model *(4)* met this criterion. The French Shell model was ultimately chosen because of its ability to incorporate asphalt properties in addition to stiffness and because it is not specific to a given geographic area. The Way model is specific to Arizona.

The French Shell model (or the Bonnaure, Gravois, and Udron model) uses three asphalt parameters to relate pavement life to the maximum horizontal tensile strain at the bottom of an asphalt layer using Equation 1:

$$e = [(4.102)\,(PI) - 0.205(PI)\,(V) + (1.094)V - 2.707]\,(S^{-0.36})\,N^{-0.2} \quad (1)$$

where

e = maximum horizontal tensile strain;
V = volumetric bitumen content of mix (%);

PI = penetration index of binder in mix;
S = stiffness modulus of mix (N/m^2) (1 N/m^2 = 1.45 × 10^{-4} psi); and
N = pavement life, loading cycles.

Using V = 9.8 percent and PI = 0, the model reduces to Equation 2:

$$N = 3.3 \times 10^4 (1/S)^{1.8} (1/e)^5 \quad (2)$$

Subgrade fatigue life was estimated using the vertical compressive strains on top of the subgrade with Equation 3, which was developed by the U.S. Army Corps of Engineers *(5)*:

$$e_v = 5.511 \times 10^{-3} [1/N^{0.1532}] \quad (3)$$

where e_v is the vertical compressive strain on the subgrade and N is pavement life, loading cycles.

FATIGUE LIFE

Pavement fatigue life is controlled by one of three strains located in the pavement structure: the vertical compressive strain on the top of the subgrade, the horizontal tensile strain at the bottom of the overlay, or the horizontal tensile strain at the bottom of the original asphalt layer. Strains at these locations can be used to determine the fatigue life of the subgrade, overlay, and original asphalt layer, respectively. The fatigue lives from these locations were compared to find the critical location in the pavement, which was indicated by the lowest fatigue life. This lowest fatigue life was assumed to control the structural life of the entire pavement.

EFFECT OF SLIPPAGE

Figure 2 shows the magnitudes of the horizontal strains in the pavement section directly under one DC–9 wheel for both frictionless slippage and full adhesion between the pavement layers. With no slippage, the maximum tensile strain in the section is located at the bottom surface of the original asphalt layer. If slippage is allowed below the overlay, tensile strain also exists at the bottom surface of the overlay. This strain was found to be larger than the strain at the bottom of the existing asphalt layer.

Vertical strains below the centerline of the wheel were also investigated. If the top asphalt layer is allowed to slip over the original asphalt layer, the effective stiffness of the two layers decreases, surface loads are less distributed at the subgrade, and vertical compressive strains on the subgrade increase.

To illustrate the effect of varying degrees of slippage, the same problem was analyzed using different slip coefficients in the BISAR computer model. The slip coefficient (K) varies from 0, no slippage, to 1,000, total slippage. Figure 3 shows the increases in horizontal strain with increasing slippage at the bottom of the overlay. Several conclusions can be drawn from this graph:

1. At the bottom of the overlay the strain increases rapidly near zero slippage and slowly near free slippage. This indicates that a small amount of slippage is all that is required to produce strains in the pavement that approach those of the free slippage case.

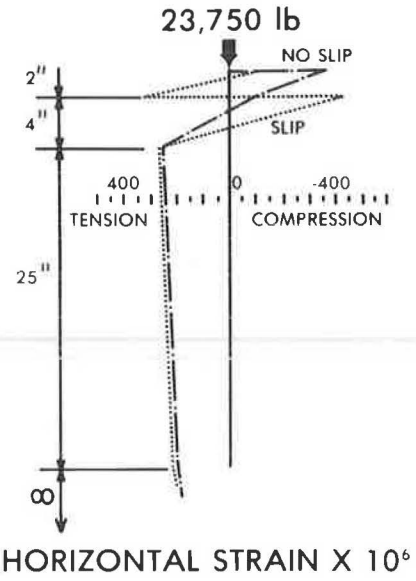

FIGURE 2 Horizontal strain under centerline of a single DC–9 wheel.

2. The bottom of the overlay goes into tension horizontally after very little slippage has taken place. Simultaneously, the top of the original asphalt layer develops a horizontal compressive strain, as shown in Figure 4. These differing strains that result from the slippage cause points in the pavement near each other (but on different sides of the interface) to distort in different directions. This further weakens the bond between the asphalt layers, allowing more slippage, which leads to higher strains.

For small amounts of slippage, the life of the original asphalt layer controls the life of the pavement, as shown in Figure 5. As the degree of slippage increases, the bottom of the overlay develops tensile strains that are larger than the strains at the bottom of the original asphalt layer. After this point the fatigue life of the overlay controls the pavement life.

The subgrade strains increase as increasing slippage allows the overlay and the original asphalt layer to act independently. Because two thinner layers are not as stiff as one layer of the

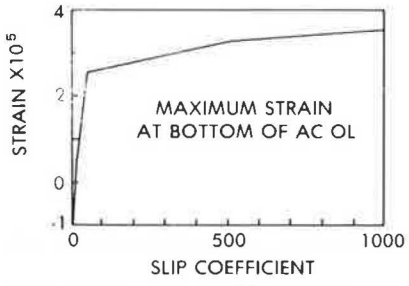

FIGURE 3 Effect of interlayer slippage on maximum horizontal strains.

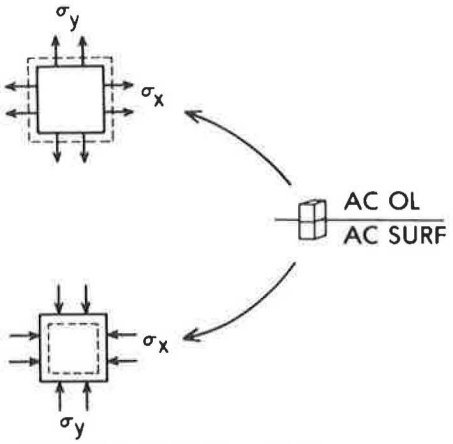

FIGURE 4 Distortion of adjacent elements across a slipping layer interface.

same overall thickness, the compressive vertical strain at the subgrade increases.

EFFECT OF OVERLAY THICKNESS

When interlayer slippage occurs, the fatigue life of a pavement is reduced because of the development of large tensile strains at the bottom of the overlay. Strains and corresponding fatigue lives at critical points in the pavement were investigated for different overlay thicknesses to find the effect of overlay thickness and slippage on payment life.

Figure 6 shows the estimated fatigue lives of the overlay and the original asphalt surface layer for various overlay thicknesses. The subgrade strains are not controlling. With free slippage allowed, increasing the overlay thickness decreases the overlay life until a thickness of 6 in. is reached. At overlay thicknesses larger than 6 in. the life of the pavement increases slightly. At an overlay thickness of 10 in. the life of the pavement still has not increased above the life of the pavement with an unslipped 2-in. overlay.

In the free slippage case, the overlay acts independently of the rest of the pavement system. Figure 7 shows a comparison of the deflections at the pavement surface and at the bottom of the overlay for various overlay thicknesses. The deflections vary linearly with overlay thickness at large thicknesses. For

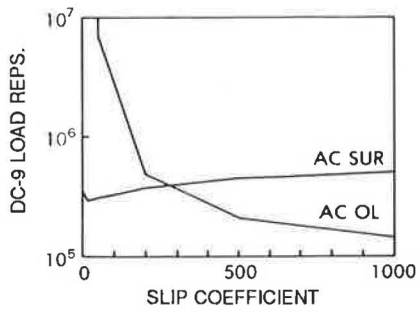

FIGURE 5 Pavement life with varying interlayer slippage.

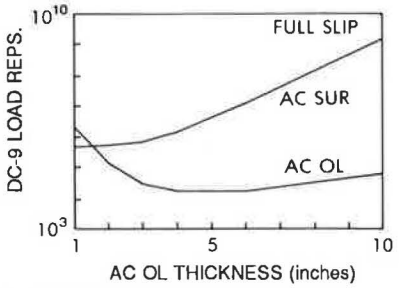

FIGURE 6 Effect of overlay thickness on the fatigue life of a pavement with interlayer slippage.

smaller overlay thicknesses (1 to 3 in.) thickness has very little effect on deflection. As the overlay increases in thickness, the structure becomes stiffer and resists more of the deflection caused by the applied load. The deflection resisted per inch of overlay will increase until the overlay thickness reaches 3 in., which causes an increase in the vertical compressive strain relative to that present at an overlay thickness of 1 in. This increase in vertical compressive strain increases the horizontal tensile strains in the asphalt overlay. At the same time, the horizontal tensile strains at the bottom of the overlay are also increasing because of bending. The horizontal strains due to vertical compression peak at an overlay thickness of 3 in.; those due to bending are maximum at 6 in. where the deflection of the pavement becomes inversely proportional to the overlay thickness, as is shown in Figure 7. With overlays larger than 6 in., the reduced deflections lead to smaller strains and an increasing fatigue life.

If complete bonding is present between the asphalt layers, overlays thicker than 2 in. will always increase the life of the pavement. This is not true when overlay slippage is present. When overlay slippage occurs, the overlay thickness must be large to restore a reasonable life to the pavement.

EFFECT OF ASPHALT STIFFNESS

The modulus of the 2-in. asphalt overlay was held constant at 500,000 psi while the 4-in. original asphalt layer modulus was

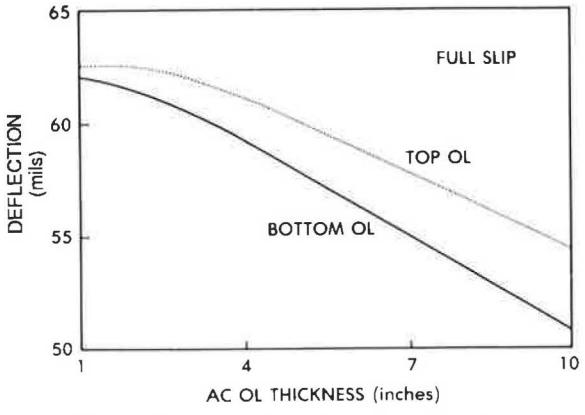

FIGURE 7 Pavement deflection at overlay top and bottom with varying overlay thickness.

varied from 250,000 to 1,000,000 psi and vice versa. Both cases were analyzed with interlayer slippage.

The effect of varying the original asphalt surface layer modulus while holding the overlay modulus constant at 500,000 psi is shown in Figure 8. The tensile strains at the bottom of the overlay control the pavement life as the original layer modulus increases to 500,000 psi. These strains are decreasing while the overlay modulus is constant, so the pavement life increases. Above 500,000 psi, the strains at the bottom of the original layer control the pavement life. These strains are decreasing as the layer stiffens, but the modulus increase causes the strain multiplier in the fatigue equation to decrease at a faster rate, yielding a reduction in pavement life.

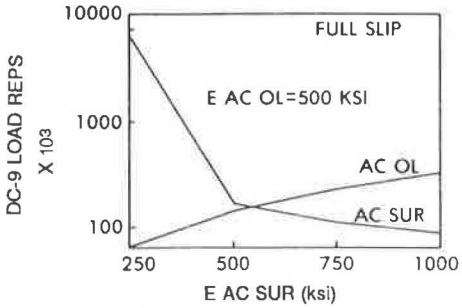

FIGURE 8 Pavement life with changing asphalt surface layer modulus.

The effect of varying the overlay modulus from 250,000 to 1,000,000 psi while holding the original layer constant at 500,000 psi is shown in Figure 9. At all values of overlay modulus, the strains at the bottom of the overlay control the pavement life. These strains decrease as the modulus increases, but the fatigue model multiplier decreases faster, causing a reduction in pavement life. The highest pavement lives in the cases examined were obtained with an overlay modulus of either 250,000 or 500,000 psi and an original surface layer modulus of 500,000 psi.

VARYING BOTH OVERLAY THICKNESS AND MODULUS

The behavior of pavement life with varying overlay thickness is similar for any single pavement modulus under vertical loading when interlayer slippage is present. The pavement life decreases as the overlay thickness increases from 2 in. to a thickness of between 4 and 6 in., after which the life begins to increase. Figure 10 shows the effect of varying both the overlay thickness and the modulus. In general, pavement moduli that perform well as thin overlays do not perform as well at higher overlay thicknesses, and vice versa.

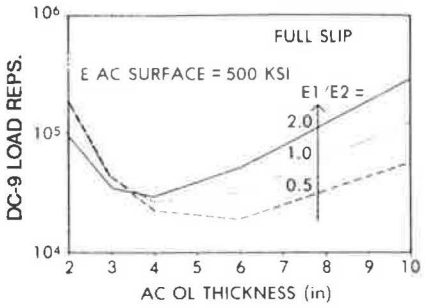

FIGURE 10 Effect of overlay thickness and modulus on pavement fatigue life.

At low overlay thicknesses of 2 or 3 in., increasing the overlay modulus decreases the pavement life as was discussed earlier. At these thin overlay thicknesses, where the overlay reacts with constant strain behavior, the strains generated in the pavement decrease as the modulus of the asphalt concrete increases. However, higher modulus asphalt concrete is more susceptible to fatigue, and pavement fatigue life decreases.

As the overlay behavior switches from constant strain behavior to a constant stress response between 3 and 4 in. of overlay thickness, the effect of varying the overlay modulus on pavement life reverses. Above 4 in., an increase in overlay stiffness decreases the induced strains enough to offset the increased fatigue susceptibility, which increases pavement life.

EFFECT OF HORIZONTAL LOADS

Pavements are usually designed only for vertical loads, but horizontal loads also act on the top pavement surface. Horizontal loads are applied to the pavement surface when aircraft stop or turn. The magnitude of the horizontal load is determined by the coefficient of friction between the tire and the pavement,

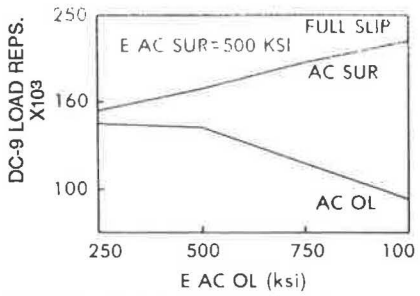

FIGURE 9 Pavement life with varying overlay modulus.

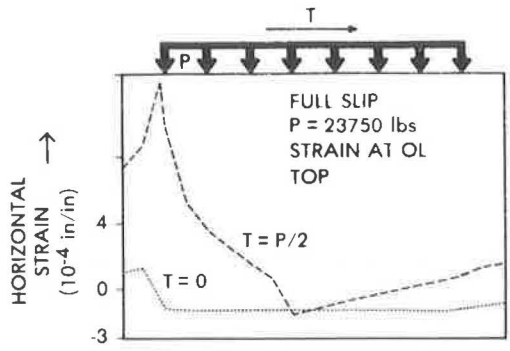

FIGURE 11 Strains generated at overlay surface by an applied shear load.

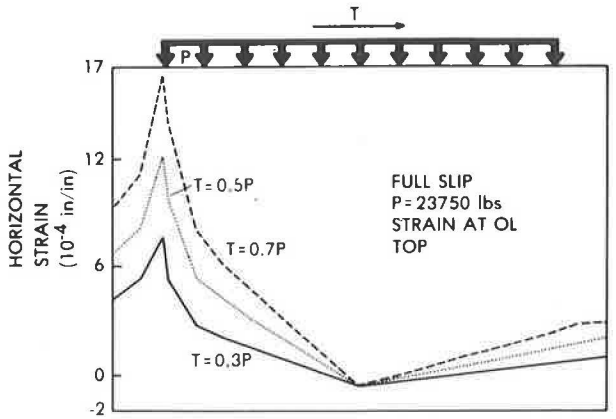

FIGURE 12 Strain magnitude at overlay surface with varying shear load.

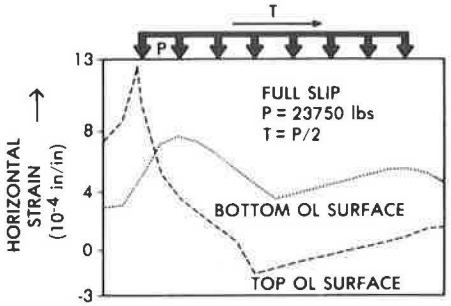

FIGURE 14 Strains generated at the top and bottom of the overlay by applied shear load.

which will vary with pavement and tire conditions up to a limiting value of 0.8 *(6)*. For this investigation a horizontal shear force of one-half the vertical load (0.5P) was assumed except where otherwise specified. The addition of a horizontal load will increase the critical stresses and strains in a pavement and will shift the location of the maximum strain from the center of the loaded area to the side of the loaded area opposite the direction of applied shear.

Figure 11 shows the distribution of the maximum horizontal strains in the top surface of the overlay along a cross section through the wheel imprint both with and without a horizontal load applied in the direction of travel for a single DC–9 wheel load. The modulus of each asphalt layer was 250,000 psi. The radius of the contact area is 7.1 in. The addition of the horizontal force generates very large tensile strains of 1.22×10^{-3} in./in. at the top of the overlay behind the wheel. This is three to four times as large as typical fatigue-generated strains that are on the order of 3×10^{-4} to 4×10^{-4} in./in.

Figure 12 shows the effect of changing the magnitude of the horizontal load applied at the pavement surface from 0.3P to 0.7P, where P is the applied vertical load. The magnitude of the maximum strain increases linearly from 0.766×10^{-3} to 1.64×10^{-3} as the horizontal load increases from 0.3P to 0.7P. The magnitude of the applied horizontal load is the single most important determinant of the magnitude of the critical strains in the pavement.

The maximum horizontal strains on the top surface of the overlay with and without interlayer slippage are compared in Figure 13. The strains are critical (0.855×10^{-3} in./in.) even with full adhesion between the layers, and they increase by almost 50 percent to 1.24×10^{-3} in./in. when the layers slip. Therefore, when analyzing a loading with an applied horizontal force, the maximum horizontal strains at the top asphalt surface should be checked in addition to the usual controlling strains, even when interlayer slippage is not present.

Figure 14 shows the strains at both the top surface of the overlay and the bottom of the overlay. The strains are lower at the bottom of the overlay, and the location of maximum strain has shifted to inside the wheel imprint. Cracks will initiate at the top of the overlay where the strains are the greatest. The cracks will propagate at an angle through the overlay to the location of maximum strain at the overlay bottom, giving an angled crack through the overlay.

Increasing the stiffness of the overlay when a horizontal force is applied reduces the magnitude of the maximum strain at both the top and the bottom surfaces of the overlay, as shown in Figures 15 and 16, respectively. The stiffer structure has less variation in strain values; the strain profile is flatter and lower. The stiffer layer is more sensitive to fatigue, but the magnitude of the induced strain decreases rapidly with increasing overlay stiffness, so pavement life will increase.

To investigate further the distribution of the maximum tensile strains and their directions, a grid of points was analyzed at the top surface of the overlay for a DC–9 aircraft with a horizontal shear force applied in the direction of travel. The horizontal force was again assumed to be one-half the vertical

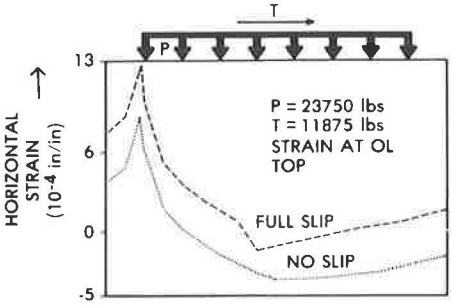

FIGURE 13 Effect of interlayer slippage on surface strain.

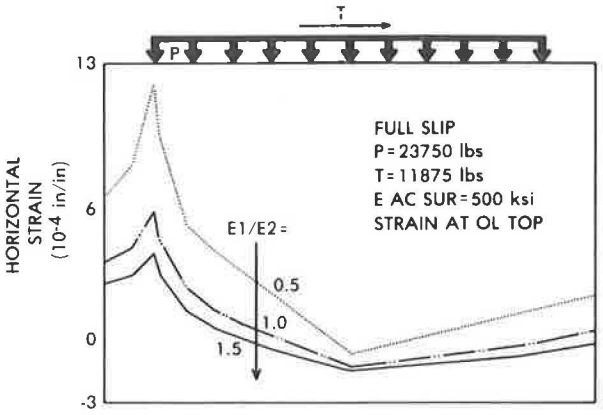

FIGURE 15 Effect of overlay modulus on surface strains from shear loading.

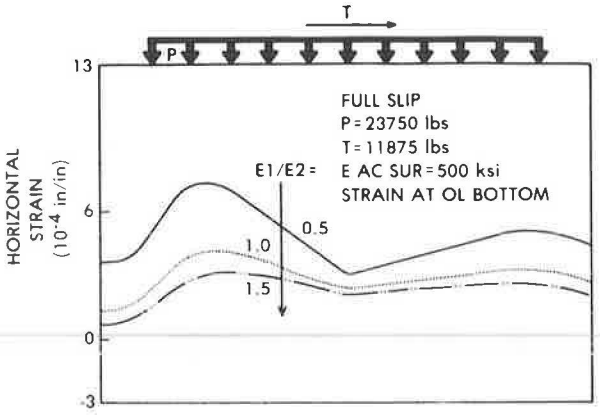

FIGURE 16 Effect of overlay modulus on strains at overlay bottom from shear loading.

FIGURE 18 Typical crescent-shaped slippage cracks.

load (0.5P). Figure 17 shows the directions of the principal tensile strains on the pavement surface. The length of the arrows indicates the magnitude of the strain. The greatest tensile strain is immediately behind the wheel imprint from the direction of the applied horizontal load.

The tensile strains along the edge of the contact area are all of the same magnitude, which can lead to progressive failure around the back edge of the contact area. A tensile failure in the overlay at the point of maximum strain would prevent stress from being transferred from the tire contact area to the area behind the wheel. This would cause a redistribution of the stress and strain at adjacent points along the edge of the contact area. Because these points are already approaching failure strain, the additional redistributed stress will cause failure at these points. This cycle of redistribution of stresses and failure of the top surface along the edge of the contact surface leads to a curved crack in the overlay. If the overlay is not properly bonded to the asphalt below, the overlay moves, which opens the crack. This behavior agrees with observed "crescent cracks" that have occurred in pavements in which the overlay has slipped, such as those shown in Figure 18. The strains generated by horizontal loads are high enough to result in significantly reduced pavement life even when interlayer slippage is not present.

Changing the direction of the horizontal load will rotate the directions of the observed strains. The relative positions of the strains do no change. In all cases investigated, the maximum strain was always 180 degrees from the direction of the applied horizontal force, just outside the wheel imprint.

REPAIR ALTERNATIVES

If overlay slippage has been detected, two alternatives exist for repair: either add a second overlay or remove the existing slipped overlay and replace it with an overlay that is properly bonded to the lower asphalt layer. Various second overlay thicknesses were assumed in the investigation of the first alternative. Stresses and strains under a DC–9 wheel were calculated and the fatigue lives of both overlays, the original asphalt layer, and the subgrade were computed.

Figure 19 shows the effect of the top overlay thickness on the fatigue life of the pavement. The curves have the same general shapes as the curves in Figure 6, in which the thickness of a single overlay was varied, because the two overlays do not slip with respect to each other but act as one layer. The bottom (existing) overlay has the lowest fatigue life and therefore controls the life of the entire pavement. It is not until the second overlay thickness is 12 in. thick that the fatigue life of the bottom overlay approaches that of the original pavement, which consisted of a 2-in. overlay without slip over a 4-in. original asphalt layer.

A cost comparison of adding a 12-in. asphalt overlay and replacing a 2-in. overlay is unnecessary. The cost of 12 in. of

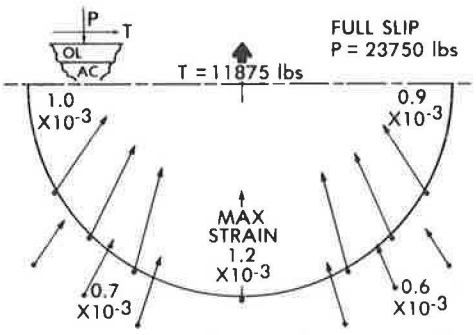

FIGURE 17 Principal maximum normal tensile strains in pavement plane of wheel imprint from shear load.

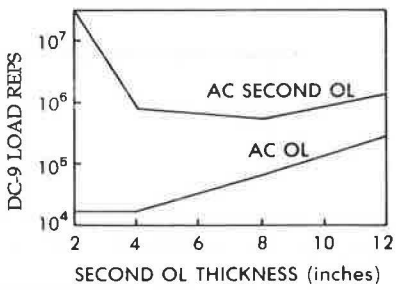

FIGURE 19 Effect of second overlay thickness on pavement fatigue life (first overlay slipped).

asphalt, along with the details required to make pavement elevations match those of existing pavements, obviously exceeds the cost of removing a slipped 2-in. overlay and replacing it with a well-bonded overlay.

SUMMARY

Layer slippage causes a redistribution of stresses and strains within a pavement. Large tensile strains occur at the bottom of the slipped layer. Asphalt at either side of the slipped interface distorts in different directions, which helps to propagate the layer slippage and further destroy the bond between the layers.

Under vertical loading in a pavement in which slippage has occurred, tensile strains due to asphalt fatigue become larger as the thickness of the slipped layer increases to about 6 in. After the slipped layer becomes larger than the underlying asphalt layer, the tensile strains gradually decrease.

High asphalt stiffness of thin overlays reduces the fatigue life of the pavement when layer slippage is present under vertical loading. This is due to stiffer materials having a lower fatigue tolerance for a given strain. For thin overlays, this decrease outweighs any advantage from the stiffer layer producing lower tensile strains.

Horizontal tangential loads cause a tensile strain behind the wheel at the top of the overlay. If the horizontal load is large enough, this strain will be the maximum tensile strain in the pavement. If slippage has occurred, the horizontal load must be completely withstood by the top slipped layer. This leads to crescent cracks in slipped overlays. The effect is smaller in stiffer layers.

When horizontal loading is present, regardless of the slippage condition, the overlays should have stiffnesses greater than or equal to 500,000 psi. The effect of overlay thickness is minor in this case; a thicker overlay gives a slightly lower strain.

Overall, a modulus of 500,000 psi would be the best compromise. If interlayer slippage is probable, a thin overlay would maximize the fatigue life in the case with no horizontal loading. A thin overlay would require the least material in areas where horizontal loading will be present. These areas will have a short pavement life and will need frequent resurfacing.

A pavement with a slipped overlay should be repaired by removing the slipped overlay and replacing it with a well-bonded overlay. Overlaying a second time requires a very large overlay to keep the tensile strains in the slipped overlay small.

ACKNOWLEDGMENTS

This paper is the result of research sponsored by the FAA, U.S. Department of Transportation, to determine the effect of asphalt layer slippage on airfield pavement management.

REFERENCES

1. *Airport Pavement Design and Evaluation.* Advisory Circular 150/5320–6C. FAA, U.S. Department of Transportation, Dec. 1978.
2. *BISAR User's Manual* (abbreviated version). Koninklijke/Shell–Laboratorium, Amsterdam, The Netherlands, 1978.
3. F. Bonnaure, A. Gavois, and J. Udron. A New Method for Predicting the Fatigue Life of Bituminous Mixes. *Proc., Association of Asphalt Paving Technologists,* Vol. 49, 1980, pp. 499–529.
4. G. Way. Asphalt Properties and Their Relationship to Pavement Performance in Arizona. *Proc., Association of Asphalt Paving Technologists.* Vol. 47, 1978, pp. 49–69.
5. T. Y. Chou. Analysis of Subgrade Rutting in Flexible Airfield Pavements. In *Transportation Research Record 616,* TRB, National Research Council, Washington, D.C., 1976, pp. 44–48.
6. E. S. Barber. Shear Loads on Pavements. *Proc., 1st International Conference on Structural Design of Asphalt Pavements,* University of Michigan, Ann Arbor, 1962, pp. 354–357.

Publication of this paper sponsored by Committee on Flexible Pavements.

The views of the authors do not purport to reflect the position of the Department of the Army or the Department of Defense.

Base Course Contamination Limits

BRUCE N. JORENBY AND R. G. HICKS

Geotextiles have been used in pavement structures for two primary purposes: subgrade reinforcement and separation. Research to date has been concentrated on developing design procedures for incorporating geotextiles for subgrade reinforcement in areas with low-strength soils [California bearing ratio (CBR) < 3]. In this paper the use of geotextiles as a separation mechanism in roadways with higher strength soils (CBR > 3) is evaluated. The primary effect of geotextiles in this application is to reduce the amount of contamination within the aggregate base layer. Contamination of this layer occurs primarily through intrusion of subgrade materials into the aggregate base. This intrusion changes the gradation of the base and results in reduced strength or stiffness as well as lower permeability. Geotextiles reduce the contamination in the aggregate base by modifying the process of subgrade intrusion, the level of stress at the subgrade interface, and the process of filtration. A laboratory study was conducted to illustrate the influence of added fines on the modulus of an aggregate base. The aggregate tested was a 1-in.-minus crushed aggregate with 5.5 percent passing the No. 200 (0.075-mm) sieve. The study showed that, for the materials tested, up to 6 percent added fines can be tolerated without adversely affecting the stiffness of the base. For U.S. Forest Service base courses, separation geotextiles need to limit subgrade intrusion to this level. In situations in which drainage controls, the geotextile needs to limit intrusion to 2.5 percent. Primary benefits from geotextiles include increased life of the pavement structure or reduced initial and long-term capital outlays, or both.

Geotextiles have been used in pavement structures for two primary purposes: subgrade reinforcement and separation. Subgrade reinforcement involves the use of geotextiles in weak soil areas to reduce the amount of aggregate base required *(1)*. Separation involves using geotextiles to reduce or prevent intrusion of subgrade materials into aggregate base courses *(1–3)*. Research to date has been concentrated on developing design procedures for incorporating geotextiles for subgrade reinforcement. The effects of geotextiles as a separation layer in pavement structures have, at present, not been evaluated to any large degree and the design criteria and recommendations for their use have been based primarily on engineering judgment *(1, 2, 4–7)*. Because the number of weak soil areas is limited, it is expected that, in the future, the greatest potential use of geotextiles and the greatest source of cost savings will be their use as a separation layer in permanent roads.

The purpose of this paper is to illustrate the effect of geotextiles on the amount of contamination of aggregate bases under repeated loadings. "Contamination" of aggregate base courses may be more properly described as the intrusion of subgrade materials into aggregate bases. The primary effect of subgrade intrusion is to change the gradation of the aggregate base. It is through this change in gradation that the strength of the aggregate base and its permeability are affected.

Geotextiles reduce the contamination of aggregate bases by changing the process of subgrade intrusion. They modify the filtration process and may change the level of stress at the subgrade-aggregate interface. The filtration process is influenced by pore water pressures at the subgrade–aggregate base interface. It is thought that one of the influences of geotextiles is to change the manner in which pore water pressures develop, although the exact nature of this change is not fully understood *(8)*.

The amount of contamination may be expressed in two ways: percent increase in the fines content of the aggregate base (S) or by the soil contamination value (SCV). Percentage of added fines (S) represents the increase in weight of the aggregate base as a result of the contamination process, expressed in terms of the original dry weight of the aggregate base. SCV is the "weight of subgrade soil . . . passing the fabric per unit area of fabric," expressed in units of g/m^2 *(4)*. When geotextiles are used as a separation layer, the amount of contamination is reduced *(4, 5)* and the amount of contamination appears to depend on porosity, percentage open area, effective opening size, and thickness of the geotextile.

LABORATORY STUDY OF SUBGRADE INTRUSION

A laboratory study was conducted to evaluate the effect of added subgrade fines on the resilient modulus of an aggregate base. The primary purpose of this study was to quantify the variation in resilient modulus with varying amounts of subgrade fines. By illustrating the effect of subgrade intrusion on resilient modulus, the benefits of using geotextiles to limit intrusion can be demonstrated. An additional benefit of this study is that the information developed can be used to better account for the effects of subgrade intrusion in pavement design.

Factors That Affect Resilient Modulus of Granular Materials

The resilient modulus of granular materials has been found to depend on a number of factors. Seed et al. *(9)* reported seven factors that influence resilient modulus. Of these, the three most significant are type of aggregate, aggregate gradation, and confining pressure (or bulk stress). Bulk stress has been used by several authors *(9–11)* to characterize the resilient modulus of granular materials. Kalcheff and Hicks *(10)* developed a general test procedure for evaluating resilient modulus in the laboratory using a triaxial testing system and expressed the results in terms of bulk stress. In 1982 AASHTO published a

B. N. Jorenby, Mount Baker–Snoqualmie National Forest, U.S. Department of Agriculture, 1022 1st Avenue, Seattle, Wash. 98104. R. G. Hicks, Department of Civil Engineering, Oregon State University, Corvallis, Oreg. 97331.

TABLE 1 INDEX PROPERTIES OF AGGREGATE BASE

Test	Property
Specific gravity	
Coarse fraction (AASHTO T–85)	
Surface saturated dry	2.71
Bulk dry	2.68
Apparent	2.77
Absorption (%)	1.18
Fine fraction (AASHTO T–100)	2.74
Maximum density [Humphres' method *(13)*]	
Grading D	141.8 pcf
Grading E	139.2 pcf

TABLE 2 GRADATIONS OF AGGREGATE

U.S. Standard Sieve	Grading D (percentage passing)	Grading E (percentage passing)
1 in. (25.0 mm)	100.0	
3/4 in. (19.0 mm)	84.0	100.0
1/2 in. (12.5 mm)	74.0	84.0
3/8 in. (9.38 mm)	64.5	75.0
No. 4 (4.75 mm)	48.0	57.0
No. 8 (2.36 mm)	36.0	42.0
No. 30 (0.600 mm)	21.5	24.5
No. 100 (0.150 mm)	8.5	10.5
No. 200 (0.075 mm)	5.5	5.5

test procedure for determining the resilient modulus of subgrade soils (T–274) *(12)*. This procedure includes methods for both granular and cohesive soils. The laboratory study for this paper used bulk stress to characterize resilient modulus, and the test procedure used generally follows that presented by AASHTO.

Selection of Materials

The aggregate base tested was a crushed aggregate produced from an intrusive igneous rock. The engineering properties of this aggregate are given in Table 1. The aggregate was sampled from an existing stockpile and was blended in the laboratory to the gradations given in Table 2.

The gradations selected are typical of those specified for aggregate base courses used with bituminous concrete pavements. The gradations represent the middle of the specification range allowed in the 1979 U.S. Forest Service Standard Specifications *(14)*. A second consideration is that the maximum particle size of each gradation should be consistent with the size of the testing apparatus used in the laboratory study. Because 4-in. (10-cm) molds were used in this study, the maximum particle size could not be larger than 1 in. (25 cm).

The subgrade material selected for use as the added fines material was a low-plasticity clay with engineering properties given in Table 3.

Test Procedures

The approach used in this study consisted of

1. Blending the aggregate to the specified gradation;
2. Determining the maximum density of the crushed aggregate using Humphres' method of granular compaction *(13)*;
3. Performing resilient modulus tests on the crushed aggregate mixture compacted to approximately 95 percent maximum density;
4. Blending mixtures of aggregate and subgrade fines using 2, 4, 6, 8, and 19.5 percent of added fines; and
5. Performing resilient modulus tests on the aggregate–subgrade fines mixtures compacted to approximately 95 percent maximum density.

All tests were performed using a triaxial cell 4 in. (10 cm) in diameter with an MTS testing machine used to apply the appropriate vertical loads. The MTS machine was set to apply a load duration of 0.1 sec, with a cycle length of 2 sec. The stress pulse was programmed to approximate a rectangular form. An initial seating pressure of 1 psi (6.9 kPa) was used for all specimens.

Test Conditions

A program was established to conduct resilient modulus testing over the range of stresses encountered in typical pavement structures used on National Forest roads. The method of analysis used to determine this range of stresses was the Boussinesq method of equivalent thickness *(15)*. Figure 1 shows the typical bituminous concrete pavement evaluated. In a linear elastic system, the computed stresses depend on the assumed relation-

TABLE 3 ENGINEERING PROPERTIES OF THE ADDED FINES

Property	Measured
Gradation	
U.S. standard sieve (% passing)	
No. 10 (2.00 mm)	99.5
No. 40 (0.425 mm)	97.8
No. 200 (0.075 mm)	90.2
(0.020 mm)	83.6
(0.002 mm)	54.9
(0.001 mm)	43.4
Atterberg Limits	
Liquid limit (AASHTO T–89), %	45.3
Plastic limit (AASHTO T–90), %	22.9
Plasticity index (AASHTO T–90), %	22.4
Soil Classification	
Unified (ASTM D2487)	CL
AASHTO (AASHTO M–145 and ASTM D3282)	A–7–6
Moisture-Density Relationship	
Maximum density (AASHTO T–99), pcf	106.2
Optimum moisture (AASHTO T–99), %	19.1
Specific gravity (AASHTO T–100)	2.75

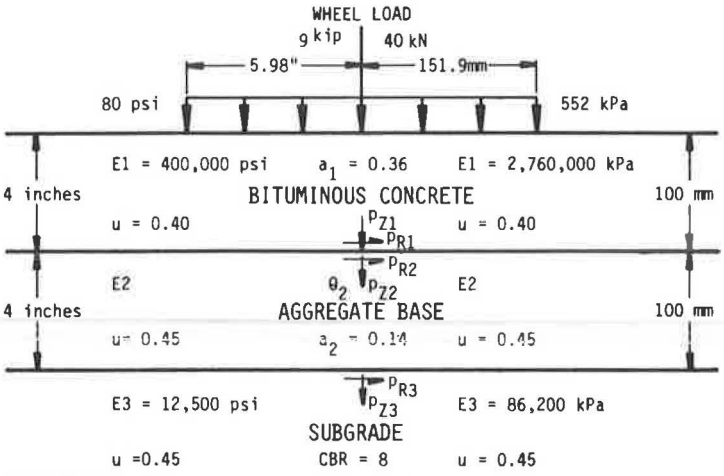

FIGURE 1 Typical pavement section.

TABLE 4 SUMMARY OF GEOTEXTILES TESTED FOR SUBGRADE INTRUSION BY WALTER *(18)*, HOARE *(4)*, AND BELL ET AL. *(5)*[1]

Geoxtexile	Researcher	S (%)	SCV (g/m^2)	EOS[2]	T[3]
MIRAFI 500X	Walter	0.00	0	0.053	0.62
TYPAR 6	Walter	0.00	0	0.175	0.48
TYPAR 6	Walter	0.09	90	0.175	0.48
TYPAR 6	Walter	0.62	600	0.175	0.48
W3	A.L. Bell	-	708	0.080	0.40
W8	A.L. Bell	-	737	0.100	na
NW4	A.L. Bell	-	777	0.170	2.00
NW5	A.L. Bell	-	839	0.170	4.00
NW3	A.L. Bell	-	849	0.130	3.50
SUPAC 4-P	Walter	0.95	910	na	1.27
BIDIM C42	Walter	1.02	980	0.175	4.03
Terram 1000	Hoare	-	1050	0.140	na
W4	A.L. Bell	-	1139	0.060	0.30
W7	A.L. Bell	-	1179	0.190	na
Neomer T425	Hoare	-	1240	0.100	na
NW1	A.L. Bell	-	1290	0.130	2.00
FIBRETEX 200	Walter	1.43	1370	0.175	2.89
Neomer PB127	Hoare	-	1400	0.110	na
W5	A.L. Bell	-	1403	0.200	0.35
FIBRETEX 200	Walter	1.51	1450	0.175	2.89
NW2	A.L. Bell	-	1605	0.130	3.00
W1	A.L. Bell	-	1922	0.300	0.03
FIBRETEX 200	Walter	2.02	1940	0.175	2.89
W6	A.L. Bell	-	2027	0.140	0.32
BIDIM C42	Walter	2.57	2470	0.175	4.03
MIRAFI 140	Walter	3.30	3170	0.150	0.77
W2	A.L. Bell	-	3766	0.430	0.60
FIBRETEX 200	Walter	3.99	3840	0.175	2.89
MIRAFI 140	Walter	3.99	3840	0.150	0.77
MIRAFI 140	Walter	5.61	5390	0.150	0.77
BIDIM C34	Walter	5.94	5720	0.175	2.82
MIRAFI 140	Walter	6.05	5820	0.150	0.77
Filter X	Walter	6.25	6010	na	na
MIRAFI 140	Walter	7.88	7570	0.150	0.77

Notes:

1. The test values above are listed in rank order of % Intruded Fines (S), and Soil Contamination Value (SCV).
2. EOS is the Equivalent Opening Size of the geotextile in mm. (Some researchers use O_{95}).
3. T is the thickness of the geotextile in mm.
   The number of load repetitions applied are as follows: Walter (18) - 100,000; Hoare (4) - 27,000; A.L. Bell (5) - Not reported.
   na = not available.

ship between the modulus of the aggregate base course (E2) and the modulus of the subgrade (E3). This ratio has been found to range between 2 and 3 for most situations *(15, 16)*. For the pavements sections analyzed in Figure 1, the following stresses were calculated, and they represent the maximum bulk stress in the aggregate base immediately below the bituminous layer:

E2/E3	*Horizontal Stress (psi)*	*Vertical Stress (psi)*	*Bulk Stress (psi)*
2	1.8	30.0	33.5
3	3.0	35.0	41.0

The percentages of added fines selected for testing were 2, 4, 6, 8, and 19.5 percent. The values 2, 4, 6, and 8 percent represent the range of added fines noted by other researchers *(4, 5, 18)* for situations in which geotextile separators are used. The 19.5 percent value represents the condition determined by Walter *(18)* when geotextiles are not used. Table 4 gives a summary of the geotextiles tested by Hoare *(4)*, Bell et al. *(5)*, and Walter *(18)* in rank order of percentage of intruded fines. It should be noted that the reported values are subject to product and soil variations.

Resilient Modulus Tests

All modulus tests were conducted over a range of confining pressures and vertical stresses. In addition, the order in which confining pressures and vertical stresses were applied to the test specimens was varied for some of the tests. Two criteria were considered in selecting the range of vertical stresses applied. The first was to select vertical stresses that would simulate the stress condition within the pavement section shown in Figure 1. The second was to select vertical stresses over a range so as to produce a ratio between deviator stress and confining pressure of between 1 and 5. Vertical stresses were applied, during testing, in 5-psi (34.5-kPa) increments.

Table 5 gives a summary of the stress conditions for each test series. The numbering system identifies each series of tests according to the incremental increase in added fines rather than the sequential order in which testing was conducted. The test series used to develop the relationship between bulk stress (θ) and resilient modulus (E2) are indicated. Grading D was selected for the tests to develop this relationship. Grading D was selected over Grading E because of its greater use on Forest Service roads.

As noted, the order of applying confining pressures was varied during the initial stages of testing. Test Series 1–4 were essentially trial tests. The most consistent results occurred when the testing was initiated with a confining pressure of 15 psi (103.5 kPa). Test Series 8 was a retest of Series 7 using the preferred order of applying confining pressures. This procedure is similar to that described in AASHTO T–274 for granular soils.

Reduction of Test Data

The relationship between state of stress and resilient modulus has been characterized for this study using bulk stress. Bulk stress (θ) is defined as the sum of the three principal stresses:

$$\theta = p_1 + p_2 + p_3 \quad (1)$$

where

p_1 = major principal stress or total vertical stress,

TABLE 5 SUMMARY OF RESILIENT MODULUS TESTING PROGRAM

Test Series	Aggregate Grading	Added Fines %	Moisture Content,%	Compaction Level,%	Order of Applying Confining Pressure, psi
1	E	0	4.14	95.0	2, 5, 10, 15, 20
2	E	0	7.13	95.0	20, 15, 10, 5
3	D	0	4.79	94.5	5, 10, 15, 20
4	E	0	4.92	95.6	20, 15, 10, 5, 2
5*	D	0	5.46	95.6	20, 5, 10, 15
6*	D	2	5.69	95.0	5, 10, 15, 20
7	D	4	5.93	95.0	20, 15, 10, 5, 2
8*	D	4	5.93	95.0	15, 10, 5, 2, 20
9*	D	6	6.27	95.8	15, 10, 5, 2, 20
10*	D	8	6.61	96.0	15, 10, 5, 2, 20
11*	D	19.5	7.50	96.5	15, 10, 5, 2, 20

*Test series used to develop the relationship between resilient modulus (E2) and bulk stress (θ).

TABLE 6 LINEAR REGRESSION ANALYSIS OF DATA: $E2 = K*\theta^n$ (psi)

Percentage of Added Fines	K	n	r^2
0	8620	0.422	0.886
2	4730	0.557	0.793
4	4210	0.625	0.698
6	4250	0.662	0.896
8	1770	0.688	0.725
19.5	9320	0.256	0.906

Note: The values of E2 have been rounded to the nearest 100 psi.

p_2 = minor principal stress, and
p_3 = minor principal stress.

For the triaxial testing system used, $p_2 = p_3$. Both of these stresses equal the confining pressure.

The test data were analyzed with linear regression techniques using the equation: $E2 = K*\theta^n$. E2 is the resilient modulus of the aggregate base, K and n are constants determined in the regression analysis, and θ is the bulk stress. The relationship between E2 and θ was developed using the data corresponding to confining pressures of 5, 10, and 15 psi (34.5, 69, and 103.5 kPa). For S-values of 4, 6, and 8 percent, some E2-values determined at a confining pressure of 5 psi (34.5 kPa) were not used in the regression analysis because some of these data did not produce reasonable results. For the situation with 19.5 percent added fines, the aggregate subgrade mixture acted more like a soil than an aggregate. This was because a total of 24 percent of the material in the specimen passed the No. 200 (0.075-mm) sieve. For this series of tests, the relationship between E2 and θ was developed using confining pressures of 2, 5, and 10 psi (13.8, 34.5, and 69 kPa). These stresses are consistent with those used to test most subgrade soils. Tables 6 and 7 give summaries of the values for K, n, θ, and E2 as a function of the percentage of added fines. Figures 2–7 show the relationship between θ and E2 for each value of percentage of added fines.

TABLE 7 RESILIENT MODULUS (E2)

Percentage of Added Fines	Bulk Stress (psi)						
	10	20	30	35	40	95	100
0	22,800	30,500	36,200	38,700	40,900	59,000	60,300
2	17,100	25,100	31,500	34,300	36,900	59,900	61,600
4	17,700	27,300	35,200	38,800	42,100	72,500	74,700
6	19,500	30,900	40,400	44,800	48,900	86,900	89,800
8	8,600	13,900	18,400	20,400	22,400	40,700	42,100
19.5	16,800	20,000	22,200	23,100	23,900	29,900	30,300

Note: The values of E2 have been rounded to the nearest 100 psi.

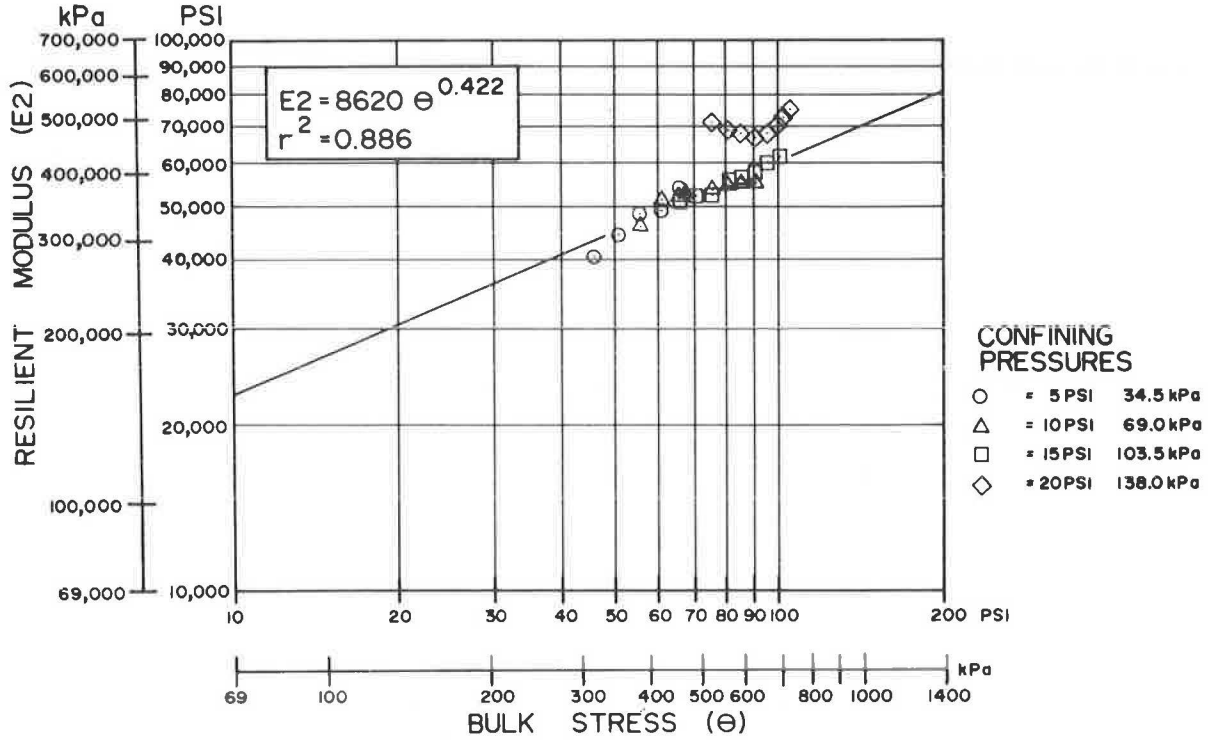

FIGURE 2 Resilient modulus versus bulk stress: Grading D (original gradation).

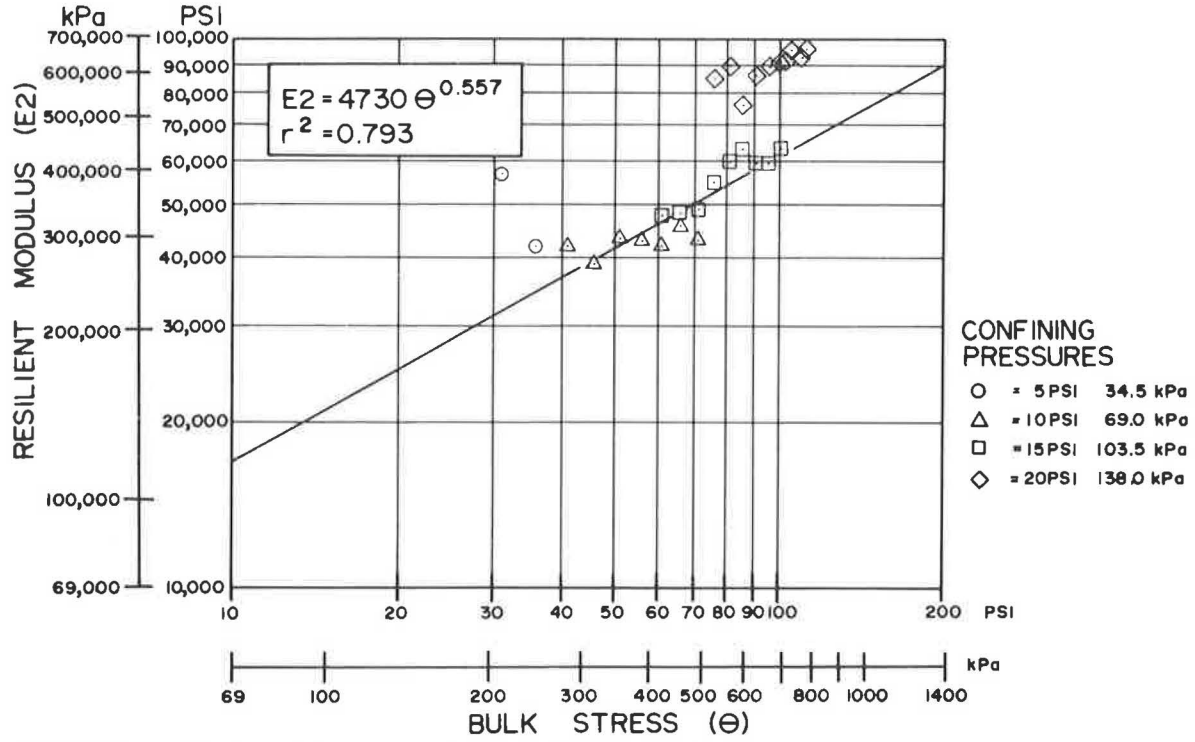

FIGURE 3 Resilient modulus versus bulk stress: Grading D with 2 percent added fines.

Relationship Between Resilient Modulus and Added Fines

The relationship between resilient modulus of the aggregate base (E2) and percentage of added fines (S) is shown in Figures 8 and 9. In Figure 8 resilient modulus has been plotted as a function of bulk stress (θ) for the various percentages of added fines (S). In Figure 9 resilient modulus is shown as a function of percentage of added fines (S) for four levels of bulk stress: θ = 10, 20, 35, and 95 psi (θ = 69, 138, 241, and 655 kPa). This encompasses the range of conditions used in the laboratory tests. A bulk stress of 35 psi represents the stress state in the

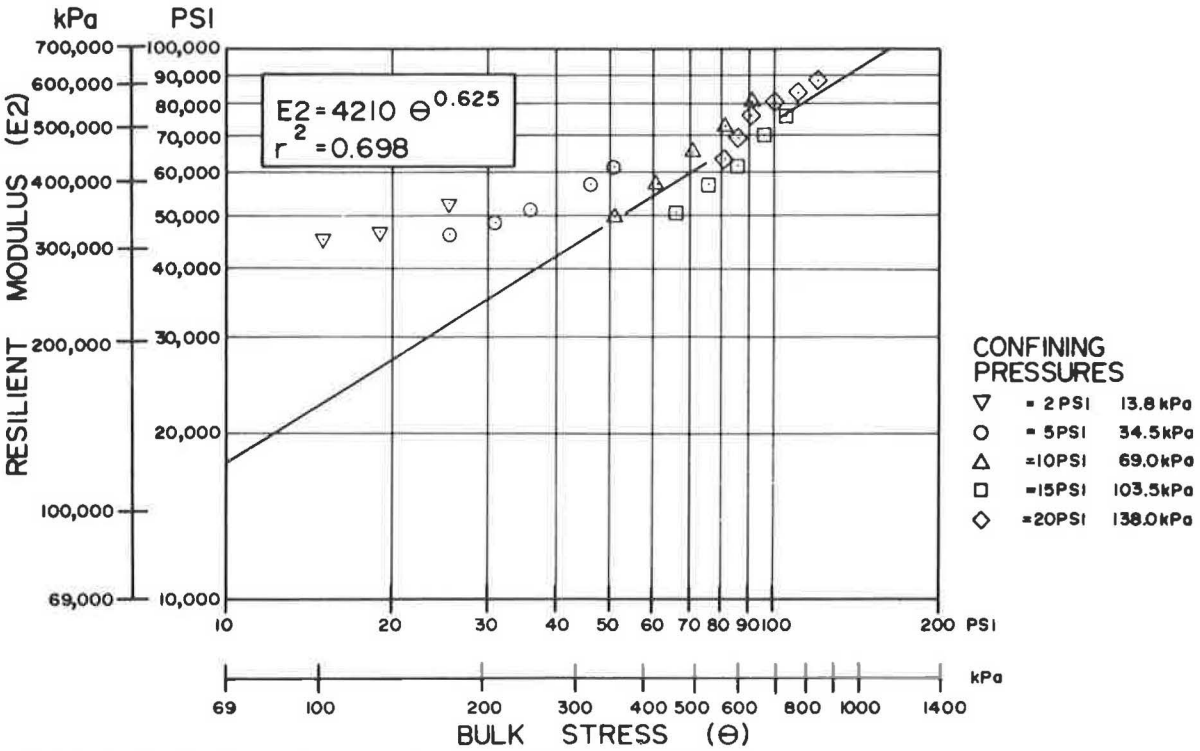

FIGURE 4 Resilient modulus versus bulk stress: Grading D with 4 percent added fines.

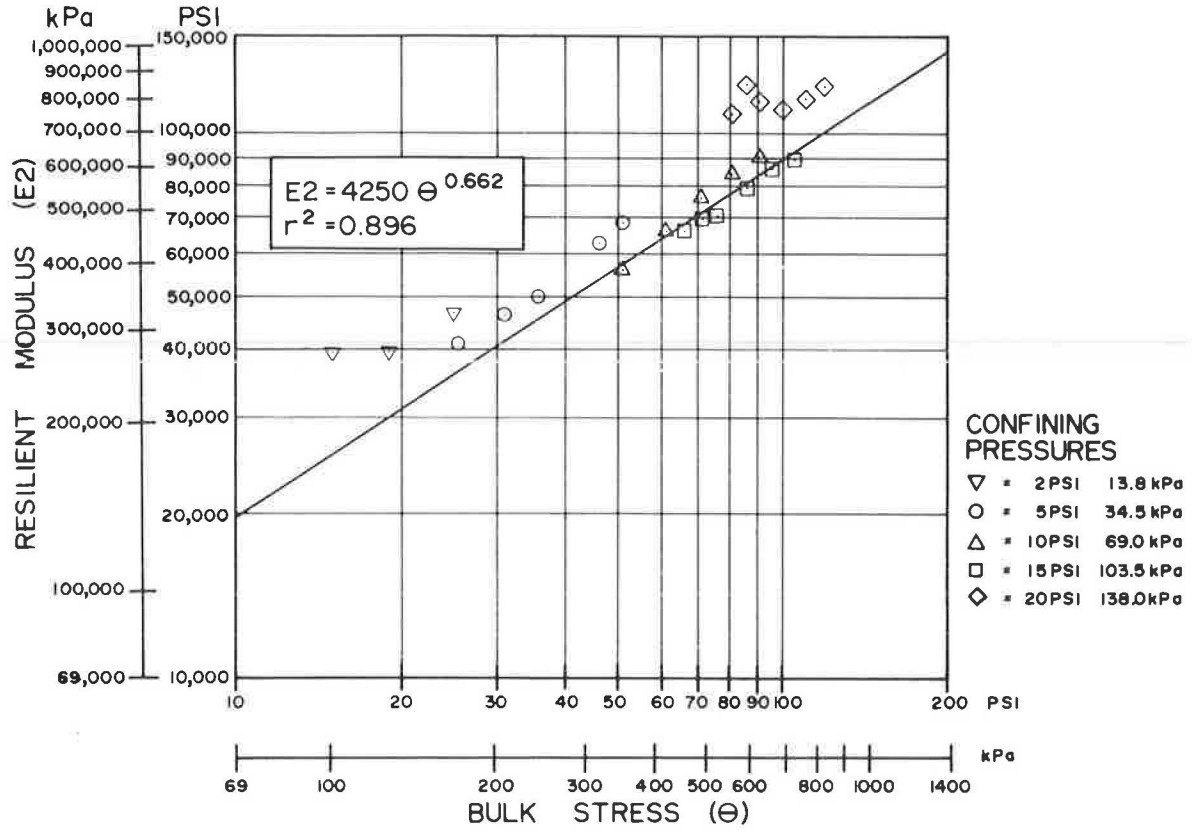

FIGURE 5 Resilient modulus versus bulk stress: Grading D with 6 percent added fines.

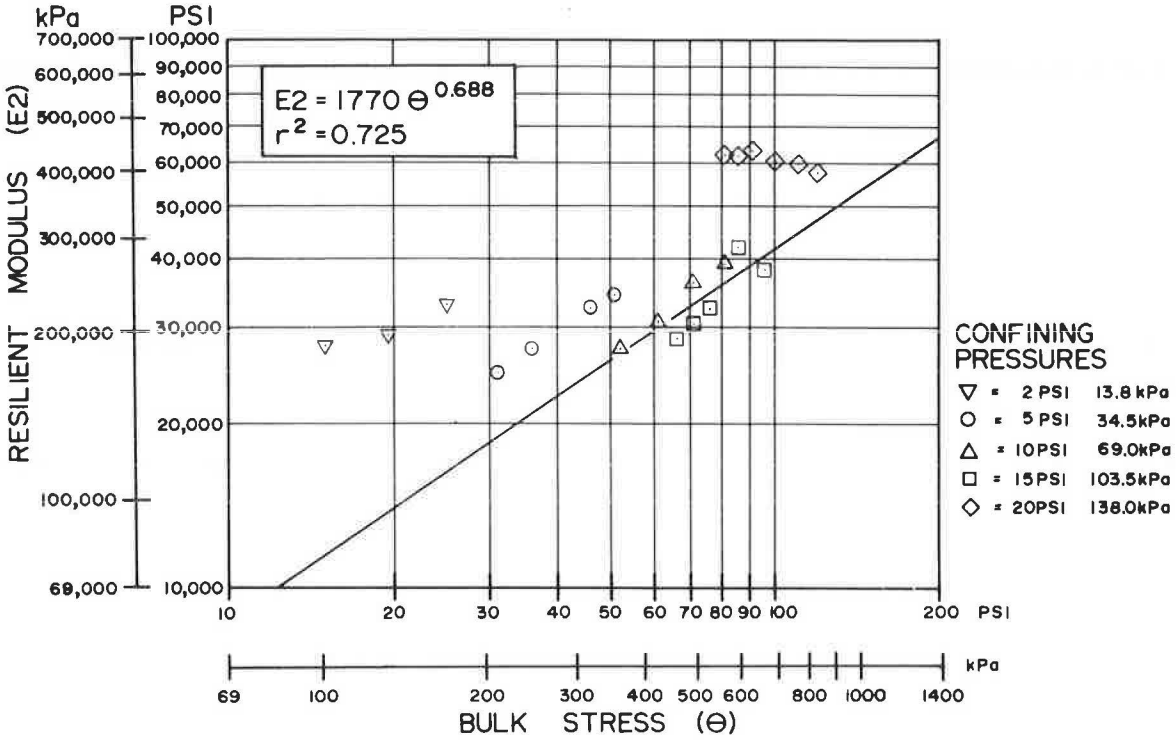

FIGURE 6 Resilient modulus versus bulk stress: Grading D with 8 percent added fines.

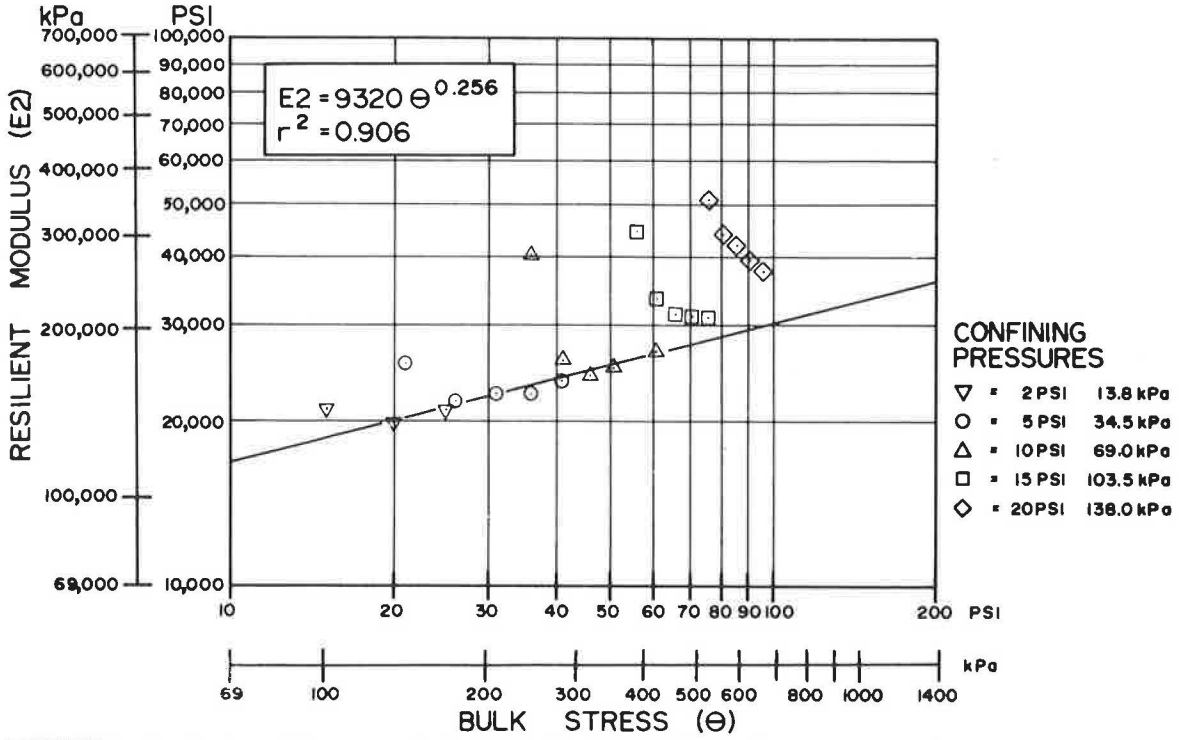

FIGURE 7 Resilient modulus versus bulk stress: Grading D with 19.5 percent added fines.

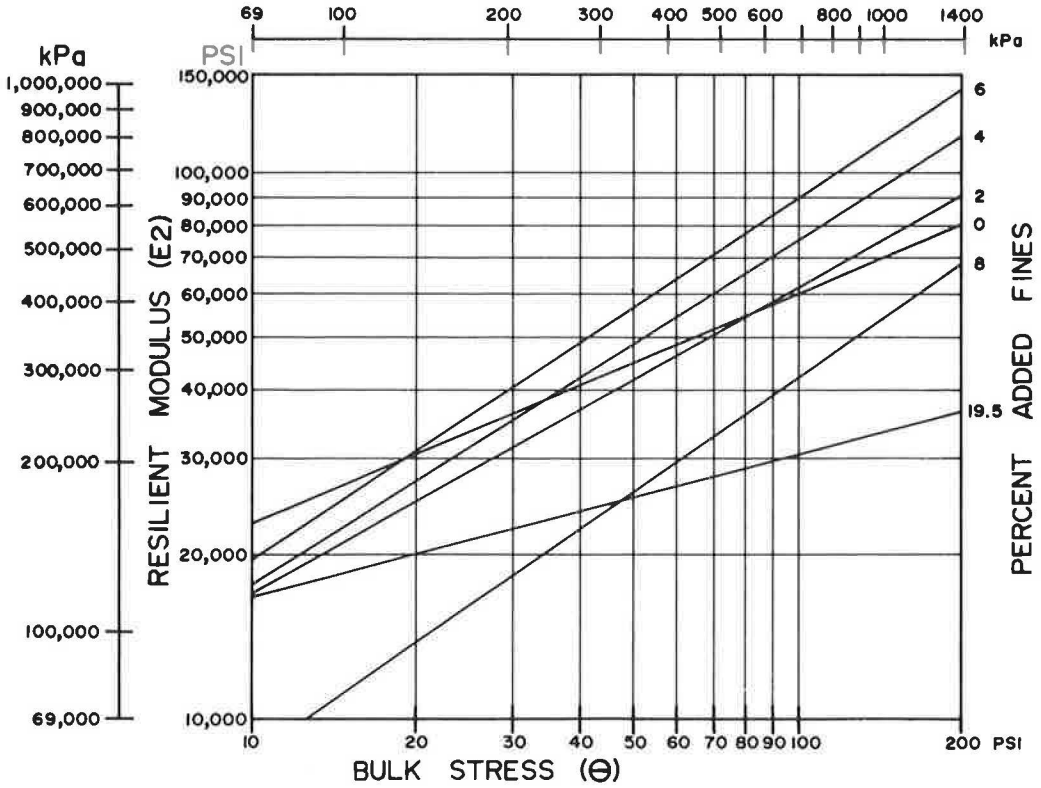

FIGURE 8 Resilient modulus versus bulk stress: Grading D as a function of percentage of added fines.

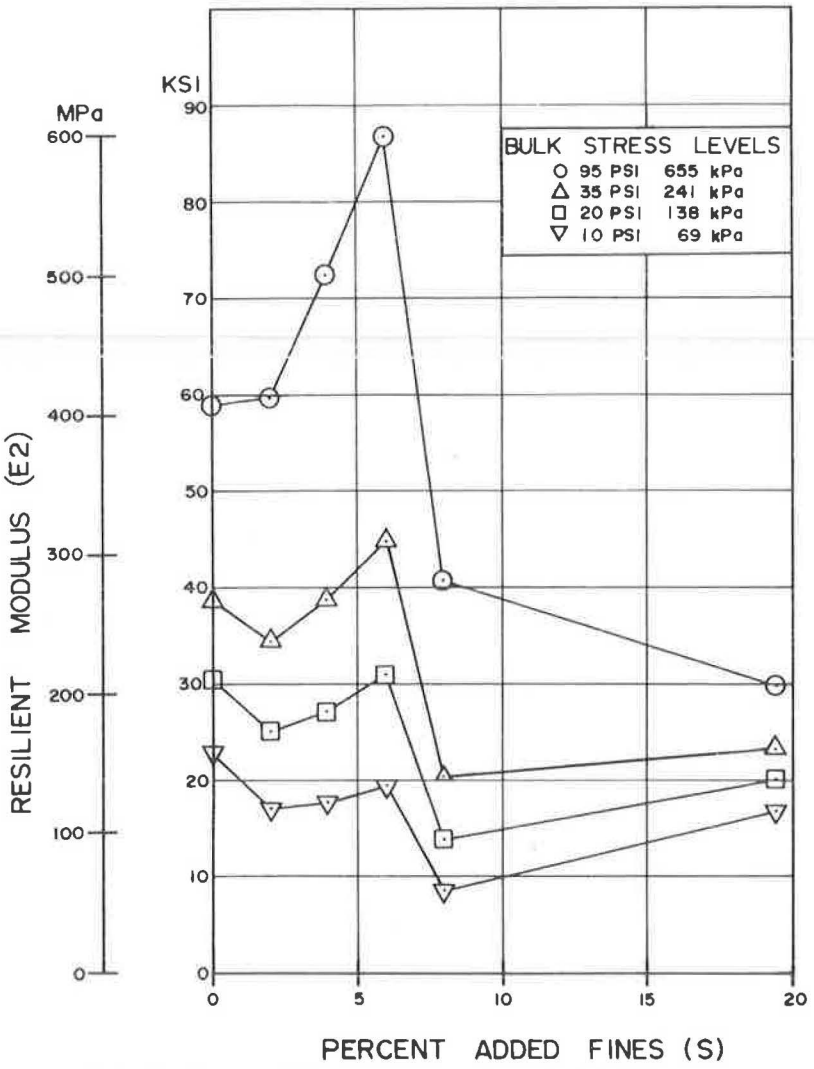

FIGURE 9 Resilient modulus versus percentage of added fines.

aggregate base course, and a bulk stress of 20 psi is representative of the stress state in the subgrade.

If the variable F is defined to represent the percentage of material passing the No. 200 (0.075-mm) sieve, then the term F includes the fines in the original aggregate base (F_0), as well as the added subgrade fines (S), or $F = F_0 + S$. For the situation tested, F_0 is 5.5 percent; E2 reaches its peak when S is 6 percent or when F is 11.5 percent. One reason for setting an upper limit for F_0 is to permit drainage within the aggregate base. For a project situation, in which the aggregate base produced has about 8 percent passing the No. 200 (0.075-mm) sieve, an additional 3.5 percent added fines can be tolerated over the life of the pavement structure before a loss in pavement strength occurs. However, under this condition, the drainage characteristics of the base material could be impaired. For a "down the middle of the spec" situation (which is the condition tested), 2.5 percent added fines should probably be considered the apparent upper limit of F (percent passing No. 200) for drainage purposes, whereas 6 percent added fines could be tolerated from a stiffness standpoint.

At a bulk stress of 95 psi (655 kPa), the test data show an increase in resilient modulus of the aggregate base (E2) as the percentage of added fines (S) increases. An apparent peak in E2 was reached when the percentage of added fines reached 6 percent. At 8 percent added fines, a dramatic drop in E2 was experienced. Coincidentally, the increase in E2 occurred over a range in S, which appears to correspond to a range of values allowed in the crushing specifications *(14)*. Grading D specifies 8 percent as a maximum allowed to pass the No. 200 (0.075-mm) sieve.

For bulk stress levels of 20 and 35 psi (138 and 242 kPa), an initial decrease in E2 was noted as S went from 0 to 2 percent. As S increased from 2 to 6 percent, an increase of E2 was experienced, and it reached an apparent peak at 6 percent. As with a bulk stress of 95 psi (655 kPa), a dramatic drop in E2 occurred when 8 percent added fines were used. It is interesting to note that E2 experienced a slight increase when S was increased to 19.5 percent. However, E2 at 19.5 percent was still significantly below the initial value of E2. In summary, it appears that up to 6 percent added fines can be tolerated in terms of stiffness criteria for aggregate bases for all the stress levels evaluated.

EVALUATION OF TEST RESULTS

Effect of Added Fines on Pavement Life

The influence of added fines on the life of a pavement structure was evaluated for added fines values of 0, 2, 4, 6, 8, 10, and 12 percent. These values represent the range of intrusion experienced in a field study of National Forest roads *(19)*, as well as those reported in several laboratory studies *(4, 5, 18)*. Also evaluated is the situation in which the aggregate base is contaminated to the point where it acts as a subgrade. This is represented by S = 19.5 percent. The three analysis procedures used were

1. U.S. Forest Service: AASHTO equation *(20)*,
2. Boussinesq method of equivalent thickness: BOUSS *(15)*, and
3. Elastic layered theory: ELSYM5 *(10)*.

In the U.S. Forest Service method, the structural strength of the aggregate base is characterized by the a-value. Resilient modulus is used to characterize the layer contribution of the aggregate base in the BOUSS and ELSYM5 analysis procedures. The structural contribution of the geotextile was ignored in all analysis methods. Only its role in preventing contamination in the base layer was considered.

Each method of characterizing the contribution of the base shows that a relative reduction in structural strength is experienced as the percentage of added fines (S) increases. To document this change, a structural equivalency ratio (SER) has been defined as the ratio of the structural contribution of a contaminated base to that of a new aggregate base as follows:

$$\text{E2 SER} = (\text{E2 for any S})/(\text{E2 for S} = 0) \quad (2)$$

$$\text{a-value SER} = (a_2 \text{ for any S})/(a_2 \text{ for S} = 0) \quad (3)$$

A bulk stress of 35 psi (241 kPa) was selected to determine the structural equivalency ratios for this paper. Table 8 gives the values of E2 calculated for each level of percentage of added fines (S) using the equations in Tables 6 and 7 as well as the associated SERs. The ratios range from 1.158 at 6 percent added fines to 0.527 at 8 percent. Structural equivalency ratios greater than 1.0 reflect the increase in resilient modulus experienced in the laboratory as S was increased from 0 to 6 percent. In subsequent analyses, the SERs for S = 0, 4, and 6 percent are set equal to 1.0. The ratio at S = 2 percent was kept as 0.886 to illustrate the effect on pavement life of a slight change in E2-values.

For a bulk stress level of 35 psi (241 kPa), SER for S = 19.5 percent was larger than for S = 8 percent. Because it is reasoned that at 19.5 percent added fines the aggregate base is acting much like a subgrade material, the ratio E2/E3 was set equal to 1.0 for all subsequent analysis. This resulted in an SER of 0.333. The SER-values for 10 and 12 percent added fines were determined using a linear interprolation after making the assumption that E2 gradually decreases between 8 and 19.5 percent added fines. The pavement section analyzed therefore had an E2-value of 37,500 psi (258 600 kPa) for the original aggregate base and a subgrade resilient modulus (E3) of 12,500 psi (86 200 kPa).

In the AASHTO design equation, the effect of added fines on the layer equivalency of an aggregate base is accounted for by varying the a-value of the aggregate base layer (a_2). The U.S. Forest Service method *(20)* incorporates a method for estimating a_2-values for aggregate base and for other materials used in layered systems. The factors that influence the a_2-values include

TABLE 8 DEVELOPMENT OF STRUCTURAL EQUIVALENCY RATIOS BASED ON RESILIENT MODULUS

S, %	E2 psi	Calculated E2 SER	Calculated E2/E3	Design E2 SER	Design E2/E3	Design E2 psi
0	38,700	1.000	3.00	1.000	3.00	37,500
2	34,300	0.886	2.66	0.886	2.66	33,225
4	38,800	1.003	3.01	1.000	3.00	37,500
6	44,800	1.158	3.47	1.000	3.00	37,500
8	20,400	0.527	1.58	0.527	1.58	19,750
10	--	--	--	0.493	1.48	18,500
12	--	--	--	0.460	1.38	17,250
19.5	23,100	0.597	1.79	0.333	1.00	12,500

Notes:
E2 = 3*E3 at S = 0 percent.

E2 at S = 19.5% set so that E2 = E3.

Design SER for S = 10 and S = 12% are based on linear interpolation.

TABLE 9 DETERMINATION OF a-VALUES AND CORRESPONDING STRUCTURAL EQUIVALENCY RATIOS BASED ON U.S. FOREST SERVICE a_2-VALUE CRITERIA *(24)*

Criteria	S (%)					
	0	2	4	6	8	10
Fractured aggregate	0.08	0.08	0.08	0.08	0.08	0.08
Plasticity, PI less than 6	0.01	0.01	0.01	0.00	0.00	0.00
Quality	0.02	0.02	0.02	0.02	0.01	0.00
P 200: 0–8	0.01	0.01	0.00	0.00	0.00	0.00
P 4: 30–65	0.01	0.01	0.01	0.01	0.01	0.01
P 1½ in: 100	0.01	0.01	0.01	0.01	0.01	0.01
Composite a-value	0.14	0.14	0.13	0.12	0.11	0.10
a-value SER	1.000	1.000	0.928	0.857	0.786	0.714

Note: Subgrade CBR = 8, which is equivalent to a = 0.07; a-value at S = 19.5 percent is set equal to the a-value of the subgrade.

1. Type of aggregate,
2. Plasticity,
3. Aggregate quality, and
4. Gradation.

Three types of aggregate are considered: cinders, sand and gravel, and fractured rock. Plasticity incorporates both plasticity index (AASHTO T–90) and sand equivalent (AASHTO T–176). Aggregate quality is a subjective determination, with three possible levels: marginal, good, and excellent. Gradation criteria include limitations on No. 200 (0.075-mm), No. 4 (4.75-mm), and 1½-in. (37.5-mm) sieves.

This method was used to determine a-values for the aggregate base over the range of percentage of added fines under consideration: 0, 2, 4, 6, 8, and 10 percent. For 10, 12, and 19.5 percent, criteria for borrow material were used to establish a-values because, at these percentages, it is reasoned that the aggregate acts more like a subgrade soil. At 10 percent added fines, a-values were determined using both criteria because 10 percent added fines is thought to represent a borderline situation. Tables 9 and 10 give summaries of the a-value determinations for use in the AASHTO equation.

The effect of added fines on the life of the pavement section under consideration is defined in terms of a pavement life ratio (PLR). PLR is defined as the allowable number of 18-kip (80-kN) equivalent axle loads for a given percentage of added fines divided by the allowable axle loads at 0 percent added fines. The U.S. Forest Service *(20)* uses the AASHTO method to determine the allowable number of axle loads. For the pavement section shown in Figure 1, the results of the analysis, including pavement life ratios, are given in Table 11.

TABLE 10 DETERMINATION OF a-VALUES AND CORRESPONDING STRUCTURAL EQUIVALENCY RATIOS BASED ON U.S. FOREST SERVICE a_3-VALUE CRITERIA *(24)*

Criteria	S (%)		
	10	12	19.5
Fractured aggregate	0.06	0.06	0.06
Plasticity, PI less than 2	0.01	0.01	0.00
Quality	0.01	0.01	0.00
P 200: 0–10	0.01	0.00	0.00
P 4: 25–60	0.01	0.01	0.01
Composite a-value	0.10	0.09	0.07
a-value SER	0.714	0.643	0.500

Note: Subgrade CBR = 8, which is equivalent to a = 0.07; a-value at S = 19.5 percent is set equal to the a-value of the subgrade.

Allowable axle loads are computed for BOUSS and ELSYM5 using fatigue criteria from Monismith, cited by Yoder and Witczak *(16)*, and the Asphalt Institute, cited by Bell *(15)*. These equations are

$$\text{Monismith equation: } N = 0.000000516\ p_{R1}^{-3.322} \quad (4)$$

$$\text{The Asphalt Institute equation: } N = 0.00000111\ p_{R1}^{-3.29} \quad (5)$$

Both of these equations are based on the following assumptions, which are considered to be representative of a typical asphalt concrete mix:

1. Asphalt content is 6 percent by weight,
2. Air void content is 5 percent by volume,
3. Resilient modulus of mix is 400,000 psi (2 760 000 kPa),
4. p_{R1} is the radial strain at the base of the bituminous concrete layer, and
5. N is the allowable number of 18-kip (80-kN) equivalent axle loads.

Table 12 gives a summary of the results of the calculations using BOUSS, and Table 13 gives similar information for ELSYM5. The Monismith and the Asphalt Institute methods differ in the number of allowable axle loads permitted for a given value of S and radial strain (p_{R1}). However, in terms of PLR, each method gives nearly identical results.

When the results of the three methods are compared (Table 14), it can be seen that each method gives a different estimate of pavement life. However, the general trend is the same for all methods; PLR decreases as the percentage of added fines increases. BOUSS generally gives the lowest estimate of pavement life, and AASHTO gives the highest estimate. However, AASHTO is in close agreement with ELSYM5. Because AASHTO is in relatively close agreement with ELSYM5, the a-values determined using the U.S. Forest Service criteria can be used to represent the effects of added fines. In terms of use

TABLE 11 PAVEMENT LIFE RATIOS FOR U.S. FOREST SERVICE METHOD

S (%)	a_2 Value	SER	SN	W	PLR
0	0.14	1.000	2.00	48,600	1.000
2	0.14	1.000	2.00	48,600	1.000
4	0.13	0.928	1.96	43,000	0.885
6	0.12	0.857	1.92	37,800	0.778
8	0.11	0.786	1.88	33,500	0.689
10	0.10	0.714	1.84	29,400	0.605
12	0.09	0.643	1.80	25,900	0.532
19.5	0.07	0.500	1.72	19,800	0.407

Notes:

SN = Structural number

$SN = a_1D_1 + a_2D_2$

$a_1 = 0.36$

$D_1 = 4$ inches

$D_2 = 4$ inches

W = Allowable number of 18 kip (80 kN) equivalent axle loads.

Subgrade CBR = 8.

TABLE 12 PAVEMENT LIFE RATIOS (PLRs) FOR BOUSS METHOD

S (%)	E2 (psi)	SER	P_{R1} (Microstrain)	N_M	PLR	N_{TAI}	PLR
0	37,500	1.000	383.8	114,700	1.000	365,500	1.000
2	33,225	0.886	415.6	88,100	0.768	281,300	0.770
4	37,500	1.000	383.8	114,700	1.000	365,500	1.000
6	37,500	1.000	383.8	114,700	1.000	365,500	1.000
8	19,750	0.527	571.7	30,500	0.266	98,500	0.270
10	18,500	0.493	593.6	26,900	0.235	87,000	0.238
12	17,250	0.460	617.6	23,600	0.206	76,400	0.209
19.5	12,500	0.333	735.7	13,200	0.115	43,000	0.118

Notes:

P_{R1} = Radial strain at the base of the bituminous concrete layer (Fig. 1).

N_M = Allowable number of 18 kip (80 kN) equivalent axle loads, using Monismith's fatigue criteria.

N_{TAI} = Allowable number of 18 kip (80 kN) equivalent axle loads, using The Asphalt Institute fatigue criteria.

TABLE 13 PAVEMENT LIFE RATIOS (PLRs) FOR ELSYM5 METHOD

S (%)	E2 (psi)	SER	P_{R1} (Microstrain)	N_M	PLR	N_{TAI}	PLR
0	37,500	1.000	333.2	183,500	1.000	581,900	1.000
2	33,225	0.886	347.7	159,300	0.868	505,800	0.869
4	37,500	1.000	333.2	183,500	1.000	581,900	1.000
6	37,500	1.000	333.2	183,500	1.000	581,900	1.000
8	19,750	0.527	403.1	97,500	0.531	311,000	0.534
10	18,500	0.493	409.4	92,600	0.505	295,500	0.508
12	17,250	0.460	415.8	88,000	0.480	280,800	0.483
19.5	12,500	0.333	443.1	71,200	0.388	227,800	0.391

Notes:

P_{R1} = Radial strain at the base of the bituminous concrete layer (Fig. 1).

N_M = Allowable number of 18 kip (80 kN) equivalent axle loads, using Monismith's fatigue criteria.

N_{TAI} = Allowable number of 18 kip (80 kN) equivalent axle loads, using The Asphalt Institute fatigue criteria.

in pavement design, the following are recommended PLRs for use in comparing alternative designs:

S	*F*	*PLR*
0–6	5.5–11.5	1.00
8	13.5	0.53
10	15.5	0.50
12	17.5	0.48
19.5	25.0	0.39

Potential Cost Savings of Using Geotextiles

Two methods are used to illustrate the potential benefits of using geotextiles as a separation layer. They involve determining *(a)* the amount of additional aggregate base needed in the original design when geotextiles are not used or *(b)* the depth of a bituminous concrete overlay needed after base contamination occurs.

The amount of additional aggregate base needed, when geo-

TABLE 14 COMPARISON OF DESIGN PAVEMENT LIFE RATIOS

S (%)	E2 (psi)	a_2 Value	AASHTO PLR	BOUSS PLR	ELSYM5 PLR
0	37,500	0.14	1.000	1.000	1.000
2	33,225	0.14	1.000	0.768	0.868
4	37,500	0.13	0.885	1.000	1.000
6	37,500	0.12	0.778	1.000	1.000
8	19,750	0.11	0.689	0.266	0.531
10	18,500	0.10	0.605	0.235	0.505
12	17,250	0.09	0.532	0.206	0.480
19.5	12,500	0.07	0.407	0.115	0.388

Notes:

AASHTO = U.S. Forest Service method (24).

BOUSS = Boussinesq Method of Equivalent Thickness (15).

ELSYM5 = Elastic layer method (17).

TABLE 15 BASE THICKNESS AND ASSOCIATED COST SAVINGS USING GEOTEXTILES, AASHTO METHOD *(24)*

	S (%)					
	0–4	6	8	10	12	19.5
Base Thickness (in.)						
Without geotextile						
a_2	0.14	0.12	0.11	0.10	0.09	0.07
D_2 (full intrusion)	4.0	5.0	5.5	6.0	6.5	8.0
D_2 (partial intrusion)	4.0	4.5	5.0	5.0	5.5	6.0
With geotextile, D_2	4.0	4.0	4.0	4.0	4.0	4.0
Cost Savings ($ per lineal foot)						
Additional aggregate cost						
Full intrusion		1.39	2.08	2.78	3.47	5.56
Partial intrusion		0.70	1.39	1.39	2.08	2.78
Geotextile cost		0.83	0.83	0.83	0.83	0.83
Cost savings						
Full intrusion		0.56	1.25	1.95	2.64	4.73
Partial intrusion		(0.13)	0.56	0.56	1.25	1.39

Note: D_2 = depth of aggregate bases rounded up to the nearest ½ in. Full intrusion assumes intrusion will occur throughout D_2. Partial intrusion assumes intrusion will be confined to first 4 in. of D_2. a_2 = 0.14 for original aggregate base and for situation with geotextile separator. Additional aggregate computed assuming a double-lane road 26 ft shoulder to shoulder at the top of pavement and having a 30-ft subgrade. Aggregate base cost = \$15/yd^3. Geotextile cost = \$0.75/yd^2.

textiles are not used, is illustrated using the cross section shown in Figure 1 and the AASHTO equation *(20)*. Table 15 gives the additional aggregate needed for various levels of percentage of added fines, as well as the estimated cost savings that may accrue from the use of geotextiles as an alternative to additional aggregate base. Two intrusion conditions are assumed: full intrusion of the aggregate base and partial intrusion. The former assumes that intrusion occurs throughout the depth of the base, whereas the latter assumes that intrusion is confined to the first 4 in. At 12 percent added fines, cost savings of up to \$2.64 per lineal foot of roadway could accrue as a result of using geotextiles as a separation mechanism. This level of added fines is typical of some National Forest roads *(19)*. Using the maximum laboratory-determined level of 19.5 percent added fines, cost savings of up to \$4.73 per lineal foot of roadway could occur.

Another way to illustrate the benefits of using geotextiles is to determine the depth of additional bituminous concrete needed during initial construction (or after contamination occurs). This is also illustrated using the AASHTO procedure *(20)*. Table 16 gives the amount of overlay needed using AASHTO *(20)* for the various levels of percentage of added

TABLE 16 COST SAVINGS USING GEOTEXTILES AS AN ALTERNATIVE TO ADDITIONAL BITUMINOUS CONCRETE, AASHTO METHOD *(24)*

S % =	0 to 2	4	6	8	10	12	19.5
	(a) Asphalt Surface Thickness, in.						
D_1 Without Geotextile	4.00	4.25	4.25	4.50	4.50	4.75	5.00
D_1 With Geotextile	4.00	4.00	4.00	4.00	4.00	4.00	4.00
D_1 Savings	0	0.25	0.25	0.50	0.50	0.75	1.00
	(b) Incremental Cost Savings, $ per lineal ft						
Overlay Cost		1.21	1.21	2.41	2.41	3.61	4.81
Geotextile Cost		0.83	0.83	0.83	0.83	0.83	0.83
Cost Savings Using Geotextiles		0.38	0.38	2.03	2.03	2.78	3.98

Notes:
D_1 = Depth of bituminous concrete with a_1 = 0.36.
Overlay assumed to be for a double lane road, 26 ft shoulder to shoulder.
Bituminous concrete cost = \$60/cy.
Geotextile cost = \$0.75/sy.

TABLE 17 U.S. FOREST SERVICE REQUIREMENTS FOR SEPARATION GEOTEXTILES *(25)*

Test Standard	Property
Geotextile properties	
Grab tensile strength (ASTM D1682)	110 lb min
Grab tensile elongation (ASTM D1682)	15% min
Equivalent opening size (U.S. standard)	
Nonwoven	20–100
Woven	20–70
Bursting strength[a] (ASTM D751)	200 lb min
Puncture strength[a] (ASTM D751)	42 lb min
Percentage open area	
Nonwoven	None specified
Woven	< 4%
Permeability	0.001 cm/sec min
Weight	4 oz/yd^2 min
Thickness	15 mils min
Soil subgrade properties	
CBR	3 min
Vane shear strength	10 psi min
Particle size of aggregate base	2 in. max

[a]Unaged fabric.

fines, as well as associated cost savings. This method indicates that a potential cost savings of $2.78 per lineal foot of roadway can accrue when the contaminated aggregate base contains up to 12 percent added fines. At 19.5 percent added fines, the savings could reach $3.98 per lineal foot of roadway. For pavement sections with thicker base layers (8 to 12 in.), it is possible that even greater cost savings could be realized.

Performance Objectives for Separation Geotextiles

This study did not evaluate the physical properties of geotextiles needed to achieve the performance objectives of a separation layer. Properties required in the 1985 U.S. Forest Service Standard Specification are given in Table 17 *(21)*.

Research by others to date suggests that the amount of contamination depends on percentage of open area, porosity, effective opening size, and thickness of the geotextile *(4, 5, 7, 8)*. Performance criteria that need to be established for separation geotextiles are those that limit the amount of added subgrade fines to an acceptable level. For the situation tested (F_0 = 5.5), the geotextile needs to limit the amount of added subgrade fines (S) to 2.5 percent to maintain drainage and to 6 percent to maintain stiffness. These criteria need to be evaluated in terms of the depth and gradation of aggregate base used because these factors influence whether full or partial intrusion is experienced.

Geotextiles used for separation must also be able to withstand the effects of abrasion during and after construction. Following construction, the geotextile should also be able to withstand compressive strains in the vertical direction and tensile strains in the horizontal direction.

SUMMARY

A laboratory study to evaluate the effects to added subgrade fines on the resilient modulus of an aggregate base has been described. The aggregate tested was a 1-in.-minus crushed aggregate with 5.5 percent passing the No. 200 (0.075-mm) sieve. Subsequent tests were conducted after adding 2, 4, 6, 8, and 19.5 percent subgrade fines to the original aggregate. The testing program showed that the resilient modulus of the aggregate-subgrade mixture increased as the percentage of added fines increased; a peak in resilient modulus occurred at 6 percent added fines. At 8 percent added fines, a dramatic drop in resilient modulus was experienced. This indicates that, from a stiffness standpoint, up to 6 percent added fines can be tolerated when the initial aggregate has 5.5 percent passing the No. 200 (0.075-mm) sieve.

When the effect of subgrade intrusion is evaluated, maintaining adequate permeability within the aggregate base also needs to be considered. U.S. Forest Service specifications *(13)* allow up to 8 percent fines in the aggregate produced for a construction contract. If it is assumed that this is to be the upper limit for proper drainage, the amount of added fines needs to be limited to 2.5 percent if the initial aggregate has 5.5 percent fines. Thus it appears that limiting subgrade intrusion for drainage purposes may take priority over limiting subgrade intrusion for stiffness purposes.

The effect of subgrade intrusion is a reduced modulus of the aggregate base and a shorter pavement life. The life of a pavement can be extended by taking this into account during design by providing either a thicker aggregate base course or a thicker bituminous concrete layer. A cost-effective alternative is the use of geotextiles as a separation layer. The potential cost savings can reach $3 to $4 per lineal foot of roadway, depending on the amount of added fines.

Available test data for geotextiles in separation applications have several limitations. One of these is the lack of a standardized test procedure for measuring soil contamination values in the laboratory. Additional research is also needed to quantify the specific geotextile properties that limit intrusion. Finally, actual geotextile installations need to be monitored to evaluate their effectiveness under field conditions.

ACKNOWLEDGMENTS

The authors wish to acknowledge the assistance of John Mohney and Richard Reay of the U.S. Forest Service Materials Laboratory in Portland, Oregon, in performing the resilient modulus tests for this study. The figures used in this paper were prepared by Brad Roberts.

REFERENCES

1. J. Steward, R. Williamson, and J. Mohney. *Guidelines for Use of Fabrics in Construction and Maintenance of Low-Volume Roads.* FHWA–TS–78–205. Forest Service (Pacific Northwest Region), U.S. Department of Agriculture, Portland, Oreg., June 1977.
2. J. R. Bell and R. G. Hicks. *Evaluation of Test Methods and Use*

Criteria for Geotechnical Fabrics in Highway Applications. FHWA/RD–80/021. FHWA, U.S. Department of Transportation, June 1980.
3. R. M. Koerner and J. P. Welsh. *Construction and Geotechnical Engineering Using Synthetic Fabrics.* John Wiley and Sons, Inc., New York, 1980.
4. D. J. Hoare. A Laboratory Study into Pumping Clay Through Geotextiles Under Dynamic Loading. *Proc., Second International Conference on Geotextiles,* Las Vegas, Nevada, Vol. 2, Aug. 1982, Session 5B, pp. 423–428.
5. A. L. Bell, L. M. McCullough, and M. S. Snaith. An Experimental Investigation of Sub-Base Protection Using Geotextiles. *Proc., Second International Conference on Geotextiles,* Las Vegas, Nevada, Vol. 2, Aug. 1982, Session 5B, pp. 435–440.
6. S. K. Saxena and D. Chiu. Evaluation of Fabric Performance in a Railroad System. *Proc., Second International Conference on Geotextiles,* Las Vegas, Nevada, Vol. 2, Aug. 1982, Session 6B, pp. 485–490.
7. G. Raymond. Geotextiles for Railroad Bed Rehabilitation. *Proc., Second International Conference on Geotextiles,* Las Vegas, Nevada, Vol. 2, Aug. 1982, Session 6B, pp. 479–484.
8. M. S. Snaith and A. L. Bell. The Filtration Behavior of Construction Fabrics Under Conditions of Dynamic Loading. *Geotechnique,* Vol. 28, No. 4, 1978, pp. 466–469.
9. H. B. Seed, F. G. Mitry, C. L. Monismith, and C. K. Chan. Factors Influencing the Resilient Deformations of Untreated Aggregate Base in Two-Layer Pavements Subjected to Repeated Loading. In *Highway Research Record 190,* HRB, National Research Council, Washington, D.C., 1967, pp. 19–57.
10. I. V. Kalcheff and R. G. Hicks. A Test Procedure for Determining the Resilient Properties of Granular Materials. *Journal of Testing and Evaluation,* ASTM, Vol. 1, No. 6, Nov. 1973.
11. Y. T. Chou. *Evaluation of Nonlinear Resilient Moduli of Unbound Granular Materials from Accelerated Traffic Test Data.* Technical Report S–76–12. U.S. Army Engineer Waterways Experiment Station, Vicksburg, Miss., Aug. 1976.
12. *Methods of Sampling and Testing,* 13th ed. AASHTO, Washington, D.C., July 1982.
13. H. W. Humphres. A Method for Controlling Compaction of Granular Materials. *Highway Research Bulletin 159,* HRB, National Research Council, Washington, D.C., 1957, pp. 41–57.
14. *Forest Service Standard Specifications for Construction of Roads and Bridges.* EM–7720–100. Forest Service, U.S. Department of Agriculture, 1979.
15. C. A. Bell. *Boussinesq Method of Equivalent Thickness.* Oregon State University, Corvallis, 1982.
16. E. K. Yoder and M. W. Witczak. *Principles of Pavement Design,* 2nd ed. John Wiley and Sons, Inc., New York, 1975.
17. R. G. Hicks. *Use of Layered Theory in the Design and Evaluation of Forest Roads.* Forest Service, U.S. Department of Agriculture, Portland, Oreg., Jan. 1976.
18. J. Walter. *Fabrics as a Separation Layer.* Oregon State University, Corvallis, 1982.
19. B. N. Jorenby. *Geotextile Use as a Separation Mechanism.* M.S. project report. Oregon State University, Corvallis, 1984.
20. *Transportation Engineering Handbook.* Forest Service (Pacific Northwest Region), U.S. Department of Agriculture, Portland, Oreg., 1974, Chapter 50.
21. *Forest Service Standard Specifications for Construction of Roads and Minor Drainage Structures.* EM–7720–100R. Forest Service, U.S. Department of Agriculture, April 1985.

Publication of this paper sponsored by Committee on Engineering Fabrics.

Hot-Mix Asphalt Railroad Trackbeds

YANG H. HUANG, JERRY G. ROSE, AND CHARLES J. KHOURY

Since 1981 about 30 experimental sections of hot-mix asphalt trackbeds have been built and evaluated. The hot-mix asphalt can be used either as an overlay placed directly under the tie or as an underlay placed under the ballast. Because of the similarity between highway pavements and railroad trackbeds, the concept developed for the design of highway pavements is investigated and extended to the design of hot-mix asphalt trackbeds. The design is based on two criteria: limiting the horizontal tensile strain at the bottom of the hot-mix asphalt to prevent fatigue cracking and limiting the vertical compressive stress on the top of the subgrade to reduce permanent deformation. The use of vertical compressive stress, instead of vertical compressive strain, is a deviation from highway practice that is found to be more applicable to railroad trackbeds. A computer program based on the finite element method and Burmister's layered theory was developed for the design and analysis of asphalt trackbeds. The results of analysis show that underlays are far superior to overlays from a structural viewpoint. Because of the difference in load distribution, an increase in the thickness of hot-mix asphalt is not as effective in reducing the stresses and strains in railroad trackbeds as it is in highway pavements. In designing underlays, the use of a thin layer of hot-mix asphalt and a thick layer of ballast is recommended. The main function of hot-mix asphalt underlays is to waterproof the subgrade, thus providing consistent load-carrying capability for the trackbed even on subgrades of marginal quality. The hot-mix asphalt mat will separate the ballast from the subgrade, confine the ballast, and eliminate pumping without substantially increasing the stiffness of the trackbed.

Although hot-mix asphalt (HMA) has been used for the construction of highway pavements for more than a century, its use in railroad trackbeds is relatively new and is still in the experimental stage. The first recorded use of hot-mix asphalt for railroad trackbeds in the United States was in 1968 when the Cleveland Transit Authority placed two 1,000-ft (305-m) asphalt test sections on a line extension near the airport *(1)*. The westbound section had 5 in. (127 mm) of hot-mix asphalt, the eastbound 4 in. (102 mm), and the asphalt mats were placed directly on the subgrade and topped with 8 in. (203 mm) of ballast. In 1969 the Santa Fe Railway placed three 700-ft (215-mm) asphalt test sections on a new line to service a coal-mining region in northeastern New Mexico *(2)*. The asphalt mats were 2.5 in. (63 mm), 5 in. (127 mm), and 7.5 in. (190 mm) thick, respectively, and were placed under a 10-in. (254-mm) ballast. In spite of the excellent performance of these experimental sections, little work was done on hot-mix asphalt trackbeds until 1981 when a research project was initiated at the University of Kentucky under the joint financial support of the National Asphalt Pavement Association and the Asphalt Institute. The overall objective of this research is to evaluate and document the technical and economic benefits of railroad trackbeds containing a layer of dense-graded hot-mix asphalt. With the cooperation of several railway companies, approximately 30 different installations of asphalt trackbeds under a variety of traffic, soil, and environmental conditions have been built. A further objective is to use the responses and performances of these test trackbeds to develop a rational method for the design of hot-mix asphalt trackbeds. It is the purpose of this paper to describe the design, construction, and performance of hot-mix asphalt trackbeds with particular emphasis on the design differences between highway pavements and railroad trackbeds.

Department of Civil Engineering, University of Kentucky, Lexington, Ky. 40506–0046.

CONSTRUCTION AND PERFORMANCE

Two methods have been used to incorporate hot-mix asphalt in railroad trackbeds. One method, which is similar to the construction of highway pavements, is to place the hot-mix asphalt on top of the subgrade or above a layer of base course. The ties are then placed directly on the asphalt mat. This type of construction is called full depth if the asphalt mat is built directly on the subgrade or overlay if a layer of granular base is used. The geometry of full depth and overlay is similar to that of highway pavements except that wheel loads are transmitted through rails and ties over a large area on the asphalt mat instead of through tires over small areas. Another method is to place the asphalt mat under the ballast. The asphalt mat actually serves as a subballast. For heavy-tonnage main lines on a poor subgrade, a granular base course or other stabilized materials may be placed between the hot-mix asphalt and the subgrade. This type of construction is called underlay and is preferred by railroad engineers because conventional railroad maintenance procedures can still be applied. Figure 1 shows typical cross sections for hot-mix asphalt trackbeds.

When the asphalt mat is placed on existing trackbeds, the track must be removed and the underlying material excavated to the desired grade. The asphalt mat may be built directly on the subgrade or a new granular base course may be constructed. The upper portion of old trackbeds can also be used as a base course. The asphalt mat is then placed by a standard highway asphalt paver and compacted by a standard roller. The track is then rebuilt or dragged back on the asphalt mat. For the full-depth and overlay sections, cribbing aggregate is spread to fill the space between the ties and to form the shoulders so the ties will not slip on the asphalt mat. For the underlay sections, ballast is spread from railroad cars and the track is raised to accommodate a specified thickness of ballast under the ties. The ballast also fills the crib areas between the ties and provides the shoulders.

The recommended asphalt mix is a slightly modified dense-graded highway mix composed of 1- to 1.5-in. (25- to 38-mm) maximum sized aggregated and AC–10 or AC–20 viscosity-graded asphalt cement. The proportions are slightly different

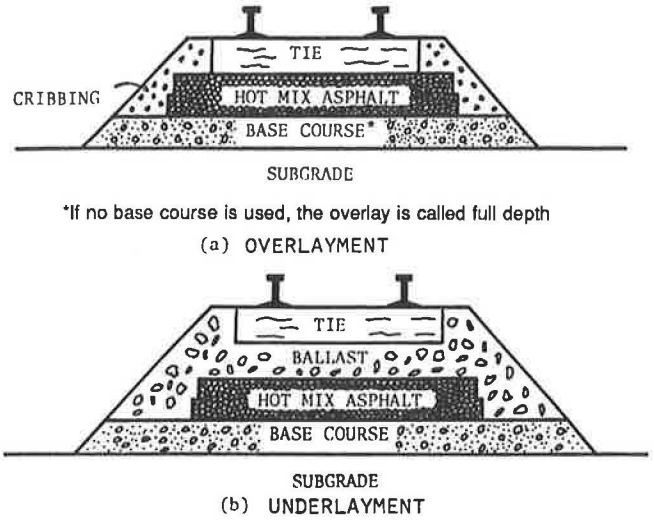

FIGURE 1 Typical cross sections of hot-mix asphalt trackbeds.

from those of typical highway dense-graded base mixes; the mix contains slightly more asphalt cement, more mineral aggregate fines, and lower air voids, which enhance compactibility and impermeability of the mat.

Approximately 30 installations, including numerous highway and railroad crossings, were constructed in Kentucky, Oklahoma, West Virginia, Massachusetts, Indiana, Louisiana, and Missouri. Several significant test tracks have been constructed since 1981 (1 ft = 0.305 m; 1 in. = 25.4 mm):

- Seaboard System Railroad, Ravenna, Kentucky, yard, 1981: two 500-ft-long, 12-ft-wide full-depth sections, one 8 in. thick, the other 12 in. thick, constructed on a curved portion of the main line.
- Santa Fe Railway, Oklahoma City, Flynn yard, 1982: one 532-ft-long, 12-ft-wide, 8-in.-thick underlay section constructed on a curved portion of the trim lead track.
- Santa Fe Railway, Oklahoma City, automobile-unloading yard, 1982: approximately 5 acres of 4-in.-thick underlay section with asphalt-paved driving areas between tracks.
- Seaboard System Railroad, Conway, Kentucky, 1983: two 1,000-ft-long, 12-ft-wide underlay sections, one 5 in. thick, the other 8 in. thick, constructed on the Cincinnati to Knoxville main line.
- Chessie System Railroads, Deepwater, West Virginia, bridge approaches, 1984: two 200-ft-long, 12-ft-wide underlay sections, 4 in. and 8 in. thick, constructed on the Huntington to Hinton main line.

The test installations have been subjected to periodic instrumented tests and measurements to monitor the performances and responses of the track system. Among the periodic measurements are the moisture contents of the subgrade and the old roadbed under the asphalt mat, the temperature distribution within the trackbed, the elevations along the top of the rail, the stiffness or track modulus under static loading conditions, and the determination of geometric parameters by track geometry vehicles.

All installations have exhibited excellent performance. Compared with that of conventional ballasted trackbeds, the moisture content of the subgrade or old roadbed directly under the asphalt mat was lower. Moisture contents directly under the asphalt mats were near optimum for maximum density and varied only slightly from as-constructed conditions. This waterproofing effect will provide consistent load-carrying capability of the subgrade, even on subgrades of marginal quality, and prevent the intrusion of subgrade soils into the ballast with subsequent fouling and pumping. The temperature fluctuations in the asphalt mat were minimal because of the insulative and temperature attenuative characteristics of the overlying ballast and cribbing aggregate. For the overlay at Ravenna yard, the maximum temperature of the asphalt mat was 35°F (1.7°C) in the winter and 80°F (26.7°C) in the summer; for the underlay at Conway, the temperature ranged from 36°F (2°C) to 79°F (26°C). The absence of extreme temperatures, such as are experienced in highway pavements, will increase fatigue life during the winter and decrease permanent deformation during the summer. It was found that no significant changes in elevation occurred, even after several years of heavy traffic on old roadbeds, which had previously exhibited frequent settlements due to soft roadbeds and pumping. The deflections and track moduli of underlays were near optimum (i.e., slightly resilient and not overly stiff) and could be maintained for a longer period of time and be less affected by variations in rainfall and other environmental conditions than are typical ballasted tracks. Track geometry tests indicated that no detectable changes in geometric parameters had ever occurred.

Asphalt cores were obtained from the Cleveland and New Mexico installations constructed during the late 1960s. Viscosity and penetration tests on the recovered asphalt indicated no hardening of the asphalt cement and no deterioration of the mixtures under the insulated environment. Because asphalt retains its resilient characteristics for a long period of time, there is a significantly reduced tendency for the asphalt mat to become brittle and cracked. This will greatly prolong the structural life of an asphalt mat in a track structure compared with that revealed by data obtained on highways.

COMPUTER MODELING

A computer program named KENTRACK *(3)* was developed for the structural analysis and design of railroad tracks. Figure 2 shows the various components of the track system to be analyzed. From top to bottom, the track is composed of rails, tie plates, ties, and the layered system. The finite element method was used in the analysis; the rails and ties were considered beam elements and the tie plates spring elements. The load is transmitted from the ties to the layered system through circular areas of equal diameter, thus Burmister's layered theory, so well known in the analysis of highway pavements, can be applied. By simply changing the properties of the layers, the program can be used for conventional ballasted tracks as well as hot-mix asphalt trackbeds. Major responses computed by the program include the deflections of rail, the bending and shear stresses in rail and tie, the contact pressure between tie and layered system, the horizontal tensile stress and strain at the bottom of hot-mix asphalt, and the vertical compressive stress

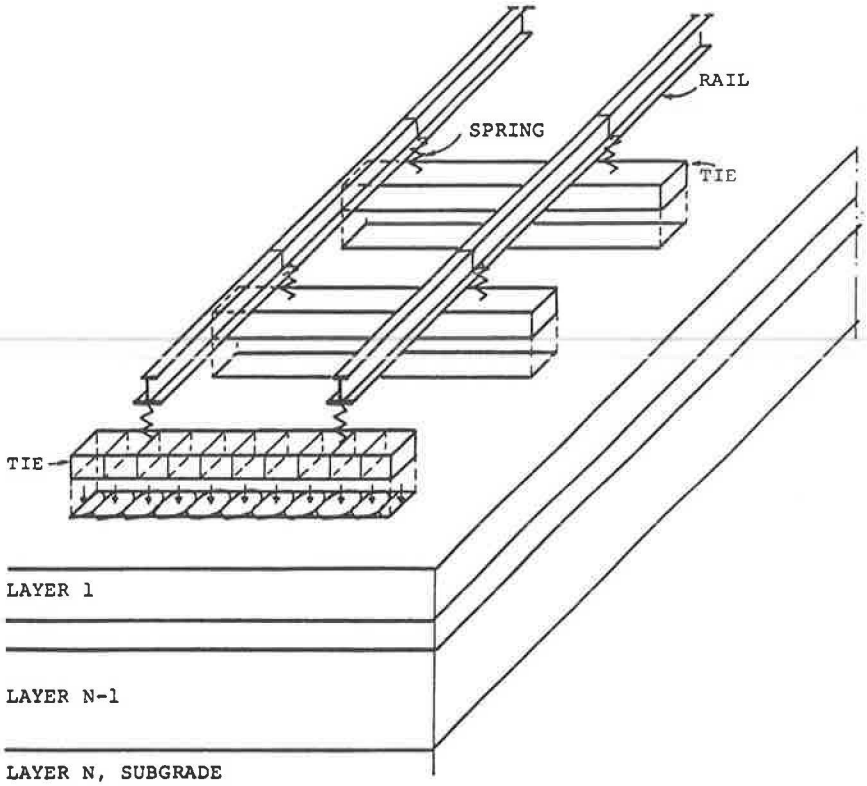

FIGURE 2 Modeling of railroad trackbeds.

and strain on the top of the subgrade. The rails, tie plates, ties, hot-mix asphalt, and subgrade are assumed to be linear elastic and the ballast and other granular layers as nonlinear elastic with an elastic modulus determined by

$$E_g = K_1\theta^{K_2} \quad (1)$$

where

E_g = elastic modulus of ballast or other granular materials,
θ = sum of the three principal stresses due to loading and overburden, and
K_1, K_2 = nonlinear coefficients.

By using the critical stress or strain in the trackbed, damage analysis can be performed by Miner's hypothesis *(4)*. Because the elastic moduli of a layered system, particularly the hot-mix asphalt, vary with the time of the year, each year can be divided into 12 months or a number of seasons for damage analysis. Damage, computed on a monthly or seasonal basis for given traffic and material properties, is accumulated up to a damage ratio of 1.0 using the concept of linear summation of cycle ratios. Two criteria, similar to those used for highway pavements, are proposed for damage analysis: limiting the horizontal tensile strain at the bottom of hot-mix asphalt to prevent fatigue cracking and limiting the vertical compressive stress on the top of the subgrade to reduce permanent deformation. The reason for using the vertical compressive stress, instead of compressive strain, as is done in standard highway practice, will be discussed later.

The purpose of damage analysis is to determine design life. In highway pavements there is only one design life because the hot-mix asphalt must be replaced or overlaid whenever the design life for fatigue cracking or pavement deformation is reached. In railroad trackbeds there are two design lives, one involving the fatigue cracking of hot-mix asphalt and the other involving the permanent deformation of the track. The required design life for fatigue cracking should be much greater than that for permanent deformation because the latter can be corrected by adjusting the ballast or shimming the rails or ties. When permanent deformation has been corrected, the track is considered new and requires further correction only when the new design life for permanent deformation is reached.

To compute the stresses and strains in highway pavements, a program called KENLAYER was also developed. KENLAYER has the same capability as KENTRACK except that wheel loads are applied directly on the layered system through single, dual, or dual-tandem circular areas.

DESIGN CRITERIA

Fatigue cracking and permanent deformation are the two criteria used most frequently for the design of highway pavements. In the Asphalt Institute's design method *(5)*, the allowable number of load repetitions for fatigue cracking (N_c) is related to the horizontal tensile strain at the bottom of hot-mix asphalt (ε_t) by

$$N_c = 0.0795\ \varepsilon t^{-3.291}\ E_a^{-0.854} \quad (2)$$

where E_a is the elastic modulus of hot-mix asphalt in psi. In the Shell design method *(6)*, the allowable number of load repetitions for permanent deformation (N_d) is related to the vertical compressive strain on the top of subgrade (ε_c) by

$$N_d = 6.15 \times 10^{-7} \varepsilon_c^{-4.0} \quad (3)$$

Equations 2 and 3 are based on long years of experience and the analysis of AASHO Road Test data. The design system is based on the asphalt surface being exposed to the atmosphere, which accelerates oxidation and hardening of the asphalt and shortens fatigue life. Because of the difference in loading conditions, environmental effects, and performance requirements, these equations may not be applicable to the design of railroad trackbeds. However, in the absence of experience in railroad applications, these equations can be used as a guide. They should be modified as more experience is gained. The reason that the Shell criterion for permanent deformation is used, instead of the Asphalt Institute's criterion, is because it allows a greater number of load repetitions and is more compatible with the larger compressive strain under railroad loadings. It is believed that the use of highway failure criteria for the design of railroad trackbeds is quite conservative because the hot-mix asphalt and subgrade are better confined and insulated and should offer greater resistance to fatigue cracking and permanent deformation.

The use of compressive strain, instead of compressive stress, in Equation 3 is a convenient way to eliminate the effect of the stiffness or modulus of the subgrade. However, it has been found that the vertical compressive stress is a much better and more sensitive indicator of structural adequacy, particularly for railroad trackbeds *(7)*. This can also be seen from Table 1 in which the stresses and strains in a 4-in. (102-mm) full depth are compared with those in an overlay composed of a 4-in. (102-mm) hot-mix asphalt on a 4-in. (102-mm) granular base. In the analysis, it is assumed that the hot-mix asphalt has an elastic modulus of 500,000 psi (3.5 GPa) and a Poisson's ratio of 0.45 and that the subgrade has an elastic modulus of 7,500 psi (51.7 MPa) and a Poisson's ratio of 0.40. The granular base is assumed to be nonlinear with K_1 of 7,500 psi and K_2 of 0.5. The highway loading is a standard 18,000-lb (80-kN) single axle load with dual tires that have a contact pressure of 70 psi (482 kPa) and a spacing of 13.5 in. (343 mm) on centers. The railroad loading consists of two 66,000-lb (294-kN) axle loads spaced 70 in. (1.78 m) apart and is applied to RE132 rails on wood ties spaced 20 in. (508 mm) on centers. These are the two axles at the end of one car. Actually, there are two more axles at the end of the adjacent car and these four axles should be grouped as a unit and considered as one load repetition. Because the stresses and strains under the two axles in one car are greater than those under the four axles in two adjoining cars, only two axles were used in the analysis. The consideration of two axles at the end of one car, or four axles on two adjoining cars, as one load repetition is also quite conservative. When a train travels at a high speed, the stress and strain under one group of axle loads is not completely released before the application of the next loads, which results in less destructive effect. The elastic modulus of wood ties is assumed to be 1.5×10^6 psi (10.3 GPa) and the tie plate stiffness is assumed to be 7×10^6 lb/in. (791 N-m/mm). Unless noted otherwise, these parameters and assumptions were used for all the analysis presented in this paper.

Table 1 gives the effect of 4-in. (102-mm) granular base on the stresses and strains in highway pavements and railroad trackbeds. Assuming the stress or strain in a 4-in. (102-mm) full depth with no base as unity, the stress and strain in a 4-in. (102-mm) hot-mix asphalt on a 4-in. (102-mm) base is expressed as a fraction, as indicated by the values in parentheses. It can be seen that the effect of granular base in reducing the horizontal tensile strain is nearly the same as that in reducing the horizontal tensile stress. Therefore it does not make any significant difference whether the horizontal tensile stress or strain is used as a design criterion. However, this is not the case for the vertical compressive stress or strain. For highway pavement, the addition of a 4-in. (102-mm) base reduces the vertical stress to 76 percent but the vertical strain to 92 percent. For railroad trackbed, the vertical stress is reduced to 88 percent but the vertical strain is increased to 106 percent. This clearly indicates that the vertical compressive strain is not a good indicator of structural adequacy because the addition of a 4-in. (102-mm) granular base does not decrease, but actually increases, the compressive strain. The reason for the increase in vertical compressive strain is the decrease in average lateral compressive stress (Table 1).

Based on the AASHTO equation, Equation 3 in terms of

TABLE 1 STRESSES AND STRAINS FOR 4-IN. HOT-MIX ASPHALT WITH AND WITHOUT GRANULAR BASE

Loading	Granular Base	Horizontal Tensile Strain ($\times 10^{-3}$)	Horizontal Tensile Stress (psi)	Vertical Compressive Strain ($\times 10^{-3}$)	Vertical Compressive Stress (psi)	Average Lateral Compressive Stress (psi)
Highway	No base	0.368(1)[a]	285(1)	1.11(1)	11.40(1)	3.78(1)
	4-in. base	0.316(0.86)	244(0.86)	1.02(0.92)	8.72(0.76)	1.30(0.34)
Railroad	No base	0.248(1)	207(1)	1.23(1)	14.77(1)	6.88(1)
	4-in. base	0.224(0.90)	183(0.88)	1.30(1.06)	12.95(0.88)	4.04(0.59)

Note: 1 in. = 25.4 mm, 1 psi = 6.89 kPa.

[a]Values in parentheses are stress and strain in a 4-in. (102-mm) hot-mix asphalt on a 4-in. (102-mm) base if the stress or strain in a 4-in. (102-mm) full depth with no base is assumed to be unity.

TABLE 2 COMPARISON OF HIGHWAY PAVEMENTS AND RAILROAD TRACKBEDS

Type	Loading	Thickness[a] (in.)	Horizontal Tensile Strain ($\times 10^{-3}$)	Horizontal Tensile Stress (psi)	Vertical Compressive Strain ($\times 10^{-3}$)	Vertical Compressive Stress (psi)	Allowable Repetitions: Tensile Strain ($\times 10^6$)	Allowable Repetitions: Compressive Strain ($\times 10^6$)	Allowable Repetitions: Compressive Stress ($\times 10^6$)	Contact Pressure (psi)
Full depth	Highway	4	3.68(1)[b]	285(1)	1.111(1)	11.40(1)	0.22	0.40	0.42	70(1)
		6	2.31(0.628)	179(0.628)	0.653(0.588)	6.43(0.564)	1.00	3.38	3.56	70(1)
		8	1.58(0.429)	122(0.428)	0.430(0.387)	4.18(0.367)	3.50	17.99	17.76	70(1)
		10	1.14(0.310)	90(0.315)	0.308(0.277)	10.24	2.93	68.34	66.93	70(1)
		12	0.87(0.236)	70(0.246)	0.233(0.210)	2.18(0.191)	24.92	208.67	201.89	70(1)
	Railroad	4	2.48(1)	207(1)	1.230(1)	14.77(1)	0.79	0.27	0.16	47.44(1)
		6	2.70(1.089)	224(1.082)	1.130(1.919)	12.84(0.869)	0.56	0.38	0.27	72.57(1.530)
		8	2.62(1.056)	216(1.043)	1.010(0.821)	11.07(0.749)	0.66	0.59	0.47	97.20(2.049)
		10	2.40(0.968)	197(0.951)	0.881(0.716)	9.53(0.645)	0.88	1.02	0.82	118.22(2.492)
		12	2.11(0.851)	173(0.835)	0.762(0.620)	8.19(0.555)	1.35	1.82	1.44	129.05(2.720)
Underlay	Highway	2	1.65(1)	124(1)	0.546(1)	6.05(1)	3.03	6.92	4.47	70(1)
		4	1.55(0.939)	119(0.960)	0.480(0.879)	5.07(0.838)	3.72	11.59	8.64	70(1)
		8	1.19(0.721)	94(0.758)	0.340(0.623)	3.34(0.552)	8.89	46.02	41.04	70(1)
		12	0.87(0.527)	70(0.565)	0.233(0.427)	2.18(0.360)	24.92	208.67	201.89	70(1)
	Railroad	2	1.47(1)	119(1)	0.883(1)	11.25(1)	4.43	1.01	0.44	48.44(1)
		4	1.66(1.129)	134(1.126)	0.870(0.985)	10.72(0.953)	2.97	1.07	0.53	54.24(1.120)
		8	1.93(1.313)	156(1.311)	0.813(0.921)	9.37(0.833)	1.81	1.41	0.87	73.56(1.519)
		12	3.11(1.435)	173(1.454)	0.762(0.863)	8.19(0.728)	1.35	1.82	1.44	129.05(2.664)
Overlay	Highway	0	1.58(1)	122(1)	0.430(1)	4.18(1)	3.50	17.99	17.76	70(1)
		4	1.50(0.949)	116(0.951)	0.415(0.965)	3.54(0.847)	4.15	20.73	33.03	70(1)
		8	1.44(0.911)	110(0.909)	0.365(0.849)	02.96(0.708)	4.75	34.65	64.43	70(1)
		12	1.39(0.880)	106(0.869)	0.313(0.728)	2.46(0.589)	5.33	64.08	128.58	70(1)
	Railroad	0	2.62(1)	216(1)	1.010(1)	11.07(1)	0.66	0.59	0.47	97.20(1)
		4	2.46(0.939)	200(0.926)	1.010(1)	9.89(0.893)	0.81	0.59	0.71	100.77(1.037)
		8	2.34(0.893)	190(0.880)	0.933(0.924)	8.80(0.795)	0.96	0.81	1.10	102.77(1.057)
		12	2.25(0.859)	182(0.843)	0.859(0.850)	7.89(0.713)	1.09	1.13	1.66	104.20(1.072)

Note: 1 in. = 25.4 mm, 1 psi = 6.89 kPa.

[a]Thickness of hot-mix asphalt for full depth and underlay and thickness of granular base for overlay.
[b]Values in parentheses are ratios with respect to the smallest thickness.

vertical compressive strain (ε_c) was converted to Equation 4 in terms of vertical compressive stress (σ_c) *(3)*:

$$Nd = 4.837 \times 10^{-5}\ \sigma_c^{-3.734}\ E_s^{3.583} \quad (4)$$

where E_s is the elastic modulus of the subgrade. It should be noted that the conversion was based on full-depth highway pavements. Significant discrepancies between Equations 3 and 4 should be expected when they are applied to railroad trackbeds or highway pavements with granular bases, as will be discussed later.

HIGHWAY PAVEMENTS VERSUS RAILROAD TRACKBEDS

Table 2 gives the critical stresses and strains, the allowable number of load repetitions, and the tire or tie contact pressure for highway pavements and railroad trackbeds. Three types of construction, viz full depth, underlay, and overlay with parameters shown in Figure 3, were investigated. In the full depth, the thickness of hot-mix asphalt varies from 4 to 12 in. (102 to 305 mm). In the underlay, the combined thickness of ballast and hot-mix asphalt is fixed at 12 in. (305 mm) but the thickness of hot-mix asphalt varies. In the overlay, the thickness of hot-mix asphalt is 8 in. (203 mm) but the thickness of granular base varies. Although underlays are not used for highway pavements, they are included in Table 2 to show their behavior under highway loadings versus that under railroad loadings. The loadings used for Table 2 are the same as those for Table 1

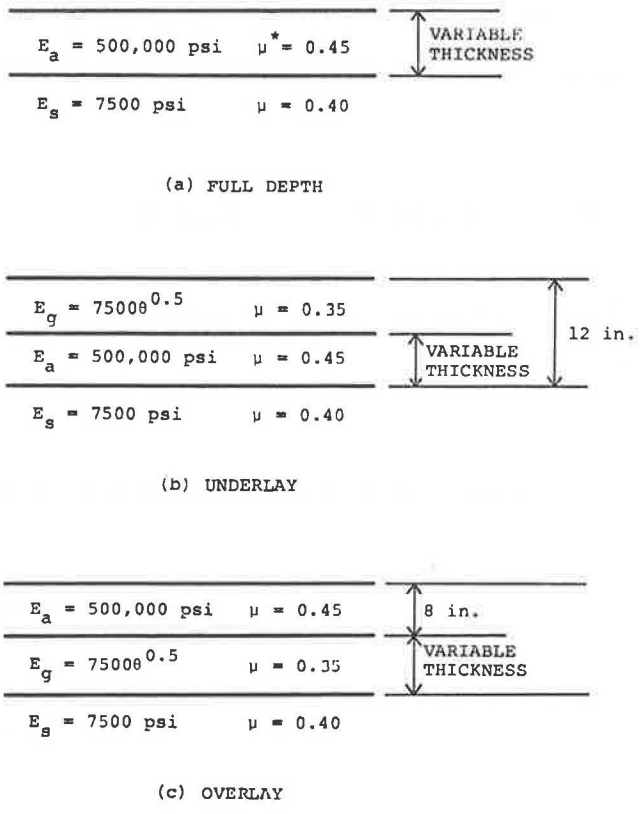

FIGURE 3 Parameters of layered system for analysis (1 in. = 25.4 mm, 1 psi = 6.9 kPa).

as described in the previous section. The values shown in parentheses are the ratios with respect to the smallest thickness. These stress or strain ratios are plotted in Figure 4. The allowable number of load repetitions was computed from Equation 2 for horizontal tensile strains, from Equation 3 for vertical compressive strains, and from Equation 4 for vertical compressive stresses. The contact pressure for highway pavements is the tire contact pressure on the layered system, and that for railroad trackbeds is the maximum contact pressure between the tie and the layered system.

Figure 4 shows the effect of hot-mix asphalt or base thickness on the stress or strain ratios. A review of Figure 4 and Table 2 reveals the following:

1. The effect of thickness on the horizontal tensile strain at the bottom of hot-mix asphalt is nearly the same as that on the horizontal tensile stress, as indicated by the close proximity of the two curves. Therefore either tensile strain or tensile stress can be used as a design criterion for fatigue cracking. Following highway practice, the use of tensile strain is recommended for railroad trackbeds.

2. An increase in the thickness of hot-mix asphalt decreases the tensile strain in highway pavements but not necessarily in railroad trackbeds. For railroad underlays with a given combined thickness of ballast and hot-mix asphalt, the tensile strain increases as the thickness of hot-mix asphalt increases, which indicates that the use of ballast is more effective than the use of hot-mix asphalt in reducing tensile strains. That the replacement of ballast by hot-mix asphalt increases the tensile strain is due to the load concentration as indicated by the tremendous increase in contact pressure near the wheel load caused by the stiffer trackbed.

3. The use of full-depth construction is effective in reducing the tensile strain in highway pavements but not in railroad trackbeds. However, the use of a thicker base course is slightly more effective in reducing the tensile strain in railroad trackbeds than in highway pavements, which indicates the importance of foundation support in railroad trackbeds to reduce tensile strains. Therefore the use of full depth is not recommended for railroad trackbeds unless a good foundation exists.

4. The effect of thickness on the vertical compressive strain at the top of the subgrade is different from that on the vertical compressive stress, particularly for railroad trackbeds, as indicated by the large spacing between the two curves. Therefore designs based on compressive strain are expected to be different from those based on compressive stress. Because compressive stress is more sensitive to changes in thickness, it is recommended for use in the design of railroad trackbeds.

5. An increase in the thickness of hot-mix asphalt or granular base decreases the vertical compressive stress on the top of the subgrade. However, the decrease is much greater in highway pavements than in railroad trackbeds. This is as expected because highway loadings are distributed through tires over small areas, whereas railroad loadings are distributed through rails and ties over a large area.

6. Except for full-depth highway pavements, the allowable number of load repetitions for permanent deformation based on compressive stress is quite different from that based on compressive strain. The close agreement in the full-depth highway pavements is as expected because the conversion from Equa-

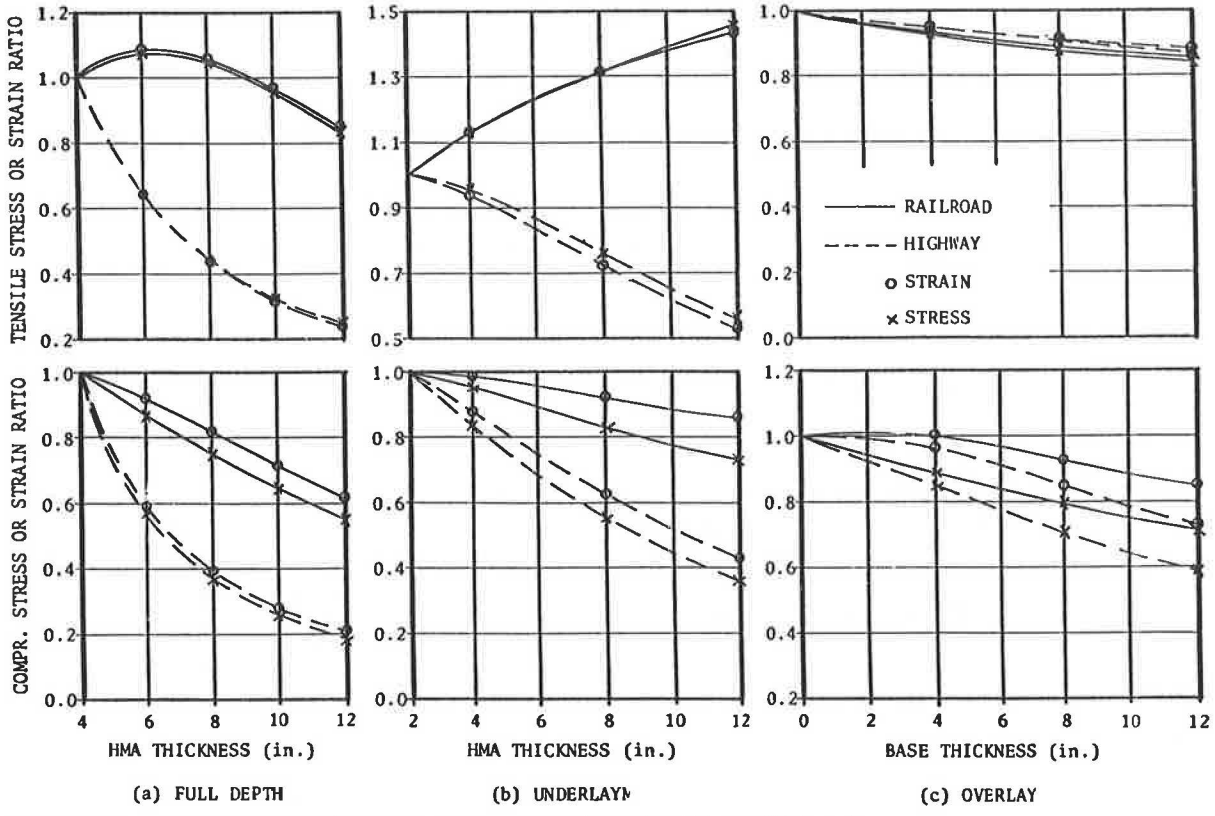

FIGURE 4 Effect of layer thickness on stress or strain ratios (1 in. = 25.4 mm).

tion 3 to Equation 4 was based on full-depth highway pavements *(3)*. This clearly indicates the inadequacy of applying highway criteria to railroad design. The highway criteria should only be used as a guide and should be revised later to meet railroad requirements. It is worthy of note that, for cases of full depth and underlay, the use of compressive stress results in a small number of allowable repetitions and is therefore on the safe side.

7. For railroad underlays with a given combined thickness of ballast and hot-mix asphalt, the vertical compressive stress decreases with an increase in the thickness of hot-mix asphalt, which indicates that the use of hot-mix asphalt is more effective than the use of ballast in reducing compressive stress. This is in contrast to horizontal tensile strain that increases with an increase in the thickness of hot-mix asphalt. The increase in tensile strain is due to the combined effect of larger contact pressures near the wheel loads, which result in greater positive moments, and smaller contact pressures away from the loads, which result in smaller negative moments. The net effect is a tremendous increase in bending moments, which overshadows the effect of increase in the thickness of hot-mix asphalt.

The allowable number of load repetitions shown in Table 2 is based on highway criteria. The application of Equations 2 and 4 to Cleveland and New Mexico test sections constructed during the late 1960s indicates that the former has a design life of 384 years for fatigue cracking and 172 years for permanent deformation and that the latter has design lives of 116 and 62 years, respectively *(8)*. The long design life at Cleveland is due to small wheel loads and light traffic, whereas that at New Mexico is due to an excellent subgrade and light traffic. Because neither installation has reached its design life, there is no way to check the validity of the criteria.

A heavy-tonnage main line may carry more than 26 million gross tons of equivalent fully loaded cars per year. Considering the passage of one car as one repetition and that each car weighs 132 gross tons, the number of load repetitions is 200,000 per year. Comparing this number with those shown in Table 2 indicates that most of the hot-mix asphalt trackbeds could last no more than a few years. Therefore the applicability of the highway criteria and the ability of hot-mix asphalt trackbeds to carry heavy-duty railroad traffic need further investigation.

DESIGN FOR HEAVY TRAFFIC

Using the loadings, material properties, and highway failure criteria described before and assuming load repetitions of 200,000 per year, the design lives, or allowable number of load repetitions, for fatigue cracking and permanent deformation of both full depth and underlay with subgrade moduli ranging from 7,500 to 30,000 psi (51.7 to 207 MPa) were determined by KENTRACK and plotted in Figure 5. For underlays, the thickness of hot-mix asphalt is 4 in. (102 mm) but the thickness of ballast varies from 5 to 15 in. (127 to 381 mm).

It can be seen from Figure 5*a* that unless a hot-mix asphalt mat more than 12 in. (305 mm) thick is built on an excellent

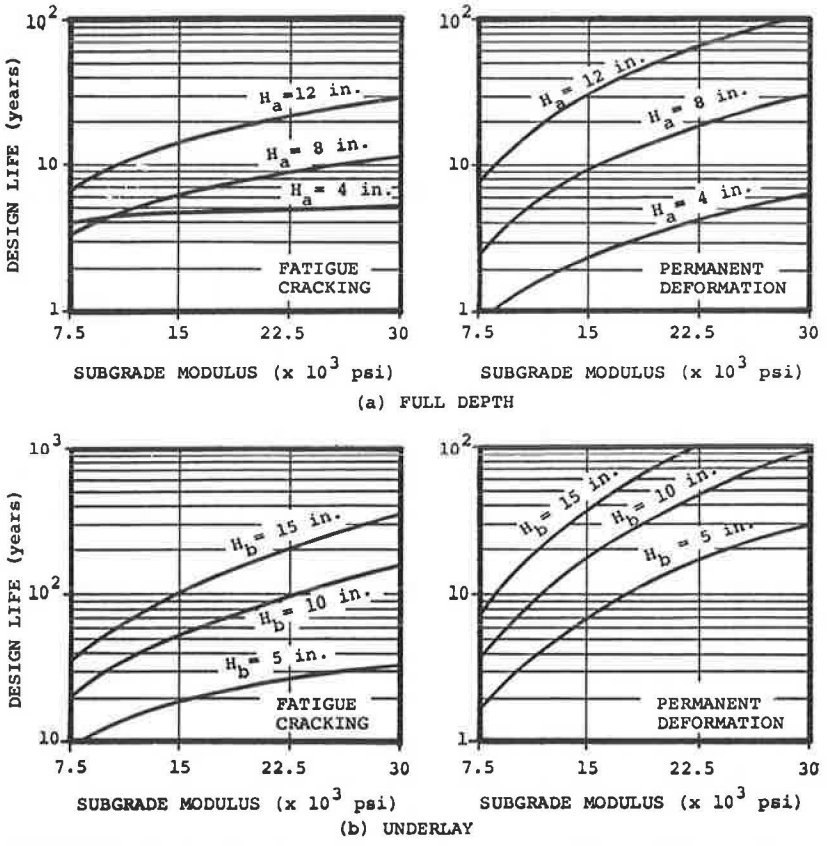

FIGURE 5 Design life of hot-mix asphalt trackbeds (1 in. = 25.4 mm, 1 psi = 6.9 kPa).

TABLE 3 COMPARISON OF UNDERLAYS AND CONVENTIONAL TRACKBEDS

Modulus of Subgrade, psi			3,000	7,500	15,000	30,000
Conventional		σ_c, psi	8.2	11.1	14.1	16.7
		N_d	5.38×10^4	4.63×10^5	2.27×10^6	1.45×10^7
Modulus of Hot-Mix Asphalt 10^3 psi	200	σ_c, psi	8.2	11.4	14.7	18.9
		N_d	5.38×10^4	4.19×10^5	1.94×10^6	9.12×10^6
	500	σ_c, psi	7.8	10.6	13.7	17.5
		N_d	6.49×10^4	5.50×10^5	2.53×10^6	1.22×10^7
	1000	σ_c, psi	7.4	10.1	12.7	16.1
		N_d	7.90×10^4	6.59×10^5	3.36×10^6	1.66×10^7

Note: 1 psi = 6.89 kPa, σ_c = vertical compressive stress on the top of subgrade, N_d = allowable number of repetitions for permanent deformation

subgrade with a modulus of 30,000 psi (207 MPa), there is no way for the full-depth trackbed to achieve a fatigue life of 30 years as recommended for fatigue cracking. The same is true for overlays unless the subgrade is greatly improved by soil stabilization or by incorporating a thick layer of granular base. The shorter fatigue life for the 8-in. (203-mm) full depth on a weak subgrade, compared with the 4-in. (102-mm) full depth, is due to the load concentration caused by the stiffer trackbed. If the track can be shimmed to adjust elevations, there should be no difficulty in achieving a design life of 5 years as recommended for permanent deformations. If the track cannot be shimmed and the design life for permanent deformation should also be 30 years, the required design life will be more difficult to obtain. Because of the high tensile strain at the bottom of hot-mix asphalt and the inapplicability of existing railroad maintenance procedures, the use of full depth and overlay for heavy-haul trackbeds is not recommended.

Figure 5*b* shows that even underlays with a 4-in. (102-mm) hot-mix asphalt can still be made to achieve a fatigue life of 30 years by simply increasing the thickness of ballast. Also there is no difficulty in achieving a design life of 5 years for permanent deformation. The use of 5 years for design life is reasonable because any permanent deformations can be easily corrected by adjusting the ballast during routine maintenance.

It can be seen that, from both the design and maintenance viewpoints, an underlay is far superior to an overlay because the required hot-mix asphalt is much thinner and the existing railroad maintenance method can still be applied.

UNDERLAYS VERSUS CONVENTIONAL TRACKBEDS

Because of the better load-carrying characteristics of hot-mix asphalt, the combined thickness of ballast and hot-mix asphalt in an underlay should be smaller than that of ballast and subballast in a conventional trackbed. It was found that a conventional trackbed with 8-in. (203-mm) ballast and 6-in. (152-mm) subballast is initially equivalent to an underlay with 8-in. (203-mm) ballast and 4-in. (102-mm) hot-mix asphalt. This equivalency is based on the vertical compressive stress on the top of the subgrade as given in Table 3. It is assumed that the ballast, subballast, and subgrade in the conventional trackbed remain separated without pumping, a condition difficult to achieve in reality. The compressive stresses were determined by KENTRACK using the geometry and material parameters described previously. The allowable number of load repetitions was computed by Equation 4. Four different moduli of subgrade were used. In the conventional trackbeds, the subballast was considered nonlinear with $K_1 = 3{,}750$ psi, $K_2 = 0.5$, and a Poisson's ratio of 0.35. In the underlays, three different moduli were assumed for the hot-mix asphalt.

It can be seen from Table 3 that the conventional trackbed and the hot-mix asphalt underlay are equivalent because the compressive stress in the conventional trackbed lies between the extreme values shown for the underlay. The comparison is based on the assumption that both systems have the same modulus of subgrade. Because of the waterproofing effect of hot-mix asphalt, the modulus of subgrade in the underlay will be kept intact, while that in the conventional trackbed will be lowered as the moisture content increases. If the modulus of subgrade is reduced from 7,500 psi (5.17 MPa) to 3,000 psi (20.7 MPa), the compressive stress in the conventional trackbed will be reduced from 11.1 to 8.2 psi (77 to 57 kPa) but the allowable number of load repetitions will be reduced from 463,000 to 53,800. In this case the design life of an underlay with 8-in. (203-mm) ballast and 4-in. (102-mm) hot-mix asphalt is more than eight times greater than that of a conventional trackbed with 8-in. (203-mm) ballast and 6-in. (152-mm) subballast.

CONCLUSIONS

The design, construction, and performance of hot-mix asphalt railroad trackbeds are presented. The excellent performance of some 30 experimental sections constructed so far has offered

the railroad industry a timely and viable option for reducing trackbed maintenance costs and improving train operating efficiency. On the basis of the critical stresses and strains in highway pavements and railroad trackbeds and the application of highway failure criteria, the following general conclusions can be drawn:

1. Similar to highway pavements, the design of hot-mix asphalt trackbeds should consider both fatigue cracking and permanent deformation. The fatigue cracking can be based on the horizontal tensile strain at the bottom of hot-mix asphalt, but the permanent deformation should be based on the vertical compressive stress on the top of the subgrade.
2. In the design of railroad trackbeds, there are two separate design lives: one that requires the replacement or rehabilitation of hot-mix asphalt that has suffered fatigue cracking and another that requires the adjustment of track that has experienced permanent deformation. In the design of highway pavements, there is only one design life because both fatigue cracking and permanent deformation occur in the hot-mix asphalt and whichever has a lesser life controls the design.
3. Because of the differences in loading conditions, environmental effects, and performance requirements, the failure criteria for highway pavements may not be applicable to railroad trackbeds. Given the lack of railroad data, highway criteria can only be used as a guide and should be revised as more experience is gained. The analysis by KENTRACK shows that underlays can be designed economically to satisfy the highway failure criteria. It is believed that the use of highway failure criteria is quite conservative because the hot-mix asphalt and subgrade in a railroad trackbed are better confined and insulated and the railroad loadings are repeated at shorter intervals.
4. Increasing the thickness of hot-mix asphalt is not as effective in reducing the critical stress and strain in railroad trackbeds as in highway pavements. The requirement of a very thick hot-mix asphalt to reduce the horizontal tensile strain makes it uneconomical to use full depth or overlays for heavy-haul trackbeds.
5. A direct comparison of predicted design life for conventional trackbeds and asphalt trackbeds must consider the effect of lowering, over time, of the subgrade modulus of the conventional trackbed, which is caused by the increased moisture content of the subgrade. Also, as the subgrade mixes with the ballast, the ballast modulus is decreased substantially. These effects decrease the number of allowable load repetitions for conventional trackbeds. Because the asphalt layer separates the ballast from the subgrade and provides a drier subgrade, optimum subgrade and ballast qualities will be maintained.
6. From both design and maintenance viewpoints, underlays are far superior to overlays. Both failure criteria can be easily satisfied by increasing the thickness of ballast.
7. In designing underlays, the use of a thick layer of hot-mix asphalt is not warranted. For a given combined thickness of ballast and hot-mix asphalt, the thicker the hot-mix asphalt, the shorter the fatigue life and the greater the contact pressure between tie and ballast. Therefore the use of a thin layer of hot-mix asphalt, say 3 to 4 in. (76 to 102 mm), with a thick layer of ballast, say 8 in. (203 mm) or more, is recommended.
8. The main function of hot-mix asphalt underlays is to waterproof the subgrade and thus provide consistent load-carrying capability for the trackbed even on marginal subgrades. The asphalt mat will confine the ballast and eliminate pumping without substantially increasing the stiffness of the trackbed.

ACKNOWLEDGMENTS

The research reported herein is funded by the National Asphalt Pavement Association and the Asphalt Institute through the University of Kentucky Research Foundation.

REFERENCES

1. A Railroad "First" is an Asphalt "First." *Asphalt*, Oct. 1968, p. 13.
2. Smoother, Stronger Roadbeds for Railway Cars. *Asphalt*, Oct. 1970, pp. 10–11.
3. Y. H. Huang, C. Lin, X. Deng, and J. G. Rose. *KENTRACK, a Computer Program for Hot-Mix Asphalt and Conventional Ballast Railway Trackbeds*. Reports RR–84–1 and QIP–105. The Asphalt Institute, College Park, Md.; National Asphalt Pavement Association, Riverdale, Md., 1984, 164 pp.
4. M. A. Miner. Cumulative Damage in Fatigue. *Transactions of the ASME*, Vol. 67, 1945, pp. A159–A164.
5. J. F. Shook, F. N. Finn, M. W. Witczak, and C. L. Monismith. Thickness Design of Asphalt Pavements—The Asphalt Institute Method. *Proc., 5th International Conference on the Structural Design of Asphalt Pavements*, Delft University of Technology, The Netherlands, Vol. 1, 1982, pp. 17–44.
6. A. I. M. Claussen, J. M. Edwards, P. Sommer, and P. Ugé. Asphalt Pavement Design—The Shell Method. *Proc., 4th International Conference on the Structural Design of Asphalt Pavements*, University of Michigan, Ann Arbor, Vol. 1, 1977, pp. 39–74.
7. Y. H. Huang, C. Lin, and J. G. Rose. Asphalt Pavement Design: Highway Versus Railroad. *Journal of Transportation Engineering*, ASCE, Vol. 110, No. 2, 1974, pp. 276–282.
8. Y. H. Huang, J. G. Rose, and C. Lin. Structural Design of Hot-Mix Asphalt Underlayments for Railroad Trackbeds. *Proc., Association of Asphalt Paving Technologists*, Vol. 54, 1985.

Publication of this paper sponsored by Committee on Railroad Track Structure System Design.

Climatic-Materials-Structural Pavement Analysis Program

BARRY J. DEMPSEY, W. ANDREW HERLACHE, AND ARTI J. PATEL

The Climatic-Materials-Structural (CMS) program has been set up to introduce climatic effects into the analysis of multilayered flexible pavement systems. The program may be used with selected pavement structural and performance models to analyze a pavement system. It can also be employed as a tool to analyze existing pavement systems in order to obtain estimates of future maintenance requirements. The CMS program is compatible with several pavement structural models for determining radial stresses, strains, and displacements. These structural models include the ILLI–PAVE model, ILLI–PAVE algorithms, and elastic layer analysis. The accuracy of the CMS output depends mainly on the quality of the inputs. It is important that boundary conditions, climatic conditions, and material properties properly represent the system to be analyzed. With representative inputs the CMS program will give realistic values for temperature and moisture profiles and material strength properties. Although future research is required to validate the overall model, the validity of the individual parts of the CMS program has been shown. Analysis of existing pavement systems and comparison of CMS outputs with actual field conditions are recommended. It is expected that further validation studies will confirm the belief that the CMS program provides an economical and realistic means of analyzing multilayered flexible pavement systems by accounting for climatic effects on pavement materials.

The detrimental effects of temperature and moisture are major problems and continue to be a significant cause of pavement deterioration leading to high maintenance costs. In many cases the cost of annual repairs and maintenance is greater than the cost of preventive measures that might have been incorporated into the original pavement design and construction.

In the past completely acceptable techniques, procedures, and criteria were not available for adequately assessing the effects of temperature and moisture changes on pavement systems. Most laboratory durability-testing procedures use arbitrary exposure conditions that are not representative of actual conditions in the field.

Further refinement of analysis procedures must take into account the changing environment in which the pavement system is located. Climatic characteristics (maximum and minimum air temperature, sunshine, wind velocity, precipitation, etc.) are known to vary with geographic location in many states. For example, the average winter temperature for northern Illinois is approximately 25°F, whereas that for southern Illinois is approximately 35°F.

The objective of this study was to develop and implement a computer-based model that would account for the influence of climate on the behavior of flexible pavement systems.

B. J. Dempsey, Department of Civil Engineering, University of Illinois, Urbana, Ill. 61801. W. A. Herlache, Harding Lawson Associates, 20 Hawthorne St., San Francisco, Calif. 94105. A. J. Patel, Illinois Department of Transportation, 2300 S. Dirksen Parkway, Springfield, Ill. 62764.

The model will take climatic parameters and material properties as inputs and from these calculate temperature profiles, moisture profiles, and structural values of the pavement system as they vary with time. The outputs will be organized so that they may be easily input into structural or performance models to fully analyze the performance of a pavement in its proposed environment.

THE PROGRAM

General

The Climatic-Materials-Structural (CMS) pavement analysis program consists of several submodels that are combined to analyze the behavior of multilayered flexible pavement systems. As shown in Figure 1, the climatic model (heat-transfer and moisture models) incorporated into the CMS program takes climatic and material data as inputs and calculates temperature and moisture profiles as they vary with time in a pavement system. This information is used in the material model to calculate the asphalt concrete, base course, subbase, and subgrade stiffness characteristics. This output can then be combined with load data and input into selected structural analysis models to generate data for analyzing flexible pavement behavior.

Heat-Transfer Model

The heat-transfer model used in the CMS program was developed from a similar model previously described by Dempsey *(1)*. The heat-transfer model uses a finite-difference solution to the one-dimensional, Fourier heat-transfer equation for transient heat flow to compute pavement temperatures as a function of time. Energy balance procedures developed by Scott *(2–3)* and Berg *(5)* are used to relate pavement surface temperatures to climatic parameters.

Finite-Difference Pavement System

Figure 2 shows a typical finite-difference pavement system used in the heat-transfer model for computing pavement temperatures. The pavement system consists of a column of nodes that have a cross-sectional area of 1 ft^2.

Nodes 2 through 37 are termed normal nodes. The nodal depth (ΔX) and the number of nodes are chosen so as to ensure mathematical stability and so that the interface between pavement layers will be located at a nodal center. Nodes 2 and 6 are also mixed nodes because the thermal properties of these nodes correspond in part to the thermal properties of the adjacent pavement layers.

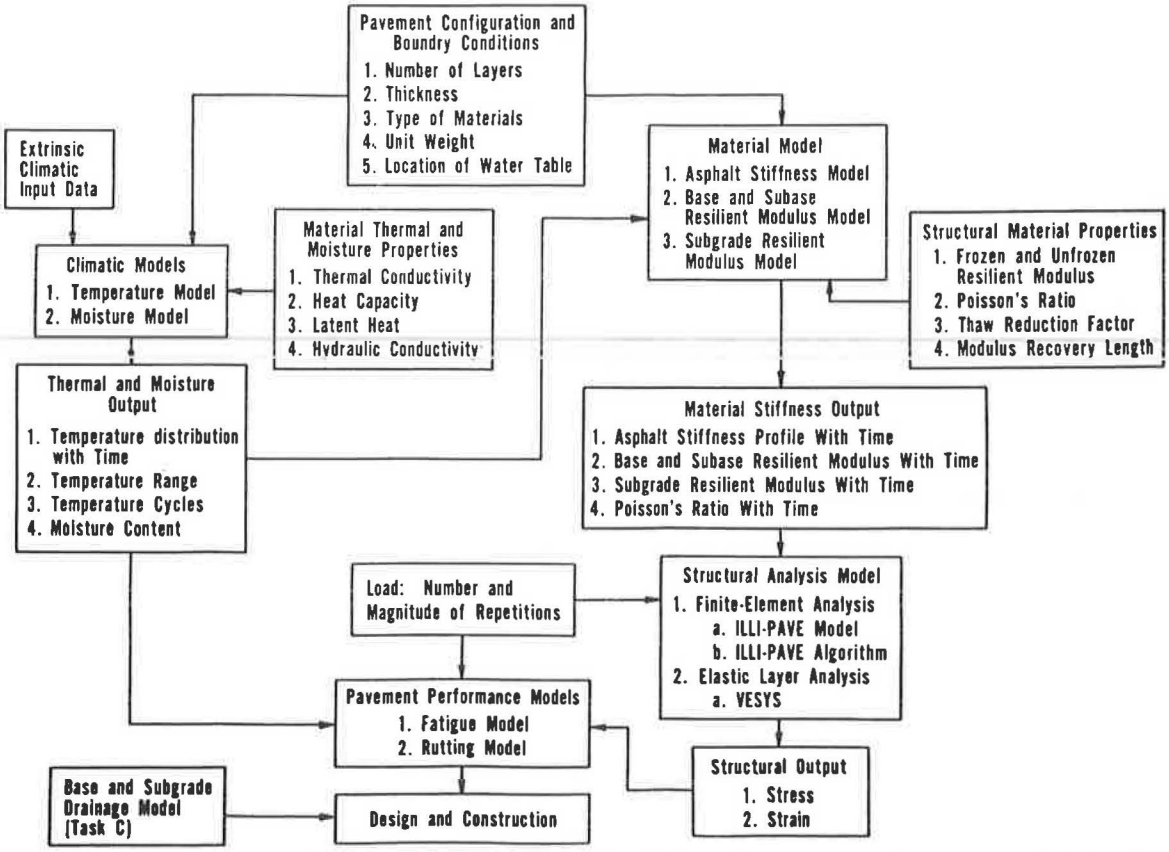

FIGURE 1 CMS program incorporated with structural analysis and pavement performance models to aid in design.

Node 1 consists of one-half of a normal node so that the nodal center will lie on the pavement surface. Node 1 at the pavement surface is the node at which the meteorological parameters are introduced and an energy balance is achieved.

Nodes 38, 39, and 40 are termination nodes and their purpose is to reduce computational time.

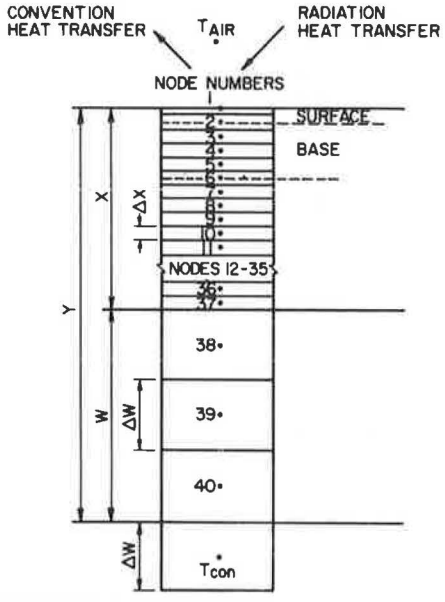

FIGURE 2 Finite-difference pavement system.

The total depth (Y) of the finite-difference pavement system is a variable input parameter in the heat-transfer model. It can be determined from a study of deep soil temperatures at a specified geographic location. For example, studies of soil temperatures in northern Illinois have indicated that the ground temperature remains essentially constant (51°F) at a depth of 144 in.

Finite-Difference Equations

Convection and radiation play a dominant role in transferring heat between the pavement surface and the air, whereas conduction plays a separate role in transferring heat within the pavement system. The general form of the one-dimensional, Fourier equation for conductive heat transfer in the heat-transfer model is expressed as follows (see Appendix for definition of terms):

$$(\partial^2 T/\partial X^2) = (1/\alpha)\ (\partial T/\partial \theta) \quad (1)$$

Dempsey *(1)* has shown that the first and second derivatives in Equation 1 can be replaced by the appropriate finite-difference terms and written as

$$[(T_{n-1} + T_{n+1} - 2T_n)/\Delta X^2] = (1/\alpha)\ [(T'_n - T_n)/\Delta \theta] \quad (2)$$

The thermal diffusivity (α) is equal to K/C_{γ_d}. By arranging

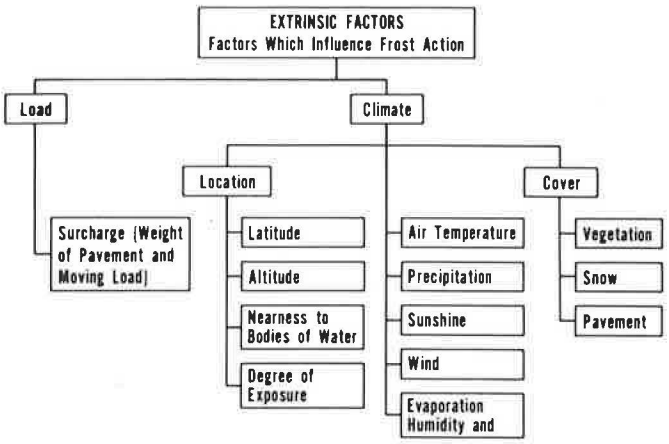

FIGURE 3 Extrinsic factors that influence temperature and frost action.

terms and substituting for α, Equation 2 can be written for the heat balance on an arbitrary interior node as

$$(K/\Delta X)\,(T_{n-1} - T_n) + (K/\Delta X)\,(T_{n+1} - T_n) = (\gamma_d C \Delta X/\Delta\theta)\,(T'_n - T_n) \quad (3)$$

The terms $(K/\Delta X)\,(T_{n-1} - T_n)$ and $(K/\Delta X)\,(T_{n+1} - T_n)$ are the equations for the thermal conductivity of a nodal volume and the term $(\gamma_d C \Delta X/\Delta\theta)\,(T'_n - T_n)$ is the heat storage in a nodal volume during an incremental time period $(\Delta\theta)$.

A more detailed description of the finite-difference equations used in the heat-transfer model can be found elsewhere *(1, 6)*.

Climatic Parameters

Numerous extrinsic climatic parameters shown in Figure 3 are considered in the heat-transfer model. The most important parameters are those related to the surface node. These are the climatic parameters concerned with the net radiation heat transfer (Q_{rad}) and the convective heat transfer (Q_c) into or out of the pavement system as shown in Figure 4.

The finite-difference equation for the surface node is ideally suited for use with the meteorological energy balance that can be expressed as follows:

$$Q_i - Q_r + Q_a - Q_e \pm Q_c \pm Q_h \pm Q_g = 0 \quad (4)$$

The importance of solar radiation in pavement temperature studies has been shown by Straub et al. *(7)* and Aldrich *(8)*. From Equation 4, the net amount of radiation (Q_{rad}) influencing heat transfer at the surface node is expressed as

$$Q_{rad} = Q_i - Q_r + Q_a - Q_e \quad (5)$$

The amount of incident short-wave radiation used in the energy balance at the surface node is determined by use of a regression equation developed by Baker and Haines *(9)* and expressed as

$$Q_i = R^* [A + B\,(S/100)] \quad (6)$$

The extraterrestrial radiation (R*) can be theoretically calculated for a given location from solar declination, latitude, zenith angle, and solar constant.

In Figure 5, it is observed that the intensity of solar radiation varies parabolically from the time of sunrise to the time of sunset. Based on this observation, the amount of short-wave radiation received at the pavement surface during a finite time increment $(\Delta\theta)$ is calculated by assuming that the extraterrestrial radiation varies in a parabolic manner from the time of sunrise to the time of sunset.

Part of the incident short-wave radiation (Q_i) is lost as reflected short-wave radiation (Q_r). The amount of short-wave radiation reflected is a function of the incident short-wave radiation (Q_i) and the absorptivity (a) of the pavement surface:

$$Q_r = (1 - a)Q_i \quad (7)$$

From Equations 6 and 7 the net amount of short-wave radiation that enters the energy balance at the pavement surface (Q_s) is derived as follows:

$$Q_s = Q_i - Q_r \quad (8)$$

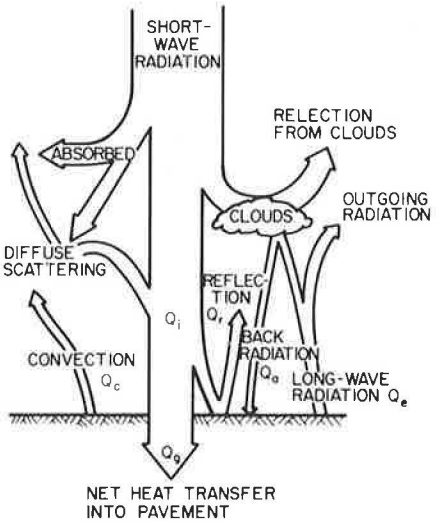

FIGURE 4 Heat transfer between pavement surface and air on a sunny day.

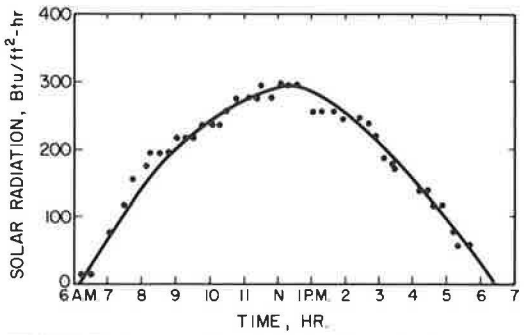

FIGURE 5 Variation in intensity of solar radiation.

By substituting for Q_r in Equation 8, the following equations are obtained:

$$Q_s = a\ Q_i \quad (9)$$

$$Q_s = a\ R^*\ [A + B\ (S/100)] \quad (10)$$

Essentially, Equation 10 considers the influence of cloud cover, reflection from clouds, diffuse scattering, absorption by the atmosphere, and reflection by the pavement surface of the extraterrestrial radiation. Discussion of the range of values for the terms in Equation 10 can be found elsewhere *(1)*.

Using the suggestion of Scott *(4)* that the net long-wave radiation entering the energy balance at the pavement surface be corrected for cloud cover in a manner similar to that used for short-wave radiation, an approach recommended by Geiger *(10)* was used:

$$Q_e = Q_x\ [1 - N\ (\overline{W}/100)] \quad (11)$$

$$Q_a = Q_z\ [1 - N\ (\overline{W}/100)] \quad (12)$$

In Equation 11, Q_x is the long-wave radiation emitted from a unit area of pavement surface with no correction for cloud cover, and, in Equation 12, Q_z is the long-wave back radiation from the atmosphere without a cloud cover correction.

In Equations 11 and 12, N is a cloud-base factor the value of which ranges between approximately 0.90 and 0.80 for cloud heights between approximately 1,000 and 6,000 ft, respectively *(10)*. The percentage of cloud cover ($\overline{W}$) is equal to 0 percent for cloudless days and 100 percent for completely overcast days.

The rate of heat transfer by convection (Q_c) between the pavement surface and the air is computed by the following method for a unit surface area:

$$Q_c = H\ (T_{air} - T_1) \quad (13)$$

The convection coefficient (H) is difficult to estimate because of the many variables involved. Previous studies by Dempsey *(1)* have shown that formulas for estimating the convection coefficient for large flat surfaces can be used for pavement systems.

In the development of the heat-transfer model, the effects of transpiration, condensation, evaporation, and sublimation were neglected because of the uncertainty in predicting their values at this time. Large error was not expected to be created in the energy balance at the pavement surface by assuming Q_h to be zero. Transpiration can be neglected in pavement studies because this is related to vegetation growth. The heat flux resulting from condensation is lost when the condensate evaporates. Heat transfer by evaporation should be minimal if rainwater quickly drains off the pavement surface. Because snow removal from most pavements takes place shortly after the snow has fallen, heat flux caused by sublimation can also be disregarded.

The climatic input for the radiation heat-transfer equations and convective heat-transfer equations can be obtained from weather station records.

Thermal Properties of Pavement Materials

Figure 6 shows the intrinsic factors that influence temperatures and frost problems in pavement systems. The heat-transfer model in the CMS program considers a majority of the factors

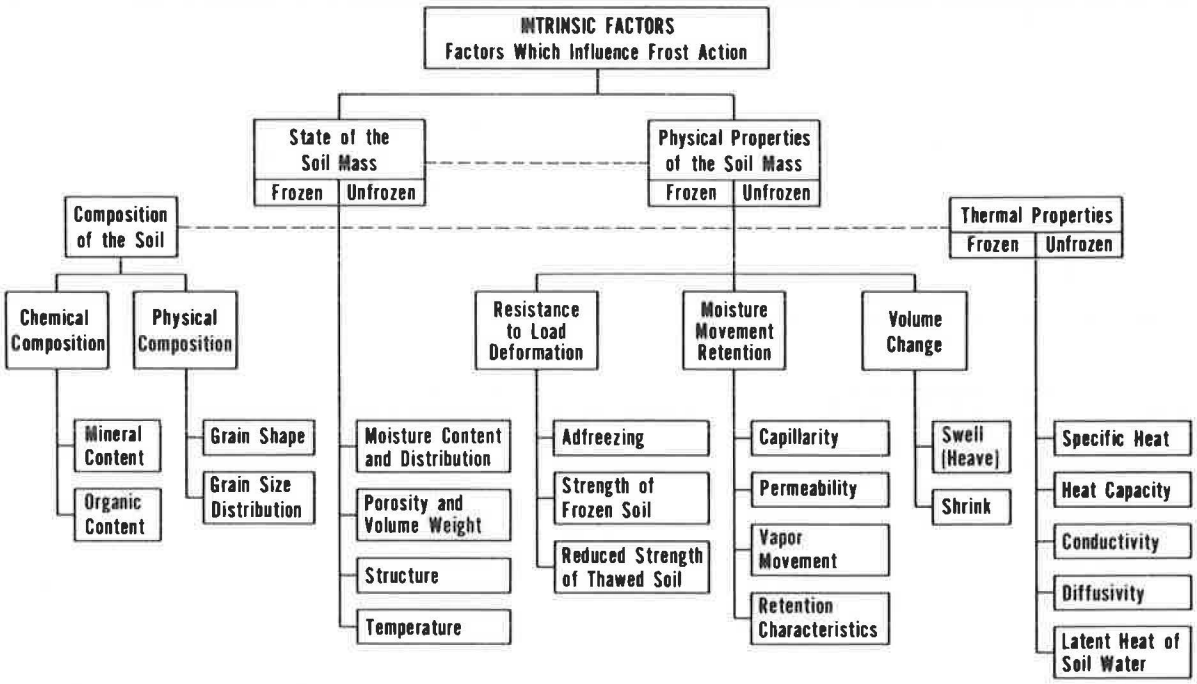

FIGURE 6 Intrinsic factors that influence temperature and frost action.

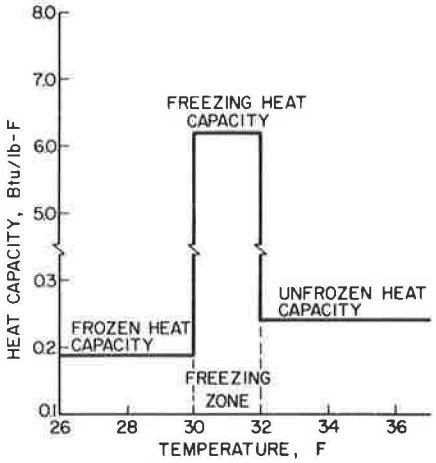

FIGURE 7 Effect of temperature on heat capacity of a granular base material.

The heat capacity of a pavement material during freezing is determined from the latent heat of fusion of the moisture in the material. When the moisture in the pavement freezes, the portion that is about to change phase remains at a constant temperature, the freezing temperature, until the latent heat of fusion is released. The time lag caused by this process retards the rate of frost penetration. The latent heat effect is incorporated into the finite-difference equations by using an approach described by Schenck *(12)*, which makes use of a freezing zone. The freezing zone is a small, hypothetical temperature range over which freezing takes place. Because only moisture effects are considered in this range, the freezing heat capacity in the freezing zone is a function of the moisture content, dry density, and the small freezing temperature range.

A comparison of the freezing heat capacity and unfrozen and frozen heat capacities for a granular base material with about 9 percent moisture is shown in Figure 7. It should be noted that even for a small moisture content the freezing heat capacity of the moisture is far greater than the unfrozen and frozen heat capacities of the material itself.

listed. The most important intrinsic factors considered in the heat-transfer model are the thermal properties of the pavement materials, which include thermal conductivity, heat capacity, and latent heat of fusion. The heat-transfer model recognizes three different sets of thermal properties depending on whether the pavement material is in an unfrozen, freezing, or frozen condition.

The procedures for determining the thermal properties of the pavement materials have been described in detail elsewhere *(1, 6)*. The thermal properties of surface materials are often determined from general tables of physical properties or from scientific research. The methods developed by Kersten *(11)* were found to be well suited for determining the thermal properties of the base, subbase, and subgrade soils.

Validation of the Heat-Transfer Model

The validity of the heat-transfer model was established by using temperature data from the AASHO Road Test at Ottawa, Illinois.

For the purpose of evaluating the heat-transfer model, a winter period at the AASHO Road Test from October 1, 1959, through March 31, 1960, was analyzed. Because pavement temperatures near the surface vary within a given day as well as from day to day, comparisons of theoretical temperatures and measured temperatures were made at 6:00 a.m. and 3:00 p.m.

Figure 8 shows a graphic comparison of measured temperature and theoretical temperature at the middepth of a 6-in.

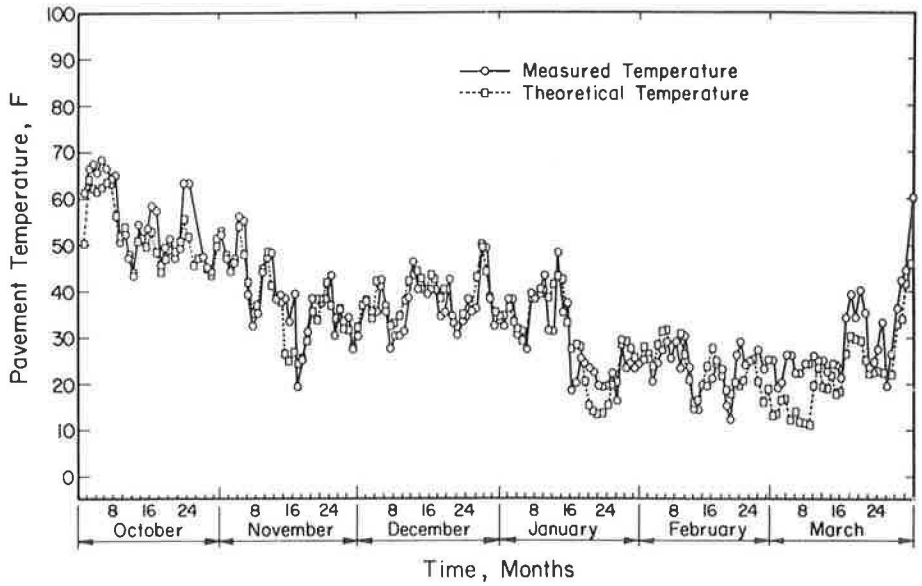

FIGURE 8 Comparison of measured and theoretical temperatures at the 3-in. depth of a 6-in. asphalt-concrete pavement at 0600 hr (AASHO Road Test 1959–1960).

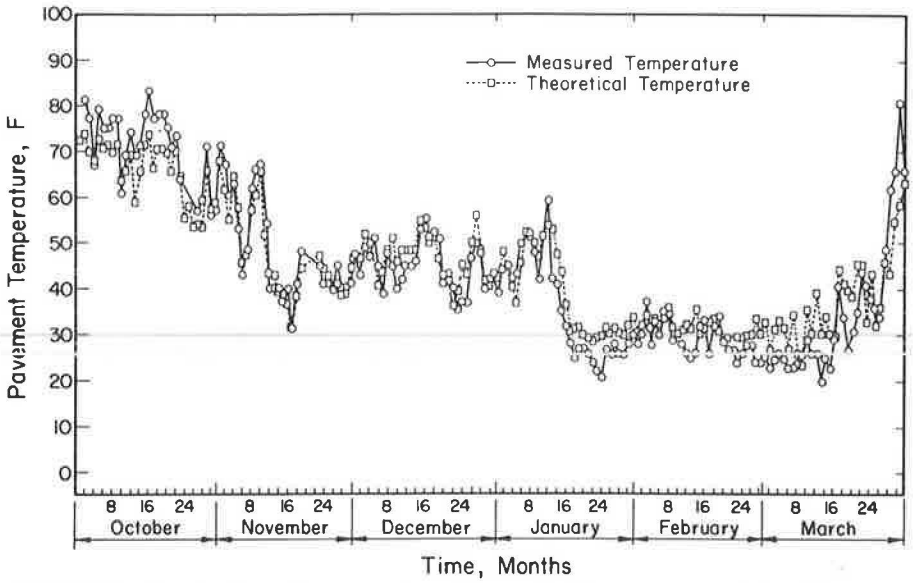

FIGURE 9 Comparison of measured and theoretical temperatures at the 3-in. depth of a 6-in. asphalt-concrete pavement at 1500 hr (AASHO Road Test 1959–1960).

asphalt-concrete pavement surface at 6:00 a.m. The average difference between the measured temperature and the theoretical temperature is 0.97°F.

A typical graphic comparison of measured temperature and theoretical temperature at 3:00 p.m. is shown in Figure 9. The average difference between the measured temperature and the theoretical temperature is 0.73°F at the 3-in. depth.

The validity of the heat-transfer model was further checked by comparing the number of freeze-thaw cycles predicted by the model with the number of freeze-thaw cycles in the actual pavement at the AASHO Road Test. Freezing in the pavement was considered to occur whenever the pavement temperature reached 30°F or less and remained at that temperature for more than 2 hr. Similarly, thawing was considered to occur whenever the pavement temperature exceeded 30°F and remained above that temperature for more than 2 hr.

At a depth of 3 in. in the pavement, 41 freeze-thaw cycles were determined from the theoretical temperatures compared with 38 freeze-thaw cycles determined by analyzing the measured hourly temperatures. At the 6-in. depth, 15 theoretical freeze-thaw cycles were observed compared with 17 freeze-thaw cycles determined from the measured temperatures for the test pavement at the AASHO Road Test.

The excellent comparisons between the theoretical temperatures and the measured temperatures and the good agreement between the number of freeze-thaw cycles at various depths indicated that the heat-transfer model was valid for predicting temperatures for use in frost action and temperature distribution studies of multilayered pavement systems.

Moisture Model

Moisture along with temperature is an important factor that influences the durability and strength parameters of highway soils and materials. Subgrades are generally constructed in the surface soil and they are usually subjected to large moisture content variations. Therefore the prediction of moisture movement and moisture equilibria are of prime importance in the CMS program.

The moisture model in the CMS program was based on procedures developed by the Road Research Laboratory *(13–15)* and a moisture model developed by Dempsey and Elzeftawy *(16)*. The moisture model is essentially an equilibrium model that is based on the following principles *(17)*:

1. The trend in pore water pressure, under certain conditions at a given level of the subgrade, is toward an equilibrium value that depends solely on the height above the groundwater level;
2. A relation exists between the pore water pressure in the soil at a given level and the suction of the soil; and
3. A relation exists between the suction and the water content of the soil.

The conditions for equilibrium to be reached depend on the following assumptions:

1. The temperature of the subgrade is constant, uniform, and above freezing;
2. The subgrade cannot receive moisture by infiltration through the highway pavement or by migration from adjacent soil masses with a higher pore water pressure, nor can it give up moisture by evaporation or migration to adjacent soil masses that have a lower pore water pressure.

In the moisture model the pressure of pore water at any given level must tend toward an equilibrium that cancels out the algebraic sum of the various water potentials. The British Road Research Laboratory has expressed the equilibrium condition as *(17)*:

$$u = -Z \tag{14}$$

In Equation 14, u is the relative pore water pressure, which is negative above the water table, and Z is the height above the groundwater table. Graphically, when the same scale is used for pressures (u) and heights (Z), the function u = f(Z) is a straight line with slope of 45 degrees regardless of the nature and dry density of the various soil layers that make up the mass in question. In principle, estimating the equilibrium pressure profile of a pavement subgrade is dependent on estimating the position of the groundwater level after the pavement is built.

A major input to the moisture model is the soil-water characteristics curve that relates water content of the soil to the water potential or pore pressure and, by Equation 14, to the height above the water table. Croney and Coleman *(18)* have discussed various methods for determining the moisture characteristics curve for soil.

Janssen and Dempsey *(19)* tested a significant number of Illinois soils and determined that an approximate soil-moisture characteristics curve could be estimated from basic soil data. Their studies indicated some similarities for a number of soil-moisture characteristics curves. From a value of zero at saturated water content, the curves first rise almost vertically and show very little moisture change with suction increase (Figure 10). The curves then show a substantial decrease in water content associated with an increase in soil suction of about 100 cm.

The midpoint of the soil-moisture characteristics curve for fine-grained soils can be approximated by determining the water content at 1000 cm of suction (W1000) and the break suction point (LSUC). The following regression equations developed by Janssen and Dempsey *(19)* for AASHTO soil groups A4 through A7 are used in the moisture model.

For A4 and A5 soils:

$$W1000 = 0.496LL + 0.297PL - 0.128SATWAT - 0.579 \quad (15)$$

$$LSUC = 0.568LL + 0.047PL - 0.009LL^2 - 0.082SATWAT - 5.811 \quad (16)$$

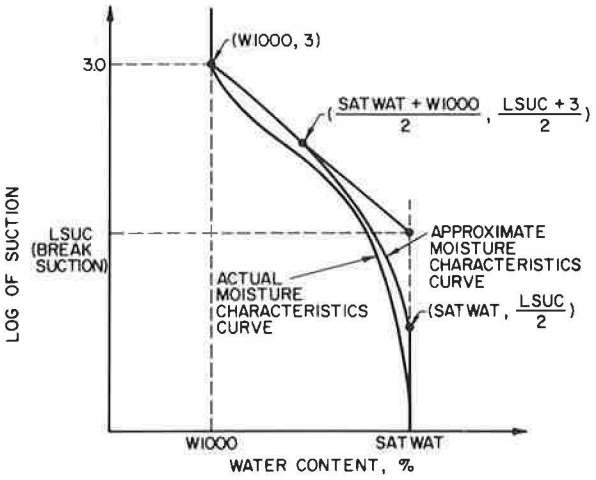

FIGURE 10 Approximation of the soil-moisture characteristics curve used in the CMS program for A4, A5, A6, and A7 soils.

For A6 soils:

$$W1000 = -0.027LL + 0.89PL + 0.0043SATWAT + 0.312 \quad (17)$$

$$LSUC = -0.273PI - 0.008PL - 0.347SATWAT + 12.873 \quad (18)$$

For A7 soils:

$$W1000 = -0.479PI - 0.215PL + 0.0077LL^2 + 0.291SATWAT + 14.46 \quad (19)$$

$$LSUC = -0.432LL - 0.022PI + 0.005LL^2 - 0.106SATWAT + 13.787 \quad (20)$$

From the midpoint of the break suction (SATWAT, LSUC/2) to a point midway between (W1000, Log of suction = 3) [note that Log of suction = 3 is equivalent to a suction of 1000 cm] and (SATWAT, LSUC), the soil-moisture characteristics curve can be modeled as a parabola (Figure 10), and the top portion of the curve can be approximated with a sloping straight line through (W1000, Log of suction = 3).

The midpoint of the soil-moisture characteristics curve for granular soils can be approximated with a series of sloping straight lines. In the program the granular material has been modeled as seen in Figure 11.

For A2 soils no data were available; therefore the water content for an A2 soil is held constant at a value input by the user.

The moisture model used by the CMS program provides a rational approach to moisture prediction in a pavement system. All that is required to predict moisture contents are standard soil properties that can be obtained from simple soil mechanics tests and knowledge of the water table position. This model serves well at the present time, but future research in developing a moisture movement model based on temperature gradients would be useful if simplicity is still maintained.

Material Model

The strength or stiffness of a pavement system is strongly dependent on the climatic conditions to which it is exposed. It has been observed that the stiffness of an asphalt layer varies with temperature, and the resilient modulus of a nonasphalt layer is dependent on its water content and condition (whether frozen, unfrozen, or thaw-recovering). The CMS program accounts for these changes and predicts the asphalt stiffness and the base, subbase, and subgrade resilient moduli on the basis of climatic conditions.

Asphalt Stiffness

The stiffness of the asphalt mixture is determined by using a model developed originally by the Shell Oil Company. The model calculates the asphalt mixture stiffness from the temperature of the asphalt and the percentage by volume of aggregate in the mix. The user must input points that define the

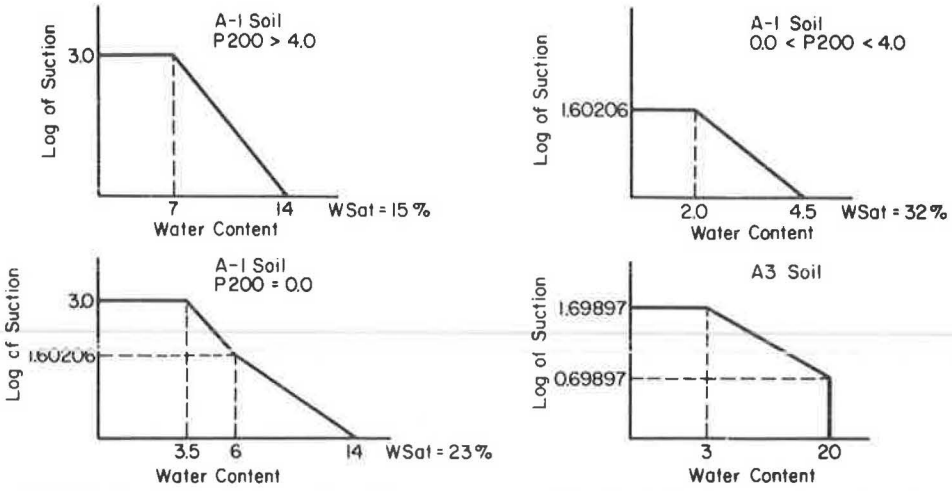

FIGURE 11 Approximate soil-moisture curves used in the CMS program for A1 and A3 soils.

temperature-stiffness relationship for the bitumen. Then, using the temperature values predicted by the heat-transfer model, the program calculates the asphalt mixture stiffness via the following equation developed by Yoder and Witczak *(20)*:

$$S_m = S_b\,[1 + (2.5/n)\,(C_v/1 - C_v)] \tag{21}$$

where

$$n = 0.83\text{Log}[(4 \times 10^5)/S_b] \text{ and} \tag{22}$$

$$C_v = VOL_{aggregate}/(VOL_{aggregate} + VOL_{asphalt}) \tag{23}$$

The term C_v is modified if the mix has an air void ratio greater than 3 percent as recommended by Van Draat and Sommer *(21)*:

$$C'_v = [C_v/(1 - H_{air})] \tag{24}$$

Here H_{air} is the actual air void content of the mix minus 3 percent.

By this procedure the asphalt stiffness is calculated for each node and then an average is determined for the entire layer as a function of time and temperature.

Base Course and Subbase Resilient Modulus Model

The resilient moduli of coarse-grained soils do not vary throughout the year to the extent that those of fine-grained soils do. For prediction of the resilient modulus, the CMS program categorizes coarse-grained soils into one of two states, frozen or unfrozen. Therefore for base and subbase materials, including stabilized materials, the user must input values for the frozen and unfrozen resilient moduli. The CMS program will then select the appropriate value depending on whether a frozen or unfrozen material condition exists.

Subgrade Resilient Modulus

The resilient modulus of the subgrade varies greatly during the year in most temperate regions. As the subgrade freezes there is a marked increase in the resilient modulus, which indicates a stiffening of the subgrade. Then as the subgrade thaws the resilient modulus drops substantially below its initial unfrozen value. This weakening of the subgrade on thawing is most apparent in fine-grained soils. Therefore the CMS program considers fine-grained soils to be in one of three conditions: frozen, unfrozen, or thaw-recovering. The resilient modulus for the frozen or unfrozen subgrade may be input by the user or calculated within the program. For coarse-grained subgrade (AASHTO classification A1 through A3 soils), the user must input the values for the frozen and unfrozen resilient moduli just as he must for the base and subbase materials.

If the user does not input a value for the unfrozen fine-grained resilient modulus, the program will calculate a value for each node based on its water content. Thompson and Robnett *(22)* derived many regression equations based on data from many Illinois subgrade soils. These equations relate the volumetric water content to the resilient modulus at a repeated deviator stress of 6 psi. The two relationships that are used in the CMS program are

For $\gamma_d \leq 100$ pcf:

$$E_{Ri} = 27.06 - 0.526\theta \tag{25}$$

For $\gamma_d > 100$ pcf:

$$E_{Ri} = 18.18 - 0.404\theta \tag{26}$$

In these equations the volumetric water content (θ) is input in percentage form, and the resilient modulus at a repeated deviator stress of 6 psi (E_{Ri}) is calculated in ksi. Also, the program does not allow the resilient modulus to drop below 1.0 ksi in the case of exceptionally high water contents.

Thompson and Robnett *(22)* found that the value of the resilient modulus at a deviator stress of 6 psi is the critical point in defining the resilient modulus versus the repeated deviator stress relationship (Figure 12). When this point has been determined, the rest of the curve may be approximated using E_{Ri} versus σ_d curve slopes of K_1 equal to –1.1 ksi/psi and K_2 equal to –0.178 ksi/psi as suggested by Thompson and Robnett *(22)*.

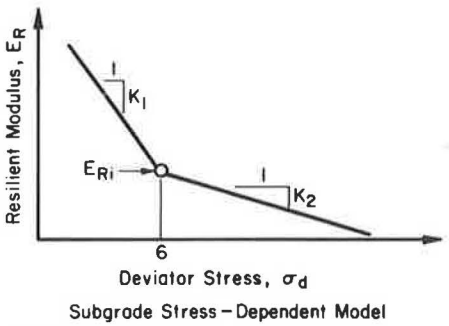

FIGURE 12 Resilient modulus versus deviator stress.

As the subgrade freezes, the resilient modulus increases to a value approximately two orders of magnitude greater than the unfrozen value. Because the resilient modulus is so high, the pavement deflections will be relatively small. Therefore great accuracy is not required in the estimation of the frozen resilient modulus (small deflections are less critical than larger deflections). If the user does not input a value for the frozen modulus, it will be assigned a value of 100 times the unfrozen value [for more information on the frozen resilient modulus refer to Vinson *(23)* and Vinson et al. *(24)*].

The final condition in which the subgrade may occur is termed thaw-recovery. At the onset of spring thawing the pavement deflections have been observed to be larger than before freezing. Johnson et al. *(25)* have found that for silt subgrades in test pavements in Hanover, New Hampshire, the resilient modulus during thawing can be as little as 1 or 2 percent of the unfrozen value (silty subgrades are most susceptible to this kind of behavior when thawing). This weakening may be attributed to a secondary structure and areas of high moisture content development during ice lens formation. As the pavement is loaded the strength increases, presumably as a result of moisture redistribution and the deterioration of the secondary structure. With repeated loading the resilient modulus nears its unfrozen or prefreezing value *(26)*. When many such cycles are being considered, it is acceptable to assume that the soil regains its full strength.

The CMS program has modeled this behavior with a linear interpolation between the high and low values of the resilient modulus. The equation is

$$E_{Ri}(t) = \{[E_{Ri}(100 - \text{REDUCT})/100]/\text{RECPER}\}\, t + E_{Ri}\text{REDUCT} \quad (27)$$

In this relationship, $E_{Ri}(t)$ is the resilient modulus at time t within the recovery period (RECPER). E_{Ri} is the value of the unfrozen resilient modulus discussed previously.

The reduction in the resilient modulus (REDUCT) is taken as a percentage of the unfrozen value. The user may input a value for the reduction factor, or a default value of 10 percent will be used.

It appears that the time required to reach 80 percent recovery varies from roughly 35 to 65 days *(27)*. This length of time is a function of the soil type and the traffic rate or number of loadings. The length of the recovery period (RECPER) may be input by the user, or a default value of 60 days will be used. The value of the resilient modulus will be calculated in this way until the end of the recovery period is reached or until the subgrade refreezes.

At the present time the moisture content of the subgrade is determined as a function of the standard soil properties and the distance to the water table. Because the unfrozen resilient modulus is based on the moisture content, it will remain constant during a period of constant water table depth. In the event that a more complex moisture movement and equilibria model, which allows for dynamic moisture content changes during a time period, is desired, the CMS program can easily be adapted to account for the changes in material properties associated with changes in moisture content.

The preceding approach to modeling the stiffness properties of a pavement system takes into account the climatic effects that result in seasonal variations at a given location. The values obtained simulate the actual conditions more realistically than does an approach that ignores the climatic effects. Therefore it is believed that this model will aid in obtaining more reliable predictions of pavement performance.

Structural Analysis Models

The problem of evaluating pavement performance is complex. The pavement structure is composed of various materials the properties of which vary diurnally, seasonally, and with repetitions of loading. All of these factors must be fully understood and accounted for when predicting pavement performance. Many mechanistic models have been developed to explain, interpret, and predict pavement load-response patterns. For any flexible pavement system, the load-response pattern is dependent on service conditions such as *(a)* stiffness of the asphalt concrete (a function of temperature) and *(b)* moisture content and physical state (frozen, unfrozen, or thaw-recovering) of the underlying layers.

Current methods of analysis consider environment by defining the most critical situation with respect to a particular distress criterion. By evaluating the properties of the materials for the critical situation, data are obtained that provide for analysis only under the most extreme conditions. This approach results in unrealistic analysis, especially if the critical situation has not been properly defined *(28)*. It is evident that there is a need to include the effect of climate on the whole structural section of a pavement throughout its entire spectrum of seasonal variation to permit accurate calculation of stress and deflection trends. The CMS program can use many of the

existing pavement structural analysis models to determine radial stresses, strains, and displacements in multilayer flexible pavements as a function of load, climatic exposure conditions, and material properties.

Elastic Layer Analysis

Application of elastic-layered system theory is the most common method used for calculating stresses and strains in multilayered flexible pavement systems *(29)*. Basic assumptions of this approach include *(a)* each layer is composed of materials that are isotropic, homogeneous, and weightless; *(b)* the system acts as a composite system such that there is continuity of stresses or displacements, or both, across the interface; and *(c)* the constituent materials are linearly elastic and can be characterized by a resilient modulus and Poisson's ratio. The use of layered elastic theory for a valid determination of stresses and deflections in a pavement system requires that resilient modulus and Poisson's ratio be properly defined.

The temperature-dependent stiffness values of the asphalt-concrete surface and appropriate resilient modulus and Poisson's ratio values for each of the underlying layers can be established from the CMS program for a specific hour, day, and year. The combined model permits prediction of stresses and deflections in a pavement system as they are influenced by the time-temperature regime.

ILLI–PAVE Model

The finite-element method has been extensively used in analysis of pavement systems in the last 15 years *(30)*. The ILLI–PAVE model is an axisymmetrical solid of revolution based on the finite-element method. The model incorporates nonlinear stress-dependent material models and failure criteria for granular and fine-grained soils. The principal stresses in the granular and subgrade layers are modified at the end of each iteration so they do not exceed the strength of the materials as defined by the Mohr-Coulomb theory of failure *(31)*.

Numerous research efforts have shown evidence of nonlinearity in flexible pavements *(32, 33)*. Therefore this pavement model offers a realistic approach to analyzing nonlinear stress-dependent materials in the pavement-subgrade system. It is possible to generate deflection basins as influenced by the time-temperature and moisture regime for each specific hour, day, and year using ILLI–PAVE and the modular values calculated in the CMS program. The main disadvantage of the finite-element approach, however, is that it will require long and expensive computer runs.

ILLI-PAVE Algorithms

Previous studies *(30, 34)* have demonstrated the validity of the algorithm approach derived from the ILLI–PAVE model. Using

TABLE 1 ILLI–PAVE DEFLECTION BASIN ALGORITHMS

For Conventional Pavements: Dependent Variable $= E_{Ri} \times p + E_{ac} \times q + T_{ac} \times r + T_{gr} \times s + o$

GROUP	Dependent Variable	o	p	q	r	s
T_{ac} = 1.5 to 3"	LogΔ	2.096	-0.0232	-0.000149	-0.0967	-0.0137
T_{gr} = 4 to 12"	Area	11.18	-0.315	0.00237	1.742	0.187
T_{ac} = 3 to 8"	LogΔ	1.878	-0.0203	-0.000194	-0.0372	-0.00694
T_{gr} = 4 to 24"	Area	13.25	-0.353	0.00383	1.040	0.0958
T_{ac} = 3 to 8"	LogΔ	1.900	-0.0197	-0.0002	-0.0451	-0.00707
T_{gr} = 6 to 18"	Area	13.21	-0.359	-0.00409	0.946	0.127

For Stabilized Pavements: Dependent Variable $= E_{Ri} \times p + E_{ac} \times t + E_{stab} \times q + T_{ac} \times r + T_{stab} \times s + o$

Dependent Variable	o	p	q	r	s	t
LogΔ	1.690	-0.0238	-0.000125	-0.0207	-0.0367	-0.000276
Area	20.046	-0.398	0.00192	0.0266	0.454	0.00519

Variables:

E_{ac} (ksi)	Modulus of Elasticity of AC Layer
E_{stab} (ksi)	Modulus of Elasticity of Stabilized Layer
E_{Ri} (ksi)	Subgrade Modulus
T_{ac} (in.)	Thickness of AC Layer
T_{gr} (in.)	Thickness of the Granular Layer
T_{stab} (in.)	Thickness of the Stabilized Layer
Δ (mils)	Equivalent 9k Moving Wheel Load Deflection
Area ($in.^2$)	Equivalent 9k Moving Wheel Load Deflection Basin Area

multiple regression techniques, Hoffman and Thompson *(30)* developed deflection basin predictive equations as a function of *(a)* the resilient modulus of the asphalt concrete (E_{ac}), *(b)* the resilient modulus of the subgrade soil (E_{Ri}), *(c)* the thickness of the asphalt layer (T_{ac}), and *(d)* the thickness of the granular base (T_{gr}) *(30)*. Table 1 gives the predictive equations developed for conventional and stabilized pavements.

There is general agreement among pavement engineers and researchers that surface deflection can be used to interpret asphalt-concrete fatigue behavior. Thompson *(35)* has shown significant correlations between ILLI–PAVE–calculated surface deflection and asphalt-concrete radial strain for conventional flexible pavements and full-depth asphalt pavements. Through statistical analyses of ILLI–PAVE data the following equations were developed:

Conventional flexible pavements:

$$\text{Log}\varepsilon_{ac} = -1.1296 + 1.1297\text{Log}\Delta \quad (\varepsilon_{ac} \times 10^{-4},\ \Delta = \text{mils}) \quad (28)$$

Full-depth flexible pavements:

$$\text{Log}\varepsilon_{ac} = 1.53\text{Log}\Delta + 0.319 \quad (\varepsilon_{ac} \times 10^{-6},\ \Delta = \text{mils}) \quad (29)$$

Based on a linear relationship of a limiting tensile strain criterion for fatigue cracking, the number of equivalent 18-kip single axle loads can be determined using the following equation *(35)*:

$$N_{18} = (6.6 \times 10^{-6})\ (1/\varepsilon_{ac})^{3.16} \quad (30)$$

Through the use of ILLI–PAVE analysis Thompson *(35)* has also developed fatigue life prediction procedures for flexible pavement systems with intact high-strength stabilized base courses.

APPLICATION OF CMS PROGRAM

Figure 13 shows a partial output from the CMS program using the ILLI–PAVE algorithm analysis for 27 days of climatic data. The flexible pavement system consisted of 8 in. of asphalt concrete over 6 in. of A2 subbase and an A6 subgrade. The strengths of the asphalt-concrete and subgrade layers were obtained through use of the heat-transfer, moisture, and material models in the CMS program. The pavement deflection and deflection basin areas were determined from the algorithms in Table 1.

Based on 27 days of climatic input data, an average deflection of 18.635 mils was determined for the analysis period. From Equation 28 a radial strain of 0.20×10^3 (0.2021E–03) in./in. was determined at the bottom of the asphalt-concrete layer. From Equation 30 the number of equivalent 18-kip single axle loads to failure at the predicted deflection is about 3.1 million. If the number of equivalent 18-kip single axle loads that actually occurred on the pavement during the study period is known, the percentage of fatigue consumption can be predicted from Minor's formula.

CONCLUSION

The CMS program was developed to introduce climatic effects into the analyses of multilayered flexible pavement systems. Figure 1 shows how this program may be used with selected pavement structural and performance models to analyze a pavement system. It can also be employed as a tool to analyze existing pavement systems in order to obtain estimates of future maintenance requirements.

The accuracy of the CMS output depends mainly on the quality of the inputs. It is important that boundary conditions, climatic conditions, and material properties properly represent the system to be analyzed. With representative inputs it is believed that the CMS program will give realistic values for the temperature profile and the material stiffness properties. The validity of the individual parts that comprise the CMS model has been shown, but the validity of the model in total has not been demonstrated. For this, analysis of existing pavement systems and comparison of the CMS outputs with actual field conditions are required. It is expected that these validation studies will confirm the belief that the CMS model provides an economical and realistic means of analyzing multilayered flex-

PAVEMENT SYSTEM

LAYER	TYPE	THICK.
1	IMPERM	4.00
2	IMPERM	4.00
3	A-2	6.00
4	A-6	130.00

DATE	AVG AC TEMP (C)	AVG AC E (KSI)	AVG SUBGRADE E (KSI)	DEFLECTION (MILS)	AREA (IN)
1	18.16	.1250E+04	.5636E+01	13.671	24.628
2	18.82	.1224E+04	.5636E+01	13.835	24.522
3	20.94	.1151E+04	.5636E+01	14.309	24.222
4	21.86	.1119E+04	.5636E+01	14.519	24.093
5	25.82	.9962E+03	.5636E+01	15.364	23.591
6	26.87	.9655E+03	.5636E+01	15.583	23.465
7	32.74	.8128E+03	.5636E+01	16.718	22.841
8	34.98	.7596E+03	.5636E+01	17.133	22.623
9	42.91	.6051E+03	.5632E+01	18.400	21.993
10	45.12	.5699E+03	.5632E+01	18.700	21.849
11	48.87	.5168E+03	.5623E+01	19.172	21.635
12	50.04	.4988E+03	.5623E+01	19.331	21.561
13	51.34	.4843E+03	.5595E+01	19.485	21.512
14	52.37	.4692E+03	.5595E+01	19.620	21.450
15	52.87	.4651E+03	.5518E+01	19.727	21.461
16	53.90	.4495E+03	.5518E+01	19.869	21.397
17	57.31	.4073E+03	.5441E+01	20.330	21.253
18	57.65	.4030E+03	.5441E+01	20.370	21.235
19	58.74	.3922E+03	.5364E+01	20.544	21.219
20	58.89	.3901E+03	.5364E+01	20.564	21.210
21	59.42	.3854E+03	.5286E+01	20.680	21.218
22	59.54	.3836E+03	.5286E+01	20.698	21.211
23	59.98	.3800E+03	.5209E+01	20.805	21.224
24	60.05	.3786E+03	.5209E+01	20.818	21.218
25	60.46	.3754E+03	.5132E+01	20.922	21.233
26	60.54	.3740E+03	.5132E+01	20.936	21.227
27	60.85	.3717E+03	.5055E+01	21.031	21.246

AVERAGE DEFLECTION OVER ANALYSIS PERIOD (MILS) 18.635

ASPHALT CONCRETE RADIAL STRAIN (IN/IN) .2021E-03

ALLOWABLE NUMBER OF 18K EQAL 3120475

FIGURE 13 Partial output from the combined CMS program and ILLI–PAVE algorithm analysis.

ible pavement systems by accounting for climatic effects on pavement materials.

ACKNOWLEDGMENT

This paper was prepared at the Department of Civil Engineering, University of Illinois at Urbana-Champaign, from research sponsored by the U.S. Department of Transportation, Federal Highway Administration.

REFERENCES

1. B. J. Dempsey. *A Heat-Transfer Model for Evaluating Frost Action and Temperature Related Effects in Multilayered Pavement Systems*. Ph.D. dissertation. Department of Civil Engineering, University of Illinois, Urbana, 1969.
2. R. F. Scott. Estimation of the Heat-Transfer Coefficient Between Air and the Ground Surface. *Transactions, American Geophysical Union*, Vol. 38, No. 1, 1957.
3. R. F. Scott. *Heat Exchange at the Ground Surface*. U.S. Army Material Command, Cold Regions Research and Engineering Laboratory, Hanover, N.H., 1964.
4. R. F. Scott. *Heat-Transfer at the Air-Ground Interface with Special Reference to Freezing and Thawing Problems Below Airfield Pavements*. Ph.D. dissertation. Massachusetts Institute of Technology, Cambridge, 1955.
5. R. L. Berg. *Energy Balance on a Paved Surface*. U.S. Army Terrestrial Sciences Center, Hanover, N.H., 1968.
6. B. J. Dempsey, W. A. Herlache, and A. J. Patel. *Environmental Effects on Pavements—Theory Manual*. FHWA/RD–84–115. FHWA, U.S. Department of Transportation, Vol. 3, 1985.
7. A. L. Straub, H. N. Schenck, Jr., and F. E. Przybycien. Bituminous Pavement Temperature Related to Climate. In *Highway Research Record 256*, HRB, National Research Council, Washington, D.C., 1968, pp. 53–77.
8. H. P. Aldrich, Jr. Frost Penetration Below Highway and Airfield Pavements. *Bulletin 135*, HRB, National Research Council, Washington, D.C., 1956, pp. 124–149.
9. D. G. Baker and D. A. Haines. *Solar Radiation and Sunshine Duration Relationships in the North-Central Region and Alaska*. Technical Bulletin 262. Agricultural Experiment Station, University of Minnesota, Minneapolis, 1969.
10. R. Geiger. *The Climate Near the Ground*. Harvard University Press, Cambridge, Mass., 1959.
11. M. S. Kersten. *Thermal Properties of Soils*. Bulletin 28. Engineering Experiment Station, University of Minnesota, Minneapolis, 1949.
12. H. Schenck, Jr. *Fortran Methods in Heat Flow*. The Ronald Press Company, New York, 1963.
13. W. P. M. Black, D. Croney, and J. C. Jacobs. *Field Studies of the Movement of Soil Moisture*. Technical Paper 41. Road Research Laboratory, Her Majesty's Stationery Office, London, England, 1958.
14. K. Russam. *The Distribution of Moisture in Soils at Overseas Airfields*. Technical Paper 58. Road Research Laboratory, Her Majesty's Stationery Office, London, England, 1962.
15. J. D. Coleman and K. Russam. The Effect of Climatic Factors on Subgrade Moisture Conditions. *Geotechnique*, Vol. 11, 1964, pp. 22–28.
16. B. J. Dempsey and A. A. Elzeftawy. Mathematical Model for Predicting Moisture Movement in Pavement Systems. In *Transportation Research Record 612*, TRB, National Research Council, Washington, D.C., 1977, pp. 48–55.
17. *Water in Roads: Prediction of Moisture Content of Road Subgrades*. Organization for Economic Cooperation and Development, Paris, France, 1973.
18. D. Croney and J. D. Coleman. Pore Pressure and Suction in Soil. *Proc., Conference on Pore Pressure and Suction in Soils*, British National Society of the International Society of Soil Mechanics and Foundation Engineering, London, 1961.
19. D. J. Janssen and B. J. Dempsey. *Final Report on Soil Water Properties of Subgrade Soils*. Transportation Engineering Series 27; Illinois Cooperative Highway and Transportation Series 184. Department of Civil Engineering, University of Illinois at Urbana-Champaign, April 1980.
20. E. J. Yoder and M. W. Witczak. *Principles of Pavement Design*, 2nd ed. Wiley-Interscience Publications, New York, 1975, 270 pp.
21. W. E. F. Van Draat and P. Sommer. Ein Geratzur Restimmung der Dynamischen Elastizitats Modulu von Asphalt. *Strasse und Autobahn*, Vol. 35, 1965.
22. M. R. Thompson and Q. L. Robnett. *Final Report: Resilient Properties of Subgrade Soils*. Civil Engineering Studies, Transportation Engineering Series 14; Illinois Cooperative Highway and Transportation Series 160. Department of Civil Engineering, University of Illinois at Urbana-Champaign, June 1976.
23. T. S. Vinson. Parameter Effects on Dynamic Properties of Frozen Soils. *Journal of the Geotechnical Engineering Division*, ASCE, Vol. 104, GT10, Oct. 1978.
24. T. S. Vinson, T. Chaichanavong, and R. L. Czajkowski. Behavior of Frozen Clay Under Cyclic Axial Loadings. *Journal of the Geotechnical Engineering Division*, ASCE, Vol. 107, GT7, July 1978.
25. T. C. Johnson, D. M. Cole, and E. J. Chamberlain. *Influence of Freezing and Thawing on the Resilient Properties of a Silt Soil Beneath an Asphalt Concrete Pavement*. CRREL Report 78–23. Cold Regions Research and Engineering Laboratory, U.S. Army, Hanover, N.H., Sept. 1978.
26. A. T. Bergan and C. L. Monismith. Characterization of Subgrade Soils in Cold Regions for Pavement Design Purposes. In *Highway Research Record 431*, HRB, National Research Council, Washington, D.C., 1973, pp. 25–37.
27. E. J. Chamberlain. *A Statistical Evaluation of Soil and Climatic Parameters Affecting the Changes in Pavement Deflection During Thawing of Subgrades*. CRREL Report 81–15. Cold Regions Research and Engineering Laboratory, U.S. Army, Hanover, N.H., 1981.
28. C. R. Marek and B. J. Dempsey. A Model Utilizing Climatic Factors for Determining Stresses and Deflections in Flexible Pavement Systems. *Proc., 3rd International Conference on the Structural Design of Asphalt Pavements*, London, England, Sept. 1972.
29. E. J. Barenberg. Summary of Methods for Incorporating Fatigue Test Results in Pavement Design. Presented at ASTM Symposium on Fatigue of Compacted Bituminous Aggregate Mixtures, June 1971.
30. M. S. Hoffman and M. R. Thompson. *Mechanistic Interpretation of Nondestructive Pavement Testing Deflections*. Transportation Engineering Series 32; Illinois Cooperative Highway and Transportation Research Program Series 190. University of Illinois at Urbana-Champaign, June 1981.
31. L. Raad and J. L. Figueroa. Load Response of Transportation Support Systems. Paper 15146. *Transportation Engineering Journal*, ASCE, Vol. 106, No. TE1, Jan. 1980.
32. R. D. Barksdale and R. G. Hicks. Material Characterization and Layered Theory for Use in Fatigue Analyses. In *Special Report 140: Structural Design of Asphalt-Concrete Pavements to Prevent Fatigue Cracking*, HRB, National Research Council, Washington, D.C., 1973, pp. 20–48.
33. G. L. Dehlen. *The Effect of Non-Linear Material Response of Granular Materials*. Ph.D. dissertation. University of California, Berkeley, 1969.
34. J. L. Figueroa and M. R. Thompson. Simplified Structural Analysis of Flexible Pavements for Secondary Roads Based on ILLI–PAVE. In *Transportation Research Record 766*, TRB, National Research Council, Washington, D.C., 1980, pp. 5–10.

35. M. R. Thompson. *Concepts for Developing a Nondestructive Testing Based Asphalt Concrete Overlay Thickness Design Procedure.* Transportation Engineering Series 34; Illinois Cooperative Highway and Transportation Series 194. University of Illinois at Urbana-Champaign, June 1982.

Publication of this paper sponsored by Committee on Environmental Factors Except Frost.

APPENDIX

A = radiation equation constant;
a = absorptivity of radiation by a surface;
B = radiation equation constant;
C_v = volume percentage of aggregate in the asphalt mixture, decimal form;
C'_v = the modified aggregate content, decimal form;
E_{ac} = the resilient modulus of the asphalt concrete layer, ksi or psi;
E_{Ri} = the resilient modulus of the nonasphalt materials at a repeated deviator stress of 6 psi, ksi, or psi;
$E_{Ri}(t)$ = the resilient modulus at time t within the recovery period, ksi or psi;
H = convection coefficient, Btu/hr-ft^2-°F;
H_{air} = the actual air void content of the asphalt mix minus 0.03, decimal form;
K_1 = slope of E_R versus σ_d for $\sigma_d < 6$ psi, ksi/psi;
K_2 = slope of E_R versus σ_d for $\sigma_d > 6$ psi, ksi/psi;
LL = the liquid limit of fine-grained soils, %;
LSUC = the break suction point on the water content versus suction plot;
N = cloud-based factor;
N_{18} = the allowable number of 18-kip single axle loads for a given surface deflection;
n = term used in the calculation of the asphalt mixture stiffness;
PI = the plasticity index for fine-grained soils, %;
PL = the plastic limit for fine-grained soils, %;
Q_a = heat flux resulting from long-wave radiation emitted by the atmosphere, Btu/ft^2-hr;
Q_c = heat flux resulting from convective heat transfer, Btu/ft^2-hr;
Q_e = heat flux resulting from long-wave radiation emitted by the pavement surface, Btu/ft^2-hr;
Q_g = heat flux conducted into pavement, Btu/ft^2-hr;
Q_h = heat flux resulting from transpiration, condensation, evaporation, and sublimation, Btu/ft^2-hr;
Q_i = heat flux resulting from incident short-wave radiation, Btu/ft^2-hr;
Q_r = heat flux resulting from reflected short-wave radiation, Btu/ft^2-hr;
Q_{rad} = net radiation flux influencing heat transfer at a surface, Btu/ft^2-hr;
Q_s = net short-wave radiation entering into the energy balance at the pavement surface, Btu/ft^2-hr;
Q_x = long-wave radiation emitted from a surface without cloud cover correction, Btu/ft^2-hr;
Q_z = long-wave back radiation not corrected for cloud cover, Btu/ft^2-hr;
RECPER = the length of the recovery period for fine-grained soils, days;
REDUCT = the reduction factor for thawing fine-grained soils, %;
R^* = extraterrestrial radiation, Btu/ft^2-day;
S = percentage of possible daily sunshine;
SATWAT = the saturated water content for fine-grained soils, %
S_b = the bitumen stiffness, kg/cm^2;
S_m = the asphalt mixture stiffness, kg/cm^2;
T_1 = temperature of surface node, °F;
T_{ac} = the thickness of the asphalt layer, in.;
T_{air} = air temperature, °F;
T_{con} = temperature of constant temperature node, °F;
T_{gr} = the thickness of the granular base, in,;
T_n = nodal temperature, °F;
T'_n = nodal temperature after a time step, °F;
T_{stab} = the thickness of the stabilized base, in.;
t = the time, days;
u = the relative pore water pressure (negative above the water table), psi;
VOL = volume;
W = total depth of termination nodes, in.;
$\overline{W}$ = percentage of cloud cover at night;
ΔW = depth of a termination node, in.;
W1000 = the water content at a suction of 1000 cm, %;
w = water content based on dry weight, %;
X = total depth of normal nodes, in.;
ΔX = depth of a normal node, in.;
Y = total depth of finite-difference pavement system, in.;
Z = the height above the groundwater table, in.;
α = thermal diffusivity, K/C, ft^2/hr;
γ = total unit weight, pcf;
γ_d = dry unit weight, pcf;
Δ = the equivalent 9-kip moving wheel load deflection, mils;
ε = emissivity of radiation by a surface;
ε_{ac} = the asphalt-concrete radial tensile strain;
θ = the volumetric water content, %;
$\Delta\theta$ = time step, hr; and
σ_d = the deviator stress, psi.